UNIVERSITAT POLITÈCNICA DE VALÈNCIA

Department of Applied Thermodynamics, School of Industrial Engineering

Application of Nanofibres in Polymer Composite Membranes for Direct Methanol Fuel Cells

Sergio Mollá Romano

Doctoral Thesis

in Electrical Technology: Materials, Generation and Distribution

Supervised by Prof. Dr. Vicente Compañ Moreno

Valencia, Spain
July 2015

Copyright ©2015, Sergio Mollá Romano.

All rights reserved.

Patience is bitter,
but its fruit is sweet

(Jean-Jacques Rousseau, 1712-1778)

Abstract

Direct methanol fuel cells are feasible devices for efficient electrochemical power generation if some issues can be solved regarding both electrodes and membranes. The research carried out in this Ph.D. thesis has particularly focused on the concerns associated with the membranes.

Nafion® is the most standard fuel cell membrane material due to its high proton conductivity and exceptional chemical and mechanical stability. However, it suffers from a considerably high methanol permeability and a limited operating temperature (< 80 ºC). The first aspect was addressed with the use of PVA nanofibres and the second one replacing Nafion® with SPEEK-based polymers.

Composite membranes of Nafion® with PVA nanofibres, surface functionalised with sulfonic acid groups, exhibited lower methanol permeabilities due to the intrinsic barrier property of PVA, although proton conductivity was also affected as a result of the non-conducting behaviour of the bulk PVA phase. Remarkably, the nanofibres provided strong mechanical reinforcement which enabled the preparation of low thickness membranes (< 20 μm) with reduced ohmic losses, thus counteracting their lower proton conductivities.

SPEEK-based membranes were examined for DMFC operation within the intermediate temperature range of 80-140 ºC, in which sluggish electrochemical reactions at the electrodes are accelerated and proton conductivity activated.

SPEEK was blended and crosslinked with PVA and PVB polymers for avoiding its dissolution in hot water conditions. SPEEK-PVA compositions showed practical proton conductivities and SPEEK-PVB blends presented very low methanol permeabilities.

Nanocomposite membranes composed of SPEEK-30%PVB nanofibres embedded in a SPEEK-35%PVA matrix were prepared and characterised. A nanocomposite membrane crosslinked at 120 ºC revealed promising results for DMFCs operating at intermediate temperatures.

Electrospinning is concluded to be a suitable technique for obtaining polymer nanofibre mats intended for advanced composite membranes with improved characteristics and fuel cell performances.

Resumen

Las pilas de combustible de metanol directo son dispositivos factibles para la generación electroquímica eficiente de energía eléctrica si se pueden solucionar algunas cuestiones relacionadas tanto con los electrodos como las membranas. La investigación llevada a cabo en esta tesis doctoral se ha centrado particularmente en los problemas asociados con las membranas.

Nafion® es el material de membrana más común para pilas de combustible debido a su alta conductividad protónica y excepcional estabilidad química y mecánica. Sin embargo, padece una considerablemente alta permeabilidad al metanol y una limitada temperatura de operación (< 80 ºC). El primer aspecto se abordó con el uso de nanofibras de PVA y el segundo reemplazando Nafion® con polímeros basados en SPEEK.

Membranas compuestas de Nafion® con nanofibras de PVA, funcionalizadas en su superficie con grupos ácidos sulfónicos, exhibieron menores permeabilidades al metanol debido a la propiedad barrera intrínseca del PVA, aunque la conductividad protónica también se vio afectada como resultado del comportamiento global no conductor de la fase de PVA. Remarcablemente, las nanofibras proporcionaron un refuerzo mecánico fuerte que permitió la preparación de membranas de bajo espesor (< 20 μm) con unas pérdidas óhmicas reducidas, así contrarrestando sus menores conductividades protónicas.

Se examinaron membranas basadas en SPEEK para la operación de pilas de combustible de metanol directo dentro del rango intermedio de temperaturas entre 80-140 ºC, en el que las lentas reacciones electroquímicas en los electrodos se aceleran y la conductividad protónica se activa.

El SPEEK se combinó y entrecruzó con los polímeros de PVA y PVB para evitar su disolución en condiciones de agua caliente. Las composiciones de SPEEK-PVA mostraron conductividades protónicas funcionales y las mezclas de SPEEK-PVB presentaron permeabilidades al metanol muy bajas.

Se prepararon y caracterizaron membranas nanocompuestas constituidas por nanofibras de SPEEK-30%PVB embebidas en una matriz de SPEEK-35%PVA. Una membrana nanocompuesta entrecruzada a 120 ºC reveló resultados prometedores para pilas de combustible de metanol directo operando a temperaturas intermedias.

Se puede concluir que la electrohilatura es una técnica apropiada para la obtención de mallas de nanofibras poliméricas destinadas a membranas compuestas avanzadas con características y rendimientos en pilas de combustible mejorados.

Resum

Les piles de combustible de metanol directe són dispositius factibles per a la generació electroquímica eficient d'energia elèctrica si es poden solucionar algunes qüestions relacionades tant amb els elèctrodes com les membranes. La investigació duta a terme en esta tesi doctoral s'ha centrat particularment en els problemes associats amb les membranes.

Nafion® és el material de membrana més comú per a piles de combustible a causa de la seua alta conductivitat protònica i excepcional estabilitat química i mecànica. No obstant això, patix una considerablement alta permeabilitat al metanol i una limitada temperatura d'operació (< 80 ºC). El primer aspecte es va abordar amb l'ús de nanofibres de PVA i el segon reemplaçant Nafion® amb polímers basats en SPEEK.

Membranes compostes de Nafion® amb nanofibres de PVA, funcionalizades en la seua superfície amb grups àcids sulfónics, van exhibir menors permeabilitats al metanol a causa de la propietat barrera intrínseca del PVA, encara que la conductivitat protònica també es va veure afectada com resultat del comportament global no conductor de la fase de PVA. Remarcablement, les nanofibres van proporcionar un reforç mecànic fort que va permetre la preparació de membranes de baixa grossària (< 20 μm) amb unes pèrdues òhmiques reduïdes, així contrarestant les seues menors conductivitats protòniques.

Es van examinar membranes basades en SPEEK per a l'operació de piles de combustible de metanol directe dins del rang intermedi de temperatures entre 80-140 ºC, en el que les lentes reaccions electroquímiques en els elèctrodes s'acceleren i la conductivitat protònica s'activa.

El SPEEK es va combinar i va entrecreuar amb els polímers de PVA i PVB per a evitar la seua dissolució en condicions d'aigua calenta. Les composicions de SPEEK-PVA van mostrar conductivitats protòniques funcionals i les mescles de SPEEK-PVB van presentar permeabilitats al metanol molt baixes.

Es van preparar i caracteritzar membranes nanocompostes constituïdes per nanofibres de SPEEK-30%PVB embegudes en una matriu de SPEEK-35%PVA. Una membrana nanocomposta entrecreuada a 120 ºC va revelar resultats prometedors per a piles de combustible de metanol directe operand a temperatures intermèdies.

Es pot concloure que l'electrofilatura és una tècnica apropiada per a l'obtenció de malles de nanofibres polimériques destinades a membranes compostes avançades amb característiques i rendiments en piles de combustible millorats.

Acknowledgements

In the first place, I want to express my heartfelt thanks to my supervisor Prof. Dr. Vicente Compañ for affording me the opportunity to work with him and complete this Ph.D. thesis. His guidance and support have been invaluable as well as our exciting scientific discussions.

My deepest sincere gratitude also goes to Prof. Dr. T.-L. Leon Yu (Yuan Ze University, Taiwan), Prof. Dr. Shih-Hung Chan (Yuan Ze University), Prof. Dr. Ulrich Stimming (Technical University of Munich, Germany) and Prof. Dr. Oliver Schneider (Technical University of Munich). I had wonderful and unforgettable research and personal experiences at their labs, which gave a strong boost to my work. All the friends I met in Taiwan and Germany will always be in my heart. Especially, I am delighted to mention that such a stay in Taiwan caused one of the most important things in my life to happen, that is, meeting my nowadays wife Mei Hua Lee.

Similarly, I fondly remember my friends and colleagues at the Department of Applied Thermodynamics and Technological Institute of Energy for their support and good moments together: Prof. Dr. Abel García, Prof. Dr. Mª Jesús Sanchis, Prof. Dr. Ricardo Díaz, Dr. Mayte Gil, Fran, Pili, Marta, Alex, Belén, Armando, Gustavo, Francisco, Rosa, both Jesús, Ángel, Jessica, Leire, Tomás...

Special mention from the bottom of my heart is dedicated to Prof. Dr. Koji Nishio (Kyoto University, Japan) for warmly accepting me to work in his group and opening my mind to the exciting world of batteries, as well as encouraging me to succesfully finish this Ph.D. thesis. I want to extend this feeling on to Prof. Dr. Zempachi Ogumi, Prof. Dr. Takeshi Abe and Prof. Dr. Kohei Miyazaki from Kyoto University, and to the friends and colleagues in our Advanced Battery Research Lab and in Toyota Motor Corporation (Higashi-Fuji Technical Centre, Japan) who were all extremely kind and nice to me: Kodera-san, Nishimura-san, Noda-san, Kobayashi-san, Ozeki-san, Nitta-san, Nakanishi-san, Iba-san, Nishikoori-san, Kotani-san, etc. I would like to include my Taiko classmates and teacher, and my friends Hirata, Yuko and Hiroyuki. Every morning in my way to work, Hiroyuki used to tell me "Ganbatte", which can be translated as "keep trying hard and do your best". This expression has somehow stuck in my mind and has helped me to keep working until the final goal of writing this book.

A very affectionate recognition deserves my beloved friends: Vicente, Esther, Ricard, Eugenia, Mei, Ramón, Berna, Laura, Quique, Mª José, Juan, etc.; and my family in general, but my parents, sister and wife in particular. I greatly want to thank my parents Mª Isabel and Mario, and my

sister Sonia for their endless love and support; and thanks a lot "mi cariño" for being a so extraordinary wife and mom, and giving me your energy, optimism, love and understanding at every moment of our lives since we are happily together.

Most of all, I want to dedicate this work to my son Isaac, who is almost 1 year old at the time these pages are being written, and might like to read this book years later so he can get to know what his father was doing in front of that machine with buttons while he was playing with his green wooden dinosaur and little orange car next to me. Isaac, I love you very much!

Finally, I would like to express my gratitude to Prof. Dr. Santiago Luis (Jaume I University, Castellon) and Prof. Dr. Javier Pozuelo (Carlos III University, Madrid), and their respective groups, for their contributions to this thesis work, and similarly to those of you who have directly or indirectly contributed to this work and have not been explicitly cited.

Again, thanks a lot you all for your support, patience and the given lessons during this amazing Ph.D. period which represents a beautiful and important experience in the life of every researcher.

Research curriculum

This thesis has led to the following research activities:

Published papers

Paper 1 Sergio Mollá, Vicente Compañ, Polyvinyl alcohol nanofiber reinforced Nafion membranes for fuel cell applications, Journal of Membrane Science 372 (2011) 191-200.

Paper 2 Sergio Mollá, Vicente Compañ, Performance of composite Nafion/PVA membranes for direct methanol fuel cells, Journal of Power Sources 196 (2011) 2699-2708.

Paper 3 Sergio Mollá, Vicente Compañ, Enrique Gimenez, Alberto Blazquez, Idoia Urdanpilleta, Novel ultrathin composite membranes of Nafion/PVA for PEMFCs, International Journal of Hydrogen Energy 36 (2011) 9886-9895.

Paper 4 S. Mollá, V. Compañ, S. L. Lafuente, and J. Prats, On the Methanol Permeability through Pristine Nafion® and Nafion/PVA Membranes Measured by Different Techniques. A Comparison of Methodologies, Fuel Cells 11 (2011) 897-906.

Paper 5 Sergio Mollá, Vicente Compañ, Polymer blends of SPEEK for DMFC application at intermediate temperatures, International Journal of Hydrogen Energy 39 (2014) 5121-5136.

Paper 6 Sergio Mollá, Vicente Compañ, Nanocomposite SPEEK-based membranes for Direct Methanol Fuel Cells at intermediate temperatures, Journal of Membrane Science 492 (2015) 123-136.

Congress presentations

(Poster) S. Mollá Romano, V. Compañ Moreno, Membranas compuestas reforzadas con nanofibras de PVA para uso en pilas de combustible de metanol directo - Composite membranes reinforced with PVA nanofibres for use in direct methanol fuel cells, CONAPPICE 2008, Zaragoza, Spain.

(Poster) S. Mollá, T. Leon Yu, E. Riande, V. Compañ, PVA nanofiber-reinforced Nafion membrane for DMFC application, EUROMEMBRANE 2009, Montpellier, France.

(Oral) Sergio Mollá, Mayte Gil, Vicente Compañ, Caracterización de membranas compuestas de Nafion/PVA para aplicación en pilas de combustible de metanol - Characterization of composite Nafion/PVA membranes for direct methanol fuel cell application, CONAPPICE 2010, Sevilla, Spain.

(Poster) Sergio Mollá, Mayte Gil, Vicente Compañ, The effect of thickness for Nafion and composite Nafion/PVA membranes for fuel cell applications, FUEL CELLS Science & Technology 2010, Zaragoza, Spain.

(Oral) Sergio Molla, Joan Prats, Mayte Gil, Vicente Compañ, Proton and methanol transport behaviour of Nafion/PVA composite membranes for fuel cell applications, XII Latin American Symposium on Polymers and X Ibero American Congress on Polymers, 2010, San José, Costa Rica.

(Poster) Sergio Mollá, Vicente Compañ, Enrique Gimenez, Alberto Blazquez, Idoia Urdanpilleta, Novel ultrathin composite membranes of Nafion/PVA for PEMFC, 15th European Fuel Cell Forum, 2011, Lucerne, Switzerland.

(Oral) Sergio Mollá, Vicente Compañ, Nanofiber-based SPEEK composite membranes for DMFC applications, The Energy&Materials Research Conference 2012, Torremolinos, Spain.

(Oral) Sergio Mollá, Vicente Compañ, Polímeros de sPEEK para su uso en membranas compuestas reforzadas con nanofibras en pilas de combustible de metanol - Polymers of sPEEK for nanofiber-reinforced composite membranes in direct methanol fuel cells, CONAPPICE 2012, Madrid, Spain.

(Poster) Sergio Mollá, Koji Nishio, Vicente Compañ, Polymer modified sulfonated PEEK ionomers for membranes in direct methanol fuel cells, 19th International Conference on Solid State Ionics, 2013, Kyoto, Japan.

Courses

High Temperature Polymer Electrolyte Membrane Fuel Cells (HT-PEMFC) Spring School, March 17-20, 2008 at the School of Chemical Engineering and Advanced Materials at Newcastle University.

Research stays

From July 26 to October 18, 2008, under the supervision of Prof. Tzyy-Lung Leon Yu, Department of Chemical Engineering and Materials Science at Yuan Ze University (Taiwan), working on the preparation and characterization of nanofibre-reinforced membranes of Nafion/PVA and organic-inorganic hybrid H_3PO_4-doped PBI membranes (for high temperature fuel cells).

From September 1 to December 9, 2011, under the supervision of Prof. Ulrich Stimming and Prof. Oliver Schneider, Physics Department at the Technical University of Munich (Germany), dealing with the synthesis of novel catalysts of titanium oxycarbide-supported platinum nanoparticles for the methanol oxidation and oxygen reduction reactions, which were studied by means of cyclic voltammetry and rotating disk techniques. In addition, basic knowledge of Li-ion batteries was also acquired and I collaborated in the preparation of anode materials of amorphous titanium dioxide.

Awards

Valencia IDEA 2010, 2nd prize in the category of energy and environment for the work entitled "Utilización de pila de combustible de metanol para la generación de energía distribuida en la ciudad de Valencia - Utilization of direct methanol fuel cell for the generation of distributed power in the city of Valencia" (in Valencia, Spain).

Christian Friedrich Schoenbein Best Poster Medal (in 15th European Fuel Cell Forum, 2011, Lucerne, Switzerland).

Other contributions

(Poster) S. Molla, N.P. Berezina, K. Suarez, O. Solorza, V. Compañ, PEMFC performance of nanocomposite membranes based on perfluorinated polymers containing polyaniline, 11th Grove Fuel Cell Symposium, 2009, London, United Kingdom.

V. Compañ, S. Molla, A.A.-R. Sytcheva, N.P. Berezina, K. Suarez, O. Solorza, E. Riande, PEMFC performance of MEAs based on perfluorinated nanocomposite membranes modified by polyaniline, ECS Transactions 25 (2009) 645-658.

J. Ferre, S. Mollá, J. Calleja, L. Zubizarreta, New composite membranes for application in a PEM electrolyser, WHEC Proceedings (2010) 145-150

(Poster) Jessica Calleja, Sergio Molla, Alberto Blazquez, Igor Cantero, Mayte Gil-Agustí, Vicente Compañ, Comportamiento de las membranas híbridas Nafion®/Sepiolita en aplicaciones PEMFC - Behaviour of hybrid Nafion®/Sepiolite membranes in PEMFC applications, CONAPPICE 2010, Sevilla, Spain.

(Poster) A. Barjola, V. Compañ, A. García, S. Mollá, Characterization of ion exchange membranes for use in fuel cells and electrolysers, XXXV Meeting of Electrochemistry of the Spanish Royal Society of Chemistry and 1st E3 Mediterranean Symposium: Electrochemistry for Environment and Energy, 2014, Burgos, Spain.

S.D. Pasini Cabello, S. Mollá, N.A. Ochoa, J. Marchese, E. Giménez, V. Compañ, New bio-polymeric membranes composed of alginate-carrageenan to be applied as polymer electrolyte membranes for DMFC, Journal of Power Sources 265 (2014) 345-355.

From August 16, 2012, to March 31, 2014, working at the Department of Energy and Hydrocarbon Chemistry at Kyoto University as a researcher on advanced batteries (metal-air) under a collaboration project with Toyota Motor. We investigated air electrodes for the oxygen reduction and evolution reactions, and some results were presented in:

(Oral) S. Molla, T. Okugaki and K. Nishio, Oxygen reduction/evolution reactions on perovskites. A comparative study of composition and performance by electrochemical methods, The 80th Spring Meeting of the Electrochemical Society of Japan, 2013, Sendai.

(Oral) S. Molla, T. Okugaki, S. Nakanishi, I. Nitta, Y. Kotani, K. Nishio, Effects of compositions of perovskite oxides on the electrochemical properties of an air electrode for metal-air batteries, The 54th Battery Symposium in Japan, 2013, Osaka.

Koji Nishio, Sergio Molla, Tomohiko Okugaki, Shinji Nakanishi, Iwao Nitta, Yukinari Kotani, Oxygen reduction and evolution reactions of air electrodes using a perovskite oxide as an electrocatalyst, Journal of Power Sources 278 (2015) 645-651.

Glossary

A, S	Geometrical surface area
C	Concentration
CH_3OH	Methanol
CTAB	Cetyltrimethylammonium bromide
D	Diffusion coefficient
Δ	Difference between two values of a same parameter
DMAc	N,N-Dimethyl acetamide
DMFC	Direct methanol fuel cell
DSC	Differential scanning calorimetry
E	Reversible open circuit voltage, Young's modulus
E_a	Activation energy
ε	Mechanical strain
η	Overpotential
f	Frequency
FTIR	Fourier transform infrared spectroscopy
HCl	Chlorhydric acid / hydrochloric acid
H_2O	Water
H^+	Proton
i	Current density
i-V	Polarization curve
IEC	Ion-exchange capacity
J	Flux
K	Partition coefficient
L	Membrane thickness
λ	A measure of water content in a membrane
LiCl	Lithium chloride
m	Membrane weight, slope of a line
MEA	Membrane-electrode assembly
NaCl	Sodium chloride
Nafion/PVA	Composite membrane of Nafion® with PVA nanofibres
Nanocomposite	A polymer matrix with embedded nanofibres
NaOH	Sodium hydroxide
OCV	Open circuit voltage
OH	Hydroxyl
P	Permeability, power density
PEM	Polymer electrolyte / proton exchange membrane
Pt	Platinum
Pt-Ru	Platinum-Ruthenium

PVA	Polyvinyl alcohol
PVB	Polyvinyl butyral
R	Resistance
RH	Relative humidity
SEM	Scanning electron microscopy
σ	Conductivity, mechanical strength
SPEEK	Sulfonated poly-ether-ether-ketone
SPEEK-PVA	Blended SPEEK and PVA polymers
SPEEK-PVB	Blended SPEEK and PVB polymers
SO_3H	Sulfonic acid
T	Temperature
t	Time
T_g	Glass transition temperature
TGA	Thermogravimetric analysis
V	Volume, Volts (potential)
Z	Impedance

Contents

Introduction

1.1. Fuel cell types. Direct methanol fuel cell (DMFC)

A fuel cell is an electricity generator device in which a fuel, typically hydrogen or methanol, is electrochemically oxidised at the anode while oxygen/air is electrochemically reduced at the cathode. An electrolyte is placed in between and separates the electrodes while enabling the conduction of ionic species, i.e. protons (H^+), hydroxides (OH^-), carbonates (CO_3^{2-}) or oxides (O^{2-}).

Proton and hydroxide species are commonly conducted through polymer electrolyte membranes (PEMs) at relatively low temperatures [1], see Table 1. On the other hand, carbonate conductivity usually takes place across a ceramic substrate soaked with a molten carbonate salt, while oxide ions are transported through a dense ceramic electrolyte. Both molten carbonate fuel cells (MCFCs) and solid oxide fuel cells (SOFCs) require temperatures above 600 ºC to operate [2].

PEM fuel cells (PEMFCs) generally refer to the use of hydrogen as a fuel and direct alcohol fuel cells (DAFCs) mainly comprises methanol and ethanol fuels. Although there is an increased interest in ethanol for fuel cells due to its easy synthesis from renewable sources, the efficient electro-oxidation of ethanol still remains challenging [3]. Because methanol can also be obtained from biomass, e.g. by pyrolysis of timber (wood alcohol), and shows a higher electrochemical activity, direct methanol fuel cells (DMFCs) are considered a suitable technology for power generation. Indeed, the liquid nature of methanol and simple refuelling make it a good candidate for portable generators, e.g. in military and leisure applications; backup systems, e.g. in telecommunication towers; and electric vehicle range extenders.

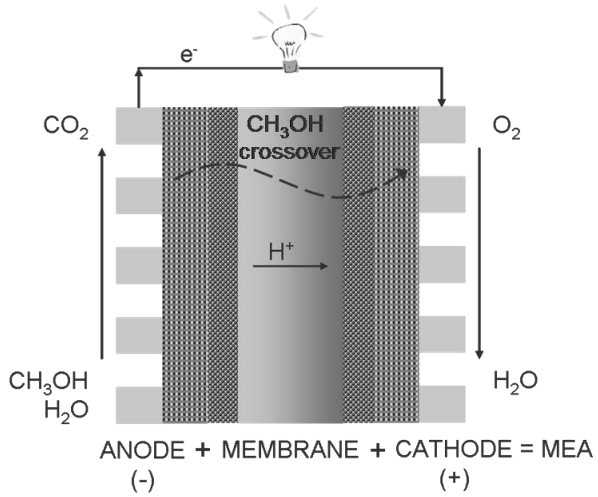

Fig. 1. Representation of the working principle of a direct methanol fuel cell (DMFC).

Table 1. Comparison between different types of polymer electrolyte membrane fuel cells (PEM: Proton exchange membrane, AEM: Alkaline exchange membrane). Adapted from [1].

Parameters	**LT-PEMFC**	**HT-PEMFC**
Electrolyte	PEM	PEM
Operating temp. (ºC)	60-80ºC	> 100
Ionic carrier	H^+	H^+
Fuel	H_2	H_2
Oxidant	O_2	O_2
Relative humidity (%)	100	< 50
Advantages	High power density, quick start up, low noise, low temperature operation	Reduced parasitic loads and system; faster electrode kinetics, improved tolerance to CO, higher efficiency of heat recovery
Drawbacks	Insufficient proton conductivity under low humidity conditions, complex and expensive heat and water management system, expensive Pt catalysts and their poor performance, sensitive to CO	Low water retention, harsher operating environment
Parameters	**DAFC**	**AEMFC**
Electrolyte	PEM	AEM
Operating temp. (ºC)	60-80	~ 60
Ionic carrier	H^+	OH^-
Fuel	Alcohol	H_2
Oxidant	O_2	O_2
Relative humidity (%)	100	100
Advantages	Liquid fuel, compact design, no compressor or humidification	Less corrosive alkaline environment, simplified water management, faster kinetics, non-precious metal catalysts
Drawbacks	Low efficiency and power and power density, high fuel permeability, catalyst poisoning, slow load response times	Inherently high thermodynamic voltage loss, low stability of AEMs, relatively lower mobility of OH-, no suitable binder for MEA.

The working principle of a DMFC is represented in Fig. 1. DMFCs are generally operated at temperatures about 80 ºC or below (Table 1). However, a goal of this thesis has included the development of membranes intended for higher temperature operation, i.e. 80-140 ºC. The values within this range

have been defined as intermediate temperatures, in order to be distinguished from the hight temperature range which is practically accepted to be 160 ºC and above. The latter is a consequence of the temperatures in which the proton conductivities of polymer electrolytes of phosphoric acid (H_3PO_4)-doped polybenzimidazole (PBI) reach acceptable levels for fuel cell operation [4].

1.2. Electro-oxidation of methanol

Methanol is electrochemically oxidised at the anode as shown in Eq. (1),

$$CH_3OH + H_2O \rightarrow CO_2 + 6H^+ + 6e^- \quad (1)$$

and simultaneously oxygen is electrochemically reduced at the cathode according to Eq. (2),

$$1.5O_2 + 6e^- + 6H^+ \rightarrow 3H_2O \quad (2)$$

correspondingly, the global reaction in the DMFC can be seen as,

$$CH_3OH + 1.5O_2 \rightarrow CO_2 + 3H_2O \quad (3)$$

Methanol electro-oxidation over a platinum (Pt) surface follows a multistep reaction mechanism, which is represented by Eqs. (4-10) [5],

$$CH_3OH + Pt(s) \rightarrow Pt\text{-}CH_2OH + H^+ + e^- \quad (4)$$
$$Pt\text{-}CH_2OH \rightarrow Pt\text{-}CHOH + H^+ + e^- \quad (5)$$
$$Pt\text{-}CHOH \rightarrow Pt\text{-}COH + H^+ + e^- \quad (6)$$
$$Pt\text{-}COH \rightarrow Pt\text{-}CO + H^+ + e^- \quad (7)$$
$$Pt(s) + H_2O \rightarrow Pt\text{-}OH + H^+ + e^- \quad (8)$$
$$Pt\text{-}OH + Pt\text{-}CO \rightarrow Pt\text{-}COOH + Pt(s) \quad (9)$$
$$Pt\text{-}COOH \rightarrow Pt(s) + CO_2 + H^+ + e^- \quad (10)$$

The main drawback is found in Eq. (7) since carbon monoxide (CO) is strongly adsorbed on platinum. This causes the available concentration of active sites to decrease thus affecting methanol adsorption as Eq. (4).

The complex Pt-CO can be eliminated by reaction with hydroxide species (Pt-OH) coming from dissociative water adsorption on the platinum surface, see Eqs. (8-10). Unfortunately, Eq. (8) is not active enough for a practical purpose.

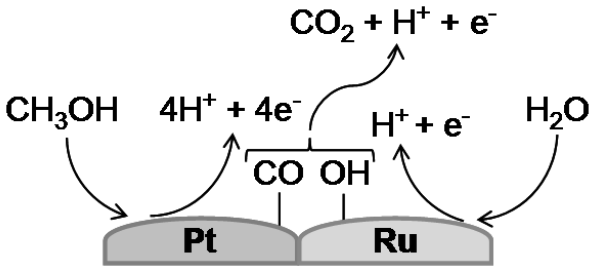

Fig. 2. Scheme of the methanol electro-oxidation mechanism on a Pt-Ru catalyst.

It was found that ruthenium (Ru) was able to promote Eq. (8), and consequently, Pt-Ru alloys have become popular catalysts for DMFC anodes [5]. In Eqs. (11-12) is detailed this catalytic synergy effect and Fig. 2 schematically represents the electro-oxidation mechanism of methanol on a Pt-Ru catalyst,

$$Ru(s) + H_2O \rightarrow Ru\text{-}OH + H^+ + e^- \quad (11)$$
$$Ru\text{-}OH + Pt\text{-}CO \rightarrow Pt\text{-}COOH + Ru(s) \quad (12)$$

An additional approach involves increasing the operating temperature of the fuel cell for accelerating the electrochemical reactions at the electrodes, in particular at the anode [7]. In this regard, SPEEK-based membranes for enabling DMFC operation well above 80 ºC are investigated in this thesis.

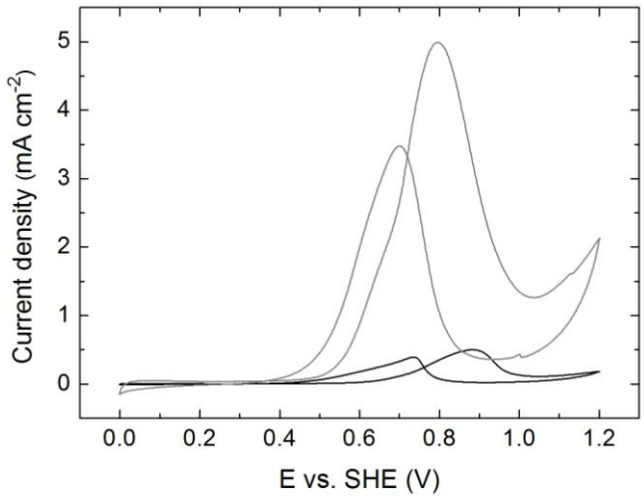

Fig. 3. Cyclic voltammetry profiles for methanol electro-oxidation of a (black) Pt/C (40 wt% Pt) and a (grey) Pt/TiO_xC_y (20 wt% Pt) catalyst.

Furthermore, extensive research is being carried out for the development of new catalyst systems with enhanced activity for methanol electro-oxidation. Among them, metal oxide-supported platinum catalysts have attracted a great attention for DMFCs and PEMFCs [8-12].

During my research stay at the Technical University of Munich (TUM), I was studying Pt/TiO_xC_y catalyst systems for the methanol oxidation and oxygen reduction reactions. In Fig. 3 is presented an experimental result of cyclic voltammetry in which a Pt/C and a Pt/TiO_xC_y catalyst are compared for the methanol electro-oxidation reaction in an aqueous solution of 0.5 M methanol and 0.1 M $HClO_4$ (perchloric acid). It is observed that Pt/TiO_xC_y is more active than Pt/C, and it is inferred to the participation in the reaction of oxygen atoms from the titanium oxycarbide lattice, while the role of carbide was increasing the electron conductivity.

1.3. DMFC membranes

The types of polymer electrolyte membranes more representative for use in direct methanol fuel cells can be classified as [13]:

- Perfluorinated membranes: They consist of chains with hydrophobic perfluorinated backbones and side chains, which are terminated in hydrophilic sulfonic acid groups thus leading to a complete phase segregation. Nafion® (DuPont™) is the most widely used commercial membrane and ionomer. Its chemical structure can be viewed in Fig. 4.

- Non-perfluorinated membranes: They are known as hydrocarbon membranes and nowadays are gaining a lot of interest as cheaper alternatives to Nafion®. Their backbone is usually formed by phenyl units linked by functional groups such us ketone, ether or sulfone. Sulfonation of the phenyl rings leads to the direct attachment of sulfonic acid groups for the proton conduction. The most considered materials are sulfonated polystyrene, sulfonated poly-ether-ether-ketone (SPEEK) and sulfonated polysulfone.

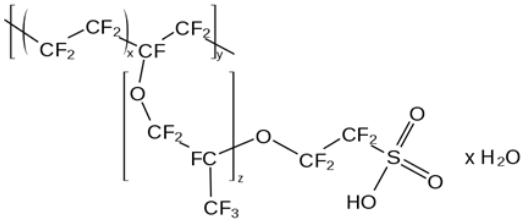

Fig. 4. Chemical structure of the perfluorosulfonic acid commercially known as Nafion®.

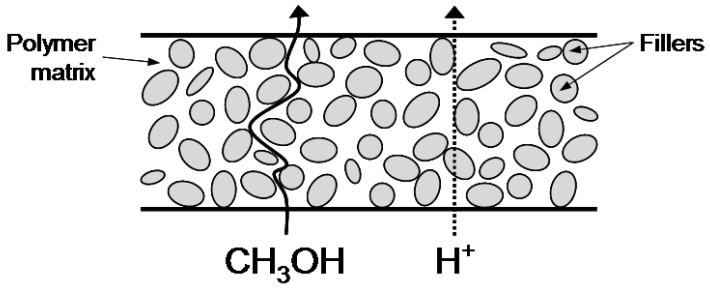

Fig. 5. Reduction of methanol permeability due to increased path tortuosity in composite membranes. Proton transport can be less affected if acid-functionalised fillers are added.

▪ Blended/crosslinked membranes: Generally, two polymers are mixed in which at least one of them is proton conducting. The function of the other polymer is enhancing mechanical, thermal and/or chemical stability of the membrane, which can be promoted by crosslinking reactions.

▪ Acid-base complex membranes: An acid polymer, i.e. containing sulfonic acid groups, is blended with a basic polymer, i.e. incorporating amino groups, and thus ionic crosslinkings are created instead of covalent bonds. Polypyrrole and PBI are some examples of basic polymers.

▪ Composite membranes: They comprise a polymer matrix in which a solid filler is added. Inorganic oxide particles and zirconium phosphate are the most common fillers [14], and they can be modified with functional groups, e.g. sulfonic or phosphonic acids, attached on their surface [15-17]. The usual role of the fillers is enhancing the water retention capacity of membranes at lower relative humidities in fuel cells operating with hydrogen, while in DMFCs they contribute to decrease methanol permeation via the associated increase of tortuosity (Fig. 5) [18].

1.3.1. Composite membranes

Three methods are reported for the preparation of organic-inorganic hybrid membranes [19]:

(1) Physical blending: The filler in form of inorganic (nano-)particles is vigorously mixed with the polymer solution and afterwards a membrane is cast from this slurry.

(2) Sol-gel: A chemical precursor of the filler is dissolved in the polymer solution and then a membrane is cast. The precursor contained in the membrane is then hydrolysed and condensates thus forming inorganic phases within the polymer matrix.

(3) Infiltration: A membrane is cast from the polymer solution and a chemical precursor of the filler is dissolved within a suitable solvent. Following, the membrane is placed within the precursor solution and the membrane correspondingly swells. The swollen membrane incorporates the filler precursor compound by diffusion. Finally, the excess solvent is removed from the membrane and the remaining precursor molecules are reacted and transformed into inorganic species.

There is a limit to the maximum content of inorganic particles which can be embedded in a polymer membrane, since an intrinsic tendency for embrittlement with increasing loadings occurs. Other composite membranes avoid this issue replacing the inorganic phase with a strong polymer support. In this direction, pore-filling type membranes were proposed for enhancing the physical properties of standard ionomers, i.e. Nafion®, and lately nanofibre-incorporating membranes have been considered.

A pore-filling type membrane is composed of a microporous film substrate with the pores filled by a proton conducting polymer electrolyte. Because the polyelectrolyte (ionomer) is confined within the pores, swelling is suppressed by the substrate matrix. Consequently, this type of membranes demonstrate low methanol permeability, relatively high proton conductivity, good mechanical strength and stability [20,21]. Fig. 6 represents a simplified view of the cross-section of a pore-filling type membrane.

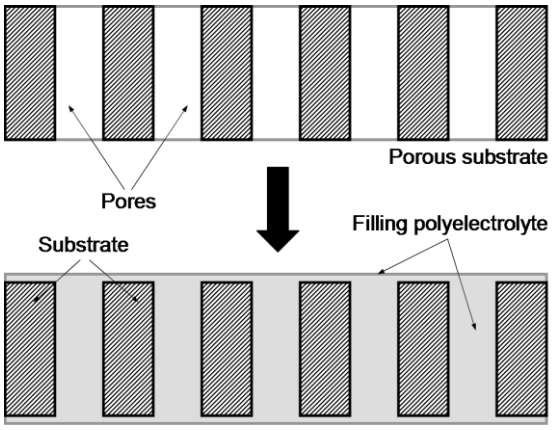

Fig. 6. Transversal representation of a pore-filling type membrane in which the pores of a microporous substrate are filled with a polyelectrolyte (ionomer).

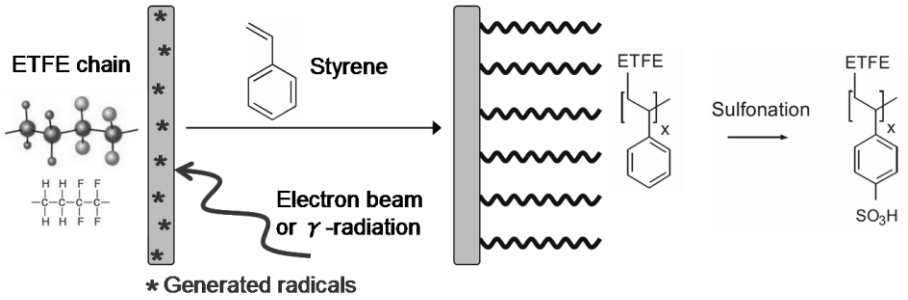

Fig. 7. Polymer electrolyte membrane prepared from a ETFE substrate. Radiation-generated radicals in ETFE chains polymerize styrene to grafted polystyrene which is then sulfonated.

Paste extrusion and solvent/non-solvent casting are some examples of the complex manufacturing processes for the formation of microporous films. Taking the concept of pore-filling membranes to a nanoscale emerges the so-called radiation grafted membranes. These latter use a fluorinated film substrate, e.g. fluorinated ethylene propylene (FEP) and poly(ethene-co-tetrafluoroethene) (ETFE), which can generate and stabilize radicals originated by electron beam or γ-radiation treatments. Swelling of the film in a solvent containing a reactive monomer with a carbon-carbon double bond, e.g. styrene with or without addition of a comoner, induces its polymerization within the free volume space between the chains of the substrate [22,23]. Then, such a grafted polymer is sulfonated to incorporate sulfonic acid groups within the membrane. Similarly, the substrate provides a robust support for constraining membrane swelling and enhancing the properties for fuel cell application. A scheme of preparation of a typical sulfonated polystyrene-based radiation grafted membrane is shown in Fig. 7.

In the last years, the pore-filling type membranes have evolved towards the utilization of electrospun nanofibres as porous polymer supports. This is justified by the wide availability of materials which can be processed by electrospinning and the relatively simple and versatile fabrication procedure [24,25]. Furthermore, nanofibres have extended their application to fuel cell catalysts and battery materials [24,25].

Different configurations are possible attending if the nanofibres are or are not proton conducting and if they are embedded in a polymer matrix which can or cannot conduct protons. In this regard, we can find (i) composite membranes with proton conducting nanofibres of sulfonated poly(ether sulfone) [26] or SPEEK/SiO_2 [27] inserted in a Nafion® matrix; (ii) composite membranes with a Nafion® matrix containing non-proton conducting nanofibres of PVA [28], polyvinylidene fluoride (PVDF) [29] or polyetherimide (PEI) [30], as well as a hydrocarbon type polyelectrolyte

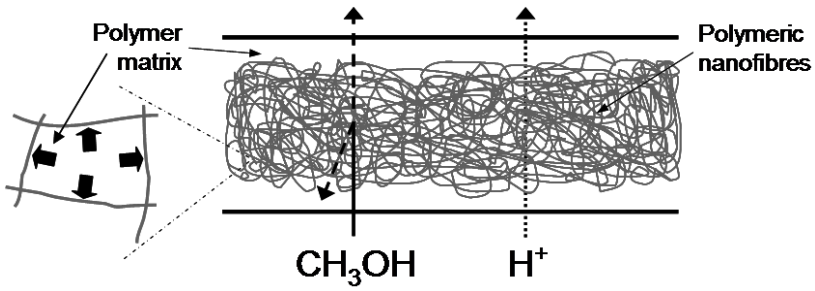

Fig. 8. Structure of a nanocomposite membrane in which electrospun nanofibres are embedded in a polymer electrolyte thus reinforcing the matrix and constraining swelling.

matrix, sulfonated poly(arylene ether sulfone), with non-conducting polyacrylonitrile (PAN) nanofibres [31]; and (iii) composite membranes based on proton conducting nanofibres of sulfonated poly(arylene ether sulfone) [32] or perfluorosulfonic acid [33] compacted within an inert polymer resin.

Fig. 8 exemplifies the typical structure of a nanocomposite membrane with nanofibres and their associated reinforcing effect which limits swelling and increases mechanical properties and stability. Moreover, this comes accompanied by a reduction of the methanol permeability, which is encouraged by nanofibres presenting an intrinsic methanol barrier property [26,28,29].

Some studies concentrate on the characteristics of proton conducting nanofibres. It seems that proton conductivity is strongly promoted along the fibre axis as a consequence of the favoured alignment of the ionic channels [34,35]. However, in a perpendicular direction, the exact proton conduction mechanism is still not clear and some authors suggest that conduction takes place on the nanofibre surface [36]. This might indeed explain the greater increments of in-plane conductivity observed in nanofibre-containing membranes with respect to the through-thickness conductivity [35-37].

This thesis compiles the investigations carried out for the preparation and characterization of composite membranes reinforced with nanofibres obtained by electrospinning. All the work has been published in journal papers, which have been collected and adapted for this book. From Paper 1 to Paper 4 are reported the studies on Nafion-PVA membranes, i.e. Nafion® infiltrated between PVA nanofibres which were crosslinked and functionalised. Specifically, Paper 1 and Paper 2 focus on their DMFC application, Paper 3 evaluates their performance in hydrogen fuel cells, and Paper 4 offers a detailed description of different techniques to measure methanol permeability. These studies concluded that PVA nanofibres acted as efficient barrier layers for methanol permeation but proton conduction

was also reduced due to the non-conducting behaviour of PVA. However, the strong reinforcement provided by the PVA nanofibres resulted to be very advantegous for fuel cell performance.

On the other hand, Paper 5 and Paper 6 describe the studies related with SPEEK-based membranes. In Paper 5, blended membranes of SPEEK with PVA and PVB are examined in terms of stability, proton conductivity and methanol permeability for application in DMFCs operating at intermediate temperatures (80-140 ºC). Paper 6 explains the preparation of nanocomposite membranes with proton conducting nanofibres (from the results in Paper 5) and discusses their properties and DMFC performance as a function of crosslinking temperature. The membranes consisted of a SPEEK-PVA matrix (composition with good proton conductivity but high methanol permeability) incorporating nanofibres of SPEEK-PVB (composition with very low methanol permeability but limited proton conductivity). It was concluded that nanocomposite membranes crosslinked at 120 ºC were promising candidates for DMFCs at intermediate temperatures.

1.3.2. Other advanced membranes

Operation above 160 ºC can be achieved with H_3PO_4-doped PBI membranes. Although acceptable performances are obtained operating with hydrogen (300-400 mW cm^{-2} at 175 ºC) [38], poor performances and a fast degradation rate are reported under DMFC operation (12-16 mW cm^{-2} at 175 ºC) [39]. This is attributed to low electrochemical kinetics in the anode due to the presence of phosphate ions and in the cathode due to methanol crossover, and as a consequence of acid loss in the membrane and catalyst layers.

A proposed attempt involves the replacement of liquid phosphoric acid in PBI with a solid polyvinylphosphonic acid (PVPA) polymer (see Fig. 9). A PBI-PVPA membrane surpassed the performance of Nafion 117 at 110 ºC feeding methanol solutions above 1 M concentration [40].

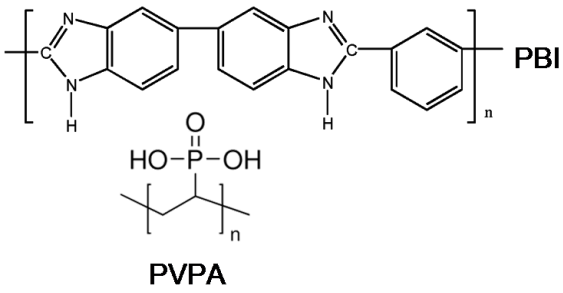

Fig. 9. Chemical structures of polybenzimidazole (PBI) and polyvinylphosphonic acid (PVPA).

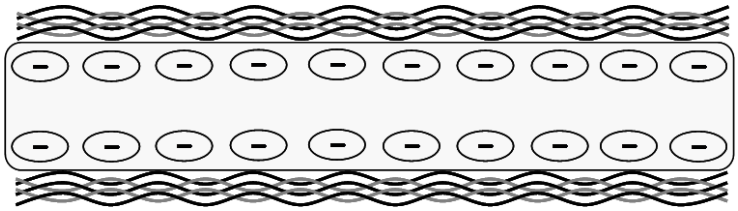

Fig. 10. Surface modification of a proton-exchange membrane (negatively charged) with a thin film formed by alternating layers of (black) cationic and (grey) anionic polyelectrolytes.

Other strategy which utilizes ionic crosslinking reactions between acid-base or cationic-anionic polymers is known as layer-by-layer assembly. In this method, a polyelectrolyte membrane such us Nafion® is typically coated on the surface with a thin film composed of alternating layers of cationic (+) and anionic (-) polymer chains (Fig. 10). Electrostatic attraction between the polyelectrolytes creates robust layers which can conduct protons but block methanol permeation [41]. Consequently, DMFC performance is improved by the surface modification.

Experimental

2.1. Electrospinning process

2.1.1. Background

Early studies on the interaction of electricity with liquids are dated in the late 16th century, in which William Gilbert noted that a spherical drop of water would change into a conical shape when an electrically charged piece of amber was placed on it.

Later, between the beginning and middle of the 20th century, some researchers set out to study this phenomenon experimentally and in 1934 Anton Formhals formalised a patent for producing polymer fibres by an electrostatic process.

However, those studies were not taken seriously until the British scientist Sir Geoffrey Taylor began to investigate the phenomena occurring when an electric field is applied to a liquid. Consequently, in 1969 he published that a drop of polymer solution at the tip of a capillary subjected to an electric field adopts the form of a cone, and that a filament emerges expelled from the vertex of such a cone, which is known as "Taylor cone".

Thereafter, studies were mainly directed to investigate the morphology and characterization of nanofibres, and from the 1980s and particularly in recent times, many efforts have been focused on the optimization of the electrospinning process. This is due to the rise of nanotechnology and the promising applications of nanofibres in different areas such us filtration membranes, special fabrics, catalyst supports, adsorbents, etc.

2.1.2. Fundamental aspects of electrospinning

An electrospinning setup (Fig. 11) basically consists of a pump, a syringe pump in a lab scale, which transfers a polymer solution at a certain flow rate to a metallic capillary or needle (spinneret) connected to a high-voltage direct current power supply. When a high electric field is applied (> 0.5 kV cm^{-1}), the liquid solution becomes charged and the equilibrium of gravity, surface tension and electrostatic forces leads to the formation of a Taylor cone (Fig. 11), and as a function of solution viscosity, drops or a continuous filament (jet) are formed. As the filament is extruded by the electrostatic repulsion (tangential component), it dries and stretches in flight. The nanofibres are finally deposited on a grounded collector which is often a metal plate or a rotating drum. The latter is preferred if aligned nanofibres are required [42].

Fig. 12 shows a picture of the experimental setup employed for the fabrication of the nanofibre mats used in this thesis work. The polymer solution was introduced in a syringe and forced to flow with a syringe pump.

A needle was placed at the top of the collector plate and was able to move alternatively from right to left and vice versa. The collector plate could move in the vertical direction for the distance between it and the needle to be fixed. Two high-voltage power supplies were incorporated, which allowed the control of voltage in both needle (positive polarization) and collector (negative). A digital camera was also present, which was very useful for monitoring the Taylor cone and adjusting the different parameters.

Two innovative extensions of electrospinning are coaxial and melt electrospinning. In the coaxial electrospinning, two immiscible polymer solutions are injected one into the other at the tip of the spinneret. The outer fluid carries the inner solution to the Taylor cone and correspondingly core-shell nanofibres are obtained [43]. On the other hand, in the melt electrospinning, a melted polymer is electrospun thus eliminating the need of solvents [44]. However, due to inherent high viscosity of polymer melts, the fibre diameters tend to be larger than those prepared by electrospinning of polymer solutions [45].

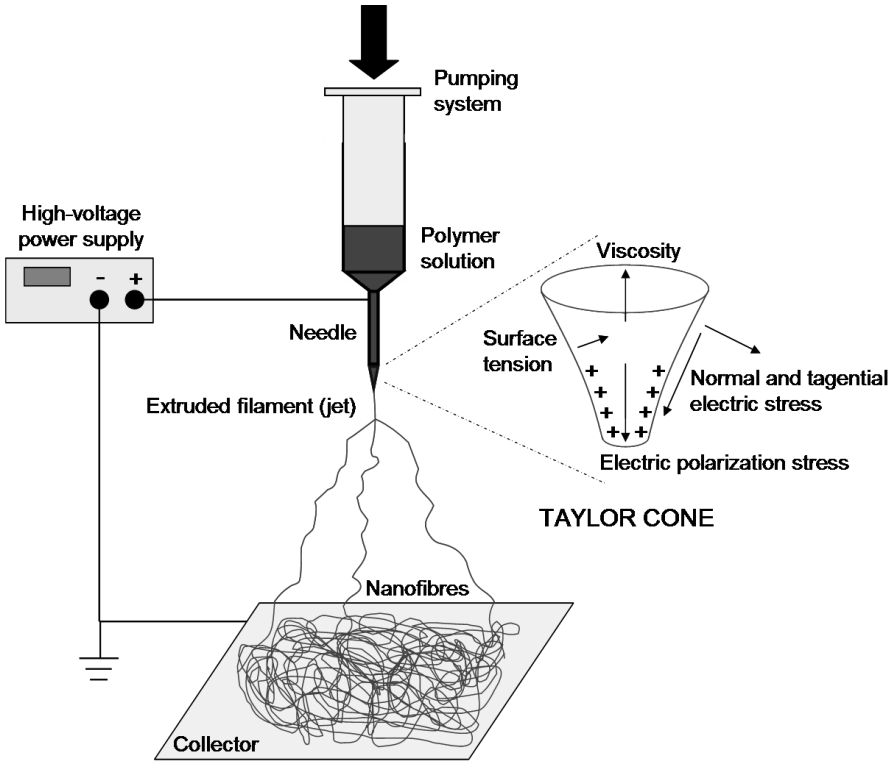

Fig. 11. Schematic representation of an electrospinning setup for the production of nanofibres from a polymer solution. The equilibrium of forces at the Taylor cone are also presented.

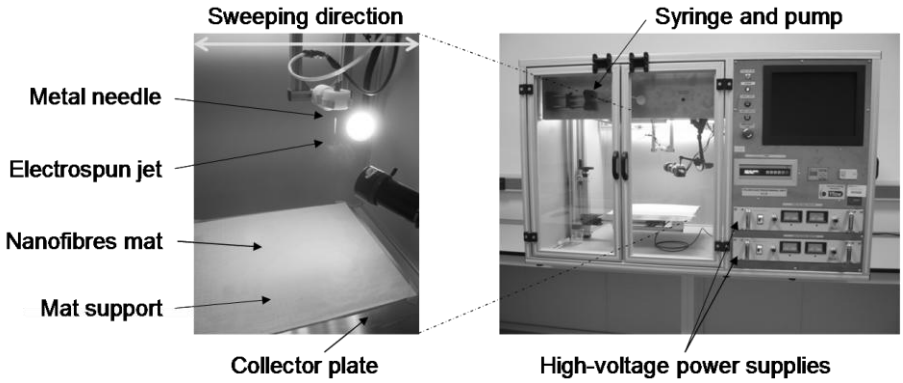

Fig. 12. Electrospinning equipment used for the preparation of nanofibres in this thesis work.

Production rates are typically low in electrospinning. Although there are several methods for scaling-up the production of nanofibres in industry, the most two common are multiplying the number of needles and using a rotating roller electrospinning system. In this last case, a metallic cylinder partially immersed in a tank with polymer solution rotates and gets coated by a thin layer of it, while a collector plate is placed at its top. Application of a high voltage difference between the cylinder and the collector causes many Taylor cones to appear on the surface of the cylinder. A backing film moving along the collector side collects the produced nanofibres in a continuous fashion (Fig. 13).

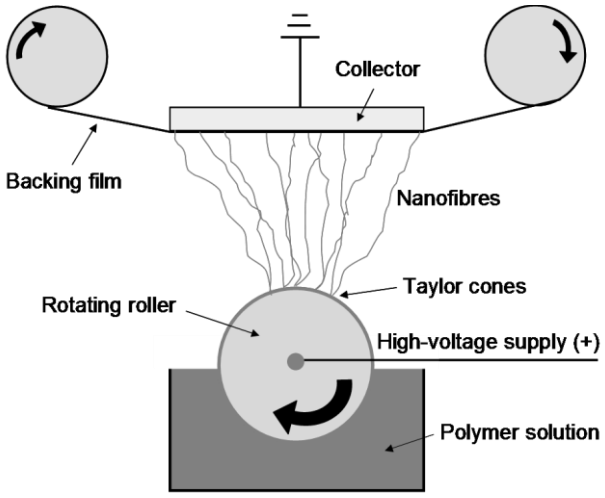

Fig. 13. Schematic representation of a rotating roller electrospinning system for scaling-up the production of nanofibres.

2.1.3. Electrospinning parameters

The electrospinning process is a simple technique but complex to optimise since it is influenced by many parameters which require an strict control. These parameters can be classified as a function of their nature:

a) Solution properties: Polymer concentration, solvent volatility, surface tension, viscosity, conductivity.

b) Process variables: Voltage applied between needle and collector, distance needle-collector, flow rate of polymer solution,

c) Environment effects: Humidity and temperature.

2.1.3.1. Solution properties

The formation of nanofibres by electrospinning is dominated by the viscosity and surface tension of the polymer solution. Therefore, each polymer-solvent system to be electrospun needs finding the optimal conditions to succeed. For example, it is reported that smooth but thicker nanofibres are formed with a polyethylene oxide (PEO) solution in water when the solvent is changed to a water/ethanol mixture. This is interpreted as a consequence of a higher viscosity and lower surface tension of the solution with increasing ethanol concentration [46]. In general, nanofibre diameters and viscosity are directly associated [42]. Consequently, increasing polymer concentration, and thereby viscosity of the solution, causes enlargement of nanofibre diameters.

The morphology of the nanofibres, i.e. formation of smooth fibres or, on the contrary, beads or beaded fibres, is mainly driven by the surface tension although viscosity plays a role too [42,46]. Decreasing the surface tension helps to eliminate the bead formation but promotes the formation of nanofibres with larger diameters. When water is used as a solvent, it is well known that surfactants must be added to the polymer solution for enabling electrospinning instead of electrospraying. In this case, the category of the surfactant (cationic, anionic, amphoteric or nonionic) also affects the aspect of the electrospun nanofibres [47].

Regarding the conductivity, it has been correlated that the net charge density carried by the moving filament is inversely proportional to the resistivity of the polymer solution [46], and therefore, directly proportional to conductivity. Increasing the conductivity, and thus the net charge density, produces greater electrostatic repulsion forces which accelerate further the jet and in turn favors smaller diameters of nanofibres. Other advantage is

that formation of beads diminishes with increasing net charge density [42,46].

Finally, the role of solvent volatility (vapour pressure) is assigned to the drying time of the nanofibres in flight. Larger times lead to wet nanofibres be reaching the collector thus obtaining mostly films instead of nanofibre mats, while shorter times are prone to block the tip of the needle during operation. Logically, a parameter of the process which depends on the solvent volatility is the distance between the needle and the collector.

2.1.3.2. Process variables

Generally speaking, increasing both the voltage applied between the needle and collector and the distance needle-collector contribute to decrease the nanofibre diameters and beads formation [42]. In the first case, this is attributed to the increment of net charge density with increasing voltage, and in the latter as a result of a greater extent of stretching associated with a larger distance of flight.

On the other hand, flow rate of the polymer solution must be conveniently fixed for achieving a stable Taylor cone at given conditions. However, as an empirical observation, relatively larger flow rates induce increased nanofibre diameters and even the formation of beads [42].

2.1.3.3. Environment effects

Relative humidity and surrounding temperature are the main factors which affect the production of nanofibres. The relative humidity seems to shield the electric field between the needle and collector thus decreasing the effective electrostatic forces. Regarding the temperature, its effect is interpreted in terms of influencing the evaporation rate of the solvent.

2.2. Preparation of nanocomposite membranes

2.2.1. Nafion/PVA membranes

Composite membranes of Nafion® containing PVA nanofibres were obtained following a sequence of steps as described next.

(a) Electrospinning of PVA nanofibre mats:

Aqueous PVA solutions were produced dissolving 8 g PVA in 80 g water with 0.04 g CTAB and stirring the mixture at 80 ºC for 2 h. The

solution, at room temperature, was introduced in a syringe (about 20 ml) which was placed at the syringe pump of the electrospinning equipment as in Fig. 12.

Electrospinning was carried out for several hours at 0.5 ml h^{-1} flow rate, with a needle-collector distance of 25 cm and a voltage difference between needle (+11 kV) and collector (-5 kV) of 16 kV. Relative humidity in the air was kept below 40% by means of a dehumidifier.

(b) Thermal treatment of the PVA nanofibres:

The mats of PVA nanofibres were annealed for 3 h at 170 ºC inside an oven (Fig. 14) below the atmospheric pressure (at a pressure of 250 mbar). Thereby, water was completely removed from the PVA phase and the mechanical properties of the nanofibres improved.

Fig. 14. Thermal treatment of a mat of PVA nanofibres at 170 ºC in vacuum (250 mbar).

(c) Surface functionalization of the PVA nanofibres:

The nanofibre mats were firmly clampled between two steel rings and then immersed in a bath with a mixture of isopropanol and water (70/30 v/v, respectively). Such a mixture contained a 0.1 M concentration of chlorhydric acid (hydrochloric acid, HCl) as a catalyst for an acetal-type reaction between the outer PVA chains and a salt of 4-formyl-1,3-benzenedisulfonic acid disodium salt (0.04 M). The reaction was performed at 60 ºC for 2 h. Fig. 15 shows a view of the functionalization reaction for the modification of the surface of the PVA nanofibres.

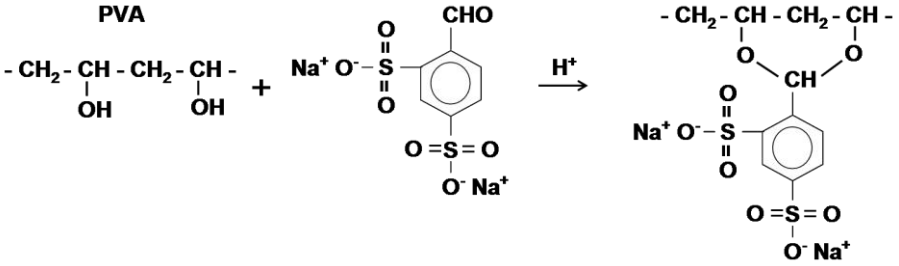

Fig. 15. Representation of the acetal-type reaction for the surface functionalization of the PVA nanofibres with sulfonic acid groups.

The sodium ions of the attached molecules were exchanged with protons from a 0.3 M HCl solution in isopropanol/water (70/30 v/v). Afterwards, the mats were washed thoroughly in an isopropanol/water mixture (70/30 v/v) and later in pure isopropanol. Finally, the mats were dried at 60 ºC inside an oven.

The purpose of the surface functionalization is providing a good interface compatibilization between the PVA nanofibres and the Nafion® matrix via hydrogen bonding associated with the respective sulfonic acids. Additionally, the plausible acid-base reaction between the OH groups of PVA and the sulfonic acids of Nafion® can be minimised or eliminated, thus allowing them to participate in the proton conductivity (Fig. 16).

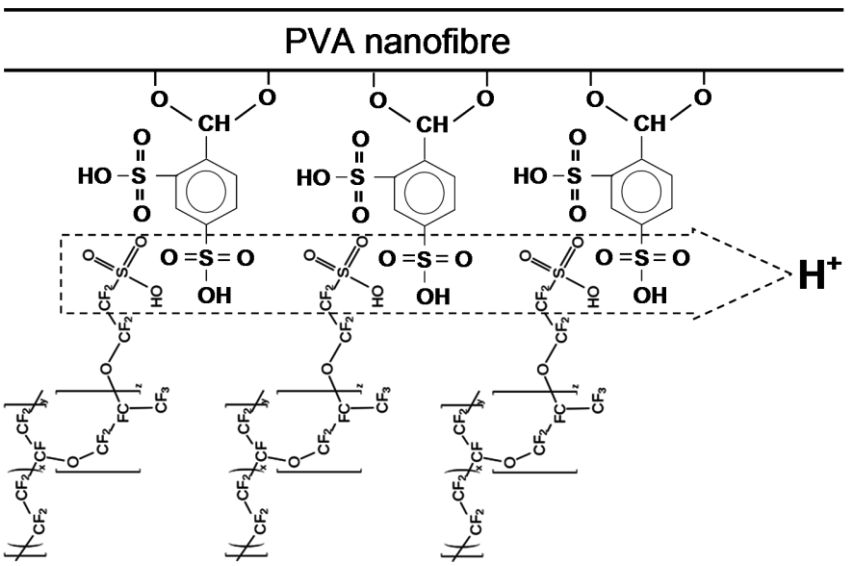

Fig. 16. Hydrogen bonding between the sulfonic acid groups of Nafion® and the surface functionalized PVA nanofibres for a better interface compatibilization and proton conduction.

(d) Chemical crosslinking of the PVA nanofibres:

The mats were placed for 24 h in a closed space at room temperature (Fig. 17). The bottom part of the container incorporated a 50 wt% solution of glutaraldehyde in water which was allowed to evaporate. Consequently, the glutaraldehyde vapour reacted and crosslinked the PVA chains favoured by the protonated sulfonic acid groups on the nanofibre surface.

Afterwards, the mats were heated at 100 ºC during 15 min with the aim to remove residual glutaraldehyde adsorbed on the nanofibres.

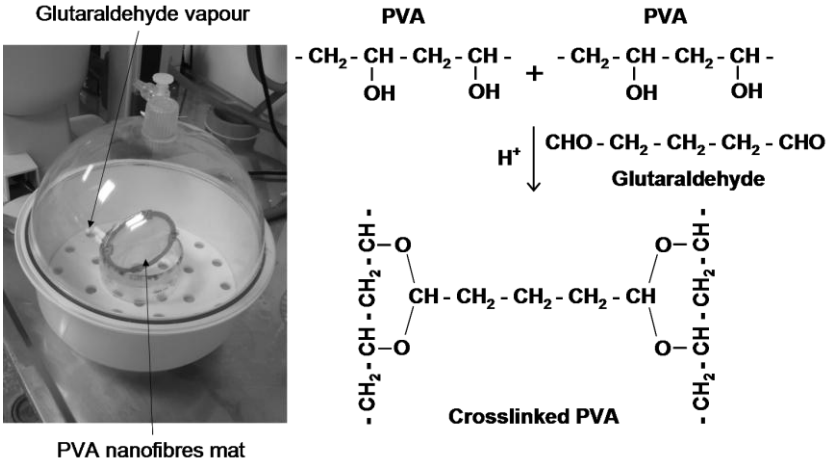

Fig. 17. The PVA nanofibres were chemically crosslinked with glutaraldehyde vapour inside a closed chamber (left). The corresponding reaction is also represented (right).

(e) Nafion® infiltration between the PVA nanofibres:

A commercial 20 wt% Nafion® dispersion was evaporated until a solid Nafion® material was collected. The Nafion® was then redissolved in a mixed solvent of isopropanol (80 wt%) and water (20 wt%). The final concentration of Nafion® was fixed at a 5 wt% value.

A customized container was filled with the prepared 5 wt% Nafion® solution for the infiltration of a Nafion® matrix between the PVA nanofibres (Fig. 18). The nanofibre mats were soaked within the Nafion® solution for 5 min, which was followed by an evaporation step in an oven at 100 ºC for other 5 min. This procedure was repeated 8 times rotating 90 degrees the mat in each time. At the end, a external layer of Nafion® became visible.

The composite membranes were cut in 5 x 5 cm^2 pieces and annealed at 125 ºC for 90 min under pressure (150 N cm^{-2}) by means of a hot-plate press.

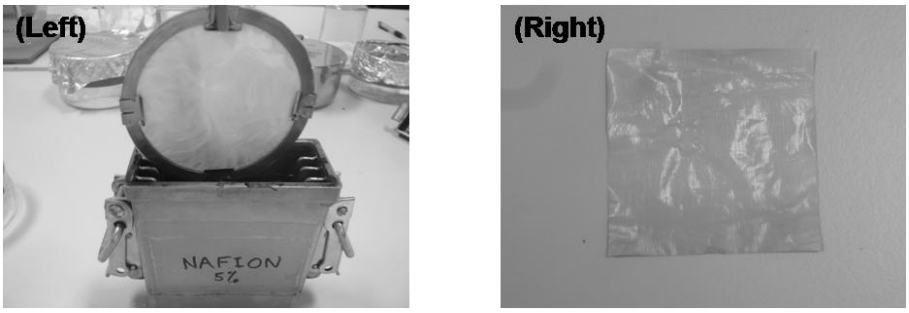

Fig. 18. (Left) The PVA nanofibres were soaked with a Nafion® solution for 5 min. This was repeated 8 times for the preparation of the nanocomposite membranes. (Right) A Nafion-PVA membrane after the conditioning process.

Finally, a conditioning process was executed which consisted in treating the nanocomposite membranes firstly with water at 85 ºC for 30 min, followed by immersion during 1 h in a 3 wt% hydrogen peroxide (H_2O_2) solution at 80 ºC, and lastly a protonation step for 1 h through ion-exchange with a 1 M HCl solution at 80 ºC.

The membranes were washed with hot water at 85 ºC, dried and stored for their later characterization (Fig. 18).

(f) Preparation of membrane electrode-assemblies (MEAs):

The Nafion/PVA membranes in an hydrated state were sandwiched between commercial anodes (Pt-Ru black) and cathodes (Pt/C) with 5 cm^2 active area and pressed at 135 ºC under a pressure of 300 N cm^{-2} for 3 min. Catalyst loading in both anode and cathode was 5 mg cm^{-2} with a 20 wt% Nafion® ionomer content.

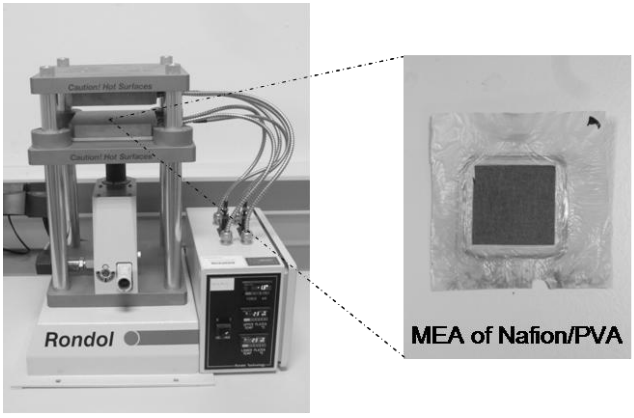

Fig. 19. Hot-plate press utilized for the preparation of the MEAs used in DMFC experiments.

2.2.2. SPEEK-PVA/SPEEK-PVB membranes

The SPEEK-based membranes comprised a SPEEK-PVA matrix embedding electrospun SPEEK-PVB nanofibres. These nanocomposite membranes were developed from the successive steps.

(a) Preparation of SPEEK-PVA and SPEEK-PVB solutions:

Solutions of SPEEK with PVA were prepared in water as a solvent. First, a SPEEK polymer with ion-exchange capacity (IEC) of 1.75 meq g^{-1} was dissolved in boiling water. Water was allowed to evaporate until a certain volume. Simultaneously, an aqueous 10 wt% PVA solution was prepared dissolving an appropriate amount of PVA in water at 80 ºC for 2 h. Then, both solutions were mixed and vigorously stirred in order to obtain a SPEEK-35%PVA composition (65 wt% SPEEK and 35 wt% PVA). Water was added to fix a 7.5 wt% SPEEK-PVA concentration. After complete homogenisation, the solution was poured into the container destined for the subsequent infiltration process.

On the other hand, solutions of 17.5 wt% SPEEK-30%PVB were prepared dissolving PVB in DMAc solvent at 80 ºC for 1 h. Afterwards, a corresponding amount of SPEEK with IEC of 2.05 meq g^{-1} was incorporated. The mixture was again stirred at 80 ºC during 1 h and the resulting polymer solution was stored and used for electrospinning.

The explanation for those selected polymer compositions is discussed in Paper 5.

(b) Production of electrospun SPEEK-PVB nanofibres:

Mats of SPEEK-30%PVB nanofibres were electrospun during 15 h with the equipment exhibited in Fig. 12. In this case, the polymer solution was fed with a flow rate of 0.2 ml h^{-1} while a potential difference of 35 kV was applied (needle at +10 kV and collector at -25 kV) with a needle-collector distance of 25 cm. Relative humidity was maintained below 40%.

The formed mats were collected and heated first at 160 ºC for 30 min and then crosslinked at 200 ºC during 1 h inside an oven. Round steel frames were laid on the mats before the crosslinking reaction. The purpose was to pull tight the nanofibres confined within the inner area of the frames because of their associated shrinking. At the end, the crosslinked mats were grasped between a pair of frames with the help of binder clips.

Fig. 20 shows a mat of electrospun SPEEK-30%PVB nanofibres before and after the crosslinking treatment. A baking paper was used as a support due to its high temperature resistance.

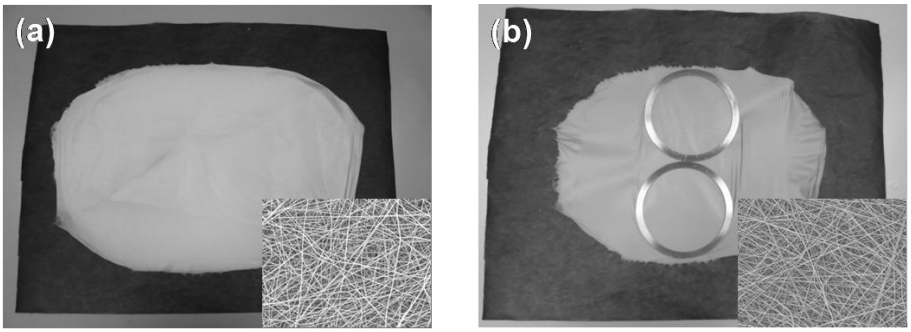

Fig. 20. Electrospun SPEEK-30%PVB nanofibre mats (a) before and (b) after crosslinking at 200 ºC. SEM views of the nanofibres are included which verify their thermal stability.

(c) SPEEK-35%PVA infiltration between the SPEEK-30%PVB nanofibres:

The procedure consisted in soaking the SPEEK-30%PVB nanofibre mats with the 7.5 wt% aqueous SPEEK-35%PVA solution for 5 min (Fig. 21). This was followed by a 5 min evaporation step inside a climate chamber at 90 ºC with a relative humidity below 10% (Fig. 22). This process was in total repeated 4 times and in between the mat was rotated 90 degrees. The last evaporation cycle was prolonged till 10 min. Afterwards, the nanocomposite membrane was collected and further dried at room temperature overnight.

Finally, square membranes (5 x 5 cm^2) were cut and crosslinked for 1 h from 110 ºC to 140 ºC (120 ºC was found to be optimal) at a pressure of 1 kN cm^{-2} between the hot plates of a press. The crosslinked nanocomposite membranes of SPEEK-PVA/SPEEK-PVB were then introduced in boiling water for 1 h and stored in water at room temperature.

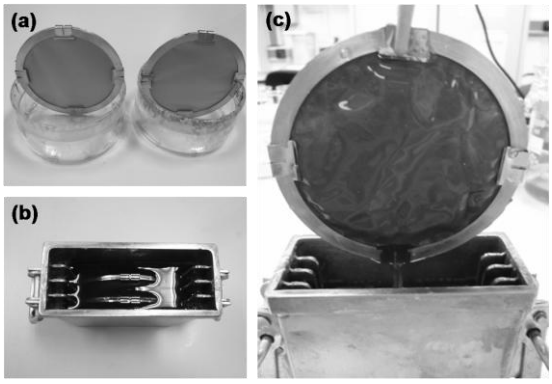

Fig. 21. (a) SPEEK-30%PVB nanofibre mats grasped between round steel frames, and (b)-(c) after immersion in a 7.5 wt% aqueous SPEEK-35%PVA solution.

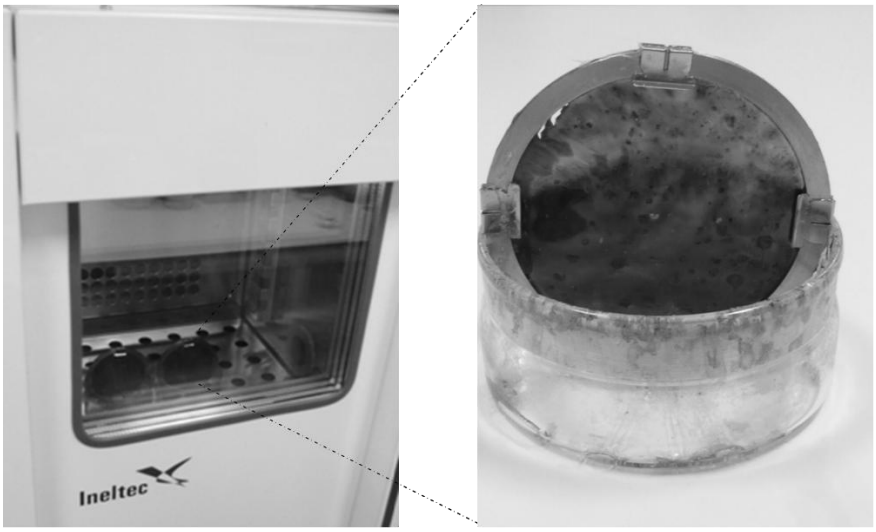

Fig. 22. Climate chamber for the evaporation of water from the SPEEK-35%PVA solution infiltrated between the SPEEK-30%PVB nanofibres thus resulting in the formation of the nanocomposite membranes.

(d) MEAs preparation:

Commercial electrodes of Pt-Ru black (anode) and Pt/C (cathode), both with a catalyst loading of 5 mg cm^{-2} and a 20 wt% Nafion® ionomer content, were sandwiched between the hydrated nanocomposite membranes.

The MEAs were formed by hot pressing at 110 ºC and a pressure of 300 N cm^{-2} for 3 min. They were stored in water until fuel cell experiments were performed. In Fig. 23 it is photographed a MEA of 5 cm^2 active area with a SPEEK-PVA/SPEEK-PVB membrane crosslinked at 120 ºC.

Fig. 23. Pictures of a prepared MEA containing a nanocomposite SPEEK-PVA/SPEEK-PVB membrane crosslinked at 120 ºC. On the left, the 5 cm^2 cell hardware used for DMFC experiments is also shown.

2.3. Characterization techniques

The experimental methods employed for the characterization of the membranes developed in this thesis are listed below. A detailed description of those techniques and their obtained results are found in the next pages from Paper 1 to Paper 6.

- Water uptake: It provides the relative amount of water taken by a polymer membrane due to its functional groups. Since water is usually required for achieving good proton conductivities, this parameter is very important to measure. Specially, a high proton conductivity with a low water uptake is desired, which is advantageous for a better mechanical stability and a reduced fuel crossover.

- Swelling degree: It is associated with the water uptake as a result of the volume occupied by the water within the polymer phase. Consequently, it informs about the dimensional changes of the membranes due to the water uptake.

- Ion-exchange capacity (IEC): It measures the relative amount of functional groups in a polymer electrolyte membrane, typically sulfonic acid groups for proton exchange membrane fuel cells. This parameter is directly related with proton conductivity, being water uptake and swelling degree also associated with it.

- Scanning electron microscopy (SEM): It allows image magnifications over a wide range, generally from 10 to 500,000 times, with high resolutions. It has been used to study the morphology and structure of the electrospun nanofibres and nanocomposite membranes.

- Differential scanning calorimetry (DSC): It monitors the flow of heat needed to maintain a sample at the same temperature than a reference. Physical transformations such us phase transitions can be elucidated, i.e. fusion, crystallization and glass transition events, as well as other exothermic or endothermic processes, e.g. vaporization of liquids and chemical reactions.

- Thermogravimetric analysis (TGA): This thermal analysis technique reports the changes of weight, generally losses, occurring in a sample as a function of temperature. Physical (vaporization, adsorption/desorption, sublimation, etc.) and chemical (decomposition, oxidation/reduction, condensation reaction, etc.) phenomena can be observed.

• Fourier transform infrared spectroscopy (FTIR): It is a very valuable technique to obtain information about the chemical structure of the materials. In polymers, FTIR can analyze the different functional groups present in a sample because of their characteristic bands, which are in turn a consequence of the chemical bonds and their vibration modes. FTIR has been helpful in this work to investigate the chemical stability of the polymers and their crosslinking reaction mechanisms.

• Dynamic mechanical thermal analysis (DMTA): It studies the viscoelastic behaviour of a polymer material as a function of temperature. Phase transitions and their associated mechanical properties can be evaluated. Remarkably, glass transition temperatures can be accurately located.

• Static tensile strength testing: It determines the main mechanical characteristics of a material, such us Young's modulus, yield strength, ultimate tensile strength and their associated elongations, by subjecting a sample to a controlled tension until failure. These tests have enabled to confirm the reinforcing effect of the nanofibres and the succesful preparation of nanocomposite membranes with no structural defects.

• Gas chromatography (GC): This type of chromatography method is very common for the separation and identification of compounds that can be vaporized without decomposition. The gaseous molecules are forced to pass along a column coated with a special material (stationary phase). Interaction with the walls causes the molecules to separate thus showing different retention times, which is the principal parameter used to identify the molecules. A detector at the end of the column can provide a signal (area under a peak) proportional to the compound concentration, and therefore, quantitative analysis can be performed. GC has been used to determine methanol concentrations and calculate the corresponding methanol permeability coefficients of membranes.

• Densimetry: It gives the value of density of a liquid. The working principle is based on the measurement of the natural vibration frequency of an oscillating U-shaped tube (Fig. 24). The natural frequency is a function of the mass of such a tube, which depends on the introduced liquid, and since the volume involved in the oscillation is constant and known, the density of the liquid inside the tube can be estimated. Importantly, a correlation between density and methanol concentration exists due to the different density values of water and methanol. It has been found very convenient for examining methanol permeabilities.

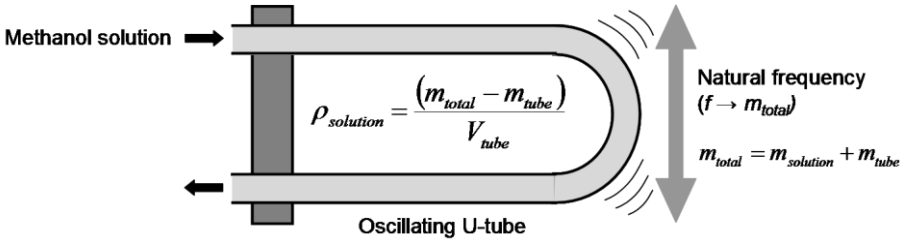

Fig. 24. Working principle of the densimetry technique, which was used for the determination of methanol concentrations and permeability coefficients. An U-shaped tube oscillates at a natural frequency which is function of its mass, and therefore, of the mass of liquid inside it.

• Potentiometry: This electrochemical method has been applied for the methanol permeability studies. The potential of a Pt-Ru electrode varies with methanol concentration, and this property was utilized for on-line monitoring the changes of methanol concentration derived from its permeation across a membrane.

• Electrochemical impedance spectroscopy (EIS): This is a versatile technique which measures the dielectric properties of a material as a function of the frequency of an electric field. In polymers, this external electric field interacts with the dipoles and ionic species of the chains. The opposition to the flow of such an alternating current is the impedance (Z), which consists of a real (Z') and an imaginary part (Z''). The Z' can be seen as the resistance whereas the Z'' is associated with occurring capacitive and inductive phenomena (reactance). The results are often expressed in terms of a Bode diagram (impedance and phase angle versus frequency) or a Nyquist plot ($-Z''$ versus Z'). The proton conductivities of the membranes prepared in this thesis have been given from the real impedance values when the phase angles approached zero, that is, the imaginary parts were minimum.

• Current-voltage characteristic: This relationship is known as *I-V* curve, in which the response of a material to an electric current is given plotting voltages versus their corresponding currents. For characterization of MEAs in fuel cells, data are generally represented as *i-V* curves, i.e. voltage outputs versus load current densities. Additionally, the result of multiplying each voltage by its current density provides curves of power density versus current density. All this information is very valuable to elucidate the performance of the membranes and electrodes under real fuel cell conditions at different operating conditions. The typical behaviour exhibitied by a MEA in a fuel cell is shown in the simulated

i-V curve of Fig. 25. Three regions can be distinguished according to their main associated losses. At low current densities, losses come from activation polarization (activation losses), which are assigned to the kinetics of the electrochemical reactions at the electrodes. In the medium region, ohmic losses due to the ionic resistance of the membrane are predominant. Finally, at high current densities, mass transport limitation phenomena (concentration polarization) can take place and cause important drops of performance. Another type of loss occurs as a consequence of fuel crossover from anode to cathode across the membrane. In this case, the open circuit voltage (OCV) diminishes in relation to the theoretical (thermodynamic) fuel cell potential due to deactivation of catalytic sites at the cathode and formation of a mixed potential, which are particularly problematic in DMFCs [48,49].

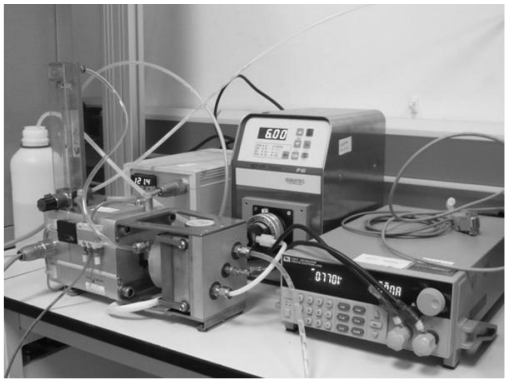

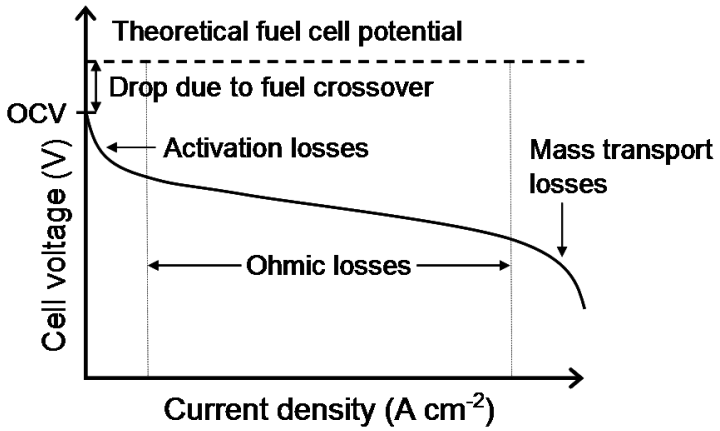

Fig. 25. Example of an *i-V* curve displaying the major types of losses encountered during fuel cell operation. The upper picture shows the setup utilized in this thesis for DMFC measurements with a single cell hardware.

Paper 1

Journal of Membrane Science 372 (2011) 191-200
(Adapted to thesis)

Polyvinyl alcohol nanofibre-reinforced Nafion® membranes for fuel cell applications

Sergio Mollá[a,b], Vicente Compañ[a,b]

[a] Dpto. Termodinámica Aplicada, ETSII, Universidad Politécnica de Valencia, 46022 Valencia, Spain.
[b] Instituto de Tecnología Energética (ITE), Universidad Politécnica de Valencia, 46022 Valencia, Spain.

Abstract

This work has been focused on the preparation and characterization of composite membranes with thickness between 19 μm and 97 μm and containing Nafion® infiltrated into a porous mat obtained by electrospinning of an aqueous solution of polyvinyl alcohol (PVA). The mat was composed of PVA nanofibres with diameters between 200 nm and 300 nm, which were functionalised on their external surface with sulfonic acid groups in order to cooperate in the proton conductivity of Nafion®. The proton conductivity of a composite membrane (47 μm thick) measured by impedance spectroscopy reached 0.022 S cm^{-1} at 70 ºC and fully hydrated. This value is lower than the conductivity measured in the same conditions for a pristine Nafion® cast membrane (46 μm), 0.032 S cm^{-1}. However, the performance of both membranes in Direct Methanol Fuel Cell tests was evaluated and showed comparable results. The proton conductivity of a series of cast Nafion® membranes with thickness similar to those of the composite membranes was found to behave linearly thickness-dependent, while Nafion/PVA composite membranes do not show such a linear behaviour due to their heterogeneous composition. Nevertheless, the composite membrane presenting a thickness of 47 μm records the maximum peak conductivities at the whole temperature range. An intrinsic value for the activation energy of our cast Nafion® membranes at fully hydrated conditions was estimated to be 7 kJ mol^{-1}.

Keywords: PEMFC, nanocomposite Nafion® membranes, PVA nanofibres, conductivity, DMFC performance.

1. Introduction

Though polymer electrolyte membrane fuel cells (PEMFC) are attractive, energy efficient and environmentally friendly power sources for many applications including transportation, distributed power and portable power systems, important scientific, technical and economical problems need to be solved before achieving mass commercialization of PEMFCs. Hydrated perfluorosulfonic acid membranes, such as Nafion®, are typically used as electrolyte in hydrogen powered fuel cells, because they combine good mechanical properties and thermal stability with relatively high protonic conductivity under high humidity conditions [1,2]. Direct Methanol Fuel Cells are promising candidates as power generators for portable devices. Easy refuelling and high energy storage capacity are their main advantages. However, it is known that application of Nafion® membranes to Direct Methanol Fuel Cells (DMFC) causes problems due to the fuel crossover and thus lowering DMFC performance [3,4], which entails the use of thicker membranes. In this context, the synthesis of efficient solid electrolytes separating the anode from the cathode together with the development of cheaper catalysts for fuel oxidation are the main issues facing the development of commercial low temperature fuel cells.

Great efforts are being made focused on the development of durable less expensive membranes, exhibiting performances equivalent or superior to those reported for membranes based on perfluorosulfonic acid polyelectrolytes [3-5]. Polyvinyl alcohol (PVA) has been proposed to be blended with Nafion® in order to diminish the methanol crossover in the membranes [6,7]. However, proton conductivity decreases as the PVA content in the composite increases.

Effective approaches seem to be the dispersion of hygroscopic metal oxide particles such as SiO_2, TiO_2, ZrO_2 and zirconium phosphate in acidic membranes. These fillers enhance both water retention and thermal stability, and contribute to lower methanol uptake and methanol permeability [8-16]. Another attractive strategy to improve the performance of PEMFCs and DMFC involves the preparation of hybrid cation-exchange membranes containing ionic functionalised inorganic fillers [17-23]. In principle, the fillers would have a dual function: enhancement of the water retention and increase of the ion-exchange capacity (IEC) of the membranes, two properties that increase the proton conductivity. In membranes with high IEC, segregation of nanosize hydrophilic domains from the hydrophobic ones to form percolation paths for proton transport may be relatively easy. It is suitable to think that ionic inorganic fillers trapped in hydrophobic domains separating hydrophilic domains might provide additional pathways for proton transport [24-27].

In earlier studies we have prepared and characterised hybrid membranes based on Nafion® and a sulfonated tri-block copolymer of polystyrene-block-poly(ethylene-ran-butylene)-block-polystyrene (sPSEBS). The hybrid membranes contained inorganic fillers such as silica, SBA-15 and sepiolite, all of them partially functionalised with phenyl sulfonic acid with the aim to increase the mechanical properties, conductivity at moderate and high temperatures and performance as PEM in fuel cell applications [22,23].

The purpose of this paper is to study novel nanocomposite membranes, Nafion/PVA, obtained by impregnation of nanofibres of polyvinyl alcohol (PVA) with a Nafion® solution. PVA is a polymer with a methanol permeability two orders of magnitude lower than Nafion®, and the nanofibres have been obtained by electrospinning of a water solution of the PVA polymer. The outer surface of such PVA nanofibres has been functionalised with sulfonic acid groups for a better interface compatibilization with Nafion® and in order to contribute to the proton conductivity, while the inner PVA phase performs as a barrier for the transport of methanol across the membrane.

In this work we have synthesized and characterised Nafion/PVA membranes with thickness ranging from 19 μm to 97 μm. The proton conductivities of membrane electrode assemblies (MEAs) prepared from (a) composite membranes of Nafion/PVA and (b) pristine Nafion® membranes with comparable thickness to those of Nafion/PVA, have been reported at different temperatures, i.e. 25 ºC, 45 ºC, 70 ºC and 95 ºC, and fully hydrated conditions. Differences observed between the membranes in function of their thickness are discussed.

Direct Methanol Fuel Cell tests at 70 ºC with a 2 M methanol solution have been also carried out for MEAs made up of pristine Nafion® and composite membranes with a thickness of 46 μm and 47 μm, respectively. The results obtained led to conclude that the composite membranes could have interesting transport properties as solid electrolytes for fuel cell applications.

2. Experimental Part

2.1. Materials

The Nafion® dispersion (DuPont Co.) was 20 wt% of 1 meq g^{-1} IEC Nafion® diluted in a mixed solvent of water, propanol, ethanol and unspecified ethers. The Nafion® was solvent exchanged by casting in order to obtain a 5 wt% solution in isopropanol and water (with isopropanol/water = 4/1, w/w). This

ratio has been previously reported to be suitable for Nafion® infiltration into porous membranes [28].

Polyvinyl alcohol, PVA Mowiol 28-99 grade, was kindly supplied by the company Kuraray Europe GmbH.

Isopropanol extra pure and cetyltrimethylammonium bromide (CTAB) were purchased from Acros Organics, and 4-formyl-1,3-benzenedisulfonic acid disodium salt from Sigma-Aldrich.

2.2. Preparation of membranes

2.2.1. Nafion® membranes

The solvent exchanged solution, with a 5 wt% Nafion® content in isopropanol and water, was used for the casting of pristine Nafion® membranes with thickness between 18 μm and 95 μm, i.e. 18, 28, 37, 46, 60 and 95 μm. The thickness was controlled in function of the volume of solution loaded in Petri glass dishes and afterwards evaporated in an oven at 60 ºC overnight.

The respective Nafion® membranes were annealed at 125 ºC for 90 min in the oven and then removed from the Petri dish by adding water.

The last step was the conditioning of the membranes by treatment with water at 85 ºC for 30 min, followed by wetting with a 3 wt% hydrogen peroxide solution during 1 h at 80 ºC and further protonation at the same temperature by ion-exchange with a 1 M chlorhydric acid solution for another 1 h. Finally, the cast Nafion® membranes were washed with hot water at 85 ºC, dried and stored.

2.2.2. PVA nanofibres

Porous PVA mats were produced by a standard electrospinning setup (Yflow S.L., Málaga, Spain) through the feeding of a water based solution of PVA (0.005:1:10 wt. CTAB:PVA:water). CTAB was used as surfactant in order to reduce surface tension of water and improve electrospinning ability.

The distance between the needle and the planar collector was fixed at 25 cm, the solution flow rate at 0.5 ml h^{-1}, the voltage of the needle at +11 kV and the voltage of the collector at -5 kV. Mats electrospinned during 8 h showed a thickness around 120 ± 10 μm, meanwhile those obtained after 4 h were approx. 60 ± 5 μm. The collected mats were heated during 3 h at 170 ºC in a vacuum atmosphere (250 mbar pressure) with the purpose of removing water and increasing manipulability.

2.2.3. Chemical functionalization of PVA nanofibres

The PVA mats were mounted on a round steel frame and then immersed into a bath with a 0.04 M concentration of the 4-formyl-1,3-benzenedisulfonic acid disodium salt and 0.1 M of chlorhydric acid as a catalyst for the schematic reaction (1), dissolved in a mixture composed of isopropanol/water (70/30 v/v):

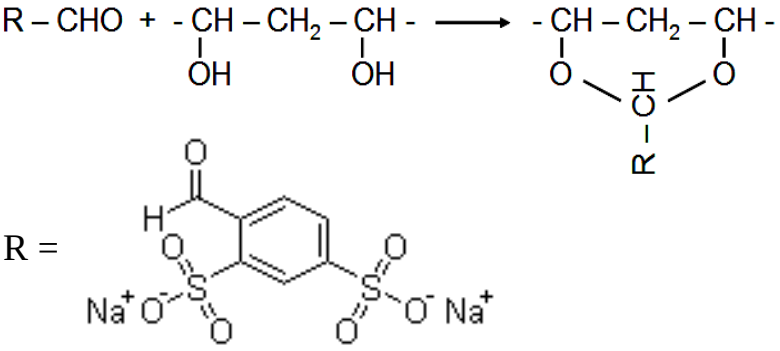

(1)

Reaction was carried out at 60 ºC for 2 h. The sodium ions present on the surface functionalised PVA nanofibres were exchanged with protons through immersion into a bath of isopropanol/water (70/30 v/v) containing chlorhydric acid with a 0.3 M concentration.

Ion-exchange was finished by washing of the mat with a solution of isopropanol/water (70/30 v/v) and further immersion in pure isopropanol. Finally, the mats were placed into an oven at 60 ºC for drying.

The last step was the crosslinking of the PVA chains in order to raise mechanical and thermal properties of the nanofibres. This was accomplished by reaction with glutaraldehyde vapor in a closed vessel during 24 h at room temperature. At the bottom of such vessel a 50 wt% water solution of glutaraldehyde was placed and let it to evaporate slowly.

After the crosslinking process, the mats were heated at 100 ºC for 15 min with the aim to remove adsorbed glutaraldehyde and water. The crosslinked mats strongly increased their chemical resistance and they were not able to dissolve in boiling water.

2.2.4. Nanofibre-reinforced Nafion® membranes

The functionalised and crosslinked mats, still mounted on the frame, were impregnated with the 5 wt% Nafion® solution in isopropanol and water (4/1 w/w, respectively).

Each impregnation step was carried out by wetting the PVA mat into the Nafion® dispersion for 5 min and followed by evaporation in an oven at 100 ºC for 5 min more. This was repeated 8 times in every mat so that an outer visible Nafion® layer was formed.

Such composite membranes obtained by infiltration of Nafion® into the PVA nanofibres were annealed at 125 ºC for 90 min under pressure in order to remove any residual solvent and enhance Nafion® can accommodate into the fibrillous structure.

Finally, the membranes were conditioned by treatment with water at 85 ºC for 30 min, followed by an oxidation with 3 wt% hydrogen peroxide during 1 h at 80 ºC and further protonation by 1 h ion-exchange with a 1 M chlorhydric acid solution at 80 ºC. Then, the composite membranes were washed with hot water at 85 ºC, dried and stored.

The thickness of the composite membranes (L) was dependent on the deposition time of the electrospun nanofibres mats, and it was measured with a digital length gauge (Heidenhain, model MT 12). The membrane thickness was calculated from the average value after ten measurements on different parts of the sample. The pertinent results are given in Table 1.

2.3. Characterizations of membranes

2.3.1. Water uptake and ionic exchange capacity

Weighed dry membranes (m_{dry}) were immersed in distilled deionized water overnight. The membranes were removed from water, gently blotted between filter paper to eliminate surface water and weighed (m_{wet}). This operation was repeated three times. Water uptake is calculated by means of the expression (2), in which m_{wet} is used as reference due to the fact that fully hydrated conditions for the membrane is the natural state into a DMFC application,

$$Water\ uptake\,(\%) = \frac{m_{wet} - m_{dry}}{m_{wet}} 100 \qquad (2)$$

The ion-exchange capacity (IEC) was obtained by immersing the membranes in the acid form in 2 M NaCl solution. The protons liberated in the exchange reaction $R–H + Na^+ \rightarrow R–Na + H^+$ were titrated with a 0.01 M NaOH solution. The IEC was obtained as

$$IEC\ (eq\ kg^{-1}) = \frac{0.01 \cdot V_{NaOH}}{m_{dry}} \qquad (3)$$

where *V* and *m* are, respectively, the volume in litres of NaOH solution spent in the titration of the protons released by *m* kilograms of dry membrane. IEC is usually given in eq kg^{-1} (meq g^{-1}) of dry membrane. In this case, Eq. (3) uses m_{dry} as reference since IEC is a property related to the chemical structure of the polymer.

2.3.2. Scanning electron microscopy (SEM) study

The morphology of the surfaces of PVA nanofibres and composite membranes, as well as their cross-sections, was investigated using a scanning electron microscope (SEM-model JSM-5410, Jeol Co., Japan). The samples were coated with gold under vacuum before SEM observations were carried out.

2.3.3. DSC analysis

Thermal analysis was carried out by differential scanning calorimetry using a DSC Q10 of TA Instruments. The heating rate was fixed at 10 ºC min^{-1} and two runs from -50 ºC to 250 ºC were performed for each sample. The experiments were performed under nitrogen atmosphere using a flux of 50 ml min^{-1}.

2.3.4. Thermogravimetric analysis (TGA) study

The thermal stability of the membranes was determined by thermogravimetric analysis using a TA Instruments TGA (model 2950) with a heating rate of 5 ºC min^{-1} from 25 ºC until 500 ºC. The experiments were carried out under nitrogen atmosphere using a flux of 60 ml min^{-1}. The samples weights for analysis were around 12-15 mg.

2.3.5. MEA preparation

Pristine Nafion® and composite membranes based on Nafion® and PVA were used for the preparation of MEAs in order to study the proton conductivity in a single cell at real fuel cell operation conditions. The anode and cathode used for MEA preparation were acquired from BalticFuelCells GmbH (Schwerin, Germany). The anode was composed of a carbon paper gas diffusion layer (GDL) from Freudenberg&Co. (Weinheim, Germany), model H2315 T105A, covered by an alloy of Pt-Ru black 50:50 (Alfa Aesar) with a catalyst loading of 5.0 mg cm^{-2} together with a 20 wt% of dry Nafion® ionomer. Similarly, the cathode was composed of a GDL from Freudenberg, model H2315 I3C4, with a catalyst loading of 5.0 mg cm^{-2} of Pt, containing

platinum nanoparticles (≈ 5 nm size) supported by advanced carbon (HiSPEC 13100, Alfa Aesar) with a Pt/C ratio of 70% (weight) and a 20 wt% of dry Nafion® ionomer.

2.3.6. Conductivity measurements

In situ conductivity experiments were carried out directly in membrane electrode assemblies (MEAs) built as described before. The conductivity was measured at 25 ºC, 45 ºC, 70 ºC and 95 ºC by impedance spectroscopy (Electrochemical workstation IM6, ZAHNER-Elektrik GmbH) in the frequency range between 100 mHz and 10 kHz, using voltage amplitudes of 50 mV. This AC potential showed a low noise in comparison to the measurement signal for a better accuracy.

The MEAs, previously equilibrated with water, were placed into a square 5 cm^2 active area fuel cell hardware (quickCONNECT, BalticFuelCells GmbH) containing graphite serpentine flow fields and equipped with a pressure-controlled clamping force system. This latter characteristic enables to exert a constant contact resistance between membrane and electrodes.

The anode side of the cell was flooded with deionized water to prevent dryness of the membrane, and thus, fully hydrated conditions were assured in the measurements. No gases were flowing across anode and cathode during the experiments.

The protonic resistance R was taken from the Bode plot as the value of the modulus of the complex impedance at which the phase angle reaches a maximum, practically zero, in the high frequency region, $|Z| \rightarrow R$. However, this resistance represents the total resistance of the real system, which is composed by the membrane and the boundary layers, and therefore, it has to be defined as an apparent value, R_{app}.

The apparent conductivity of the membranes, which represent the average value measured for the total system, was calculated from the apparent proton resistance R_{app} by means of the following expression,

$$\sigma_{app} = \frac{L}{R_{app} \cdot S} \qquad (4)$$

where L is the thickness of the membrane (cm) and S = 5 cm^2, the electrode area in contact with the membrane.

2.3.7. DMFC performance of Nafion® and composite Nafion/PVA membranes

MEAs prepared with a 46-μm Nafion® membrane and a 47-μm composite Nafion/PVA membrane were tested in the single cell hardware described previously. A 2 M concentration methanol solution in water pumped at a flow rate of 5 ml min^{-1} was used to feed the anode. The cathode was directly fed with oxygen gas at a flow rate of 150 ml min^{-1} and atmospheric pressure.

Polarization curves of *i-V* (current density versus potential) were obtained at 70 ºC from OCV (open circuit voltage) conditions up to 0.2 V by manual stepwise increment of the current density and waiting for 1 min in each measurement in order to assure the reading of a voltage near a steady-state value. Power density values were then calculated and represented.

Before *i-V* measurements, the MEAs were activated for 5-6 h by alternating different current demands until a stable operation was achieved. This is helpful for increasing the activity of the catalytic sites and enhancing the performance of the electrodes.

3. Results and discussion

3.1. Water uptake and ionic exchange capacity

In general, the conductivity of acidic membranes involves dissociation of protons from $–SO_3H$ groups and their transport across water and fixed $–SO_3^-$ ionic groups. Then, the conductivity depends on the water uptake and the

Table 1. Thickness, water uptake, ionic exchange capacity and nanofibre deposition time for composite Nafion/PVA. Nafion® is included for comparison.

Membrane	Thickness (μm)	Water uptake (%)	IEC (eq kg^{-1})	Deposition time (h)
Nafion/PVA	19 ± 1	26.4 ± 0.1	0.47	3
Nafion/PVA	26 ± 2	19.3 ± 0.1	0.33	6
Nafion/PVA	39 ± 3	27.9 ± 0.1	0.45	9.5
Nafion/PVA	47 ± 3	25.8 ± 0.1	0.58	13.5
Nafion/PVA	61 ± 3	22.9 ± 0.1	0.57	16
Nafion/PVA	97 ± 5	35.8 ± 0.1	0.55	[2 x 13.5][a]
Nafion® (casting)	[18-95] ± 1-2	27.0 ± 0.1	0.93	-
Nafion 117 (commercial)	216 ± 4	21.5 ± 0.1	0.91	-

[a] Membrane prepared by assembly under hot pressure welding of two membrane pieces derived from mats deposited 13.5 h.

ion-exchange capacity (IEC) of the membranes. Values of the water uptake and the ionic exchange capacity (IEC) obtained for all the studied membranes are given in third and fourth columns of Table 1.

Water uptake of both Nafion® and composite Nafion/PVA membranes exhibits alike values. However, the IEC values of the Nafion/PVA membranes are nearly the half of the ones corresponding to Nafion® materials, presumably as a consequence of the fact that the amount of Nafion® polymer hold by the composite membrane is limited by the presence of the PVA nanofibre phase.

PVA is a very hydrophilic polymer and can hold water in its structure. This is the reason for the water uptake behaviour found in the Nafion/PVA membranes. Thus, water is both attached to the sulfonic acid groups of Nafion® and incorporated into the PVA structure.

3.2. SEM results

The technology of electrospinning has allowed the obtaining of mats made up of PVA nanofibres with diameters ranged between 200 nm and 300 nm. It has been possible to reach these diameters by means of the optimization of different parameters of the electrospinning equipment such as the concentration of the PVA solution (1:8 w/w PVA:water), the distance needle-collector (25 cm) and the applied potential (V_+ = 11 kV, V_- = 5 kV). In Fig. 1 we show the SEM micrographs of the nanofibres, the transversal cut and the surface of a Nafion/PVA membrane, respectively.

The micrograph of Fig. 1a shows that the nanofibres adapt a totally cylindrical morphology in which the fibres appear as welded between them, with a negligible amount of beads and possessing a great open porosity along the mat surface. In Fig. 1b is shown a micrograph of the same nanofibres given in Fig. 1a but after the first impregnation with the Nafion® dispersion. This tends to increase the grade of compactness and the size of the nanofibres with a progressive reduction of the porosity.

In Figs. 1c and 1d we observe the images of the transversal section and surface of a composite membrane Nafion/PVA with a thickness around 20 μm. From Fig. 1c we can distinguish that the nanofibres are totally immersed into a Nafion® phase and a pure Nafion® layer exists on each external surface of the membrane. Thus, the Nafion® polymer is shaping a continuous phase between both faces of the composite membrane, which is necessary for the transport of protons from the anode to the cathode. It is worth mentioning that the voids observed in the SEM picture (Fig. 1c) are due to the nanofibres tore apart during the cutting of the membrane for the observation of the transversal section, so it is not porosity left during the membrane preparation.

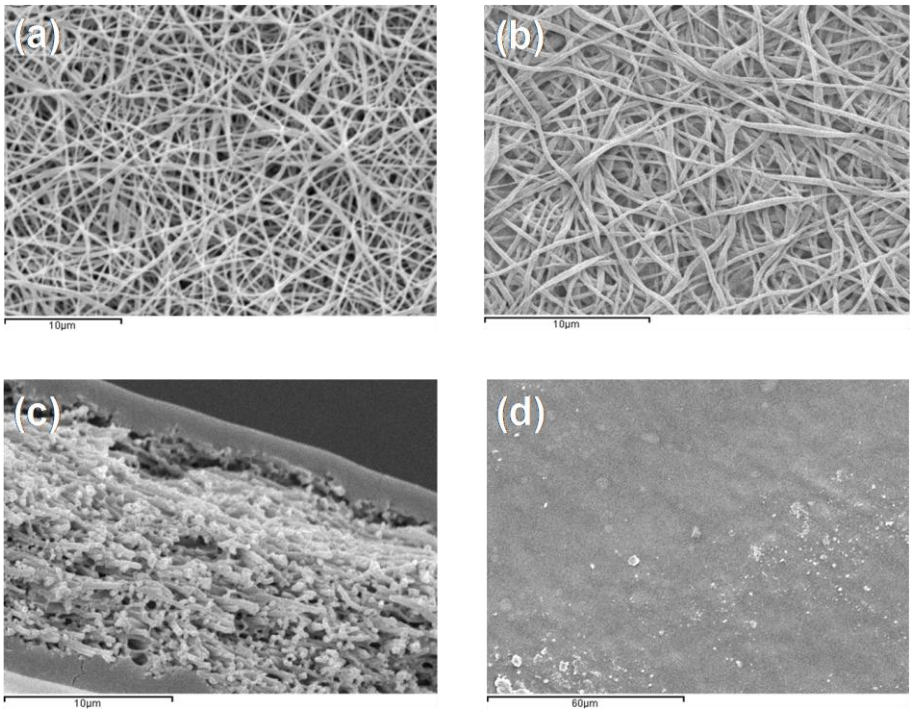

Fig. 1. SEM image of a composite Nafion/PVA membrane. (a) Mat of nanofibres functionalised and crosslinked. (b) Mat of nanofibres after its first impregnation within the Nafion® dispersion. (c) Transversal section of a composite membrane Nafion/PVA. (d) The surface image of the composite membrane.

Finally, in Fig. 1d we show a surface image of the composite membrane where it can be appreciated that the membrane is totally compact, that is, no porosity can be observed, what confirms that the Nafion® dispersion prepared in isopropanol/water 4:1 is a suitable mixture for the penetration of the polymer into the mat. Other formulations of Nafion® dispersion, for example as received from commercial supplier, were not found to be appropriate and surfaces with micropores resulted when used for impregnation of a porous PTFE membrane, due to the larger aggregated Nafion® particles in comparison to the smallest sizes formed in the isopropanol/water mixture solvent [28].

Thus, the SEM images permit us to corroborate that the morphology of the Nafion/PVA membranes resembles a sandwich, in which the external surfaces are composed of Nafion® and the inner layer is made up of PVA nanofibres perfectly surrounded by Nafion® polymer.

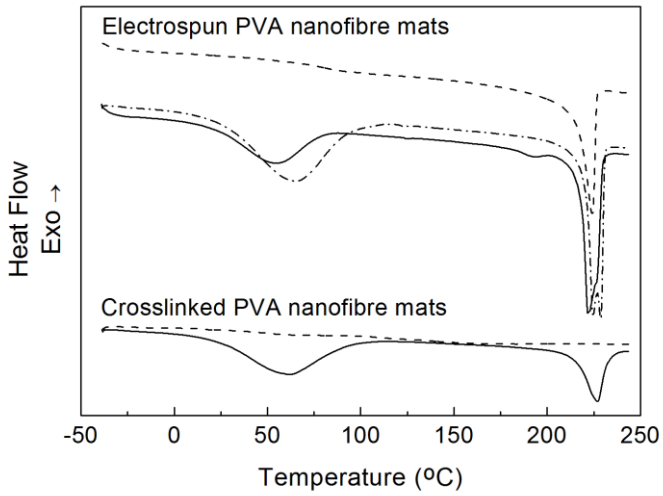

Fig. 2. DSC curves for PVA nanofibres without heat treatment (dash dot-style), after heat treatment at vacuum (solid-style) and their second run (dash-style). First run of chemically crosslinked PVA nanofibres is given by a solid line and their second run by a dashed line.

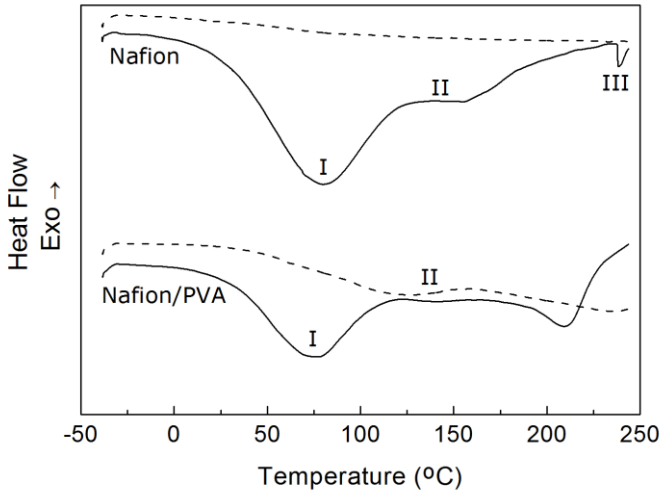

Fig. 3. DSC curves for Nafion® membrane (solid line) and its second run (dashed line), and for a composite membrane of Nafion/PVA (solid line) and its second run (dashed line).

3.3. DSC results

In Fig. 2 are shown the DSC measurements of a PVA nanofibre mat after the different steps, while in Fig. 3 are represented the DSC curves of both Nafion® and Nafion/PVA membranes. The peaks ranging from 200 ºC to

230 ºC correspond to the melting of the crystalline phase of PVA, which occurs with an enthalpy of 138.6 J g^{-1} (for a 100% crystalline material) [29]. From the DSC curves of Fig. 2 we have determined that the degree of crystallinity of the electrospun PVA nanofibres is approximately 57%. After heat treatment of the mats under vacuum, water is removed from the PVA phase as the peak under 100 ºC narrows, while crystallinity is kept constant.

On the other hand, the second run applied to the PVA nanofibres sample treated thermally reveals the total absence of water in its structure, and this suggests a change in the baseline of the curve at a temperature around 85 ºC, which is a typical value found for the glass transition temperature of PVA [30]. Similarly, it has been measured its enthalpy of fusion and was found a degree of crystallinity around 40%. Its lower value when compared with the initial 57% shows that during the electrospinning process, the fibres undergo a tensile strength/elongation inducing a preferred orientation of the chains and this favours crystallization.

Fig. 2 also shows the DSC curve of PVA nanofibres after being subjected to crosslinking reaction with glutaraldehyde vapor. It can be seen again a broad peak in the range of 25-100 ºC due to the presence of water retained in the amorphous phase. A close inspection of Fig. 2 reveals that the degree of crystallinity of PVA decreases sharply to almost 30%. Addition of glutaraldehyde to form covalent bridges between the PVA chains might act as a separator and therefore causes a reduction in the crystallinity.

DSC curves in the range -50 ºC to 250 ºC are presented in Fig. 3 showing the thermal stability of the Nafion® membranes obtained in this study by casting and the Nafion/PVA composite membranes. Continuous and dashed lines correspond to the first and second runs. The region I is related to phase transitions in clusters/ion channels as a result of water present. The region II is related to the melting of micro-regions in the hydrophobic part of the polymer. Finally, region III corresponds to the rupture of ionic clusters. Once this has happened is no longer possible to recover the polymer morphology, as suggested by the DSC curve obtained after the second run, which adopts a flat shape.

The study of the DSC curve of a membrane composed of Nafion/PVA shows the same appearance as that of Nafion®, with the exception that integrates a melting peak of the crystal phase present in the PVA nanofibres. It is not possible to observe the peak assigned to the region III cited above. Perhaps the hydrophilic character of PVA helps to stabilize the ionic clusters. The second run applied to the sample of Nafion/PVA reveals a small peak which might be associated with the region II. It is inferred that the intimate contact between the PVA nanofibres and Nafion® promotes a noticeable phase separation between the hydrophobic Nafion® backbone and the hydrophilic PVA.

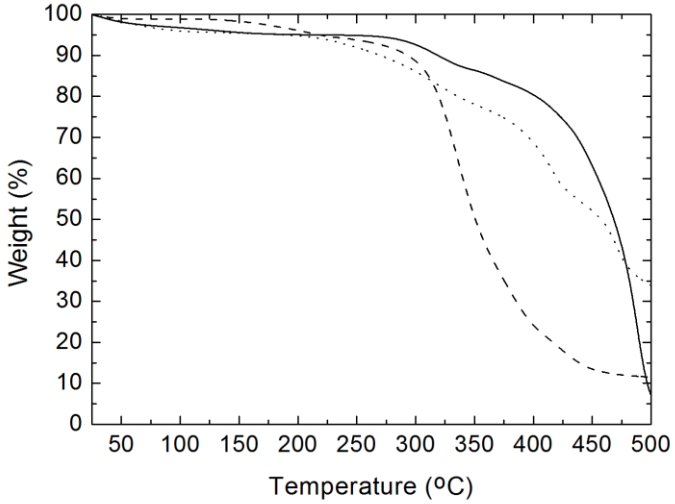

Fig. 4. Thermo-gravimetric analysis (TGA) of a Nafion® membrane (solid line), PVA nanofibres (dashed line) and a composite Nafion/PVA membrane (dotted line).

3.4. TGA analysis

A curve showing the thermal degradation of a composite membrane by means of the weight loss profile is presented as a function of temperature in Fig. 4. For comparative purposes, the curve describing the thermal stability of a pristine Nafion® membrane and a PVA nanofibre mat are also shown.

The loss of mass observed for the Nafion® and Nafion/PVA membranes up to 150 ºC in Fig. 4 corresponds to traces of water, whereas the mass loss in the 275-400 ºC temperature range is caused by degradation of sulfonic groups due to decomposition of Nafion® side chains $–OCF_2CF_2–SO_3H$. The rather sharp weight loss taking place in the range 400-500 ºC proceeds from degradation of the polymer backbone, i.e., decomposition of $CF_2–CF_2$ main chains of Nafion® [31,32].

It is worth noting that the degradation curves show that the Nafion® membrane is more stable than the composite one below 475 ºC. The organic nature of the nanofibre filler within the Nafion/PVA membrane is responsible of the larger weight losses at temperatures above 230 ºC, as polyvinyl alcohol starts to dehydrate and decompose [33]. However, the residual mass of the composite membrane at 500 ºC is much larger than the obtained for pristine Nafion® and pure PVA, thus indicating that total PVA decomposition might be inhibited by the Nafion® phase and even the Nafion® backbone might also be more protected by the introduction of the nanofibres.

The good thermal stability of Nafion/PVA up to 200 ºC suggests that no degradation of the composite membrane is expected during a broad range of fuel cell operating temperatures, i.e. between 50 ºC and 140 ºC.

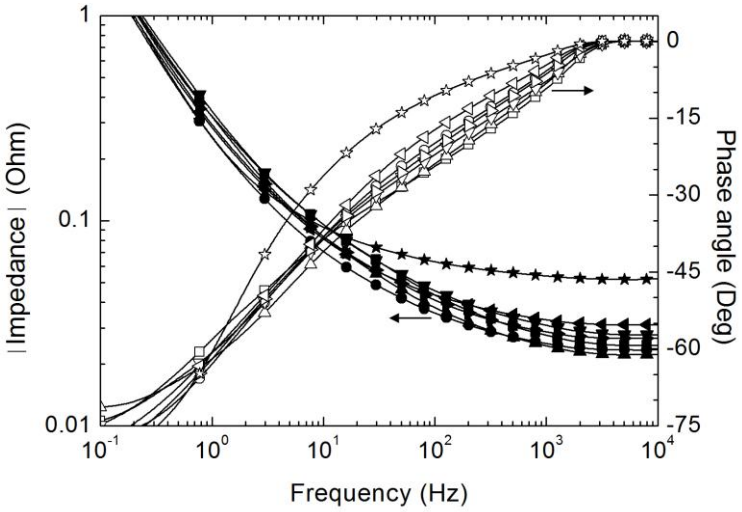

Fig. 5. Bode diagram at 70ºC for fully hydrated Nafion® membranes with different thickness: (■) 18 μm, (▲) 28 μm, (●) 37 μm, (▼) 46 μm, (►) 60 μm, (◄) 95 μm, and (□) 216 μm for commercial N117.

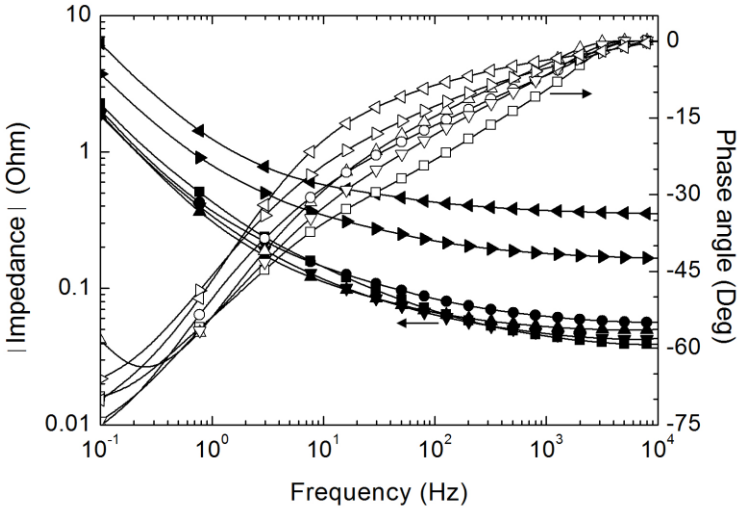

Fig. 6. Bode diagram at 70ºC for fully hydrated Nafion/PVA membranes with different thickness: (■) 19 μm, (▲) 26 μm, (●) 39 μm, (▼) 47 μm, (►) 61 μm, and (◄) 97 μm.

3.5. Conductivity results of MEAs

The conductivity of the membranes was obtained from impedance measurements from the Bode diagram plotted in Figs. 5 and 6, for Nafion® and composite Nafion/PVA membranes, respectively. Notice that in the

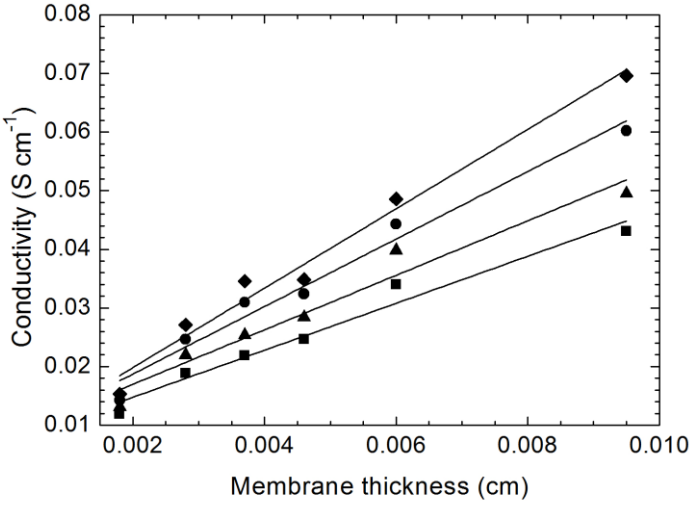

Fig. 7. Proton conductivity of cast Nafion® membranes as a function of temperature and thickness: (■) 25ºC, (▲) 45ºC, (●) 70ºC, and (♦) 95ºC.

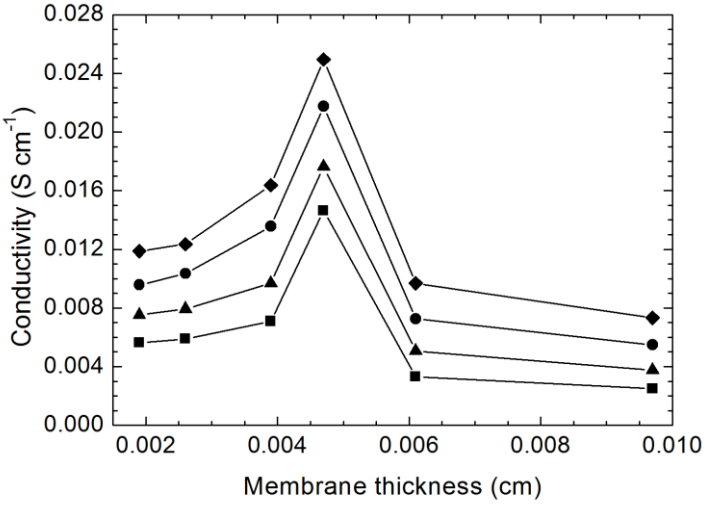

Fig. 8. Proton conductivity of NAFION/PVA membranes as a function of temperature and thickness: (■) 25ºC, (▲) 45ºC, (●) 70ºC, and (♦) 95ºC.

region of high frequency the value of $|Z|$ tends to a constant value when the phase angle reaches zero. This constant value correspond to the apparent resistance of the MEA and the apparent conductivity can be obtained taking into account the thickness of the membrane, L, given in Table 1, and the area of the electrodes, $S = 5\ cm^2$, through the Eq. (4). In Figs. 7 and 8 we resume the values of the apparent conductivity for the different membranes at each temperature. It can be seen that the conductivities of the Nafion/PVA composite membranes are below those of the pristine Nafion® membranes, which is related with the lower ion-exchange capacity found in the former membrane.

From Fig. 7 it is observed, as opposed to what would be expected, the existence of a linear correlation between the apparent conductivity and thickness for the Nafion® membranes. This makes evident that the proton conductivity measured for each membrane is just an apparent value and not an intrinsic one. From our point of view, this should be related to the presence of two different conductive phases, i.e., the Nafion® bulk content under full hydrated conditions and a skin layer comprising the boundary effect between membrane and electrode and a superficial low conductive Nafion® phase. Thus, in order to measure the true conductivity of a membrane, skin layer effects should be eliminated from the experimental results. A similar behaviour has been pointed out before by Tsampas *et al.* [34] and Slade *et al.* [35], who explained it as the consequence of a surface skin layer with a low proton conductivity behaviour, whereas the inner Nafion® phase, whose amount depends on membrane thickness, should present a higher intrinsic conductivity value.

The work of Slade *et al.* is based on extruded Nafion® membranes. They performed *ex situ* conductivity experiments in a four electrode glass cell filled with an aqueous 1 M H_2SO_4 solution, and *in situ* conductivity measurements in a PEM fuel cell hardware using MEAs previously conditioned at 538 mA cm^{-2} until a steady-state operation. The membrane resistance in each MEA was obtained using the current-interrupt technique, which does not include the bulk electrode resistances, and the electronic resistances of the gas distribution plates and the gas diffusion layers were also subtracted from the measurements. In both cases, the results clearly demonstrate a decrease in the membrane conductivity as the membrane thickness is reduced [35]. While electrode-membrane contact resistance could account for part of the behaviour found during the *in situ* experiments, this combined with the *ex situ* measurements points to an effect of membrane structure. They report that the most likely explanation for the unexpected decrease in conductivity for thin membranes must be related to their production method, that is, by the extrusion process, since the temperatures and pressures must have a pronounced effect on the surface

Table 2. Values of the parameters of the intrinsic conductivity (thickness-dependent), conductivity of the boundary layer and true activation energy for the pristine Nafion® membranes at different temperatures.

Temperature (ºC)	σ_s^0 (S cm^{-2})	$\sigma_{B.L}$ (S cm^{-1})	E_a^{true} (kJ mol^{-1})
25	4.0051	0.0068	7.0
45	4.6438	0.0077	
70	5.7540	0.0072	
95	6.7687	0.0063	

structure of the material. Thinner membranes may have been produced with a higher roller pressure, resulting in increased local temperature and the melt flow of surface layers, and in some closing of ion and water channels, reduction in their size or an increase in their tortuosity.

However, the membranes prepared in our work have been obtained by casting inside an oven where homogeneous temperatures are applied and no external pressures are exerted. Thus, it cannot be assumed that the production process is responsible for the observed phenomenon. A more plausible explanation would describe it as a consequence of the fact that membranes should intrinsically contain surface layers whose structure and hydrophobic/hydrophilic properties change from those found in the bulk material as a consequence of a different segregation of phases between outer and inner parts of the membrane.

Discontinuities in structure between the surface and the bulk have been measured in Nafion® membranes by means of neutron reflectometry [36]. When a glassy carbon layer was deposited on the surface of a Nafion® membrane, imitating a MEA, it was found that Nafion® adopted an outer less hydrophilic region followed by a middle hydrophobic region and an inner more hydrophilic area.

A model of equation suitable to describe the observed apparent conductivity phenomenon for a membrane with a thickness *L* (cm) is showed through the Eq. (5):

$$\sigma_{App}(L,T) = \sigma_s^0(T) \cdot L + \sigma_{BL} \qquad (5)$$

where $\sigma_s^0(T)$ represents the intrinsic or true conductivity of the bulk membrane and σ_{BL} is the conductivity associated to the skin layer effect [34].

Table 2 gives the $\sigma_s^0(T)$ and σ_{BL} values at each studied temperature. It is remarkable to mention that $\sigma_s^0(T)$ is a temperature-dependent parameter, obtained from the slope of the lines in Fig. 7, whereas σ_{BL} tends to be fixed at a common point (ordinate at the origin), showing an average value of $(7 \pm 0.7) \cdot 10^{-3}$ S cm^{-1}.

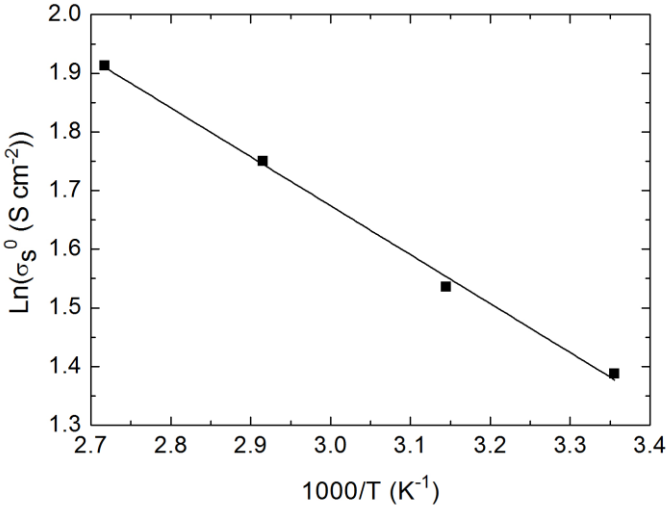

Fig. 9. Arrhenius plot of the intrinsic conductivity parameters $\sigma_s^0(T)$ obtained from the representation of conductivity of the Nafion® films versus thickness at several temperatures.

Fig. 9 represents $\sigma_s^0(T)$ in an Arrhenius-type plot. The corresponding slope provides the true activation energy, E_a^{true}, for the conductivity process of the bulk material of Nafion® pristine membranes at fully hydrated conditions, which is found to be 7 kJ mol^{-1}. This value is about 20% minor than 9.34 kJ mol^{-1} and 9.82 kJ mol^{-1} found for pure Nafion® and composite Nafion/zirconium phosphate, respectively [37].

Nafion/PVA membranes do not show such a linear behaviour due to their heterogeneous composition. Nevertheless, the composite membrane presenting a thickness of 47 μm records the maximum peak conductivities at the whole temperature range. The explanation for this peak conductivity has to be referred to the preparation method, and consequently, it is not expected in all cases to be fully reproducible at such a thickness value since some factors are difficult to control and polymer electrospinning involves a random process itself, although the observed trend should remain as explained next. Thicker membranes are prepared from thicker PVA nanofibre mats, and therefore, the Nafion® dispersion requires diffusing longer lengths into the mats, which at the same time become more compact after each infiltration step. It is suggested that the central inner layer of the membrane might not be sufficiently covered by the Nafion® polymer and proton conduction between both faces of the membrane should become more restricted. As a consequence of this, the IEC values measured for the membranes above 50 μm are almost similar to the value obtained for the 47-μm composite membrane (Table 1) whereas their conductivities are much lower.

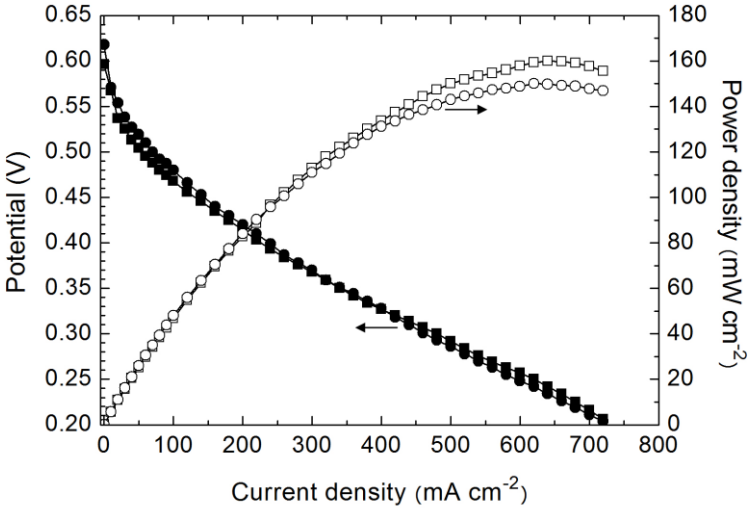

Fig. 10. Polarization curves (*i*-*V*) of DMFC experiments performed at 70 ºC with a 2 M methanol solution for (■) a pristine Nafion® membrane of 46 µm thick, and (●) a composite NAFION/PVA membrane with a thickness of 47 µm.

On the other hand, thinner membranes come from thinner PVA mats, and therefore, less free volume (space between nanofibres) is present and a reduced amount of Nafion® can be infiltrated and hold by the mat. This can be confirmed by the lower values of IEC found in the membranes with thickness below 47 µm. In addition, lower conductivities would be also expected in the thinnest membranes due to the mentioned skin effects.

The 47-µm composite membrane is placed within a range in which both consequences are minimized and it is reached an optimum condition for the Nafion® phase, and thus, for the proton conductivity.

3.6. DMFC performance of MEAs

Fig. 10 shows the polarization curves for comparison between the MEAs prepared with a pristine Nafion® membrane of 46 µm of thickness and a composite Nafion/PVA membrane of 47 µm, when the DMFC is operating at 70 ºC with a methanol feed concentration of 2 M.

The open circuit voltage (OCV) of the cell usually does not reach the theoretical value of the overall reversible cathode and anode potential at the given temperature and pressure. The reduction of the OCV from the theoretical voltage has been attributed to the penetration of the fuel across the membrane, and thus, these values are an indicator of the degree of methanol crossover by diffusion and the catalyst efficiency [38,39]. The OCV value of the composite membrane, 0.618 V, is higher than the OCV for

the Nafion®, 0.596 V. Therefore, the PVA nanofibres perform as effective methanol barriers for methanol diffusion.

Although proton conductivity of the composite membrane at these conditions, 0.022 S cm^{-1}, is around 31% lower than the one measured for the pristine Nafion®, 0.032 S cm^{-1}, the resistance found in the ohmic region of the *i-V* curve (linear behaviour after i > 300 mA cm^{-2}) is 0.078 Ω for the Nafion/PVA membrane and 0.074 Ω for the Nafion®, just a 5.4% difference. The reason for this much shorter difference in the ohmic resistance exhibited by the MEAs under real DMFC operation can be explained again by the fact that the composite Nafion/PVA membrane accomplishes a lower methanol crossover, and thus, cathode losses caused by the methanol can be kept reduced in the case of the composite membrane. For the Nafion® membrane, the higher proton conductivity is almost counteracted by the also larger methanol crossover.

The maximum power density for the MEA with Nafion®, 160 mW cm^{-2}, is just slightly above the peak power density showed by the MEA with Nafion/PVA membrane, 150 mW cm^{-2}. However, in terms of the Nafion® content, which is related to the IEC value, it is remarkable to mention the lower amount needed to constitute the composite membrane, and therefore, the material and economic yield of the Nafion/PVA membrane is much superior when compared with pristine Nafion®. For this reason, the performance of the Nafion/PVA membrane suggests a high degree of utilization of Nafion® as proton conductive material within the composite membrane, and therefore, significant savings in the consumed amount of Nafion® are potentially able to be achieved.

While in the literature one can find several papers reporting the performance of pristine Nafion®, composites of Nafion® and impregnated membranes, the results cannot always be easily compared with each other since the experimental conditions can differ. For example, the results of polarization curves and power density obtained in this paper are very similar to those found for PVI/Pd-modified Nafion® and Nafion 115 membranes, where at 80 ºC the power density reached the value of 140 mW cm^{-2} for Nafion 115 and 160 mW cm^{-2} for PVI/Pd-impregnated Nafion® membranes [40], but our experiments were carried out with thinner membranes than those ones and at a lower temperature. Others researchers have found that introducing Nafion® into a very thin microporous UHMWPE film (Solupor®) causes reduction of both methanol crossover and proton conductivity, and the lower proton conductivity of the impregnated membranes is compensated by the significant reduced methanol crossover and thinnest thickness, which leads to better DMFC performance at different methanol concentrations in comparison to Nafion 117 and cast Nafion® membranes [41]. Such membranes feed with a 1 M methanol solution reached the best

performances with average maximum power densities around 275 mW cm^{-2}, 240 mW cm^{-2} and 220 mW cm^{-2} for the impregnated, the Nafion 117 and the cast Nafion® membranes, respectively. These values are higher than the performance showed by our Nafion/PVA and cast Nafion® membranes, although there are great differences in the experimental conditions. In our case the concentration was 2 M at 70 ºC without pressure while Yildirim *et al.* [41] used a methanol feed of 1 M at 80 ºC and 2 atm of oxygen pressure. In the latter, these better results are ascribed to the fact that working at a lower methanol concentration and higher oxygen pressure and temperature strongly favours the performance due to the reduced methanol permeation and the more enhanced electrochemical reactions at the cathode for both oxygen reduction and oxidation of the permeated methanol.

4. Conclusions

In this work we have successfully obtained porous mats of PVA nanofibres with 200-300 nm diameter sizes from aqueous solutions of this polymer and using an equipment of electrospinning.

The thermal treatment, the surface functionalization with sulfonic acid groups and the chemical crosslinking which were applied to PVA nanofibres, did not alter the porous and fibrillar structure of the mats, while even helped to improve their properties.

The method used to infiltrate Nafion® between the PVA nanofibres has managed to produce composite membranes with good mechanical and thermal properties where co-continuous phases of Nafion® and PVA are present.

The proton conductivity of the composite membranes is lower than that of pure Nafion® as the functionalization of the nanofibres with acidic groups is only superficial and does not compensate the reduction caused by the presence of PVA.

It is observed, as opposed to what would be expected, the existence of a linear correlation between conductivity and thickness for the Nafion® membranes. This points out that experimental conductivity measurements lead to apparent values and does not correspond with an intrinsic property of the material due to skin layer effects. An estimation of the thickness-dependent conductivity parameter $\sigma_s^0(T)$ has been obtained. Likewise, the intrinsic activation energy for the bulk phase of the Nafion® membranes has been found to reach 7 kJ mol^{-1}.

Direct Methanol Fuel Cell tests at 70 ºC and 2 M methanol solution confirmed the lower methanol crossover exhibited by the composite Nafion/PVA membranes due to the barrier property of the PVA nanofibres.

The performance of pristine Nafion® and composite membranes with similar thickness (46-47 μm) was comparable and suggested a high degree of utilization of Nafion® as proton conductive material within the composite membrane, and therefore, significant savings in the consumed amount of Nafion® are potentially able to be achieved.

Acknowledgements

This work has been supported by the Valencian Institute of Small and Medium-Sized Enterprises (IMPIVA) and the European Regional Development Funds, through the project IMIDIC/2009/155.

References

[1] M. Peneri, A. Eisemberg, Structure and Properties of Ionomers NATO ASI Series 198, Reidel Publishing Co., Dordrecht, The Netherlands, 1987.
[2] S.R. Samms, S. Wasmus, R.F. Savinell, Thermal stability of Nafion in simulated fuel cell environments, J. Electrochem. Soc. 143 (1996) 1498.
[3] J. Muller, G. Frank, K. Colbow, D. Wilkinson, in: W. Vielstich, A. Lamm, H.A. Gasteiger (Eds.), Handbook of Fuel Cells-Fundamentals Technology and Applications, vol. 4, John Wiley & Sons Ltd., 2003 (Chapter 62).
[4] M. Neergat, K.A. Friedrich, U. Stimming, in: W. Vielstich, A. Lamm, H.A. Gasteiger (Eds.), Handbook of Fuel Cells-Fundamentals Technology and Applications, vol. 4, John Wiley & Sons Ltd, 2003 (Chapter 63).
[5] S. Sambandam, V. Ramani, SPEEK/functionalised silica composite membranes for polymer electrolyte fuel cells, J. Power Sources 170 (2007) 259.
[6] N.W. DeLuca, Y.A. Elabd, Direct methanol fuel cell performance of Nafion®/poly (vinyl alcohol) blend membranes, J. Power Sources 163 (2006) 386-391.
[7] Z.-G. Shao, X. Wang, I.-M. Hsing, Composite Nafion/polyvinyl alcohol membranes for the direct methanol fuel cell, J. Membr. Sci. 210 (2002) 147-153.
[8] Z.-G. Shao, H. Shu, M. Li, I.-M. Hsing, Hybrid Nafion-inorganic oxides membrane doped with heteropolyacids for high temperature operation of proton exchange membrane fuel cell, Solid State Ionics 177 (2006) 779.
[9] X. Zhu, H. Zhang, Y. Liang, X. Wang, B. Yi, An ultrathin self-humidifying membrane for PEM fuel cell application: fabrication, characterization, and experimental analysis, J. Phys. Chem. B 110 (2006) 14240.
[10] V. Ramani, H.R. Kunz, J.M. Fenton, Investigation of Nafion®/HPA composite membranes for high temperature/low relative humidity PEMFC operation, J. Membr. Sci. 232 (2004) 31.
[11] U.H. Jung, K.T. Park, E.H. Park, S.H. Kim, Improvement of low-humidity performance of PEMFC by addition of hydrophilic SiO_2 particles to catalyst layer, J. Power Sources 159 (2006) 529.
[12] E. Chalkova, M.B. Pague, M.V. Fedkin, D.J. Wesolowski, S.N. Lvov, Nafion/TiO_2 proton conductive composite membranes for PEMFCs operating at elevated temperature and reduced relative humidity, J. Electrochem. Soc. 152 (2005) A1035.

[13] E. Chalkova, M.V. Fedkin, S. Komarneni, S.N. Lvov, Nafion/zirconium phosphate composite membranes for PEMFC operating at up to 120 ºC and down to 13% RH, J. Electrochem. Soc. 154 (2007) B288.
[14] Q. Li, R. He, J.A. Gao, J.O. Jensen, N.J. Bjerrum, The CO poisoning effect in PEMFCs operational at temperatures up to 200 ºC, J. Electrochem. Soc. 150 (2003) A1599.
[15] A.S. Arico, V. Baglio, A. Di Blasi, V. Antonucci, FTIR spectroscopic investigation of inorganic fillers for composite DMFC membranes, Electrochem. Commun. 5 (2003) 862.
[16] H.L. Tanga, M. Pan, Synthesis and characterization of a self-assembled nafion/silica nanocomposite membrane for polymer electrolyte membrane fuel cells, J. Phys. Chem. C 112 (2008) 11556.
[17] P.L. Antonuci, A.S. Arico, P. Creti, E. Ramunni, V. Antonuci, Investigation of a direct methanol fuel cell based on a composite Nafion®-silica electrolyte for high temperature operation, Solid State Ionics 125 (1999) 431.
[18] M.A. Navarra, C. Abbati, B. Scrosati, Properties and fuel cell performance of a Nafion-based, sulfated zirconia-added, composite membrane, J. Power Sources 183 (2008) 109.
[19] S. Malhotra, R. Datta, Membrane-supported nonvolatile acidic electrolytes allow higher temperature operation of proton-exchange membrane fuel cells, J. Electrochem. Soc. 144 (1997) L23.
[20] B. Tazi, O. Savadogo, Parameters of PEM fuel-cells based on new membranes fabricated from Nafion®, silicotungstic acid and thiophene, Electrochim. Acta 45 (2000) 4329.
[21] K.D. Kreuer, On the development of proton conducting polymer membranes for hydrogen and methanol fuel cells, J. Membr. Sci. 185 (2001) 29.
[22] F.J. Fernández-Carretero, V. Compañ, E. Riande, Hybrid ion-exchange membranes for fuel cells and separation processes, J. Power Sources 173 (2007) 68.
[23] F.J. Fernández-Carretero, E. Riande, C. Del Rio, F. Sanchez, J.L. Acosta, V. Compañ, Preparation and characterization of hybrid membranes based on Nafion® using partially sulfonated inorganic fillers, J. New Mater. Electrochem. Syst. 13 (2010) 83.
[24] K.D. Kreuer, Proton conductivity: materials applications, Chem. Mater. 8 (1996) 610-641.
[25] J.F. Synder, M.A. Ratner, D.F. Shriver, Polymer electrolytes and polyelectrolytes: Monte Carlo simulations of thermal effects on conduction, Solid State Ionics 147 (2002) 249.
[26] S.J. Paddison, Proton conduction mechanisms at low degrees of hydration in sulfonic acid-based polymer electrolyte membranes, Ann. Rev. Mat. Res. 33 (2003) 289.
[27] J. Pozuelo, E. Riande, E. Saiz, V. Compañ, Molecular dynamics simulations of proton conduction in sulfonated poly (phenyl sulfone)s, Macromolecules 39 (2006) 8862.
[28] H.-L. Lin, T.L. Yu, L.N. Huang, L.C. Chen, K.S. Shen, G.B. Jung, Nafion/PTFE composite membranes for direct methanol fuel cell applications, J. Power Sources 150 (2005) 11-19.
[29] Y. Liu, L.M. Geever, J.E. Kennedy, C.L. Higginbotham, P.A. Cahill, G.B. McGuinness, Thermal behaviour and mechanical properties of physically crosslinked PVA/Gelatin hydrogels, J. Mech. Behav. Biomed. Mater. 3 (2010) 203-209.
[30] N.A. Peppas, E.W. Merrill, Differential scanning calorimetry of crystallized PVA hydrogels, J. Appl. Polym. Sci. 20 (1976) 1457-1465.
[31] Q. Deng, C.A. Wilkie, R.B. Moore, K.A. Mauritz, TGA–FTi.r. investigation of the thermal degradation of Nafion® and Nafion®/[silicon oxide]-based nanocomposites, Polymer 39 (1998) 5961–5972.
[32] V. Di Noto, R. Gliubizzi, E. Negro, G. Pace, Effect of SiO_2 on relaxation phenomena and mechanism of ion conductivity of [Nafion/$(SiO_2)_x$] composite membranes, J. Phys. Chem. B 110 (2006) 24972-24986.
[33] Z. Peng, L.X. Kong, A thermal degradation mechanism of polyvinyl alcohol/silica nanocomposites, Polym. Degrad. Stab. 92 (2007) 1061-1071.

[34] M.N. Tsampas, A. Pikos, S. Brosda, A. Katsaounis, C.G. Vayenas, The effect of membrane thickness on the conductivity of Nafion, Electrochim. Acta 51 (2006) 2743-2755.
[35] S. Slade, S.A. Camphell, T.R. Ralph, F.C. Walsh, Ionic conductivity of an extruded Nafion 1100 EW series of membranes, J. Electrochem. Soc. 149 (2002) A1556-A1564.
[36] D.L. Wood, J. Chlistunoff, J. Majewski, R.L. Borup, Nafion structural phenomena at platinum and carbon interfaces, J. Am. Chem. Soc. 131 (2009) 18096-18104.
[37] P. Costamagna, C. Yang, A.B. Bocarsly, S. Srinivasan, Nafion® 115/zirconium phosphate composite membranes for operation of PEMFCs above 100 ºC, Electrochim. Acta 47 (2002) 1023-1033.
[38] J. Larminie, A. Dicks, Fuel Cell System Explained, John Wiley&Sons Ltd., Chichester, England, 2000 (Chapter 3).
[39] L.-C. Chen, T. Leon Yu, H.-L. Lin, S.-H. Yeh, Nafion/PTFE and zirconium phosphate modified Nafion/PTFE composite membranes for direct methanol fuel cells, J. Membr. Sci. 307 (2008) 10-20.
[40] A.H. Tian, J.-Y. Kim, J.Y. Shi, K. Kim, Poly(1-vinylimidazole)/Pd-impregnated Nafion for direct methanol fuel cell applications, J. Power Sources 183 (2008) 1-7.
[41] M.H. Yildirim, D. Stamatialis, M. Wessling, Dimensionally stable Nafion-polyethylene composite membranes for direct methanol fuel cell applications, J. Membr. Sci. 321 (2008) 364-372.

Paper 2

Journal of Power Sources 196 (2011) 2699-2708
(Adapted to thesis)

Performance of composite Nafion/PVA membranes for direct methanol fuel cells

Sergio Mollá[a,b], Vicente Compañ[a,b]

[a] Dpto. Termodinámica Aplicada, ETSII, Universidad Politécnica de Valencia, 46022 Valencia, Spain.
[b] Instituto de Tecnología Energética (ITE), Universidad Politécnica de Valencia, 46022 Valencia, Spain.

Abstract

This work has been focused on the characterization of the methanol permeability and fuel cell performance of composite Nafion/PVA membranes in function of their thickness, which ranged from 19 μm to 97 μm. The composite membranes were made up of Nafion® polymer deposited between polyvinyl alcohol (PVA) nanofibres. The resistance to methanol permeation of the Nafion/PVA membranes shows a linear variation with the thickness. The separation between apparent and true permeability permits to give an estimated value of $4.0 \cdot 10^{-7}$ cm^2 s^{-1} for the intrinsic or true permeability of the bulk phase at the composite membranes. The incorporation of PVA nanofibres causes a remarkable reduction of one order of magnitude in the methanol permeability as compared with pristine Nafion® membranes. The DMFC performances of membrane-electrode assemblies prepared from Nafion/PVA and pristine Nafion® membranes were tested at 45 ºC, 70 ºC and 95 ºC under various methanol concentrations, i.e., 1 M, 2 M and 3 M. Nanocomposite membranes of 19 μm and 47 μm thickness reached power densities of 211 mW cm^{-2} and 184 mW cm^{-2} at 95 ºC and 2 M methanol concentration. These results are comparable to those found for Nafion® membranes with similar thickness at the same conditions, which were 210 mW cm^{-2} and 204 mW cm^{-2} respectively. Due to the lower amount of Nafion® polymer present within the composite membranes, it is suggested a high degree of utilization of Nafion® as a proton conductive material within the Nafion/PVA membranes, and therefore, significant savings in the consumed amount of Nafion® are potentially able to be achieved. In addition, the reinforcement effect caused by the PVA nanofibres offers the possibility of preparing membranes with a very low thickness and good mechanical properties, while on the other hand, pristine Nafion® membranes are unpractical below a thickness of 50 μm.

Keywords: DMFC, methanol permeability, nanocomposite Nafion® membranes, PVA, nanofibres.

1. Introduction

Perfluorinated polyelectrolytes, such as Nafion®, are up to date the best proton conductors for low temperature fuel cells because of their combination of good chemical and mechanical stability in addition to relatively high conductivity of about 0.08 S cm^{-1} [1-4]. Though polymer electrolyte membranes (PEMs) for fuel cells are promising candidates for transportation, distributed power, and portable power applications, important scientific, technical and economical problems need to be solved before commercialization is possible.

Direct methanol fuel cells (DMFCs) are promising candidates as power generators for portable devices. Easy refuelling and high energy storage capacity are their main advantages. However, it is known that the use of Nafion® membranes in DMFCs causes problems such as methanol crossover, which entails the utilization of very thick membranes, and thus performance is reduced [5,6].

Recently, extensive work has been focused on Nafion® membranes modified with conducting polymers, such as polyaniline [7], polyaniline/silica [8] and polypyrrole [9], paying special attention to the methanol crossover in the composite membranes. It is worth noting that the mix of electronic conductivity of polyaniline with the ionic conductivity of cation-exchange membranes has also promoted the study of these composites for electrode modifications [10-14]. Mauritz *et al.* [15,16] demonstrated that hybrid Nafion/silica membranes in PEM applications produce advantages such as higher water uptake, lower methanol uptake, and greater mechanical strength than unmodified Nafion®. Sorption studies showed that the Nafion/silica membranes had a larger affinity for water over methanol, whereas the order is reversed for unmodified Nafion®. Consequently, these experimental results suggest that the methanol permeability through the hybrid membranes will be smaller than in unmodified membranes [17-19]. However, such a reduction of methanol crossover usually leads to a decrease in proton conductivity.

In this context, the synthesis of efficient solid electrolytes separating the anode from the cathode together with the development of cheaper catalysts for fuel oxidation are the main issues facing the development of commercial low temperature DMFCs. In principle, proton conducting ionic fillers would have a dual function: enhancement of the water retention and increase of the ion-exchange capacity (IEC) of the membranes, two properties that increase the proton conductivity. In membranes with high IEC, segregation of nanosize hydrophilic domains from the hydrophobic ones to form percolation paths for proton transport may be relatively easy. It is possible to think that ionic inorganic fillers trapped in hydrophobic domains separating

hydrophilic domains might provide additional pathways for proton transport [20-22].

In this work we report the methanol permeability and DMFC performance of novel nanocomposite membranes as a function of thickness. They were prepared from mats of sulfonic acid functionalised nanofibres of polyvinyl alcohol (PVA) in which Nafion® has been infiltrated. Advantages provided by the PVA nanofibres are an increase of mechanical properties (reinforcement effect), which allows obtaining composite films much thinner than commercial Nafion® membranes, and a decrease of methanol permeation. The thickness of the composite membranes prepared in our laboratory ranged from 19 ± 1 μm to 97 ± 5 μm. Thin membranes were particularly searched for lowering the ohmic resistance of proton transport.

MEAs prepared from composite membranes of Nafion/PVA have been examined via polarization curves at different temperatures and methanol concentrations. For comparison, Nafion® membranes presenting similar thicknesses have been cast and their performance analyzed. The differences observed between the membranes are discussed, paying special attention on methanol concentration, temperature and membrane thickness.

2. Experimental Part

2.1. Materials

A commercial 20 wt% Nafion® dispersion (DuPont Co.) was solvent exchanged in order to prepare a 5 wt% dispersion in isopropanol/water mixture, 4:1 w/w respectively.

Polyvinyl alcohol, PVA Mowiol 28-99 grade, was kindly supplied by the company Kuraray Europe GmbH.

Isopropanol extra pure and cetyltrimethylammonium bromide (CTAB) were purchased from Acros Organics, and 4-formyl-1,3-benzenedisulfonic acid disodium salt from Sigma-Aldrich.

2.2. Preparation of the membranes

2.2.1. Nafion® membranes

The solvent exchanged solution, with a 5 wt% Nafion® content in isopropanol and water, was used for the casting of pristine Nafion® membranes with thickness values between 18 μm and 95 μm. The respective Nafion® membranes were annealed at 125 ºC for 90 min in the oven and then removed from their Petri glass dishes by adding water.

The last step was the conditioning of the membranes by treatment with hot hydrogen peroxide and chlorhydric acid solutions. Finally, the cast Nafion® membranes were washed with hot water, dried and stored.

2.2.2. PVA nanofibre-reinforced Nafion® membranes

A description of the preparation method and characterization of composite Nafion/PVA membranes has been previously reported by the authors [23]. Porous PVA mats were produced by an electrospinning setup (Yflow S.L., Málaga, Spain) through the feeding of an aqueous solution of PVA (0.005:1:10 wt. CTAB:PVA:water) at a flow rate of 0.5 ml h^{-1}. CTAB was used as surfactant in order to reduce surface tension of water and facilitate the process. A potential difference of 16 kV was applied between the needle and the planar collector, which were separated a distance of 25 cm.

The collected mats were heated during 3 h at 170 ºC in a vacuum atmosphere (250 mbar pressure) with the purpose of removing water and increasing manipulability. The PVA mats were then mounted on a round steel frame and immersed into a bath in which the disodium salt of the 4-formyl-1,3-benzenedisulfonic acid was dissolved by a mixture of isopropanol/water (70/30 v/v), incorporating chlorhydric acid as a catalyst for the acetal reaction, which was carried out at 60 ºC for 2 h:

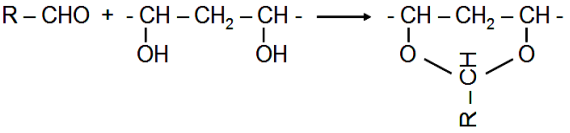

(1)

The sodium ions were exchanged with protons by immersion of the mats in a HCl solution. Subsequently, the mats were crosslinked with the aim to improve their mechanical, chemical and thermal properties. This was accomplished by reacting glutaraldehyde vapor with the PVA nanofibres during 24 h at room temperature. Afterwards, the mats were heated at 100 ºC for 15 min with the aim to remove adsorbed glutaraldehyde and water.

The treated mats were then impregnated with the prepared 5 wt% Nafion® dispersion in isopropanol/water 4:1 w/w. This ratio has been previously reported to be suitable for Nafion® infiltration into porous membranes [24]. Each impregnation step was carried out by wetting the PVA mat into the Nafion® dispersion for 5 min and followed by evaporation in an oven at 100 ºC for 5 min more. This was repeated 8 times in every mat so that an outer visible Nafion® layer was formed.

Finally, the composite membranes were annealed at 125 ºC for 90 min under pressure and then conditioned with hot aqueous solutions of hydrogen peroxide and chlorhydric acid, washed with hot water, dried and stored.

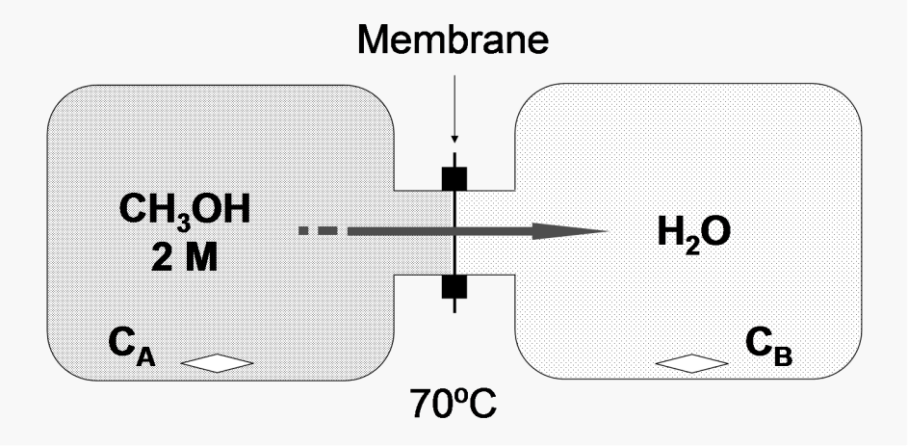

Fig. 1. Schematic representation of the experimental setup for the determination of the methanol permeability across the membranes.

2.3. Characterization of membranes

2.3.1. Coefficients of methanol permeability

In order to determine the methanol permeability coefficient through the composite membranes, an experimental setup as shown in Fig. 1 was used. Chamber A was filled with a 2 M aqueous solution of methanol, while chamber B was filled with water. Both chambers were kept under stirring and thermostatized at 70 ºC. A sample of 500 µl from chamber B was taken every certain time and then introduced into a vial containing 500 µl of water. The composition of the vial content was analyzed by gas chromatography (GC, HP Co. model 8590A) with a capillary column (Agilent Co., 30 m × 0.53 mm × 20 µm) and a TCD detector. Seven patron solutions were previously prepared in order to obtain a calibration curve representing peak areas versus methanol concentrations.

The diffusion process of methanol across a membrane, in the stationary state, is described by the Fick's first law:

$$J = -D\frac{\partial C^m}{\partial x} = D\frac{\Delta C^m}{L} \qquad (2)$$

where ΔC^m represents the variation in methanol concentration between the right and left sides of the membrane, with a thickness L, and can be expressed as $C_B - C_A$.

However, from a strict point of view, the methanol concentrations at both sides of the membrane, C_B^m *and* C_A^m, cannot be considered the same as the concentrations in bulk solution, since this transfer process is governed by the methanol solubility in such a membrane. Thus, we can define the membrane partition coefficient *K* as,

$$K = \frac{C_A^m}{C_A} = \frac{C_B^m}{C_B} \tag{3}$$

and therefore, the variation in the methanol concentration across the membrane will be given by,

$$\Delta C^m = C_B^m - C_A^m = K \cdot (C_B - C_A) = K \cdot \Delta C \tag{4}$$

The flux of methanol *J* can also be expressed as the amount of methanol in moles *n* crossing the membrane (thickness *L*) per unit of time *t* and area *A*. We can rewrite the Fick's law as:

$$J = \frac{dn}{A \cdot dt} = D \cdot K \frac{\Delta C}{L} \tag{5}$$

where,

$$n = C_B \cdot V_B \rightarrow dn = V_B \cdot dC_B \tag{6}$$

Thus:

$$\frac{V_B \cdot dC_B}{A \cdot dt} = D \cdot K \frac{\Delta C}{L} \tag{7}$$

If we take into account that the difference in concentration between both sides of the membrane, $\Delta C = C_B - C_A$, is practically constant due to the fact that $C_A >> C_B$, then:

$$dC_B = \frac{D \cdot K \cdot A}{L \cdot V_B} C_A \cdot dt \tag{8}$$

Integrating Eq. (8), the following expression is obtained:

$$C_B = \frac{D \cdot K \cdot A}{L \cdot V_B} C_A \cdot t \qquad (9)$$

The product between the diffusion coefficient, *D*, and the membrane partition coefficients, *K*, measures the apparent permeability coefficient *P*:

$$P = D \cdot K \qquad (10)$$

in which the name apparent refers to the permeability through the whole system (membrane + boundary layers) and not only to the membrane.

Combining Eqs. (9) and (10), we can obtain the final expression which shows how varies the concentration of methanol in chamber B as a function of time:

$$C_B = \frac{P \cdot A}{L \cdot V_B} C_A \cdot t \qquad (11)$$

where, C_B: Concentration of methanol in chamber B, C_A: Concentration of methanol in chamber A (2 M), *P*: Coefficient of apparent methanol permeability across the membrane ($cm^2\ s^{-1}$), *A*: Area of the membrane (2.27 cm^2), *L*: Membrane thickness (cm), V_B: Volume of water which fills the chamber B (150 cm^3), and *t*: Time reached at each measurement (s).

Plotting C_B versus time will show a straight line of which slope *m* the apparent permeability can be calculated,

$$m = \frac{P \cdot A}{L \cdot V_B} C_A \qquad (12)$$

The apparent transmissibility of methanol through the membrane system is defined by the relation *P/L*. The inverse of the slope *m* is,

$$\frac{1}{m} = \frac{L}{P} \cdot \frac{V_B}{A \cdot C_A} \qquad (13)$$

while the reciprocal of the apparent transmissibility, *L/P*, is related with the resistance of the total system to the methanol flux.

The total resistance of the system has two components: One derived from the intrinsic material properties of the membrane and other due to the boundary layers, that is, the transfer process between the bulk solution and the membrane surface [25]:

$$\left(\frac{L}{P_{App}}\right)=\left(\frac{L}{P_{True}}\right)+R_{B.L.} \qquad (14)$$

The values of resistance to the methanol flux (L/P_{App}) of each membrane, calculated from the apparent permeability, plotted versus their values of thickness (L) will develop a straight line of slope equal to $1/P_{True}$. Thereby, the true methanol permeability coefficient of the membrane material (P_{True}) can be obtained.

2.3.2. MEA preparation

Composite membranes of Nafion/PVA, as well as pristine Nafion® membranes, were used for the preparation of membrane electrode assemblies (MEAs) in order to study their DMFC performance.

The anode and cathode electrodes used for MEA preparation were acquired from Baltic Fuel Cells GmbH (Schwerin, Germany). The anode was composed of a carbon paper gas diffusion layer (GDL) from Freudenberg & Co. (Weinheim, Germany), model H2315 T105A, covered by an alloy of Pt-Ru black 50:50 (Alfa Aesar) with a catalyst loading of 5.0 mg cm^{-2} together with a 20 wt% of dry Nafion® ionomer. Similarly, the cathode was composed of a GDL from Freudenberg & Co., model H2315 I3C4, with a catalyst loading of 5.0 mg cm^{-2} of platinum nanoparticles supported by advanced carbon (HiSPEC 13100, Alfa Aesar) with a Pt/C ratio of 70 wt%, and the electrode also contained a 20 wt% of dry Nafion®.

2.3.3. DMFC performance of Nafion/PVA and Nafion® membranes

The MEAs were previously equilibrated with water and then placed into a single fuel cell hardware with a square 5 cm^2 active area (quick CONNECT, Baltic Fuel Cells GmbH), containing graphite serpentine flow fields and equipped with a pressure-controlled clamping force system.

Different concentrations of aqueous methanol solution, i.e. 1 M, 2 M and 3 M, were pumped at a flow rate of 5 ml min^{-1} to feed the anode. The cathode was directly fed with oxygen gas at a flow rate of 150 ml min^{-1} and atmospheric pressure.

Polarization curves of *i-V* (current density versus potential) were obtained at several temperatures, i.e. 45 ºC, 70 ºC and 95 ºC, from open circuit voltage (OCV) conditions up to 0.2 V by stepwise increment of the current density. Power density values were consequently calculated and represented. Before *i-V* measurements, the MEAs were activated at least for 5 h until reproducible results were achieved.

Table 1. Thickness, water uptake at 70ºC, ion-exchange capacity and proton conductivity at 95 ºC and fully hydrated conditions for composite Nafion/PVA membranes. Nafion® is included for comparison.

Membrane	Thickness (μm)	Water uptake (%)	IEC (meq g^{-1})	λ $\left(\frac{mol\ H_2O}{mol\ SO_3H}\right)$	$\sigma^{95ºC}$ (S cm^{-1})
Nafion/PVA	19 ± 1	26.4 ± 0.1	0.47 ± 0.1	42	0.012
Nafion/PVA	26 ± 2	19.3 ± 0.1	0.33 ± 0.1	44	0.012
Nafion/PVA	39 ± 3	27.9 ± 0.1	0.45 ± 0.1	47	0.016
Nafion/PVA	47 ± 3	25.8 ± 0.1	0.58 ± 0.1	34	0.025
Nafion/PVA	61 ± 3	22.9 ± 0.1	0.57 ± 0.1	30	0.010
Nafion/PVA	97 ± 5	35.8 ± 0.1	0.55 ± 0.1	49	0.007
Nafion®	18 ± 1	27.0 ± 0.1	0.93 ± 0.1	22	0.015
Nafion®	28 ± 1	27.0 ± 0.1	0.93 ± 0.1	22	0.027
Nafion®	37 ± 1	27.0 ± 0.1	0.93 ± 0.1	22	0.034
Nafion®	46 ± 1	27.0 ± 0.1	0.93 ± 0.1	22	0.035
Nafion®	60 ± 2	27.0 ± 0.1	0.93 ± 0.1	22	0.049
Nafion®	95 ± 2	27.0 ± 0.1	0.93 ± 0.1	22	0.070
Nafion 117 (commercial)	216 ± 4	21.5 ± 0.1	0.91 ± 0.1	18	0.096

3. Results and discussion

3.1. Properties of the Nafion/PVA membranes

Table 1 summarizes thickness, water uptake, ion-exchange capacity (IEC) and conductivity of the composite Nafion/PVA membranes. The absolute values for the water uptake at 70 ºC of the Nafion/PVA membranes are similar to those of pristine Nafion® membranes prepared in our laboratory by casting and slightly higher than the value obtained for commercial Nafion 117. However, the λ values, which relate the molar content of water molecules to the total number in moles of sulfonic acid groups within the membrane, show values between 18 and 22 for the pristine Nafion® materials, as expected since Nafion® saturates at $\lambda = 22$, whereas the Nafion/PVA membranes show much larger values. This observation would suggest that the PVA nanofibres of the composite membranes are also swelling in a certain degree due to the strong hydrophilic character of the PVA molecule.

Ion-exchange capacities of the Nafion/PVA membranes are nearly the half of the typical values observed for pure Nafion® materials, assumed to be

due to the replacement of Nafion® polymer by the PVA nanofibre phase. Consequently, the proton conductivities of the Nafion/PVA membranes fall below the values measured in pristine Nafion® membranes (see Table 1 and [23]). This confirms that the superficial functionalization of the PVA nanofibres hardly influences the total ion-exchange capacity (IEC) of the composite membranes. However, it has been desired just to functionalize the surface of the nanofibres in order to keep the barrier properties associated with bulk PVA. If the PVA phase would have been fully sulfonated, the methanol crossover across its volume would have strongly increased, and therefore, the nanofibre phase would have not showed barrier properties against methanol.

The nanocomposite membrane with a thickness of 47 μm showed the maximum proton conductivity at the whole studied temperature range, achieving 0.025 S cm^{-1} at 95 ºC under fully hydrated conditions.

3.2. Apparent and true methanol permeabilities across the composite membranes

It has been characterised the methanol transport across Nafion/PVA membranes with different thicknesses by means of the setup already described in Fig. 1. The temperature of the bath was fixed at 70 ºC and the chamber A was filled with a 2 M methanol solution.

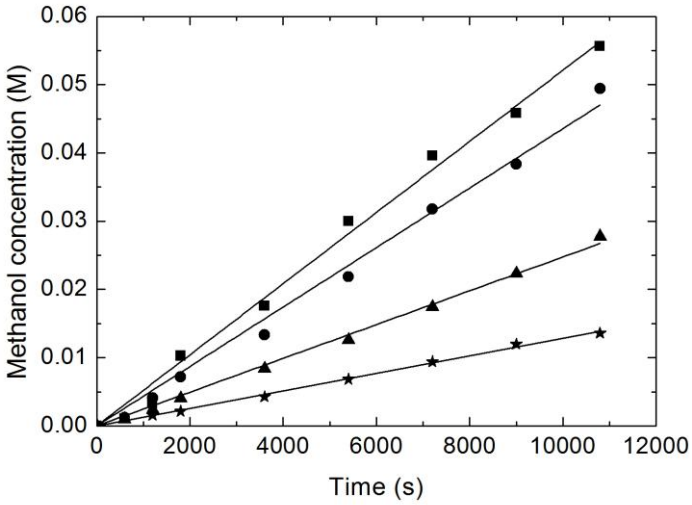

Fig. 2. Methanol concentration (C_B) versus time for permeability experiments at 70 ºC of composite Nafion/PVA membranes having different thickness values: (■) 26 μm, (●) 39 μm, (▲) 61 μm, and (★) 97 μm.

Table 2. Apparent methanol permeabilities (P_{App}) at 70 ºC for several composite Nafion/PVA membranes and for both cast and commercial Nafion® membranes.

Membrane	Thickness (µm)	$m = C_B/t$ (mol l^{-1} s^{-1})	P_{App} methanol (cm^2 s^{-1})
Nafion/PVA	26 ± 2	$5.21295 \cdot 10^{-6}$	$4.13 \cdot 10^{-7}$
Nafion/PVA	39 ± 3	$4.35606 \cdot 10^{-6}$	$5.33 \cdot 10^{-7}$
Nafion/PVA	61 ± 3	$2.47526 \cdot 10^{-6}$	$4.99 \cdot 10^{-7}$
Nafion/PVA	97 ± 5	$1.28308 \cdot 10^{-6}$	$4.11 \cdot 10^{-7}$
Nafion [26][a]	175	-	$5.58 \cdot 10^{-6}$
Nafion 117 [26]	178	-	$4.36 \cdot 10^{-6}$

[a] Cast membrane using Nafion® dispersion in isopropanol/water (4:1 w/w). C_B measured by densimetry.

Samples (500 µl) from the chamber B were taken within a period between 0 and 3 h, i.e. 600 s, 1200 s, 1800 s, 3600 s, 5400 s, 7200 s, 9000 s and 10,800 s. These were analyzed by gas chromatography and their chromatograms compared with the calibration curve, correlating the chromatograms peak areas with methanol concentrations.

Fig. 2 depicts the variation of methanol concentration in the chamber B versus time. Straight lines with different slopes ($m = C_B/t$) have been obtained as a function of the membrane thickness. By application of Eq. (1) with the experimental parameters and the values of the obtained slopes, the apparent methanol permeability of the membranes can be calculated.

Table 2 shows the apparent permeability coefficients obtained for

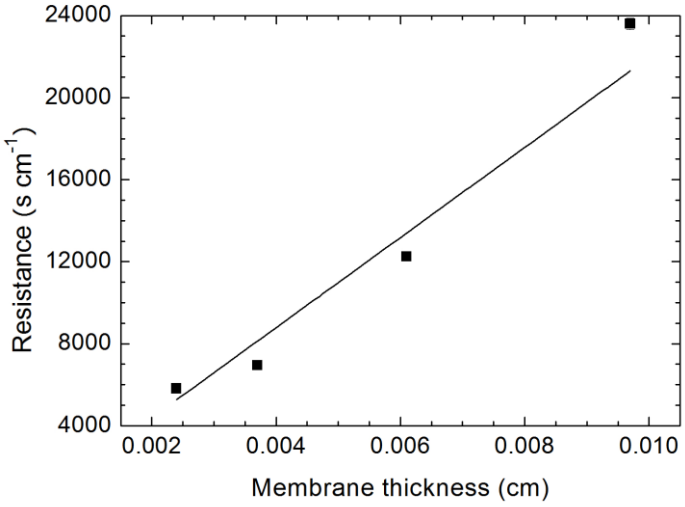

Fig. 3. Representation of the resistance to the methanol permeation across the Nafion/PVA membranes as a function of their thickness.

Nafion/PVA membranes and are compared with those reported for both a cast Nafion® membrane, prepared with a similar Nafion® dispersion composition, and for a commercial Nafion 117 membrane.

With the purpose of obtaining the true or intrinsic permeability of the membranes Nafion/PVA, it has been plotted the reciprocal of the transmissibility of the membranes, that means the resistance that the membrane offers to methanol flux, *L/P*, as a function of the membrane thickness (Fig. 3).

The value of the true methanol permeability, P_{True}, can be given from the reciprocal of the slope of the straight-line plotted in Fig. 3, that is $m = (2.196 \pm 0.195) \cdot 10^{6}$. This parameter represents an intrinsic property of the material and a value of $(4.55 \pm 0.40) \cdot 10^{-7}$ cm^2 s^{-1} is calculated for the Nafion/PVA membranes.

These results of methanol permeability for the nanocomposite membranes prepared in our work are very promising and validate the capacity of the PVA nanofibres to perform as barriers for the methanol diffusion. It is worth noting that the intrinsic methanol permeability coefficient of the Nafion/PVA membranes are one order of magnitude below the permeabilities at 70 ºC of Nafion® membranes prepared by casting in our laboratory, as well as much lower than the typical permeability coefficients reported for commercial Nafion 117 membranes at room temperature $(2.3 \pm 0.2) \cdot 10^{-6}$ cm^2 s^{-1}, according to the literature [27-30].

3.3. Performance of MEAs in direct methanol fuel cell operation

Figs. 4 and 5 are graphically represented data of the cell potential, *V*, and power density curves versus current density, *i*, for the MEAs prepared with pristine Nafion® membranes (18 μm and 46 μm thickness) and composite Nafion/PVA membranes (19 μm and 47 μm), when DMFC was operated at 45 ºC, 70 ºC and 95 ºC, and fed with 1 M, 2 M and 3 M methanol solutions.

The cell potential at OCV conditions ($i = 0$) usually does not reach the theoretical value of the overall reversible cathode and anode potential at the given pressure and temperature. The drop of the OCV from the theoretical voltage has been attributed to the penetration of the fuel across the membrane, and thus, these values are a good indicator of the degree of methanol crossover by diffusion [31].

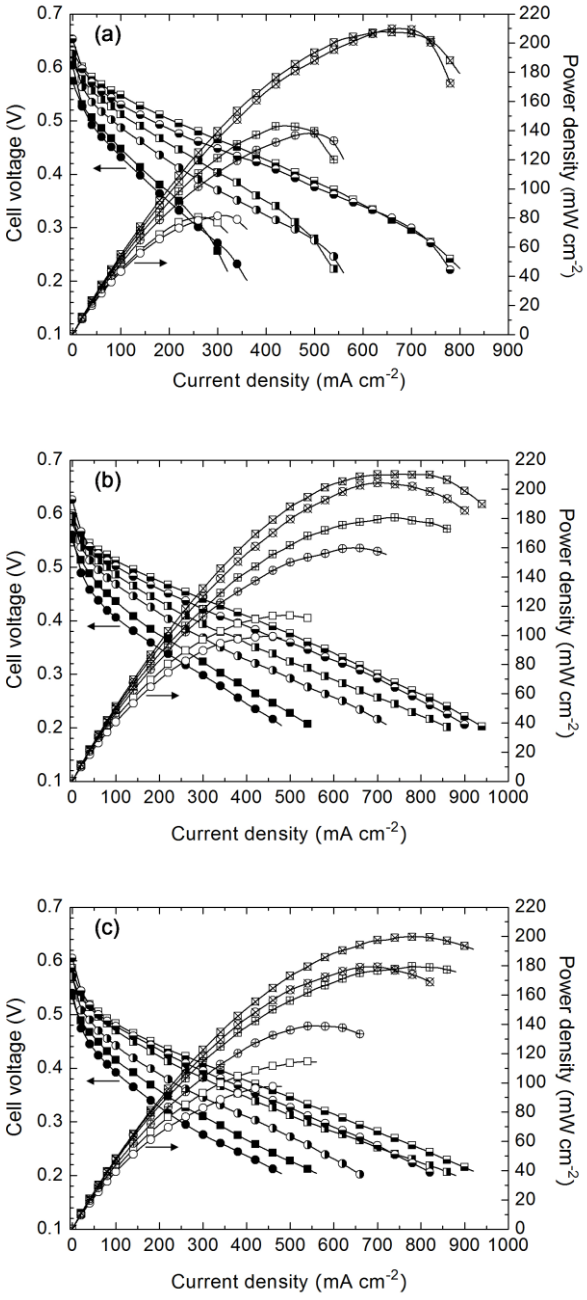

Fig. 4. Curves of i-V and power density profiles obtained with methanol solutions of (a) 1 M, (b) 2 M, and (c) 3 M concentration for pristine Nafion® membranes at different conditions of temperature and thickness: (■)(□) 45 ºC, 18 µm; (◧)(⊞) 70 ºC, 18 µm; (⬓)(⊠) 95 ºC, 18 µm; (●)(○) 45 ºC, 46 µm; (◑)(⊕) 70 ºC, 46 µm; and (◒)(⊗) 95 ºC, 46 µm.

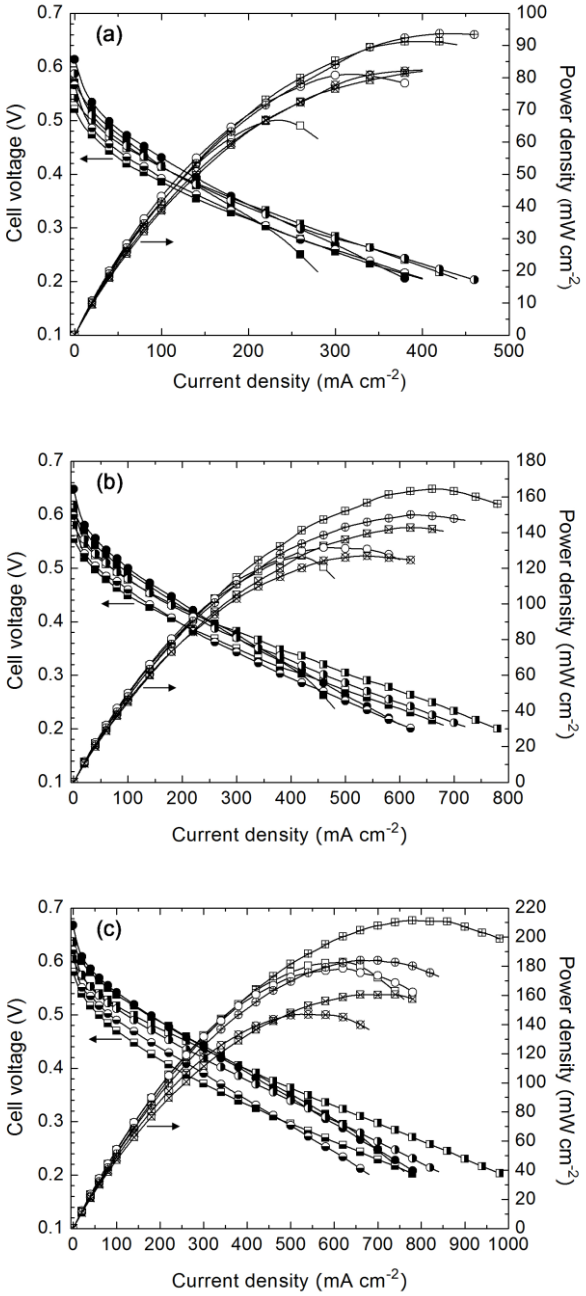

Fig. 5. Curves of i-V and power density profiles obtained at cell temperatures of (a) 45 ºC, (b) 70 ºC, and (c) 95 ºC for Nafion/PVA membranes at different conditions of methanol concentration and thickness: (■)(□) 1 M, 19 µm; (◧)(⊞) 2 M, 19 µm; (⬓)(⊠) 3 M, 19 µm; (●)(○) 1 M, 47 µm; (◑)(⊕) 2 M, 47 µm; and (◒)(⊗) 3 M, 47 µm.

Table 3. Values of open circuit voltage (OCV) for Nafion/PVA and Nafion® membranes at different conditions of temperature and methanol concentration.

Membrane	L (μm)	OCV (V)			$[CH_3OH]$ (M)
		45 ºC	70 ºC	95 ºC	
Nafion/PVA	19 ± 1	0.570	0.608	0.635	1
		0.541	0.580	0.604	2
		0.521	0.554	0.580	3
Nafion®	18 ± 1	0.574	0.610	0.631	1
		0.552	0.583	0.600	2
		0.534	0.569	0.586	3
Nafion/PVA	47 ± 3	0.614	0.648	0.668	1
		0.587	0.618	0.637	2
		0.566	0.598	0.621	3
Nafion®	46 ± 1	0.604	0.625	0.653	1
		0.560	0.596	0.626	2
		0.540	0.571	0.605	3
Nafion 117	216 ± 4	0.673	0.688	0.708	1
		0.650	0.653	0.668	2
		0.624	0.653	0.673	3

Table 3 summarizes the OCV values of MEAs prepared with Nafion® and composite Nafion/PVA membranes fed by 1 M, 2 M and 3 M methanol solutions at 45 ºC, 70 ºC and 95 ºC. Those OCV values decrease in all cases with the increase in methanol concentration, due to a larger fuel permeation, while at a fixed methanol concentration, the values of OCV increase with the temperature favoured by the accelerated electrochemical reactions. These results obtained indicate that the effect of the activation energy in the electrochemical reaction (voltage increment) is higher than the opposite effect caused by the increased methanol crossover (voltage reduction), and thus, the combined effect is only a moderate increase of the cell potential with the temperature.

However, at a fixed temperature and methanol concentration, the OCV follows the trend Nafion (18 μm) ≈ Nafion/PVA (19 μm) < Nafion (46 μm) < < Nafion/PVA (47 μm) < Nafion 117. At very low thickness levels, Nafion® and Nafion/PVA behave very similar, while at medium size thicknesses, Nafion/PVA exceeds pristine Nafion®. Commercial Nafion 117 is a very large thickness membrane, and therefore, its OCV values surpass the others.

It would be expected that the comparison between membranes of pristine Nafion® and Nafion/PVA with similar thickness would show higher OCV values for the composite ones as a more reduced methanol crossover is reported. However, not only the methanol crossover is known to be

responsible on the OCV parameter. Another factors as homo/heterogeneity of the membrane and electrodes, catalyst loading, MEA preparation, water management and blocking of pores in gas diffusion layers, catalytic activity and reaction kinetics, proton conductivity, gradient of methanol concentration within the catalytic layer, porosity of gas diffusion and catalytic layers, air/oxygen flow rates, contact pressures, temperature, etc. can influence the OCV values. Unfortunately, all these parameters are difficult to control together.

For example, it has been reported that the ability of air/oxygen to reach the catalyst layer is a very important factor with regards to the OCV parameter, since the OCV values diminish due to the competitive reaction of methanol oxidation against oxygen reduction over the cathode catalyst, and thus it depends on the methanol crossover, but the available amount of oxygen, depending on the flow rate, strongly affects this reaction as well, and therefore, the OCV typically increases with the oxygen/air flow rate since more methanol is dissipated from the cathode [32].

It is also worth to mention that our composite membranes showed lower proton conductivity values than the pristine Nafion® membranes with similar thickness, and it has been reported by another authors that proton conductivity can influence the OCV values too, since from a practical point of view, the OCV values cannot be obtained at conditions of null intensity ($I = 0$), and at least $I = 0.01$ A is usually necessary. Thus, this factor must be also taken into account [33]. In fact, taking a look at Table 3, it is possible to remark that the Nafion/PVA membrane which showed the highest proton conductivity among the composite membranes (47 μm thickness) exceeds the OCV values measured for the Nafion® membrane with comparable thickness (46 μm).

Fig. 4 clearly shows that the DMFC performances follow the order 95 ºC > 70 ºC > 45 ºC. The differences in performance, especially between 70 ºC and 95 ºC, become smaller with increasing methanol concentration. At 1 M, due to the low methanol concentration, the temperature effect is very significant. On the other hand, Fig. 5 elucidates an optimal methanol concentration at 2 M. Due to mass transport problems, 1 M concentration results are not convenient, although at 95 ºC the performance with 1 M methanol solution surpasses that one showed by the 3 M concentration. This is inferred to the higher methanol crossover with increasing temperature and concentration.

Figs. 6 and 7 represent the performances of the MEAs prepared with both pristine Nafion® and composite Nafion/PVA membranes ranging different thicknesses, at the conditions of 2 M methanol solution and 95 ºC. In the case of pristine Nafion® (Fig. 6), the maximum power density is achieved with the thinnest (18 μm) membrane, reaching 210 mW cm^{-2},

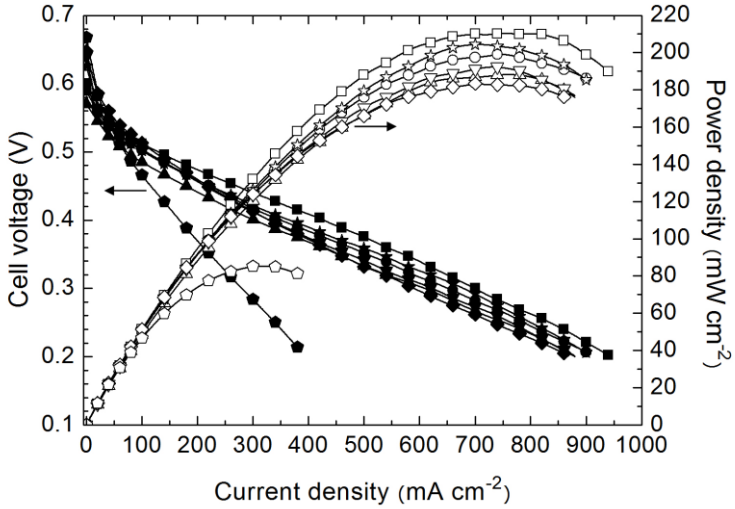

Fig. 6. DMFC performances at 95 ºC and 2 M methanol concentration for pristine Nafion® membranes with different thickness: (■) 18 µm, (▲) 28 µm, (●) 37 µm, (★) 46 µm, (▼) 60 µm, (◆) 95 µm, and (⬟) 216 µm, commercial N117.

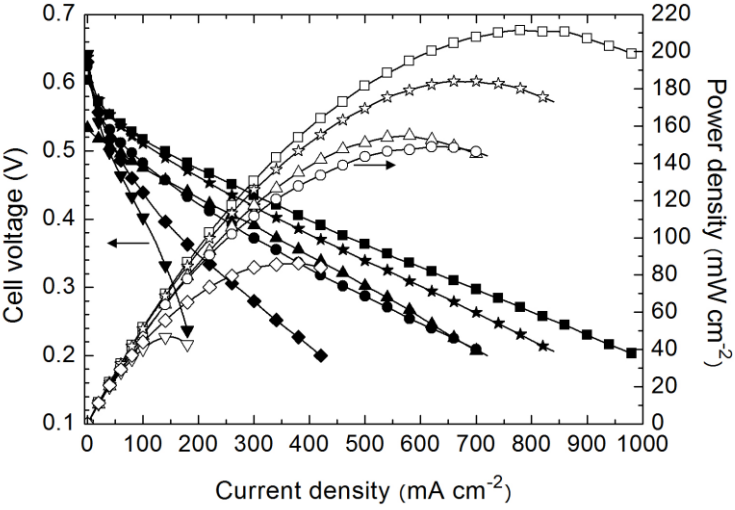

Fig. 7. DMFC performances at 95 ºC and 2 M methanol concentration for composite Nafion/PVA membranes with different thickness: (■) 19 µm, (▲) 26 µm, (●) 39 µm, (★) 47 µm, (▼) 61 µm, and (◆) 97 µm.

assumed to be due to its very low protonic resistance which greatly compensates the negative effect of the high flux of methanol permeating across. However, the 28 µm thickness membrane shows a lower performance, which might be attributed to the larger resistance while

methanol flux still keeps being high. For the 37 μm and 46 μm membranes, performance increases with the thickness, and thus, the membrane of 46 μm thickness shows the second maximum power density, 204 mW cm^{-2}. A reasonable explanation of this phenomenon suggests that the reduced methanol flux with increasing thickness compensates the correspondingly increase of protonic resistance.

The benefit on the methanol permeation caused by the effect of thickness applies up to 50 μm, and those membranes presenting thicknesses higher than that value show performances decreasing accordingly. In this sense, the membrane with 60 μm thickness has a performance similar to that one of 28 μm, and the 95 μm membrane slightly below those ones. The poorest performance has been found for the commercial Nafion 117 membrane, with a power density of 85 mW cm^{-2}, since it presents a very large thickness (216 μm at fully hydrated conditions) and thus undergoes an important protonic resistance, although on the other hand, its methanol permeation rate is the lowest as suggested by its OCV value.

Fig. 7 represents the performances of the prepared Nafion/PVA membranes. Again, the membranes with thicknesses of 19 μm and 47 μm show the best performances, 211 and 184 mW cm^{-2} respectively, which are almost similar to those ones showed by the Nafion® membranes of comparable thickness. As mentioned before, a thickness below 20 μm involves a very low protonic resistance and the best performance result. In the case of the Nafion/PVA membrane of 47 μm, Table 1 confirms the largest conductivity value achieved for a composite membrane, 0.025 S cm^{-1} at 95 ºC under fully hydrated conditions. This combined with the intrinsically reduced methanol permeability would explain its very good performance.

The low conductivities found for the composite membranes when compared with Nafion® makes the protonic resistance to be the most important parameter, and therefore, the effect of thickness has a more profound impact on the performance. Thus, the composite membranes with thickness larger than 50 μm performed very poor. With regard to this, the 97 μm membrane was found to perform better than the membrane of 61 μm thickness. The former was built by hot pressing of two thinner pieces of Nafion/PVA membrane, while the last one was prepared from a single PVA nanofibre mat. This experimental result advises that large thickness PVA mats are not suitable for the infiltration of Nafion® polymer, since diffusion of the dispersion within the inner part of the porous mat should become more restricted.

A close inspection on the *i*-*V* curves (Figs. 4-7) shows two different regions: Region-I, in which the activation process of the MEA occurs, is characteristic of low current densities; and region-II, typically at current

densities *i* above 100 mA cm^{-2}, is characterised by showing a linear negative slope. The latter region is dominated by the protonic resistance of the membrane and its methanol crossover, which can be attributed to mechanisms of diffusion and electro-osmosis [34-36]. The cell voltage of a DMFC can be written as,

$$V = E - A_1 \cdot \ln\left(\frac{i}{i_0}\right) - \frac{i \cdot L}{\sigma} - \eta_{cros} \qquad (15)$$

where V is the cell voltage, E the reversible open circuit voltage, i the current density, i_0 the current density at which the over-voltage begins to move from zero, A_1 the sum of the slopes of the polarization curves for anode and cathode, L is the thickness of the membrane clamped between the anode and cathode electrode layers, σ the conductivity of the membrane and η_{cros} is the overpotential caused by methanol crossover [31].

The methanol crossover produces depolarization losses at cathode, by competitive reaction with oxygen, and concentration losses in anode as fuel permeates. The overpotential due to the methanol crossover, η_{cros}, can be calculated following the procedure described by Huang *et al.* [36], by mean of the expression:

$$\eta_{cros} = \chi \cdot J_{MeOH} = \chi \cdot (J_{con} + i \cdot J_{cros}) \qquad (16)$$

where χ is a constant and J_{MeOH} the flux of methanol crossing the membrane. This flux has a current independent term affected by methanol concentration C_{an} at anode, i.e. J_{con}, and a current dependent term due to electro-osmosis of methanol, i.e. J_{cros}. Substituting Eq. (16) into Eq. (15), we obtain,

$$V = E - A_1 \cdot \ln\left(\frac{i}{i_0}\right) - \frac{i \cdot L}{\sigma} - \chi \cdot (J_{con} + i \cdot J_{eos}) \qquad (17)$$

Ficken diffusion and a linear concentration gradient across the thickness direction of the membrane is assumed, i.e. diffusion coefficient is independent of the concentration differential between anode and cathode sides, as well as the methanol molecules crossing from anode to cathode are catalytically oxidised. Thus, J_{con} becomes a dependent term of the methanol concentration in anode,

$$J_{con} = k \cdot C_{an} \qquad (18)$$

being k a constant which depends on the methanol diffusivity across the membrane. Substituting Eq. (19) into Eq. (17), rearranging Eq. (18) and separating the C_{an}-dependent and i-dependent terms, it results the following expression,

$$V(i, C_{an}) = E - A_1 \cdot \ln\left(\frac{i}{i_0}\right) - A_2 \cdot C_{an} - A_3 \cdot i \qquad (19)$$

with

$$A_2 = \chi \cdot k \qquad (20)$$

$$A_3 = \frac{L}{\sigma} + \chi \cdot J_{eos} \qquad (21)$$

where A_2 is a term relating the overvoltage to the methanol crossover by diffusion, A_3 is a term relating the overvoltage influenced by the sum of the protonic resistance and the methanol electro-osmotic effects. These equations are only valid in the region-II of *i-V* curves. The derivative *dV/di* when the concentration of methanol in the anode is constant, is equal to,

$$\frac{dV}{di} = -\frac{A_1}{i} - A_3 \qquad (22)$$

At current densities above 100 mA cm^{-2}, $(A_1/i) < (A_1/100) << A_3$. Thus, A_3 can be obtained from the slope of the plot of V versus i at a fixed temperature and methanol feed concentration C_{an} when $i > 100$ mA cm^{-2}.

Table 4. Values of the $\chi \cdot J_{eos}$ parameter (V cm^2 mA^{-1}) for the electro-osmotic diffusion of methanol across Nafion/PVA and pristine Nafion® membranes at different methanol concentrations and temperatures.

Membrane	1 M	2 M	3 M	T (ºC)
Nafion/PVA	$(4.09 \pm 0.09)\cdot10^{-4}$	$(2.82 \pm 0.10)\cdot10^{-4}$	$(2.95 \pm 0.08)\cdot10^{-4}$	70
(19 ± 1 μm)	$(3.16 \pm 0.05)\cdot10^{-4}$	$(2.41 \pm 0.06)\cdot10^{-4}$	$(3.35 \pm 0.10)\cdot10^{-4}$	95
Nafion®	$(4.15 \pm 0.03)\cdot10^{-4}$	$(3.37 \pm 0.08)\cdot10^{-4}$	$(3.16 \pm 0.09)\cdot10^{-4}$	70
(18 ± 1 μm)	$(2.91 \pm 0.07)\cdot10^{-4}$	$(2.39 \pm 0.05)\cdot10^{-4}$	$(2.51 \pm 0.07)\cdot10^{-4}$	95
Nafion/PVA	$(4.03 \pm 0.11)\cdot10^{-4}$	$(3.30 \pm 0.12)\cdot10^{-4}$	$(3.69 \pm 0.14)\cdot10^{-4}$	70
(47 ± 3 μm)	$(3.25 \pm 0.07)\cdot10^{-4}$	$(2.70 \pm 0.08)\cdot10^{-4}$	$(3.07 \pm 0.04)\cdot10^{-4}$	95
Nafion®	$(4.48 \pm 0.09)\cdot10^{-4}$	$(3.63 \pm 0.09)\cdot10^{-4}$	$(3.40 \pm 0.10)\cdot10^{-4}$	70
(46 ± 1 μm)	$(2.80 \pm 0.10)\cdot10^{-4}$	$(2.63 \pm 0.06)\cdot10^{-4}$	$(2.88 \pm 0.06)\cdot10^{-4}$	95

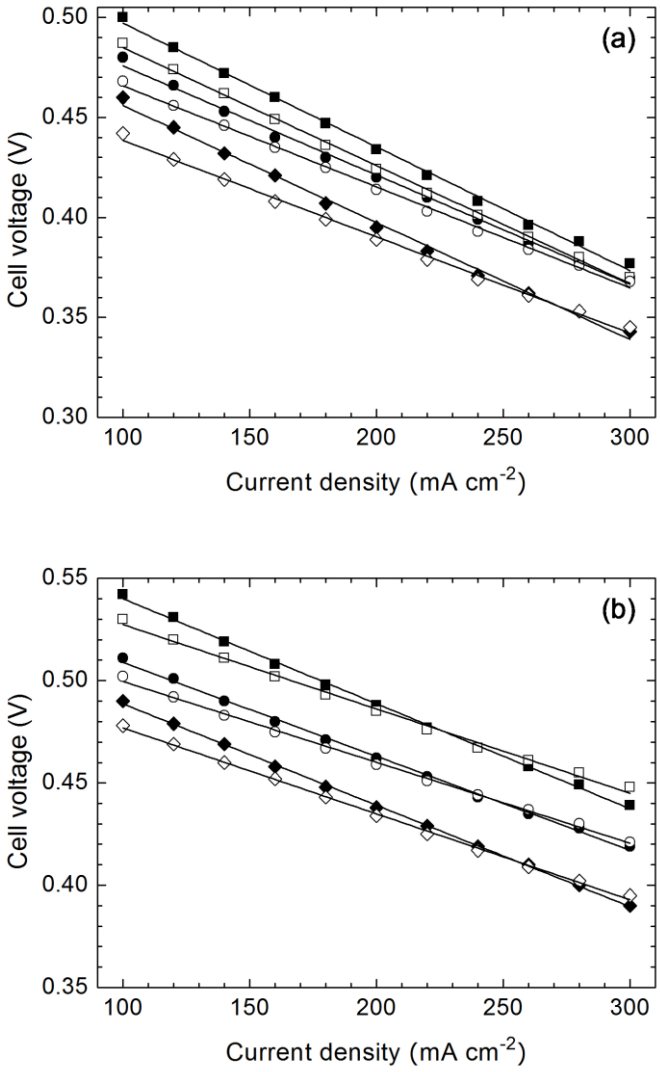

Fig. 8. Profiles of cell voltage versus current density (between 100 and 300 mA cm^{-2}) for MEAs of 46-µm Nafion® (open symbol) and 47-µm Nafion/PVA (filled symbol) membranes operated at (a) 70 ºC, and (b) 95 ºC, with methanol feed concentrations of (square) 1 M, (circle) 2 M, and (diamond) 3 M.

Fig. 8 shows the variation of cell voltage, *V*, versus *i* for MEAs prepared with Nafion® and Nafion/PVA membranes of thickness between 46 µm and 47 µm operated at 70 ºC and 95 ºC with methanol feed concentrations of 1 M, 2 M and 3 M. Since A_3 relates the overvoltage to a combination of protonic resistance, i.e. L/σ, and methanol crossover by electro-osmosis, i.e.

$\chi \cdot J_{eos}$, this latter parameter can be estimated by subtracting L/σ from A_3. In Table 4 we summarize the values of $\chi \cdot J_{eos} = (A_3 - L/\sigma)$ as a function of methanol concentration and temperature for different MEAs. It can be observed from Table 4 that $\chi \cdot J_{eos}$ decreases in the Nafion/PVA membrane in comparison with Nafion® at 70 ºC and methanol concentrations of 1 M and 2 M. However, at the other conditions, $\chi \cdot J_{eos}$ tends to be similar for both Nafion® and Nafion/PVA membranes.

It is also remarkable to notice that the electro-osmotic drag effect becomes reduced with temperature. This behaviour has also been found by other authors [37]. However, Luo *et al*. have reported that electro-osmotic drag coefficient of water in Nafion® membrane raises with increasing temperature due to the higher amount of protons transported by diffusion with relation to those transported by the Grotthuss mechanism [38]. In the case of a methanol solution, the observed phenomenon seems to indicate a weakening of the interaction between protons and methanol molecules in relation to the proton-water system as the temperature increases.

Finally, we have fitted the experimental data of the *i-V* curves with a model based on Eq. (19), and thus, the parameters A_1, i_0 and A_2 have been estimated, while keeping E and A_3 fixed. For A_3, the values calculated for obtaining $\chi \cdot J_{eos}$ have been used. Table 5 summarizes the values of the cited parameters. A_2 has not been included since it resulted to be negligible in all the modeled experiments.

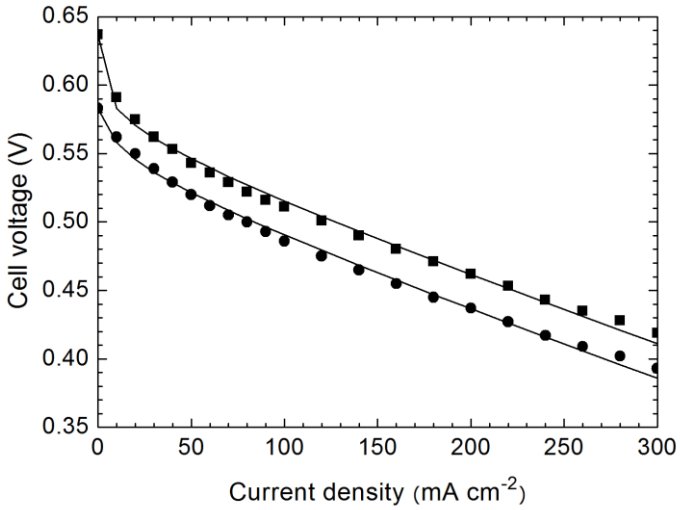

Fig. 9. Fitting between experimental (solid symbol) and modelled (line) results of *i-V* curves obtained with 2 M methanol solutions for (●) a pristine Nafion® membrane of 46 µm thickness measured at 70 ºC, and (■) a Nafion-PVA membrane of 47 µm thickness at 95 ºC.

Table 5. Fitting parameters for the *i-V* curves of Nafion® and Nafion/PVA membranes which showed the best performances using 2 M methanol solutions at 70ºC and 95ºC conditions.

Membrane	E (V)	i_0 (mA cm^{-2})	A_1 (V)	A_3 (Ω cm^{-2})	T (ºC)
Nafion/PVA (19 ± 1 μm)	0.580	2.368	$1.319 \cdot 10^{-2}$	0.481	70
	0.604	1.229	$9.778 \cdot 10^{-3}$	0.401	95
Nafion® (18 ± 1 μm)	0.583	1.618	$1.118 \cdot 10^{-2}$	0.463	70
	0.600	0.636	$9.562 \cdot 10^{-3}$	0.356	95
Nafion/PVA (47 ± 3 μm)	0.618	0.243	$1.324 \cdot 10^{-2}$	0.546	70
	0.637	0.129	$1.138 \cdot 10^{-2}$	0.459	95
Nafion® (46 ± 1 μm)	0.596	0.546	$1.385 \cdot 10^{-2}$	0.505	70
	0.626	0.129	$1.184 \cdot 10^{-2}$	0.395	95

Fig. 9 shows the fitting between some experimental and modelled curves, where it can be observed that Eq. (19) fits very well with the results of performance obtained at 2 M methanol concentration. As usual, the open circuit voltage E sharply decreases from the thermodynamic electromotive force of the cell to a value in the vicinity of 0.58-0.64 V. This sharp decrease is caused by internal currents, activation energy and by fuel crossover. The parameter A_3, which is related to the ohmic resistance of the membrane, decreases in each membrane as the temperature increases due to the activation of the protonic conductivity.

For a similar thickness and temperature, the Nafion/PVA membranes show higher values of A_3 in comparison with those of pristine Nafion®, since the composite membranes have lower protonic conductivity than the Nafion® membranes [23], which is in agreement with their reduced values of ion-exchange capacity (see Table 1). For each membrane, the parameters i_0 and A_1 also show a decrease as the temperature increases. Since both parameters are related with the catalytic activity of the catalyst layer at the electrodes, this would suggest that as the methanol crossover rises with the temperature, the specific activity of the catalyst diminishes as a consequence of the undesired reaction between methanol and oxygen.

4. Conclusions

Novel nanocomposite membranes made up of Nafion® polymer infiltrated between functionalised polyvinyl alcohol (PVA) nanofibres have been prepared and characterised regarding their methanol permeability and DMFC performance. It was found that the reinforcement effect caused by the PVA nanofibres enabled the preparation of composite membranes with very low thickness and good mechanical properties, whereas the

manipulation of pristine Nafion® membranes resulted to be unpractical below a thickness of 50 μm.

The apparent methanol permeability has been distinguished from the true permeability property intrinsic to the membrane material. In this regard, the composite membranes showed a methanol permeability coefficient with one order of magnitude reduction in comparison to pristine Nafion®, as a consequence of the barrier effect caused by the nanofibres. However, the nanofibre phase does not seem to influence the electro-osmotic drag coefficient of methanol, although at certain conditions lower values were observed in the Nafion/PVA membranes. Interestingly, the electro-osmotic drag coefficient of methanol was found to decrease with increasing temperature, as opposed to the water behaviour which has been reported to increase with temperature.

Direct methanol fuel cell tests at different conditions of temperature and methanol concentration showed the maximum performances to be achieved at 95 ºC and 2 M solutions. At those conditions, the Nafion/PVA membranes of 19 μm and 47 μm thickness performed similarly to those Nafion® membranes with comparable thickness.

The incorporation of a nanofibre phase within the Nafion® matrix and the use of thin membranes suggest that significant savings in the consumed amount of Nafion® polymer are able to be potentially afforded while keeping high performances.

Acknowledgements

This research is in the frame of IMIDIC/2009/155 project granted by Generalitat Valenciana through Institute for Small and Medium Industry (IMPIVA) and European Union by FEDER funds. The IMIDIC/2009/155 project belongs to the call for Technological Centres of IMPIVA Network.

References

[1] B. Smitha, S. Sridhar, A.A. Khan, J. Membr. Sci. 259 (2005) 10 (review).
[2] S. Tan, D. Bélanger, J. Phys. Chem. 109 (2005) 23480.
[3] D.H. Jung, S.Y. Cho, D.H. Peck, D.R. Shin, J.S. Kim, J. Power Sources 106 (2002) 173-177.
[4] M. Fujimura, T. Hashimoto, H. Kawai, Macromolecules 14 (1981) 1309.
[5] J. Müller, G. Frank, K. Colbow, D. Wilkinson, in: W. Vielstich, A. Lamm, H.A. Gasteiger (Eds.), Handbook of Fuel Cells-Fundamentals, Technology and Applications, vol. 3, Wiley, Chichester, 2003 (Chapter 62).
[6] M. Neergat, K.A. Friedrich, U. Stimming, Fuel Cells 2 (2002) 25-30.
[7] T. Shimizu, T. Naruhashi, T. Momma, T. Osaka, Electrochemistry 70 (2002) 991.

[8] C.-Y. Chen, J.I. Garnica-Rodriguez, M.C. Duke, R.F. Dalla Costa, A.L. Dicks, J.C. Diniz da Costa, J. Power Sources 166 (2007) 324.
[9] A. Sungpet, J. Membr. Sci. 226 (2003) 131-134.
[10] Q.M. Huang, Q.L. Zhang, H.L. Huang, W.S. Li, Y.J. Huang, J.L. Luo, J. Power Sources 184 (2008) 338-343.
[11] N. Li, J.Y. Lee, L.H. Ong, J. Appl. Electrochem. 22 (1992) 512.
[12] C. Barthet, M. Guglielmi, Electrochim. Acta 41 (1996) 2791.
[13] P. Aldebert, P. Audebert, M. Armand, G. Bidan, M. Pineri, Chem. Soc., Chem. Commun. (1986) 1636.
[14] S. Tan, A. Laforgue, D. Bélanger, Langmuir 19 (2003) 744.
[15] K.A. Mauritz, D.A. Mountz, D.A. Reuschle, R.I. Blackwell, Electrochim. Acta 50 (2004) 565-569.
[16] Q. Deng, Y. Hu, R.B. Moore, C.L. McCormick, K.A. Mauritz, Chem. Mater. 9 (1997) 36-44.
[17] N. Miyake, J.S. Wainright, R.S. Savinell, J. Electrochem. Soc. 148 (8) (2001) A905-A909.
[18] W.C. Choi, J.D. Kim, S.I. Woo, J. Power Sources 96 (2001) 411.
[19] Z.G. Shao, X. Wang, I.M. Hsing, J. Membr. Sci. 210 (2002) 147.
[20] D. Kreuer, Chem. Mater. 5 (1996) 610.
[21] J.F. Synder, M.A. Ratner, D.F. Shriver, Solid State Ionics 147 (2002) 249.
[22] S.J. Paddison, Annu. Rev. Mater. Res. 33 (2003) 289.
[23] S. Mollá, V. Compañ, J. Membr. Sci. 372 (2011) 191-200.
[24] H.-L. Lin, T.L. Yu, L.N. Huang, L.C. Chen, K.S. Shen, G.B. Jung, J. Power Sources 150 (2005) 11-19.
[25] V. Compañ, A. Andrio, A. López-Alemany, E. Riande, M.F. Refojo, Biomaterials 23 (2002) 2767-2772.
[26] C.-H. Ma, T. Leon Yu, H.-L. Lin, Y.-T. Huang, Y.-L. Chen, U.-S. Jeng, Y.-H. Lai, Y.-S. Sun, Polymer 50 (2009) 1764-1777.
[27] N.W. DeLuca, Y.A. Elabd, J. Membr. Sci. 282 (2006) 217-224.
[28] P. Mukoma, B.R. Jooste, H.C.M. Vosloo, J. Membr. Sci. 243 (2004) 293-299.
[29] D.W. Kim, H.-S. Choi, C. Lee, A. Blumstein, Y. Kang, Electrochim. Acta 50 (2004) 659-662.
[30] J.-C. Tsai, H.-P. Cheng, J.-F. Kuo, Y.-H. Huang, C.-Y. Chen, J. Power Sources 189 (2009) 958-965.
[31] J. Larminie, A. Dicks, Fuel Cell System Explained, John Wiley & Sons Ltd., Chichester, England, 2000 (Chapter 3).
[32] Z. Qi, A. Kaufman, J. Power Sources 110 (2002) 177-185.
[33] V.S. Silva, A. Mendes, L.M. Madeira, S.P. Nunes, J. Membr. Sci. 276 (2006) 126-134.
[34] G. Murgia, L. Pisani, A.K. Shukla, K. Scott, J. Electrochem. Soc. 150 (2003) A1231-A1245.
[35] K. Scott, W. Taana, J. Cruickshank, J. Power Sources 65 (1997) 159-171.
[36] L.-N. Huang, L.-C. Chen, L.T. Yu, H.-L. Lin, J. Power Sources 161 (2006) 1096-1105.
[37] L.-C. Chena, T.L. Yu, H.-L. Lin, S.-H. Yeh, J. Membr. Sci. 307 (2008) 10-20.
[38] Z. Luo, Z. Chang, Y. Zhang, Z. Liu, J. Li, Int. J. Hydrogen Energy 35 (2010) 3120-3124.

Paper 3

International Journal of Hydrogen Energy 36 (2011) 9886-9895
(Adapted to thesis)

Novel ultrathin composite membranes of Nafion/PVA for PEMFCs

Sergio Mollá[a,b], Vicente Compañ[a,b], Enrique Gimenez[c], Alberto Blazquez[d], Idoia Urdanpilleta[d]

[a] Dpto. Termodinámica Aplicada, ETSII, Universidad Politécnica de Valencia, 46022 Valencia, Spain.
[b] Instituto de Tecnología Energética (ITE), Universidad Politécnica de Valencia, 46022 Valencia, Spain.
[c] Dpto. de Ingeniería de Materiales, Universidad Politécnica de Valencia, 46022 Valencia, Spain.
[d] CIDETEC-IK4, Centro de Tecnologías Electroquímicas, Parque Tecnológico de San Sebastián, Paseo Miramón 196, 20009 San Sebastián, Spain.

Abstract

The electrospinning approach is an easy and useful method to fabricate porous supports with tailored properties for the preparation of impregnated membranes with enhanced characteristics. Therein, this technique was used to obtain polyvinyl alcohol (PVA) nanofibre mats in which Nafion® polymer was infiltrated. These Nafion/PVA membranes were characterised in their mechanical properties, proton conductivity and fuel cell performance. Conductivity of the composite membranes was below the showed by pristine Nafion® due to the non-ionic conducting behaviour of the PVA phase, although the incorporation of the PVA nanofibres strongly reinforced the mechanical properties of the membranes. Measurements carried out in a single cell fed with H_2/Air confirmed the high performance exhibited by a 19-μm thick nanofibre reinforced membrane owing to its low ionic resistance. These reasons make ultrathin (< 20 μm) Nafion/PVA composite membranes promising candidates as low cost ion-exchange membranes for fuel cell applications.

Keywords: Nanocomposite, Nafion® membranes, PVA nanofibres, mechanical properties, conductivity, PEMFC performance.

1. Introduction

The synthesis of cation-exchange membranes that combine low protonic resistance and good mechanical properties and thermal stability in hot oxidative atmospheres is nowadays a flourishing field of research. The interest in membranes arises in part from the potential use of these materials as electrolytes in low temperature fuel cells [1].

Perfluorinated ionomers are currently the best materials to develop polymer electrolyte membranes (PEM) that meet the requirements of high protonic conductivity and good mechanical and thermal stability at temperatures lying in the range 50-90 ºC [2-4]. However, the need of working at higher temperatures requires the development of membranes that maintain high conductivity in low humidity environments. This is a key issue in the progress of the development of medium temperature PEM fuel cells (PEMFC) for practical purposes [5,6]. Fillers may improve water retention in polyelectrolytes under low relative humidity (RH) conditions thus preserving the protonic conductivity of membranes at temperatures above 100 ºC [5,7].

Fillers may also reduce fuel and gas permeabilities across membranes by increasing tortuosity [8]. The information at hand suggests that modification of Nafion® membranes can be performed by inclusion of inorganic fillers such as oxides, phosphates and heteropolyacids [7-12].

Pursuing in this line of research, many researchers report the preparation of hybrid membranes by incorporating phenyl-sulfonated inorganic materials into Nafion® in order to build composite membranes with improved ionic conductivity and mechanical properties when the membranes are working at moderate and high temperatures [13]. An alternative to increase the conductivity of a membrane is to reduce its thickness [14], which also favours back diffusion of water from cathode to anode [15]. However, this procedure is not that simple with Nafion® materials because their mechanical properties diminish drastically when the membranes become very thin.

Porous polytetrafluoroethylene (PTFE) films, under the Gore trademark, have been proposed as supports for Nafion® resins, in impregnated-type membranes, for the preparation of mechanically reinforced membranes of relatively thin thickness for PEMFC and Direct Methanol Fuel Cell (DMFC) applications [16,17]. Furthermore, hybridizing the Nafion® matrix with nano-inorganic particles, such as silica and zirconium phosphate, results in Nafion/PTFE membranes which demonstrate improved performance than pristine Nafion® at temperatures above 100 ºC [18,19].

PTFE belongs to the family of perfluorinated polymers, the same as Nafion®, and thus environmental and cost issues can still concern. Porous supports prepared from different materials in a convenient and easy way

would be a clear advantage. In this sense, electrospinning is nowadays being proposed for the fabrication of porous mats of nanofibres based on polyvinylidene fluoride (PVDF) [20] and polyvinyl alcohol (PVA) [21].

Recently, we have prepared novel nanocomposite membranes made up of Nafion® polymer infiltrated between sulfonic acid-functionalised nanofibres of polyvinyl alcohol. These membranes, presenting thicknesses from around 20 μm till 100 μm, have been characterised regarding their thermal stability, proton conductivity, methanol permeability and DMFC performance [22,23]. It was found that the reinforcement effect caused by the PVA nanofibres enabled the preparation of composite membranes of very low thickness and good mechanical properties, whereas the manipulation of pristine Nafion® membranes under fully hydrated conditions showed to be unpractical below a thickness of 50 μm. The results obtained let us to conclude that the thinner Nafion/PVA composite membranes present interesting transport properties as solid electrolytes for fuel cells as well as for separation processes based on membrane technologies.

In this work we have prepared cast Nafion® membranes and Nafion/PVA nanocomposite membranes of similar thickness between each other, ranging from 18 μm to 60 μm, with the aim of investigating and comparing the mechanical properties of the membranes through isothermal stress-strain curves and by dynamic mechanical thermal analysis. The properties were measured with membranes under dry conditions to neglect any effect of water.

The in-plane proton conductivity of both Nafion® and Nafion/PVA membranes has been measured at different conditions of relative humidity at 80 ºC. The differences observed between the membranes in function of their thickness are discussed.

Finally, fuel cell performance tests of membrane electrode assemblies (MEAs) were also investigated by measuring their polarization curves in different operating conditions. The differences of performance distinguished between the membranes are discussed, paying special attention on the behaviour as a result of the membrane thickness.

2. Experimental

2.1. Materials

The Nafion® dispersion (DuPont Co.) was 20 wt% of 1 meq g^{-1} IEC Nafion® diluted in a mixed solvent of water, propanol, ethanol and unspecified ethers. The Nafion® was solvent exchanged by casting in order to obtain a 5 wt% solution in isopropanol and water (with isopropanol/water = 4/1, w/w). This

ratio has been previously reported to be suitable for Nafion® infiltration into porous membranes [17,24].

Polyvinyl alcohol, PVA Mowiol 28-99 grade, was kindly supplied by the company Kuraray Europe GmbH.

Isopropanol extra pure and cetyltrimethylammonium bromide (CTAB) were purchased from Acros Organics, and 4-formyl-1,3-benzenedisulfonic acid disodium salt from Sigma-Aldrich.

2.2. Preparation of membranes

2.2.1. Nafion® membranes

The solvent exchanged solution, with a 5 wt% Nafion® content in isopropanol and water, was used for the casting of pristine Nafion® membranes with thickness between 18 μm and 60 μm. The thickness was controlled in function of the volume of solution loaded in Petri glass dishes and afterwards evaporated in an oven at 60 ºC overnight.

The respective Nafion® membranes were annealed at 125 ºC for 90 min in the oven and then removed from the Petri dish by adding water.

The last step was the conditioning of the membranes by treatment with water at 85 ºC for 30 min, followed by immersion in a 3 wt% hydrogen peroxide solution during 1 h at 80 ºC and further protonation at the same temperature by ion-exchange with a 1 M chlorhydric acid solution for another 1 h. Finally, the cast Nafion® membranes were washed with hot water at 85 ºC, dried and stored.

2.2.2. PVA nanofibres

Porous PVA mats were produced by a standard electrospinning setup (Yflow S.L., Málaga, Spain) through the feeding of a water based solution of PVA (0.005:1:10 wt. CTAB:PVA:water). CTAB was used as surfactant in order to reduce surface tension of water and improve electrospinning ability.

The distance between the needle and the planar collector was fixed at 25 cm, the solution flow rate at 0.5 ml h^{-1}, the voltage of the needle at +11 kV and the voltage of the collector at -5 kV. Mats electrospinned during 8 h showed a thickness around 120 ± 10 μm, meanwhile those obtained after 4 h were aprox. 60 ± 5 μm. The collected mats were heated during 3 h at 170 ºC in a vacuum atmosphere (250 mbar pressure) with the purpose of removing water and increasing manipulability.

2.2.3. Chemical functionalization of PVA nanofibres

The PVA mats were mounted on a round steel frame and then introduced into a bath with a 0.04 M concentration of the 4-formyl-1,3-benzenedisulfonic acid disodium salt and 0.1 M of chlorhydric acid as a catalyst for the schematic reaction (1), solved in a mixture composed of isopropanol/water (70/30 v/v):

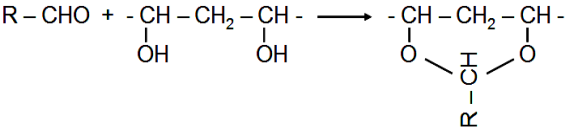

(1)

Reaction (1) was carried out at 60 ºC for 2 h. The sodium ions present on the surface of the functionalised PVA nanofibres were exchanged with protons through immersion in a bath of isopropanol/water (70/30 v/v) containing chlorhydric acid with a 0.3 M concentration.

Ion-exchange was finished by washing of the mat with a solution of isopropanol/water (70/30 v/v) and further immersion in pure isopropanol. Finally, the mats were placed in an oven at 60 ºC for drying.

The last step was the crosslinking of the PVA chains in order to raise mechanical and thermal properties of the nanofibres. This was accomplished by reaction with glutaraldehyde vapour in a closed vessel during 24 h at room temperature. At the bottom of such vessel, a 50 wt% water solution of glutaraldehyde was placed and let it to evaporate slowly.

After the crosslinking process, the mats were heated at 100 ºC for 15 min with the aim to remove adsorbed glutaraldehyde and water. At this point, the PVA nanofibres were very stable and could not be dissolved in boiling water.

2.2.4. Nanofibre-reinforced Nafion® membranes

The functionalised and crosslinked mats, still mounted on the frame, were impregnated with the 5 wt% Nafion® solution in isopropanol and water (4/1 w/w, respectively).

Each impregnation step was carried out by introducing the PVA mat into the Nafion® dispersion for 5 min and followed by evaporation in an oven at 100 ºC for 5 min more. This was repeated 8 times in every mat until an outer visible Nafion® layer was formed.

The prepared nanocomposite membranes were annealed at 125 ºC for 90 min under a slight pressure (by a hot press) in order to remove any residual solvent and enhance Nafion® can accommodate into the fibrillous structure.

Finally, the membranes were conditioned by treatment with water at 85 ºC for 30 min, followed by an oxidation with 3 wt% hydrogen peroxide during 1 h at 80 ºC and further protonation by 1 h ion-exchange with a 1 M chlorhydric acid solution at 80 ºC. Then, the Nafion/PVA membranes were washed with hot water at 85 ºC, dried and stored.

The thickness of the composite membranes was dependent on the deposition time of the electrospun nanofibres mats, and it was measured with a digital length gauge (Heidenhain, model MT12). The membrane thickness was calculated from the average value after ten measurements on different parts of the sample. The pertinent results are varying from 19 μm to 61 μm.

3. Membranes characterization

3.1. FTIR analysis

IR spectroscopy was used to check polymer matrix-filler interactions and molecular structure of the materials. The spectra was obtained using a JASCO, FT/IR6200 with microscope IRT-300 IRTRON.

3.2. Mechanical tests

Dynamic mechanical thermal analysis (DMTA) was performed with a Perkin-Elmer DMA7e analyzer at a constant frequency of 1 Hz from 20 ºC to 400 ºC. A temperature ramp rate of 5 ºC min^{-1} and a constant strain of 0.1% in tensile mode were used.

All the samples were dried in a vacuum steam autoclave at 25 ºC. The experiments were carried out using a rectangular tension fixture with a gap width of 10 mm. The samples were cut in pieces of 15 x 10 mm^2 and measurements of thickness and width were conducted by means of a length calibrator.

Static tensile strength tests were carried out at room temperature using a Microtest Tensile stage controller DEBEN (Gatan). A crosshead rate of 0.4 mm min^{-1} collecting data each 500 ms was used in each measurement. The separation between the clamps was fixed at 10 mm and the maximum force was set at 150 N with an initial static force of 0.1 N. The samples were also cut in rectangular pieces with 15 x 10 mm^2 dimensions.

3.3. Proton conductivity

The proton conductivity of the membranes was measured by using a BT-512 In-Plane Membrane Conductivity Test System (BekkTech LLC) under N_2

atmosphere. The in-plane 4 electrode measurement (scanning DC with voltage sweeps from +0.1 V to -0.1 V) was performed at 80 ºC as a function of relative humidity (%RH) and the conductivity values (mS cm^{-1}) taken from stable regions were plotted as a function of %RH.

3.4. Fuel cell tests

The measurements were performed using a single cell hardware of 5 cm^2 active area with serpentine anode and cathode flow fields. MEAs of different membranes were prepared using a catalyst ink which consisted of a Nafion® dispersion, isopropanol and 60 wt% Pt on carbon particles. The catalyst ink was sprayed onto the gas diffusion layer (GDL) made up of carbon paper (Freudenberg). The anode and cathode loadings were kept constant at 0.5 mg Pt cm^{-2}.

The cell was initially tested at 60 ºC with fully humidified H_2 and Air supplied at the anode and cathode sides. The fuel and oxidant stoichiometry were 1.5 and 3.0, respectively. Typically, tests were performed at constant voltage and 100% RH, supplemented with polarization (*i-V*) curves which started from open circuit voltages (OCV) to 0.4 V.

4. Results and discussion

4.1. FTIR analysis

The results of FTIR spectra corresponding to a pristine Nafion® membrane, a PVA nanofibre mat and a Nafion/PVA composite membrane are showed in Fig. 1.

As it can be observed, Nafion® shows characteristic absorption peaks between 910 cm^{-1} and 1410 cm^{-1}. Vibrational bands associated with the sulfonic acid groups are found at 910 cm^{-1} and 1410 cm^{-1} corresponding to the S=O and S-OH stretching bands [25]. Additionally, a band at about 1057-1062 cm^{-1} is assigned to -SO_3H groups [25-27]. The intense bands at ca. 1200 cm^{-1} and 1300 cm^{-1} are assigned to CF_2 vibrations and stretching of the C-F bonds [25,26]. The small peaks towards 1700 cm^{-1} can be explained by the presence of a low water content in form of hydronium ions [27].

The FTIR spectra of PVA show a broad peak around 3297 cm^{-1} indicating stretching of the hydroxyl groups, whereas the peak at 1093 cm^{-1} indicates the C-O stretch of the secondary alcoholic groups. The peak at 2918 cm^{-1} is due to symmetric C-H stretching in -CH_2- species [28].

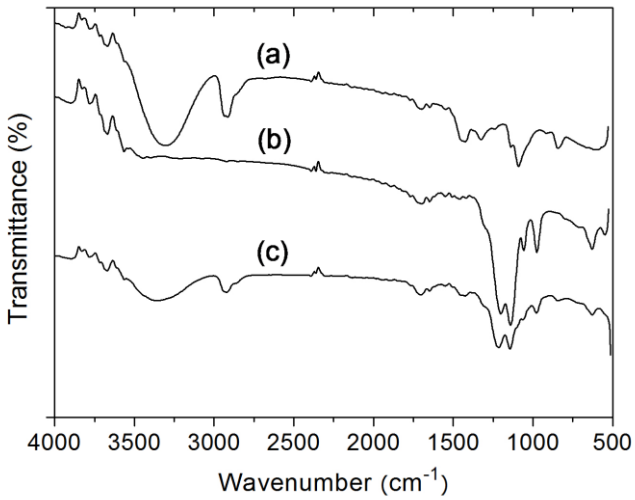

Fig. 1. FTIR spectra for (a) PVA nanofibre, (b) pristine Nafion® and (c) Nafion/PVA membrane.

The composite membrane of Nafion/PVA reveals an FTIR curve clearly dominated by the Nafion® bands. However, the bands corresponding to the stretching of both OH groups and C-H bonds in PVA are still able to be distinguished from the spectra.

4.2. Mechanical properties

The real part of the elastic modulus *E'*, so-called storage modulus, and the loss tangent *Tan δ* of the membranes were measured in dry conditions by means of dynamic mechanical thermal analysis at a frequency of 1 Hz. The results are shown in Fig. 2 and Fig. 3.

It is important to understand the behaviour of these membranes in the vicinity of 80 ºC as this is the most typical operating temperature in many fuel cell applications. Curves in Figs. 2 and 3 reveal a change in storage modulus and *Tan δ* over a large temperature range for Nafion® and Nafion/PVA membranes. Two temperature regions are discerned for the Nafion® membranes. Between room temperature and 80 ºC, *E'* and *Tan δ* of Nafion® show practically a constant behaviour. However, above 80 ºC the storage modulus shows a continuous loss in stiffness with increasing temperature, whereas the loss tangent shows a pronounced increment up to a maximum value reached around 110 ºC, which is attributed to the α-relaxation associated with the glass-transition temperature (T_g) of dry Nafion® polymer. Similar results have been found by other researchers [29-31].

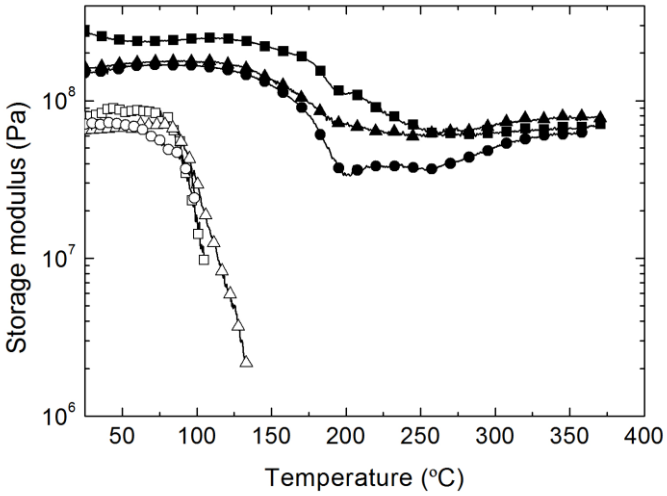

Fig. 2. Storage modulus E' at 1 Hz as a function of temperature for Nafion® (□) 60 µm, (Δ) 37 µm, (○) 28 µm; and Nafion/PVA membranes (■) 61 µm, (▲) 39 µm, (●) 25 µm.

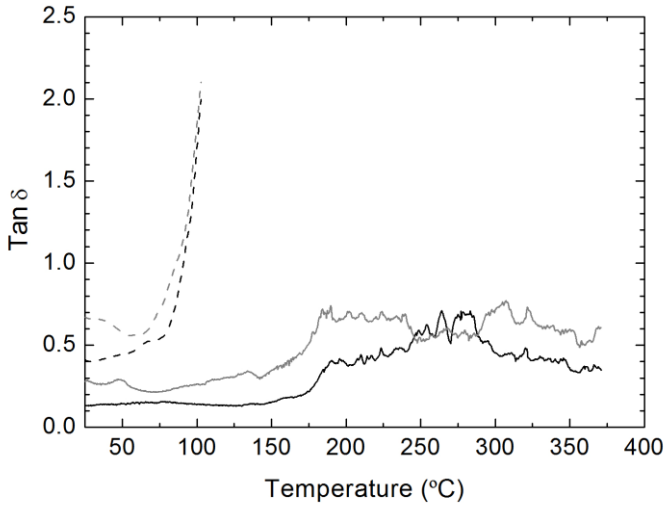

Fig. 3. Loss tangent Tan δ at 1 Hz as a function of temperature for Nafion® (dashed grey line) 60 µm, (dashed black) 37 µm; and Nafion/PVA membranes (solid black line) 61 µm, (solid grey) 39 µm.

In comparison with their homologous membranes of pristine Nafion®, the composite membranes present higher *E'* modulus associated with the significant mechanical reinforcement provided by the PVA nanofibres. A close inspection of Fig. 2 shows that *E'* of the composite membranes remains constant up to about 150 ºC. Above this temperature, *E'* starts to decline and

only near 200 ºC a pronounced drop is observed. This may be due to the softening of the crystalline phase of the PVA which melts between 200 ºC and 230 ºC [22,32]. However, above 200 ºC the storage modulus tends to reach a plateau region which goes beyond 300 ºC. This suggests that crosslinking of the PVA phase by means of the glutaraldehyde vapour forms stable bonds able to keep good mechanical properties at very high temperatures. On the other hand, thermal decomposition of PVA chains into polyenes and their further cyclization reactions might provide additional crosslinks able to maintain a rigid structure at those temperatures [33,34].

From the loss tangent profiles of the Nafion/PVA membranes plotted in Fig. 3, we cannot conclude the presence of a clear α-relaxation although *Tan δ* slightly increases above 150 ºC and especially near 200 ºC. The values of *Tan δ* of the composite membranes are considerably lower than those observed for Nafion®, which confirms the enhanced mechanical stability derived from the introduction of nanofibres within the Nafion® matrix.

Static mechanical testing of the samples were performed and their results of stress versus strain are presented in Fig. 4 and Fig. 5 for Nafion® and Nafion/PVA membranes, respectively. In Fig. 4, the Nafion® membranes show higher values of ultimate tensile strength (σ_{ult}) and yield strength (σ_y) with increasing thickness. Strain values follow a similar trend. It is remarkable the large values of strain found for the Nafion® membranes, which can explain the well known ductile behaviour associated with this kind of fluoropolymers [35].

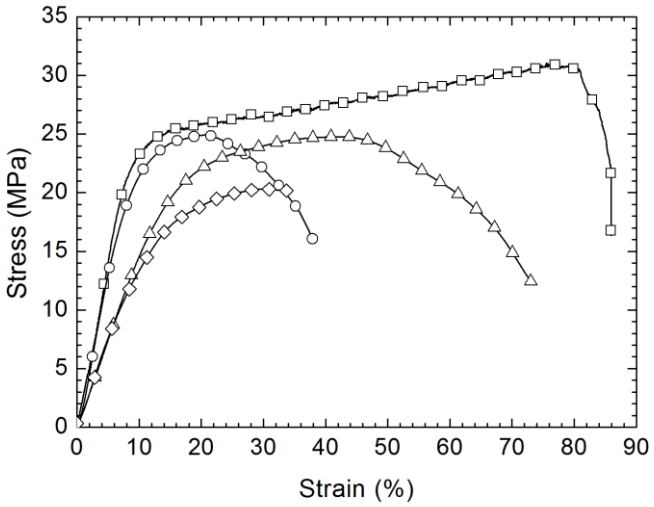

Fig. 4. Stress-strain curves for Nafion® membranes of (□) 60 µm, (○) 46 µm, (Δ) 37 µm, and (◇) 18 µm thickness.

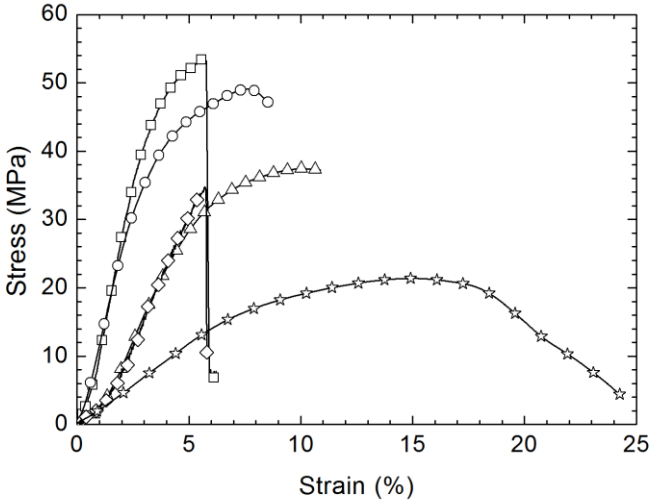

Fig. 5. Stress-strain curves for composite Nafion/PVA membranes of (□) 61 µm, (○) 47 µm, (Δ) 39 µm, and (◇) 19 µm thickness. A (☆) PVA nanofibre mat (10 µm) has been included for comparative purposes.

Electrospun nonwoven mats usually also show large strain values and a ductile behaviour in which the mechanical properties mainly depend on the morphology and bonding structure of the fibres such as the arrangement and orientation between fibres [36,37]. In this sense, the PVA mat in Fig. 5 does not exhibit a defined rupture point but a continuous tear of the mat as a consequence of the inter-fibre sliding between the random oriented nanofibres.

The ultimate tensile strength of the Nafion/PVA membranes as shown in Fig. 5 increases with increasing thickness too. However, the strain seems to follow two different behaviours, increasing up to the 39 µm thickness range, as it would be expected, and then diminishing from that point with increasing thickness. This unusual observation may indicate that Nafion® and PVA nanofibre make a strong bond with each other, and thus, large deformation of both Nafion® and fibres phases are hindered. If a force is applied, inter-fibre sliding causes the fibres to move apart following the direction of force and to get closer perpendicularly to such a direction (necking). When Nafion® is filling the space between the fibres, the first physical consequence will be a strong friction which will difficult the movement of the nanofibres. Additionally, the necking phenomenon will exert a compression force over the confined Nafion® phase, and the resulting counterforce of Nafion® will also block displacement of the nanofibres. All these effects acting jointly should be responsible of the small strain values showed by the nanocomposite membranes.

Table 1. Mechanical parameters of Young's modulus (E), yield strength (σ_y), strain at yield point (ε_y), ultimate tensile strength (σ_{ult}) and strain at ultimate tensile strength point (ε_{ult}) for Nafion® and Nafion/PVA membranes of different thicknesses. The number after the sample's name indicates the average thickness in μm.

Sample	E (MPA)	σ_y (MPa)	ε_y (%)	σ_{ult} (MPa)	ε_{ult} (%)
Nafion® 18	112 ± 2	17.5 ± 0.2	15.8 ± 0.3	20.3	30.9
Nafion® 37	131 ± 7	19.7 ± 0.5	15.3 ± 0.7	24.8	41.6
Nafion® 46	215 ± 7	21.7 ± 0.3	10.3 ± 0.4	24.9	20.4
Nafion® 60	245 ± 1	22.7 ± 0.2	9.4 ± 0.1	31.0	75.8
NanoPVA mat 10	221 ± 11	16.6 ± 0.4	7.6 ± 0.3	21.4	14.9
Nafion/PVA 19	607 ± 6	34.6 ± 0.5	5.7 ± 0.1	34.8	5.8
Nafion/PVA 39	559 ± 6	30.6 ± 0.5	5.6 ± 0.1	37.5	10.2
Nafion/PVA 47	1103 ± 5	39.4 ± 0.5	3.7 ± 0.1	49.1	7.6
Nafion/PVA 61	1198 ± 3	49.7 ± 0.5	4.3 ± 0.1	53.5	5.8

In Table 1 we compare the mechanical parameters obtained from Figs 4 and 5 for Nafion® and Nafion/PVA membranes. In all cases, the composite membranes show much higher values of σ_y, σ_{ult} and E (Young's modulus), while strains ε_y and ε_{ult} are much more reduced in comparison with pristine Nafion®. This is again a proof of the good mechanical reinforcement achieved by the incorporation of PVA nanofibre mats into the Nafion® matrix.

4.3. Conductivity measurements

The ionic conductivity of the membranes was measured in-plane by means of a test bench developed by CIDETEC according to the criteria of the U.S. Department of Energy (DOE), which allows obtaining automatically the conductivity of a membrane at different relative humidity conditions (RH) as shown in Fig. 6.

First, we can observe that conductivity of both Nafion® and composite membranes increases with water content (%RH) in an exponential manner as it has been observed before [38]. Relative humidity is directly related to water activity, and it is known that high values of water activity involves a larger number of water molecules attached to each sulfonic acid group and thus increasing overall proton conductivity.

In our previous work, through-plane proton conductivity of Nafion/PVA membranes was measured by impedance spectroscopy from MEAs fully hydrated in liquid water at different temperatures. It was observed that proton conductivity of the composite membranes increased with increasing thickness up to a maximum value found at 47 μm, and the reason was

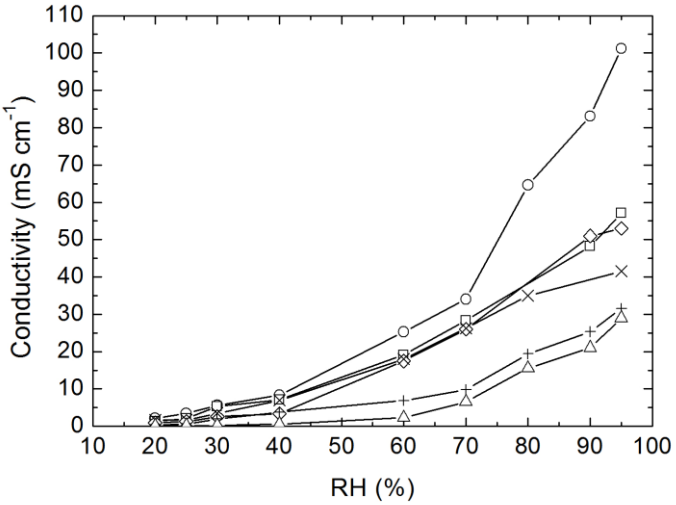

Fig. 6. Proton conductivities of Nafion® and Nafion/PVA membranes as a function of relative humidity at 80 ºC: (○) Nafion-212 (50 µm), (□) Nafion/PVA 19 µm, (◇) Nafion/PVA 25 µm, (X) Nafion/PVA 31 µm, (+) Nafion/PVA 39 µm, and (Δ) Nafion/PVA 47 µm.

explained as a consequence of the preparation method [22]. However, a detailed inspection of Fig. 6 reveals an opposite trend, proton conductivities decreasing with increasing thickness when conductivities of the Nafion/PVA membranes are measured in-plane. Again, a feasible explanation for those differences has to be related to the preparation method and the special membrane structure. The number of nanofibre layers within the Nafion® matrix of composite membranes must increase with increasing thickness since electrospun nanofibres are deposited on the collector oriented parallel to the plane, and then it may be assumed that percolation of the Nafion® phase following the in-plane direction will become more restricted as more compacted layers of nanofibres are present. Thus, large anisotropies are introduced in the membrane properties due to this nanofibre morphology.

In Fig. 6, the conductivity of pristine Nafion® exceeds considerably the conductivities reached by the composite membranes at high RH levels, in which the Nafion® conductivity is strongly activated by the water content. This was also observed in the cited work [22] and it was attributed to the non-ionic conducting behaviour of the bulk PVA phase.

Interestingly, at RH levels under 40%, the conductivities of the Nafion/PVA membranes, especially of those thinner, reach values close to those exhibited by the Nafion® membrane, which suggests a higher relative capacity of the composite membranes to work under low humidity conditions.

4.4. Fuel cell performance

The performance of MEAs prepared with Nafion/PVA membranes measured in a single cell operating with H_2/Air was evaluated over a long operation time (6-10 h) at a constant voltage of 0.5 V and 100% RH in anode and cathode. A Pt loading of 0.5 mg cm^{-2} per electrode was used. In Fig. 7 it is shown the plot of current density versus time for such Nafion/PVA membranes at different temperatures, i.e. 70 ºC, 80 ºC and 90 ºC.

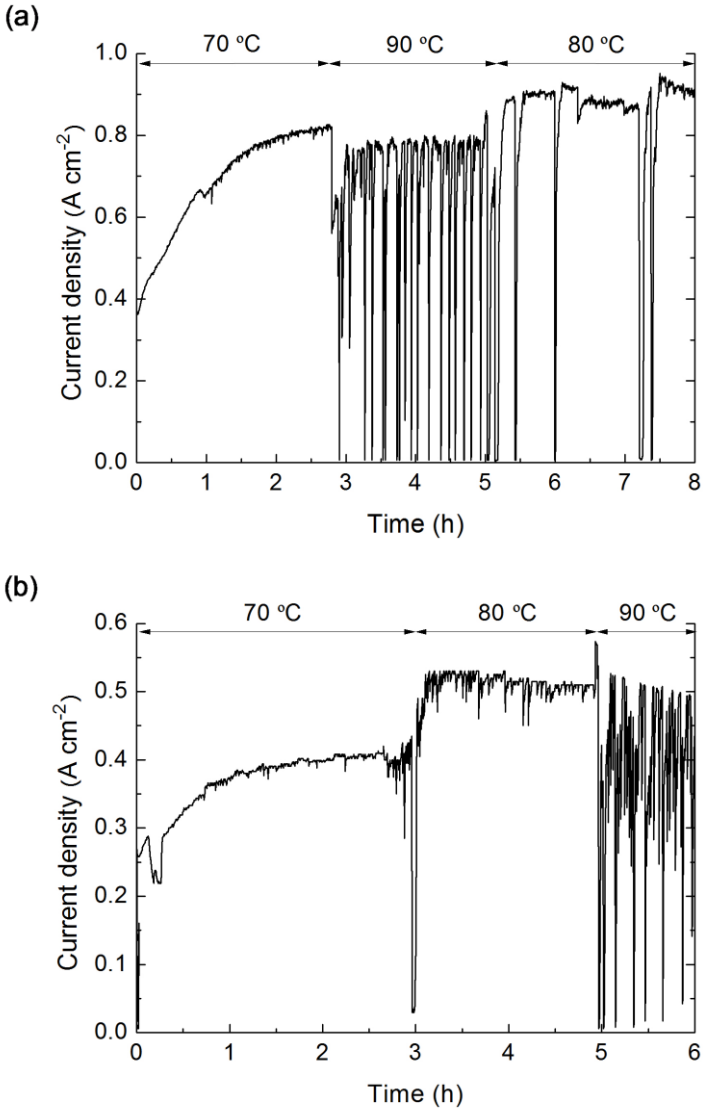

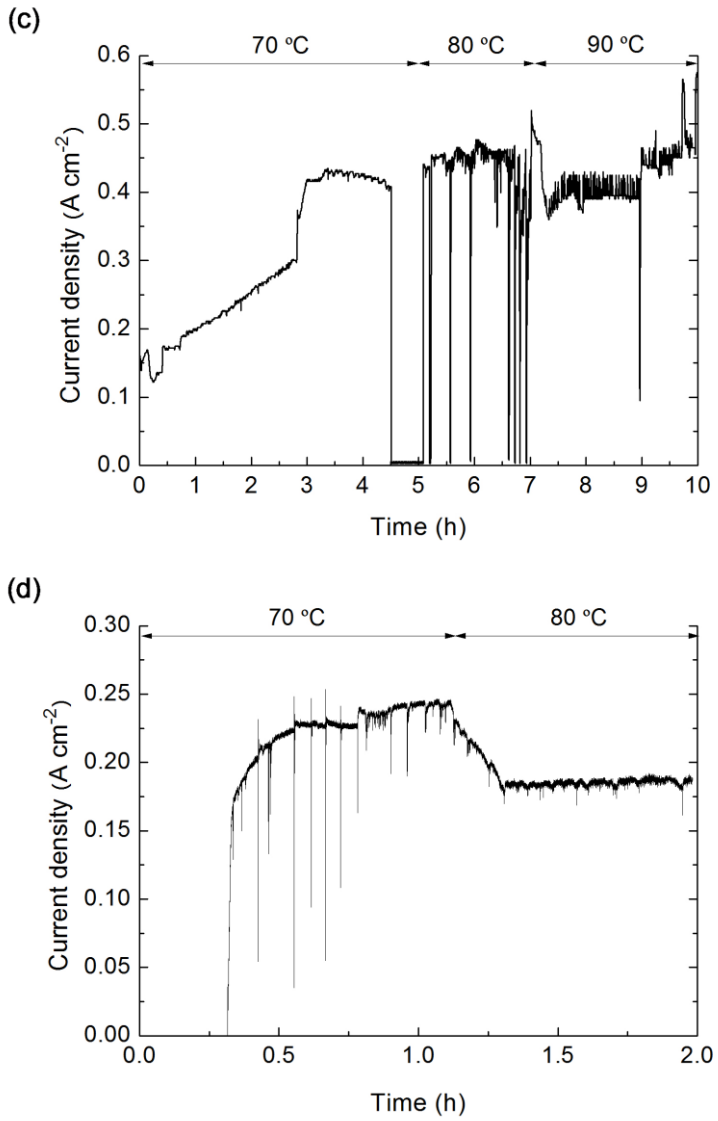

Fig. 7. Profiles of current density versus time at different temperatures under a constant voltage of 0.5 V for Nafion/PVA membranes of (a) 19 µm, (b) 25 µm, (c) 31 µm, and (d) 47 µm thickness. Conditions: 100% RH in anode and cathode under H_2/Air operation.

The current densities generally follow the trend: i(90 ºC) ≤ ≤ i(70 ºC) < i(80 ºC). Between 80 ºC and 90 ºC a certain degree of drying of the membrane and/or the catalyst layers can occur and it would explain the observed drop in performance.

Paying attention to the profiles obtained at 80 ºC, it is clearly observed that performance increases with decreasing thickness. Obviously, the thinnest membranes should present the lowest protonic resistances. Average current densities at 80 ºC range from about 0.19 A cm^{-2} up to 0.92 A cm^{-2}, i.e. 0.19, 0.45, 0.52 and 0.92 A cm^{-2}, for the Nafion/PVA membranes of 47 μm, 31 μm, 25 μm and 19 μm thickness, respectively.

The polarization curves of MEAs containing Nafion/PVA membranes of 19 μm, 25 μm and 31 μm are shown in Fig. 8 under operation with H_2/Air at 80 ºC and 100% RH in anode and cathode. In all cases, an open circuit voltage (OCV) near 1.0 V is found, which is a well known typical value for Nafion® membranes.

The cell voltage of a PEM fuel cell can be modelled by means of Eq. (2) as reported by several authors [39-41],

$$V = V_{OC} - A \cdot \ln\left(\frac{i}{i_0}\right) - R \cdot S \cdot i - m \cdot \exp(n \cdot i) \qquad (2)$$

where V is the cell voltage, V_{OC} the reversible open circuit voltage, i the cell current density, i_0 the forward and reverse (exchange) current density at equilibrium in open circuit conditions, $R{\cdot}S$ is the protonic resistance of the membrane per unit of area, and m and n are empirical parameters associated with mass transport limitation phenomena. Finally, A is the sum of the slopes

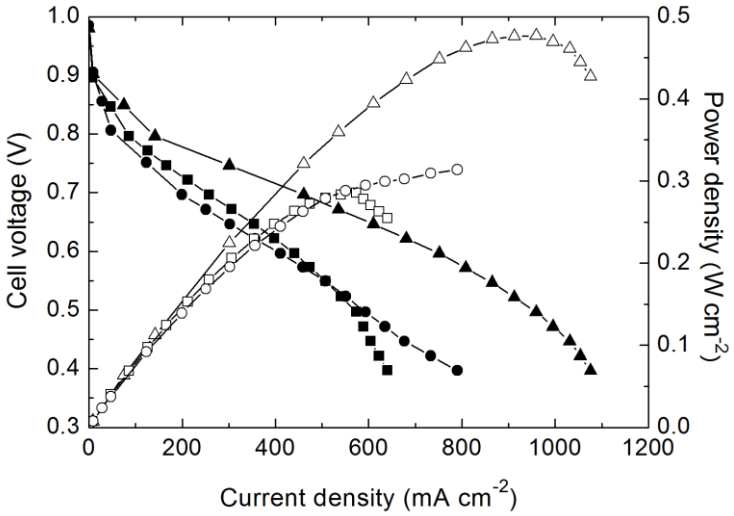

Fig. 8. Polarization curves of MEAs with Nafion/PVA membranes of (▲) 19 μm, (■) 25 μm, and (●) 31 μm thickness at 80 ºC and 100% RH in anode and cathode under H_2/Air operation. Voltages are given in closed symbols and power densities in open symbols.

of the Tafel equations for anode and cathode, $A = R \cdot T/(2 \cdot \alpha \cdot F)$, with α being the charge-transfer coefficient.

A nonlinear least-squares fitting procedure was used to obtain the values of V_{OC}, A, α, i_0, $R \cdot S$, m and n for the experimental polarization curves. In Fig. 9 a comparison between modelled and experimental curves is shown and Table 2 summarizes the obtained results including the maximum power densities P achieved by each membrane.

The Tafel slopes, A, increase with increasing thickness, which is consistent with the observations made by other authors [42,43]. This is explained by differences in the oxygen reduction reaction at the cathode as the protonation step of the oxygen molecule becomes influenced by the proton transport limitation associated with the ionic resistance of the membrane, and thus, with the thickness.

The charge-transfer coefficient, α, describes the portion of the electrical energy applied that is harnessed in lowering the free energy barrier for the electrochemical reaction. Its value must be in the range 0-1 depending on the reaction involved and the material of the electrode, being accepted a standard value of 0.5 for the electrochemical reactions occurring in PEMFCs over Pt catalysts [44]. However, in practical terms, values of α between 0.4 and 0.7 are estimated from experimental PEMFC polarization curves [45-47], which are in the range of our measurements (Table 2).

The Nafion/PVA membrane of 19 µm thickness exhibits the best

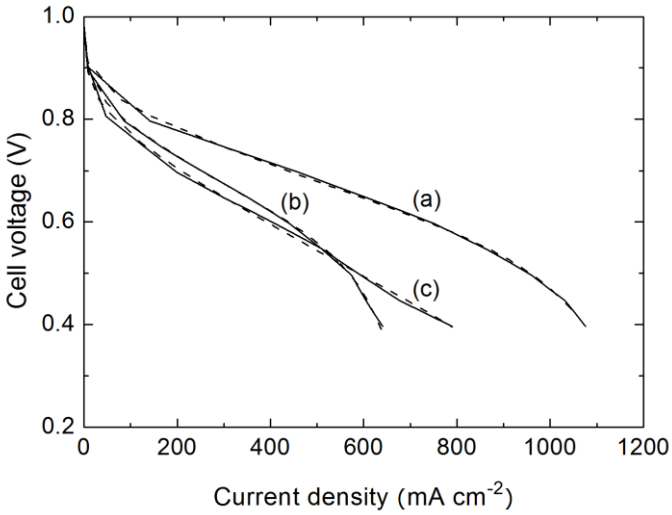

Fig. 9. Comparison between experimental (solid line) and modelled (dashed) polarization curves of (a) 19 µm, (b) 25 µm, and (c) 31 µm thick Nafion/PVA membranes at 80 ºC and 100% RH in anode and cathode under H_2/Air operation.

Table 2. Fitting parameters for the experimental *i-V* curves of several Nafion/PVA membranes under fuel cell operation with H_2/Air.at 80 ºC and 100% RH conditions in anode and cathode. The reached values of maximum power density are included.

Membrane	Nafion/PVA		
L (μm)	19 ± 1	25 ± 1	31 ± 2
V_{OC} (V)	0.980	0.982	0.985
A (mV)	24.44	29.53	33.57
α	0.62	0.52	0.45
i_0 (mA cm^{-2})	0.58	0.60	0.61
R·S (Ω cm^{-2})	0.27	0.41	0.43
m·10^5 (V)	1.30	1.35	1.41
n·10^3 (cm^2 mA^{-1})	8.40	14.30	8.35
P (W cm^{-2})	0.477	0.285	0.314

performance, with a power density of 0.477 W cm^{-2} at 0.5 V and 960 mA cm^{-2}. Comparable levels of performance are reported for Nafion/PTFE membranes of low thickness (≈ 20 μm) [48-50]. Although such composite membranes show conductivities below pristine Nafion®, their performances are similar to a Nafion-112 membrane (50 μm) owing to the shorter pathway for transporting H^+ ions and thus a lower "ohmic loss". Other advantages are improved mechanical strength and good thermo-stability. More reduced costs are also suggested for these Nafion/PTFE membranes as they contain much less of the expensive Nafion® resin than the traditional membranes. The characterization of the Nafion/PVA membranes performed in this work shows that similar conclusions are valid for our composite membranes.

Nevertheless, PTFE is a material support with a very low surface energy, strong hydrophobic behaviour [51], making difficult to find a liquid solvent with lower surface tension that can wet it successfully. In fact, this would be another feasible reason to explain the better characteristics found in Nafion/PTFE membranes when a surfactant, Triton-X, is incorporated into the Nafion® solution before the impregnation step [52]. Furthermore, lack of interfacial bonding between the polar side chains of Nafion® containing sulfonic acid groups and the PTFE walls might explain the observed creep deformation for those composite membranes under a severe RH-cycling test which apparently does not affect pristine Nafion® MEAs [48].

The 25 μm and 31 μm thick Nafion/PVA membranes seem to perform similarly (Fig. 8) as their protonic resistances *R·S* are almost identical (Table 2). However, by some unknown reason, the 25 μm thick membrane exhibited an unexpected loss of performance at higher current densities, likely as a consequence of mass transport limitations since the parameter *n*

shows a sharp rise, which was not observed on the 31 μm thick composite membrane.

In comparison with commercial porous membranes as that of Gore, electrospinning provides a flexible approach to produce polymeric supports with a high porosity from a wide range of materials [53]. Hydrophobic and hydrophilic surfaces, tailored core-shell nanofibres [54], surfaces functionalised with organic groups [55] and nanofibres containing nanoparticles [56] can be conveniently obtained. In the present work, PVA nanofibres were selected due to their economic price, high mechanical and thermal stability, easy way to carry out chemical modification by reactivity of the OH groups, and their ability to be electrospun from water solutions.

Platinum doped nanofibres for self-humidifying membranes [49], fast ionic conducting membranes containing proton conductive nanofibres [57-61] and mechanically more stable membranes via strong interfacial bonding between fibre and matrix, i.e. acid-base reactions of sulfonic acid with amino groups [62], are just a few examples of promising possibilities offered by the application of electrospun nanofibre mats for fuel cell membranes.

Summarizing, our novel ultrathin membranes based on PVA nanofibre reinforced Nafion® show a great potential as ion-exchange membranes for fuel cell applications, although further optimization should still be achieved, and they represent a first step in the development of new membranes and materials.

5. Conclusions

Novel composite membranes of Nafion/PVA have been successfully prepared by electrospinning of aqueous solutions of polyvinyl alcohol and further infiltration of Nafion® between the nanofibres.

The electrospinning technique represents a versatile tool for the preparation of porous polymer supports from a wide range of materials enabling tailored properties in order to obtain improved fuel cell membranes in terms of mechanical, thermal, conductive, fuel crossover characteristics and so on.

Mechanical studies have revealed that the composite membranes are strongly reinforced by the incorporation of the PVA nanofibres showing higher tensile strength and Young's modulus values in comparison with pristine Nafion®. In addition, the behaviour of the mechanical properties with temperature is also improved, from 80 ºC for mechanically stable operation of Nafion® up to 150 ºC for the composite membranes.

The proton conductivity of the Nafion/PVA membranes has been found to be a very anisotropic property. Conductivities below that of pristine

Nafion® have been measured for all the composite membranes, explained by the non-ionic conductivity behaviour of the PVA phase. However, an ultrathin Nafion/PVA membrane of thickness under 20 μm has showed a very good performance in fuel cell operation at 80 ºC and 100% RH in anode and cathode. The low ionic resistance of the membrane by its reduced thickness together with its good mechanical properties makes these ultrathin ion-exchange membranes potential candidates for fuel cell applications. Moreover, the incorporation of cheap nanofibre phase within the Nafion® matrix and the use of membranes of very low thickness ensure that significant savings in Nafion® material can be afforded while keeping high performances.

Acknowledgements

This research is in the frame of IMIDIC/2009/155 project granted by Generalitat Valenciana through Institute for Small and Medium Industry (IMPIVA) and European Union by FEDER funds. The IMIDIC/2009/155 project belongs to the call for Technological Centres of IMPIVA Network.

References

[1] Sata T. Ion exchange membranes: preparation, characterization, modification and application. Cambridge: Royal Society of Chemistry; 2003.
[2] Kreuer KD. On the development of proton conducting polymer membranes for hydrogen and methanol fuel cells. J Membr Sci 2001;185:29-39.
[3] Shao Y, Yin G, Wang Z, Gao Y. Proton exchange membrane fuel cell from low temperature to high temperature: material challenges. J Power Sources 2007;167:235-42.
[4] Alberti G, Casciola M. Solid state protonic conductors, present main applications and future prospects. Solid State Ionics 2001;145:3-16.
[5] Li Q, He R, Jensen JO, Bjerrum NJ. Approaches and recent development of polymer electrolyte membranes for fuel cells operating above 100 ºC. Chem Mater 2003;15:4896-915.
[6] Alberti G, Casciola M. Composite membranes for medium temperature PEM fuel cells. Annu Rev Mater Res 2003;33:129-54.
[7] Fernández-Carretero FJ, Compañ V, Riande E. Hybrid ion-exchange membranes for fuel cells and separation processes. J Power Sources 2007;173:68-76.
[8] Felice C, Ye S, Qu D. Nafion-Montmorillonite nanocomposite membrane for the effective reduction of fuel crossover. Ind Eng Chem Res 2010;49:1514-9.
[9] Ke C-C, Li X-J, Shen Q, Qu S-G, Shao Z-G, Yi B-L. Investigation on sulfuric acid sulfonation of in-situ sol-gel derived Nafion/SiO_2 composite membrane. Int J Hydrogen Energy 2011;36:3606-13.
[10] Alberti G, Casciola M, Capitani D, Donnadio A, Narducci R, Pica M, Sganappa M. Novel Nafion-zirconium phosphate nanocomposite membranes with enhanced stability of proton conductivity at medium temperature and high relative humidity. Electrochim Acta 2007;52:8125-32.

[11] Amjadi M, Rowshanzamir S, Peighambardoust SJ, Hosseini MG, Eikani MH. Investigation of physical properties and cell performance of Nafion/TiO_2 nanocomposite membranes for high temperature PEM fuel cells. Int J Hydrogen Energy 2010;35:9252-60.
[12] Shao Z-G, Xu H, Li M, Hsing I-M. Hybrid Nafion-inorganic oxides membrane doped with heteropolyacids for high temperature operation of proton exchange membrane fuel cell. Solid State Ionics 2006;177:779-85.
[13] Navarra MA, Abbati C, Scrosati B. Properties and fuel cell performance of a Nafion-based, sulfated zirconia-added, composite membrane. J Power Sources 2008;183:109-13.
[14] Haddad D, Benmoussa H, Bourmada N, Oulmi K, Mahmah B, Belhamel M. One dimensional transient numerical study of the mass heat and charge transfer in a proton exchange membrane for PEMFC. Int J Hydrogen Energy 2009;34:5010-4.
[15] Vengatesan S, Kim H-J, Cho EA, Jeong SU, Ha HY, Oh I-H, Hong S-A, Lim T-H. Operation of a proton-exchange membrane fuel cell under non-humidified conditions using thin cast Nafion membranes with different gas-diffusion media. J Power Sources 2006;156:294-9.
[16] Liu F, Yi B, Xing D, Yu J, Zhang H. Nafion/PTFE composite membranes for fuel cell applications. J Memb Sci 2003;212:213-23.
[17] Lin H-L, Yu TL, Huang LN, Chen LC, Shen KS, Jung GB. Nafion/PTFE composite membranes for direct methanol fuel cell applications. J Power Sources 2005;150:11-9.
[18] Jung G-B, Weng F-B, Peng C-C, Jao T-C. The development of PTFE/Nafion/TEOS membranes for application in moderate and high temperature proton exchange membrane fuel cells. Int J Hydrogen Energy 2011;36:6045-50.
[19] Lin H-L, Yeh S-H, Yu TL, Chen L-C, Silicate and zirconium phosphate modified Nafion/PTFE composite membranes for high temperature PEMFC. J Polym Res 2009;16:519-527.
[20] Choi SW, Fu Y-Z, Ahn YR, Jo SM, Manthiram A. Nafion-impregnated electrospun polyvinylidene fluoride composite membranes for direct methanol fuel cells. J Power Sources 2008;180:167-71.
[21] Lin H-L, Wang S-H, Chiu C-K, Yu TL, Chen L-C, Huang C-C, Cheng T-H, Lin J-M. Preparation of Nafion/poly(vinyl alcohol) electro-spun fiber composite membranes for direct methanol fuel cells. J Memb Sci 2010;365:114-22.
[22] Mollá S, Compañ V. Polyvinyl alcohol nanofiber reinforced Nafion membranes for fuel cell applications. J Memb Sci 2011;372:191-200.
[23] Mollá S, Compañ V. Performance of composite Nafion/PVA membranes for direct methanol fuel cells. J Power Sources 2011;196:2699-708.
[24] Ma C-H, Yu TL, Lin H-L, Huang Y-T, Chen Y-L, Jeng U-S, Lai Y-H, Sun Y-S. Morphology and properties of Nafion membranes prepared by solution casting. Polymer 2009;50:1764-77.
[25] Ludvigsson M, Lindgren J, Tegenfeldt J. FTIR study of water in cast Nafion films. Electrochim Acta 2000;45:2267-71.
[26] Liang Z, Chen W, Liu J, Wang S, Zhou Z, Li W, Sun G, Xin Q. FT-IR study of the microstructure of Nafion® membrane. J Membr Sci 2004;233:39-44.
[27] Laporta M, Pegoraro M, Zanderighi L. Perfluorosulfonated membrane (Nafion): FT-IR study of the state of water with increasing humidity. Phys Chem Chem Phys 1999;1:4619-28.
[28] Chang Y-W, Wang E, Shin G, Han J-E, Mather PT. Poly(vinyl alcohol) (PVA)/sulfonated polyhedral oligosilsesquioxane (sPOSS) hybrid membranes for direct methanol fuel cell applications. Polym Adv Technol 2007;18:535-43.
[29] Bauer F, Denneler S, Willert-Porada M. Influence of temperature and humidity on the mechanical properties of Nafion® 117 polymer electrolyte membrane. J Polym Science Part B Polym Phys 2005;43:786-95.

[30] Jalani NH, Dunn K, Datta R. Synthesis and characterization of Nafion®-MO_2 (M = Zr, Si, Ti) nanocomposite membranes for higher temperature PEM fuel cells. Electrochim Acta 2005;51:553-60.
[31] de Almeida SH, Kawano Y. Thermal behaviour of Nafion membranes. J Thermal Anal Calorimetry 1999;58:569-77.
[32] Park J-S, Park J-W, Ruckenstein E. Thermal and dynamic mechanical analysis of PVA/MC blend hydrogels. Polymer 2001;42:4271-80.
[33] Peng Z, Kong LX. A thermal degradation mechanism of polyvinyl alcohol/silica nanocomposites. Polym Degrad Stabil 2007;92:1061-71.
[34] Gilman JW, VanderHart DL, Kashiwagi T. Thermal decomposition chemistry of poly(vinyl alcohol). Fire and polymers II: materials and test for hazard prevention. In: ACS Symposium Series 599. Washington DC: American Chemical Society; August 21-26, 1994 [Chapter 11].
[35] Brown EN, Dattelbaum DM. The role of crystalline phase on fracture and microstructure evolution of polytetrafluoroethylene (PTFE). Polymer 2005;46:3056-68.
[36] Kim GH. Electrospun PCL nanofibers with anisotropic mechanical properties as a biomedical scaffold. Biomed Mater 2008;3:025010.
[37] Jung YH, Kim HY, Lee DR, Park SY, Khil MS. Characterization of PVOH nonwoven mats prepared from surfactant-polymer system via electrospinning. Macromol Res 2005;13:385-90.
[38] Anantaraman AV, Gardner CL. Studies on ion-exchange membranes. Part 1. Effect of humidity on the conductivity of Nafion®. J Electroanalytical Chem 1996;414:115-20.
[39] Kim J, Lee SM, Srinivasan S, Chamberlin CE. Modeling of proton exchange membrane fuel cell performance with an empirical equation. J Electrochem Soc 1995;142:2670-4.
[40] Laurencelle F, Chahine R, Hamelin J, Agbossou K, Fournier M, Bose TK, Laperrière A. Characterization of a Ballard MK5-E proton exchange membrane fuel cell stack. Fuel Cells 2001;1:66-71.
[41] Pisani L, Murgia G, Valentini M, D'Aguanno B. A new semi-empirical approach to performance curves of polymer electrolyte fuel cells. J Power Sources 2002;108:192-203.
[42] Chu D, Jiang R. Comparative studies of polymer electrolyte membrane fuel cell stack and single cell. J Power Sources 1999;80:226-34.
[43] Du X, Yu J, Yi B, Han M, Bi K. Performances of proton exchange membrane fuel cells with alternate membranes. Phys Chem Chem Phys 2011;3:3175-9.
[44] Larminie J, Dicks A. Fuel cell systems explained. 2nd ed. England: John Wiley & Sons Inc; 2003. 42.
[45] Danilov VA, Tade MO. An alternative way of estimating anodic and cathodic transfer coefficients from PEMFC polarization curves. Chem Eng J 2010;156:496-9.
[46] Fernandez-Carretero FJ, Suarez K, Solorza O, Riande E, Compañ V. PEMFC performance of MEAs based on Nafion® and sPSEBS hybrid membranes. J New Mater for Electrochemical Syst 2010;13:191-9.
[47] Kunusch C, Puleston PF, Mayosky MA, Moré JJ. Characterization and experimental results in PEM fuel cell electrical behaviour. Int J Hydrogen Energy 2010;35:5876-81.
[48] Jao T-C, Ke S-T, Chi P-H, Jung G-B, Chan S-H. Degradation on a PTFE/Nafion membrane electrode assembly with accelerating degradation technique. Int J Hydrogen Energy 2010;35:6941-9.
[49] Liu Y, Nguyen T, Kristian N, Yu Y, Wang X. Reinforced and self-humidifying composite membrane for fuel cell applications. J Memb Sci 2009;330:357-62.
[50] Yu TL, Lin H-L, Shen K-S, Huang L-N, Chang Y-C, Jung G-B, Huang JC. Nafion/PTFE composite membranes for fuel cell applications. J Polym Res 2004;11:217-24.
[51] Burkarter E, Saul CK, Thomazi F, Cruz NC, Roman LS, Schreiner WH. Superhydrophobic electrosprayed PTFE. Surf Coatings Technol 2007;202:194-8.

[52] Lin H-L, Yu TL, Shen K-S, Huang L-N. Effect of Triton-X on the preparation of Nafion/PTFE composite membranes. J Memb Sci 2004;237:1-7.
[53] Huang Z-M, Zhang Y-Z, Kotaki M, Ramakrishna S. A review on polymer nanofibers by electrospinning and their applications in nanocomposites. Composites Sci Technol 2003;63:2223-53.
[54] Zhang J-F, Yang D-Z, Xu F, Zhang Z-P, Yin R-X, Nie J. Electrospun core-shell structure nanofibers from homogeneous solution of Poly(ethylene oxide)/Chitosan. Macromolecules 2009;42:5278-84.
[55] Kim TG, Park TG. Surface functionalised electrospun biodegradable nanofibers for immobilization of bioactive molecules. Biotechnol Prog 2006;22:1108-13.
[56] Hong KH, Park JL, Sul IH, Youk JH, Kang TJ. Preparation of antimicrobial Poly(vinyl alcohol) nanofibers containing silver nanoparticles. J Polym Science Part B Polym Phys 2006;44:2468-74.
[57] Choi J, Lee KM, Wycisk R, Pintauro PN, Mather PT. Nanofiber network ion-exchange membranes. Macromolecules 2008;41:4569-72.
[58] Dong B, Gwee L, de la Cruz DS, Winey KI, Elabd YA. Super proton conductive high-purity Nafion nanofibers. Nano Lett 2010;10:3785-90.
[59] Choi J, Wycisk R, Zhang W, Pintauro PN, Lee KM, Mather PT. High conductivity perfluorosulfonic acid nanofiber composite fuel-cell membranes. ChemSusChem. 2010;3:1245-8.
[60] Shabani I, Hasani-Sadrabadi MM, Haddadi-Asl V, Soleimani M. Nanofiber-based polyelectrolytes as novel membranes for fuel cell applications. J Memb Sci 2011;368:233-40.
[61] Tamura T, Kawakami H. Aligned electrospun nanofiber composite membranes for fuel cell electrolytes. Nano Lett 2010;10:1324-8.
[62] Pak SH, Caze C. Acid-base interactions on interfacial adhesion and mechanical responses for glass-fiber reinforced low-density polyethylene. Appl Polym Sci 1997;65:143-53.

Paper 4

Fuel Cells 11 (2011) 897-906
(Adapted to thesis)

On the methanol permeability through pristine Nafion® and Nafion/PVA membranes measured by different techniques. A comparison of methodologies

S. Mollá[1,2], V. Compañ[1,2], S.L. Lafuente[3], and J. Prats[1]

[1] Dpto. Termodinámica Aplicada, ETSII, Universidad Politécnica de Valencia, 46022 Valencia, Spain.
[2] Instituto de Tecnología Energética (ITE), Universidad Politécnica de Valencia, 46022 Valencia, Spain.
[3] Dpto. de Química Orgánica, Universidad Jaume I, 12072 Castellón, Spain.

Abstract

Methanol crossover through polymer electrolyte membranes is a critical issue and causes an important reduction of performance in direct methanol fuel cells (DMFCs). Measuring the evolution of CO_2 gas in the cathode is a common method to determine the methanol crossover under real operating conditions, although an easier and simpler method is preferable for the screening of membranes during their step of development. In this sense, this work has been focused on the *ex situ* characterization of the methanol permeability in novel nanofibre-reinforced composite Nafion/PVA membranes for DMFC application by means of three different experimental procedures: (a) potentiometric method, (b) gas chromatography technique, and (c) measuring the density. It was found that all these methods resulted in comparable results and it was observed that the incorporation of the PVA nanofibre phase within the Nafion® matrix causes a remarkable reduction of the methanol permeability. The optimal choice of the most suitable technique depends on the accuracy expected for the methanol concentration, the availability of the required instrumental, and the complexity of the procedure.

Keywords: DMFC, methanol permeability, nanocomposite Nafion® membranes, nanofibres, PVA.

1. Introduction

Though polymer electrolyte membrane fuel cells (PEMFCs) are attractive, energy efficient, and environmentally friendly power sources for many applications including transportation, distributed power, and portable power systems, important scientific, technical, and economical problems need to be solved before PEMFC commercialization is possible. Direct methanol fuel cells (DMFCs) are promising candidates to replace existing batteries as power generators in portable devices. Easy refuelling and high energy storage capacity are their main advantages.

It is known that perfluorosulfonic polymers, such as Nafion®, are the most commonly used proton conductors in membranes for fuel cells due to their good mechanical and chemical properties, thermal stability, and high protonic conductivity. However, Nafion® materials suffer from a significant methanol crossover which lowers the performance of the DMFCs [1,2], and therefore, thicker membranes are required.

In order to reduce the methanol permeability within the polymeric matrix, great efforts have been made to modify Nafion® or preparing new hybrid cation-exchange membranes containing ionic functionalised inorganic fillers [3,4]. Composite membranes using a wide variety of materials such as Pd alloy [5], polypyrrole [6], polyaniline [7], silica [8], sepiolite [9], SEBS [10], PVA [11,12], etc., have been studied. Although those fillers can provide properties as methanol barriers by increasing tortuosity, the fillers would also have a dual function: (a) enhancement of the water retention and (b) increase of the ion-exchange capacity (IEC) of the membranes, two characteristics which favors the proton conductivity. In membranes with high IEC, segregation of nanosized hydrophilic domains from the hydrophobic ones to form percolation paths for proton transport may be relatively easy. It may be assumed that ionic inorganic fillers trapped in hydrophobic domains separating hydrophilic domains might provide additional pathways for proton transport [13-15].

In DMFC, the methanol crossover occurs by diffusion as a result of the concentration gradient and also by the electro-osmotic drag. Diffusion dominates when the cell runs at low currents, whereas the electro-osmotic drag mode dominates when the cell is operating at elevated current densities, and this effect is even more pronounced at higher methanol concentrations in the anode [16]. As a consequence of the methanol crossover, a decrease of the coulombic efficiency is produced due to the loss of fuel and additionally, the crossed methanol undergoes oxidation on the cathode, at which oxygen reduction alone is intended to occur, producing into the cathode a mixed potential which causes a global reduction of the potential, and non-oxidised methanol is also susceptible to poison the catalyst surface. Due to these

phenomena, the cathode overvoltage increases and the cell performance drops.

The most common method used for the *in situ* determination of the methanol crossover in DMFCs consists in monitoring the CO_2 concentration within the gaseous products of the cathode. This technique uses an optical infrared CO_2 sensor to know the amount of methanol crossing the membrane [17]. It is assumed that the methanol crossing from the anode is completely oxidised to CO_2 on the catalyst layer of the cathode. However, the methanol being evaporated by the air/oxygen flow [18] and the carbon dioxide which may be permeating from anode to cathode are often ignored. It has been observed by mass spectrometry that CO_2 crossover from anode to cathode and unreacted methanol passing through the cathode increase with increasing current density [19]. With the aim to obtain better results, another authors have performed *in situ* measurements using gas chromatography (GC) to measure both the methanol concentration in the condensed phase (methanol + water), after cooling of the cathode outlet stream, and the carbon dioxide concentration in the remaining gas phase [20]. Furthermore, a precise measurement of the cathode gas flow rate is expected to be needed for an accurate result.

Although those systems are the best approach to follow the methanol permeation across the membrane during real operating conditions, in which diffusion and electro-osmotic drag effects simultaneously occur, it is important to take into account that they are complex systems and it is not always possible to carry out fuel cell performance experiments or on-line sensors/equipments are available. Thereby, membrane development specialists require a larger range of options for the screening of their membranes behaviour. Among those, *ex situ* methods based on placing the membrane between two separated reservoirs are usually used. One of them initially contains pure water and the other reservoir is containing a methanol-water mixture. The concentration of methanol crossing the membrane can be measured versus time using GC or connecting the cell to a differential refractometer [21, 22].

The *ex situ* procedure is appropriate for the characterization of membranes under DMFC operation as their results of methanol flux will tend to be similar to those obtained *in situ* at low current densities, in which a small electro-osmotic effect is present and gradient concentration between the anode-membrane-cathode interfaces is the main driving force for the crossover. At higher current densities the results may differ as the electro-osmotic effect will become more significant while the gradient concentration will diminish due to the increased methanol consumption at the anode [23]. Generally, methanol transport across the membrane and methanol crossover overpotential at the cathode both decrease with increasing current

density [23-25]. Thus, methanol permeability predominates at low current density (via overpotential losses at cathode) while proton conductivity predominates at high current density (via ohmic losses in membrane) on the DMFC performance [23]. In principle, neglecting mass transport phenomena in gas diffusion layers (GDLs), results obtained *in situ* at open circuit voltage (OCV) conditions, if CO_2 and unreacted methanol are analyzed, should be equivalent to those values measured by *ex situ* methods. Therefore, *ex situ* methanol permeability measurements involve the most unfavourable case (higher methanol flux crossover) than those conditions normally taking place under DMFC operation, and they can represent a good filter for the selection of membranes.

Additional techniques to measure the change in methanol concentration imply potentiometry and densimetry. The potentiometric method has been developed for Nafion® membranes [26], SPEEK/TPA/MCM-41 composite membranes [27] and for Nafion-polyfurfuryl alcohol nanocomposite membranes [28]. The crossover rate of methanol is obtained from the recording of the potential (E) given by an electrode coated with a black Pt-Ru catalyst and immersed in an aqueous 0.2 M H_2SO_4 solution as a supporting electrolyte during the methanol crossover. The slope dE/dt is proportional to the crossover rate.

On the other hand, the densimetry method uses the property of mass density variation as a function of concentration, taking advantage of the considerable difference in density between water and methanol. Thus, the methanol concentration versus time in the methanol receiver reservoir is obtained from the density of the solution at each instant of time.

The purpose of this paper is the study of the methanol permeation on cast Nafion® and novel Nafion/PVA membranes by means of different techniques, i.e. potentiometry, GC and densimetry; motivated by the importance of an accurate characterization of the methanol permeability of membranes to be used in DMFCs, since this parameter will be helpful to predict their usefulness and performance.

The Nafion/PVA membranes were prepared by successive loading of Nafion® into a mat of nanofibres of polyvinyl alcohol (PVA), which was obtained by electrospinning [12,29]. The main advantages given by the nanofibres involve the mechanical reinforcement of the composite films and the methanol barrier effect caused by the low methanol permeability of the PVA phase.

2. Methodology

2.1. Potentiometry

The membranes were successively treated in aqueous 5 wt% H_2O_2 solution, distilled water, and 0.2 M H_2SO_4, and finally stored in a 0.2 M H_2SO_4 solution. The membrane was clamped between two glass cells of about 150 cm^3 capacity by means of an O-ring joint with an inner area of 2.27 cm^2 (Figure 1). The methanol receiver reservoir was filled with 150 ml of an aqueous 0.2 M H_2SO_4 solution. A working electrode composed of a catalyst layer of black Pt-Ru particles supported on a carbon paper was introduced and potential measured against a reference electrode of Ag/AgCl in 3 M KCl solution (AgCl sat.). The experiment was started by introducing into the opposite cell 150 ml of an aqueous 2 M methanol solution containing 0.2 M H_2SO_4. By this procedure, the hydrostatic pressure gradient and the concentration of the supporting electrolyte at both sides of the membrane is maintained. Both cells were stirred by means of Teflon coated magnetic bars during the experiments, which were carried out at 25 °C. The potential of the working Pt-Ru electrode (cell R) was recorded using a multimeter (Fluke 8842A).

After each measurement, the membrane was cleaned with distilled water and then left for 24 h immersed in distilled water to remove any residual concentration into the pores of the membrane. The asymmetry potential of the membrane was measured before performing another experiment following the procedure described in the literature [30].

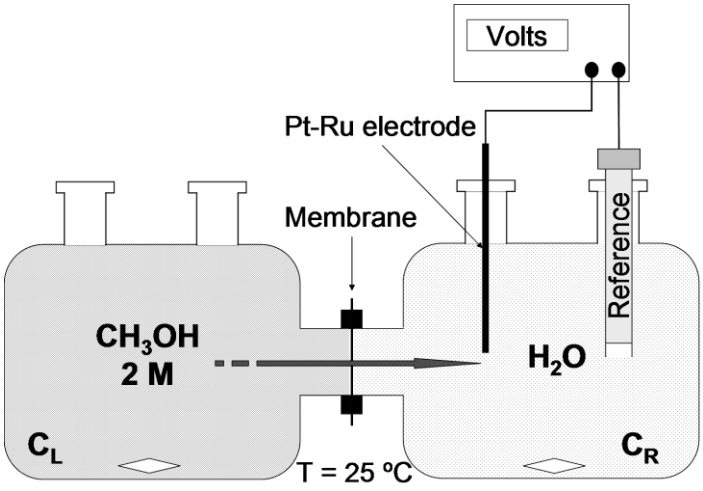

Fig. 1. Schematic representation of the experimental setup used for the determination of the methanol permeability across the membranes. The potentiometric method is specifically represented.

Previously, a calibration curve was obtained at different methanol concentrations. In this case, the working and reference electrodes were introduced into a 0.2 M H_2SO_4 solution. The potential was monitored until a steady-state value, which reached 0.705 V. In successive steps, different amounts of methanol were added and it was observed the potential versus each methanol concentration.

It is known that the diffusion process of methanol across a membrane in the stationary state is described by the Fick's first law, which relates the diffusive flux to the concentration field:

$$j = \frac{dn}{A \cdot dt} = D_m \frac{\Delta \bar{c}_m}{L} \qquad (1)$$

where j is the flux density of methanol, n the amount of methanol crossing the membrane expressed in moles, A is the area, t the time, $\bar{c}_m$ the methanol concentration into the membrane ($\Delta \bar{c}_m$ represents the variation in methanol concentration between the right and left side of the membrane, with a thickness L, and can be expressed as $\bar{c}_{m,L} - \bar{c}_{m,R}$), L the average thickness of the membrane system, and D_m the methanol diffusion coefficient into the membrane. This coefficient is not a quantity measurable because the concentration profile into the membrane is not known. However, from a strict point of view, the methanol concentrations at both sides of the membrane, $\bar{c}_{m,L}$ and $\bar{c}_{m,R}$, cannot be considered the same as the concentrations in bulk solution, since this transfer process is governed by the methanol solubility in such a membrane and by the mass transport limitation within the boundary layers (BLs) (Figure 2). Thus, we can define the membrane partition coefficient k_m as,

$$k_m = \frac{\bar{c}_m}{c_s} = \frac{\bar{c}_{m,L}}{c_L} = \frac{\bar{c}_{m,R}}{c_R} \qquad (2)$$

being c_s the solute concentration in the bulk solution, c_L and c_R the bulk concentrations in the left or right side of the membrane. From Eqs. (1) and (2) we can easily probe that,

$$j = D_m \cdot k_m \frac{(c_L - c_R)}{L} = P \frac{(c_L - c_R)}{L} \qquad (3)$$

where P is the apparent permeability coefficient.

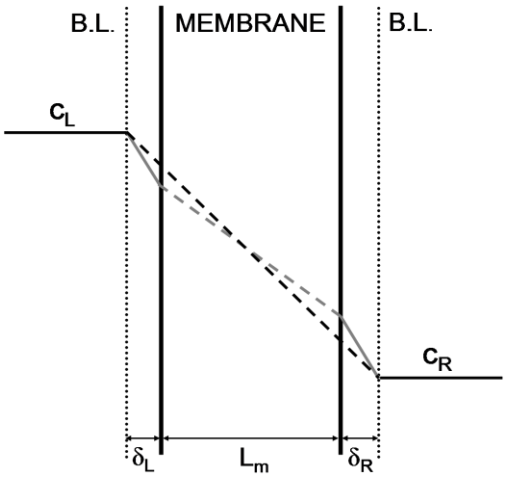

Fig. 2. Scheme of the permeation phenomenon across a membrane. The grey profile represents the real process occurring, while the black discontinuous line represents the apparent permeability of the membrane by neglecting the boundary layer (BL) effects. The grey discontinuous line inside the membrane shows the true (intrinsic) permeability profile.

Combining Eqs. (1) and (3), and taking into account that the concentration can be expressed by $c = n/V$, we can easily obtain,

$$\ln\left(1-\frac{2\cdot c_R(t)}{c_{L,0}}\right)=-\frac{2\cdot A\cdot P}{V_R\cdot L}(t-t_0) \qquad (4)$$

in which $c_R(t)$, A, L, V_R, and $c_{L,0}$ are known. Thus, from the slope of Eq. (4) we can obtain the apparent methanol permeability of the membrane, furthermore the average methanol flux density is obtained from the expression of $dc_R(t)/dt$ together with the values of V_R and the area, A, of the membrane.

From Eq. (4), the methanol concentration in the receiver compartment can be expressed as,

$$c_R(t)=\frac{c_{L,0}}{2}\left[1-\exp\left(\frac{-2\cdot A\cdot P}{V_R\cdot L}\right)(t-t_0)\right] \qquad (5)$$

and the methanol flux,

$$J(t)=\frac{c_{L,0}\cdot A\cdot P}{V_R\cdot L}\left[\exp\left(\frac{-2\cdot A\cdot P}{V_R\cdot L}\right)(t-t_0)\right] \qquad (6)$$

In case of $c_L(t) >> c_R$, as it happens in our experiments, we can obtain,

$$c_R = \frac{P \cdot A \cdot c_{L,0}}{V_R \cdot L}(t - t_0) \quad (7)$$

being $c_{L,0}$ the initial concentration of methanol in the compartment on the left side of the membrane and t_0 the time lag.

It is known that platinum-ruthenium (Pt-Ru) is the best catalyst for methanol oxidation [30]. The mechanism of electro-oxidation of methanol is complex because the reaction involves a transfer of six electrons and the formation of several by-products and finally carbon dioxide. In our experiments, under the presence of methanol, the main reaction assumed to take place in the equilibrium is,

$$PtRu + CH_3OH \Leftrightarrow PtRu(CH_2OH) + H^+ + e^- \quad (8)$$

The potential of the reaction is related with the concentrations as follows,

$$E = E^0 - \frac{R \cdot T}{F} \ln\left(\frac{c_R}{\theta_{ad} \cdot c_{H^+}}\right) \quad (9)$$

where E^0 is the standard electrode potential and θ_{ad} the surface coverage by the adsorbed species [31]. By differentiation of Eq. (9) we can obtain,

$$\frac{dc_R}{dt} = -k' \cdot \exp\left(\frac{F \cdot (E^0 - E)}{R \cdot T}\right)\frac{dE}{dt} = k\frac{dE}{dt} \quad (10)$$

in which is assumed that the concentrations terms, θ_{ad} and c_{H+} are invariant with time, $k' = \theta_{ad} \cdot c_{H+}$ is a empirical constant introduced, and $k = k' \cdot exp(F \cdot (E^0 - E)/R \cdot T)$.

Thus, assuming that the measured potential (E) of the Pt-Ru electrode, which is a mixed potential and varies only according the reaction given in Eq. (8), the dE/dt of Eq. (10) can be estimated and consequently the concentration of methanol in the receiver compartment (c_R) can be calculated from the Eq. (10) taking into account the calibration curve experimentally obtained, in which the potential values were correlated with the methanol concentration.

2.2. Gas chromatography technique

The methanol crossover of the Nafion® and Nafion/PVA membranes was investigated using a similar experimental setup as described for the potentiometric technique. However, in this case, both the solutions containing methanol (left reservoir) and pure water (right reservoir) did not contain sulfuric acid as a supporting electrolyte. Again, the experiments were carried out at 25 °C and the initial methanol concentration (c_L) was fixed at 2 M.

The change in methanol concentration with time in the right compartment (c_R) was measured using a GC (HP Co., model 8590 A) with a capillary column (Agilent Co., 30 m × 0.53 mm × 20 μm) and a TCD detector. Samples of 2.5 ml from the receiver reservoir were taken at certain time intervals and mixed with 2.5 ml of pure water before the measurements in the GC. The carrier gas of the GC was helium and the injection sample size was 5 μl. The injector, oven and detector temperature were fixed at 120 ºC. Previously to characterize the methanol permeability of the membranes, five aqueous methanol solutions with a known concentration were prepared to obtain the calibration curve by relating the methanol concentration with the area of the peaks represented in the chromatograms. From this standard calibration curve, the methanol concentration in the receiver compartment (c_R) was calculated for each time interval, and the permeability coefficient (P) was determined with Eq. (7).

2.3. Densimetry

Using the same experimental setup described above, the apparent methanol permeability of the membranes was measured at 25 °C by density measurements. The variation of methanol concentration with time in the receiver reservoir (c_R) was determined by means of a densimeter (Anton-Paar, DMA 4500 M). The sample (≈ 1 ml) is introduced into a U-shaped borosilicate glass tube that is being excited to vibrate at its characteristic frequency, which changes depending on the density of the sample. Through a precise determination of the characteristic frequency and a mathematical conversion, the mass density (g cm^{-3}) of the sample can be given.

A calibration curve of density versus methanol concentration was obtained before the permeation measurements. During those experiments, a small sample of solution from the receiver compartment was taken at certain time intervals and the density recorded. In order to avoid the volume of liquid in the receiver reservoir (V_R) to change, the samples were recovered from the densimeter after each measurement. Representing c_R versus time,

the flux (*J*), and apparent permeability (*P*) of the methanol across the membranes can be determined.

3. Experimental section

3.1. Materials

A commercial Nafion® membrane NR-212 (dispersion-cast type film) and a 20 wt% Nafion® dispersion (DuPont Co.), which was subsequently solvent exchanged in order to prepare a 5 wt% dispersion in isopropanol/water mixture, 4/1 (w/w), respectively, both were purchased from Ion-Power.

PVA, Mowiol 28-99 grade, was kindly supplied by the company Kuraray Europe GmbH.

Isopropanol extra pure and cetyltrimethylammonium bromide (CTAB) were purchased from Acros Organics, and 4-formyl-1,3-benzenedisulfonic acid disodium salt from Sigma-Aldrich.

3.2. Preparation of Nafion/PVA membranes

A detailed procedure of the preparation and characterization of the composite Nafion/PVA membranes has been previously described by the authors [12,29] and it is summarized as follows.

Porous PVA mats were produced by a standard electrospinning setup (Yflow S.L., Málaga, Spain) through the feeding of an aqueous solution of PVA (0.005:1:10 wt. CTAB:PVA:water). CTAB was used as surfactant in order to reduce surface tension of water and improve electrospinning ability. A potential difference of 16 kV was applied between the needle and the planar collector, which were separated 25 cm, and a flow rate of 0.5 ml h^{-1} was used for the electrospinning process.

The collected mats were heated during 3 h at 170 °C in a vacuum atmosphere (250 mbar pressure) with the purpose of removing water and increasing manipulability. The PVA mats were then mounted on a round steel frame and immersed into a bath in which the disodium salt of the 4-formyl-1,3-benzenedisulfonic acid was solved by a mixture of isopropanol/water (70/30, v/v), incorporating chlorhydric acid as a catalyst for the acetal-type reaction, which was carried out at 60 °C for 2 h. The sodium ions were exchanged with protons by means of a chlorhydric acid solution.

Subsequently, the PVA chains were crosslinked in order to raise mechanical, chemical, and thermal properties of the nanofibres. This was accomplished by reaction with glutaraldehyde vapor in a closed vessel

during 24 h at room temperature. After the crosslinking process, the mats were heated at 100 °C for 15 min with the aim to remove adsorbed glutaraldehyde and water.

Finally, the functionalised and crosslinked mats were impregnated with the prepared 5 wt% Nafion® dispersion in isopropanol and water. Each impregnation step was carried out by wetting the PVA mat into the Nafion® dispersion for 5 min and followed by evaporation in an oven at 100 °C for 5 min more. This was repeated 8 times in every mat so that an outer visible Nafion® layer was formed. Afterwards, the composite membranes were annealed at 125 °C for 90 min under pressure and then conditioned with hot aqueous solutions of hydrogen peroxide and chlorhydric acid, washed with hot water, dried, and stored.

3.3 Electrodes

The working electrode, a typical anode composition for DMFCs, was acquired from BalticFuelCells GmbH (Schwerin, Germany) and it is composed of a carbon paper GDL from Freudenberg&Co. (Weinheim, Germany), model H2315 T105A, covered by an alloy of Pt-Ru black 50:50 (Alfa Aesar) with a catalyst loading of 5.0 mg cm^{-2} together with a 20 wt% dry Nafion® ionomer.

The reference electrode is based on a Ag/AgCl reference system immersed in a 3 M KCl solution saturated with AgCl. It was purchased from CRISON (model 5261). This is a combined type electrode which additionally contains a Pt ring as counter electrode for electrochemical measurements.

4. Results and discussion

4.1. Methanol permeability by potentiometry

Figure 3 shows the variation of the open circuit potential (E) by stepwise addition of different amounts of methanol into the aqueous 0.2 M H_2SO_4 solution during the calibration experience. When the system is in absence of methanol, the difference of potential in potentiometric conditions ($i = 0$) between the Pt-Ru working electrode and the reference electrode of Ag/AgCl is 0.705 V. The addition of methanol causes the potential to drop immediately due to methanol electro-oxidation on the working electrode. Since a large volume of solution is used in the experiment, the methanol consumption is practically negligible and its concentration remains almost unchanged. After 2-3 h, the potential observed is fairly stable. These

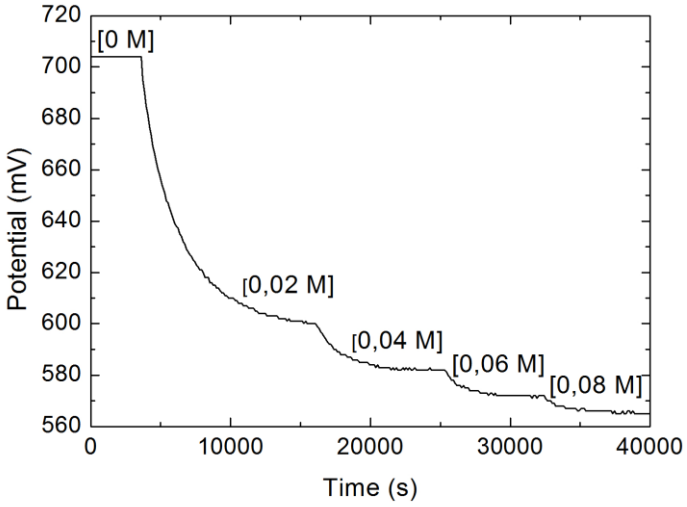

Fig. 3. Measurements of the potential shift at the Pt-Ru working electrode by stepwise addition of methanol in order to obtain the potentiometric calibration curve at 25 ºC.

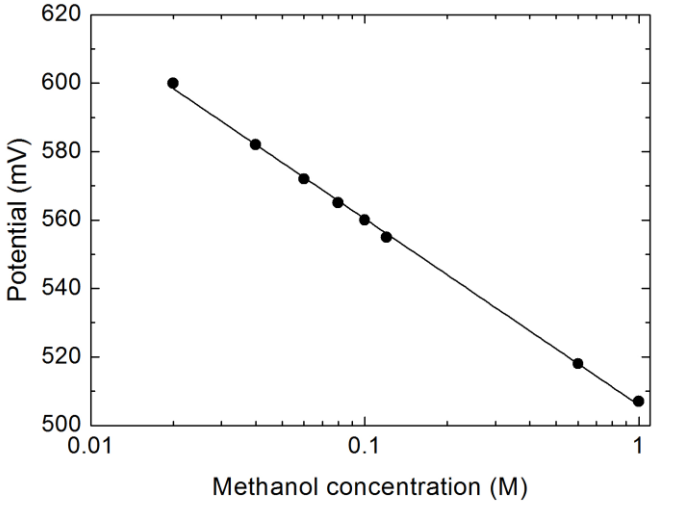

Fig. 4. Calibration curve for methanol concentration versus potential at 25 ºC by the potentiometric method.

measurements have been repeated five times and the average values have been used to obtain the calibration curve for the potentiometric method.

In Figure 4 is showed the calibration curve for almost two orders of magnitude of methanol concentration. The potential shift has a linear correlation with methanol concentration in natural logarithmic scale with a slope of 23.63 ± 0.30 mV, which is close to 25.68 mV as expected from

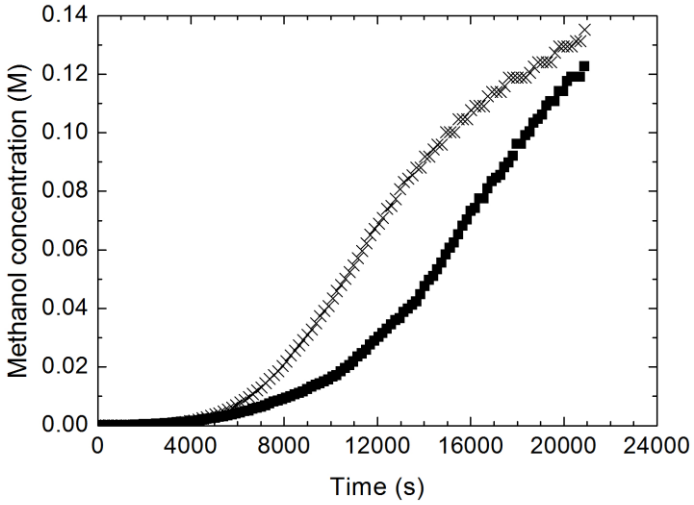

Fig. 5. Methanol concentration (c_R) versus time for (■) pristine Nafion® and (X) Nafion/PVA membranes measured by potentiometry at 25 ºC with $c_{L,0}$ = 2 M.

Eq. (9) for reaction (8). The methanol flux across pristine Nafion® and Nafion/PVA membranes was determined by measuring the variation of potential versus time in potentiometric conditions. Combining the values of $\Delta V(t)$ with the calibration curve permit us to obtain the variation of concentration in compartment R versus time (dc_R/dt). The pertinent results are given in Figure 5 for a pristine Nafion® (hydrated thickness L_{wet} of 60 μm) and a Nafion/PVA membrane (L_{wet} of 44 μm).

In Figure 5 we can see that the analyzed curves have two regions. During the first 4 h of experiment, we can observe a transitory part where the working electrode needs to reach a steady state in which the potential shifts correspond to the real variation in methanol concentration due to the flux of methanol across the membrane. The explanation for this delayed time has to be found in the fact that the response time of the electrode is not instantaneous. In this sense, it can be observed from Figure 3 that after each methanol addition the equilibrium potential was reached after at least 2-3 h. As during the permeation measurements the methanol concentration changes with time, it is assumed that a longer stabilization time is necessary.

After such a transitory part, the curve of concentration versus time presents a straight line, from which slope is calculated the apparent methanol permeability. Figure 6a and 6b focuses on those non-transitory profiles (t > 14,500 s) for the Nafion® and Nafion/PVA membranes, respectively. The values obtained are given in Table 1.

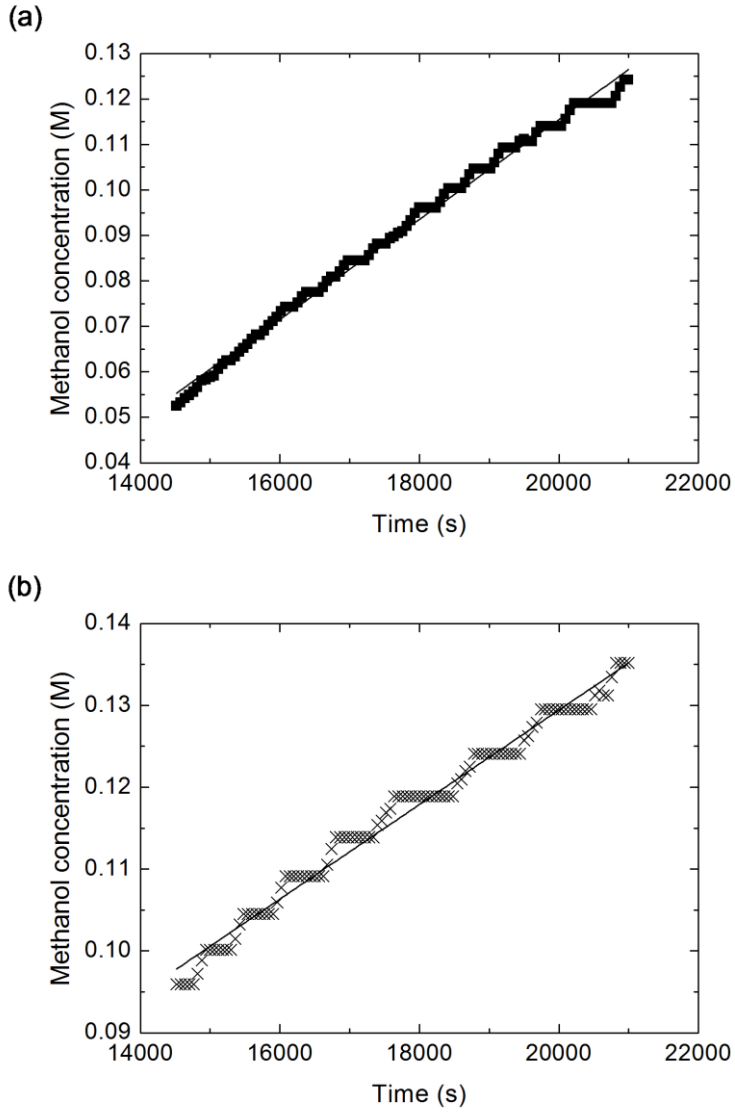

Fig. 6. Stationary regime representing c_R versus time for the (a) pristine Nafion® film and (b) Nafion/PVA membrane during the methanol permeation experiments by potentiometry at 25 ºC with $c_{L,0}$ = 2 M.

It is worth mentioning that the absolute values of concentration versus time given by the potentiometric method did not correspond with the real values which should be found at those time intervals. Due to the large response time of the electrode, this technique is only valid for relative

Table 1. Flux density of methanol (j_{MeOH}) and apparent permeability (P_{app}) constants of the Nafion® and Nafion/PVA membranes obtained at 25 ºC by means of the different methods, with experimental parameters $A = 2.27$ cm^2, $V_R = 150$ cm^3, and $c_{L,0} = 2$ M. L_{wet} is the thickness of the hydrated membrane in water.

Technique	Membrane	L_{wet} (μm)	j_{MeOH} (mol cm^{-2} s^{-1})	P_{app} (cm^2 s^{-1})
Potentiometry	Nafion-212	60 ± 1	$(7.25 \pm 0.05)\cdot10^{-4}$	$(2.18 \pm 0.05)\cdot10^{-6}$
	Nafion/PVA	44 ± 2	$(3.81 \pm 0.05)\cdot10^{-4}$	$(8.39 \pm 0.49)\cdot10^{-7}$
Chromatography	Nafion-212	60 ± 1	$(7.28 \pm 0.12)\cdot10^{-4}$	$(2.19 \pm 0.07)\cdot10^{-6}$
	Nafion/PVA	44 ± 2	$(3.43 \pm 0.08)\cdot10^{-4}$	$(7.56 \pm 0.53)\cdot10^{-7}$
Densimetry	Nafion-212	60 ± 1	$(7.31 \pm 0.06)\cdot10^{-4}$	$(2.19 \pm 0.05)\cdot10^{-6}$
	Nafion/PVA	44 ± 2	$(2.72 \pm 0.02)\cdot10^{-4}$	$(5.98 \pm 0.31)\cdot10^{-7}$

measurements, such as the methanol permeability, in which the slope dc_R/dt is the main experimental parameter required.

From Table 1 it is observed that the apparent methanol permeability obtained for the Nafion/PVA membrane ($\approx 8.39\cdot10^{-7}$ cm^2 s^{-1}) is about 2.6 times lower than that of pristine Nafion® ($\approx 2.18\cdot10^{-6}$ cm^2 s^{-1}). This latter value is in very good agreement with the methanol permeability coefficients reported for Nafion® by several authors [11,32-34].

4.2. Methanol permeability by gas chromatography technique

Previously to the characterization of the methanol transport across the membranes, a calibration curve correlating methanol concentrations with peak areas was prepared by means of chromatograms obtained from five aqueous methanol solutions with known concentration (Figure 7). It has been included a view of the peak shapes as recorded from the chromatograms. The maximum of each peak was formed at a retention time of approximately 4.53 min (see inset in Figure 7). Several repeated measurements revealed that the deviation of the peak area for a constant methanol concentration ranges between 2-4%. The calibration patrons were made up of pure water/methanol solution with different concentrations.

The apparent methanol permeability across the membranes was obtained from a similar experimental setup as showed in Figure 1. Chamber L was filled with a 2 M aqueous methanol solution, while chamber R was filled with deionized water. Both chambers were kept under stirring and thermostatized at 25 °C. Samples of 2.5 ml from chamber R were taken within a period between 0 and 3 h. These were analyzed by GC and their chromatograms compared with the calibration curve showed in Figure 7 in

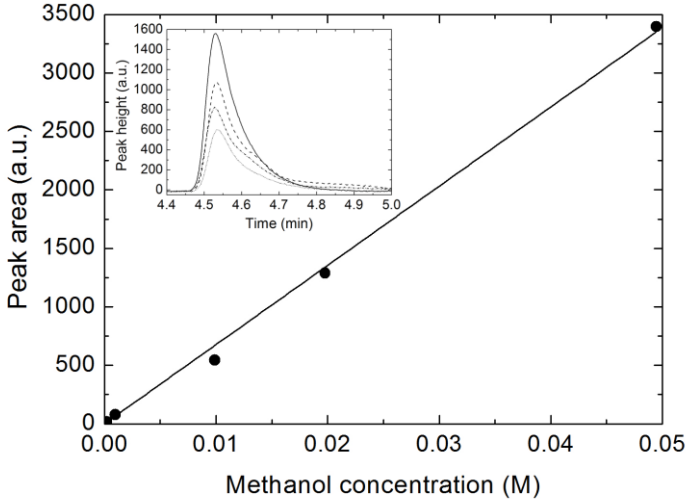

Fig. 7. Calibration curve for different methanol solutions at 25 ºC by gas chromatography.

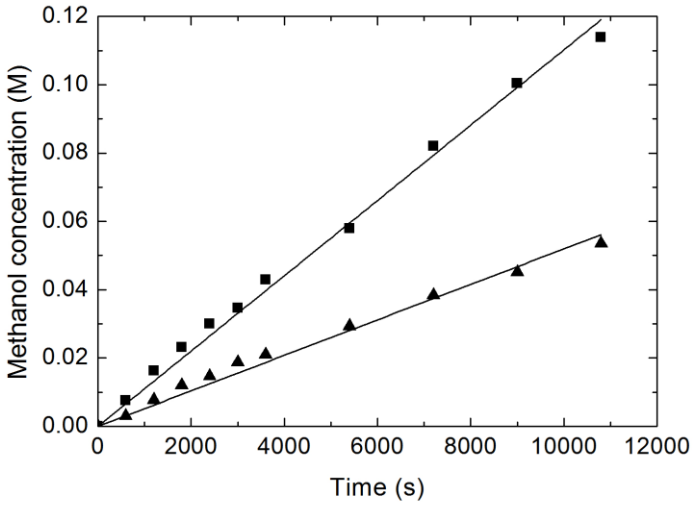

Fig. 8. Methanol concentration (c_R) versus time for (■) pristine Nafion® and (▲) Nafion/PVA membranes measured by gas chromatography at 25 ºC and $c_{L,0}$ = 2 M.

order to correlate between the obtained peak areas and the methanol concentrations at each time instant.

Figure 8 depicts the variation of methanol concentration in chamber R versus time. Straight lines with different slopes ($m = dc_R/dt$) have been obtained for both pristine Nafion® and composite Nafion/PVA membranes.

By application of Eq. (7), the apparent methanol permeability coefficients have been calculated and are given in Table 1. It is again observed a methanol permeability value for Nafion® ($\approx 2.19 \cdot 10^{-6}$ cm^2 s^{-1}) in total accordance with the literature [11,32-34]. The composite membrane of Nafion/PVA with an apparent permeability coefficient of $7.56 \cdot 10^{-7}$ cm^2 s^{-1} shows a permeability reduction about three times of the value for pristine Nafion®.

Similar procedures have been used by other researchers to determine the methanol permeability through membranes [35]. Although it is not the case by using methanol, the main limitation of this technique is the fact that only liquid/vaporizable solutes can be measured. Moreover, a precise column is important to be selected for a good separation of solvent and solute during the chromatography process.

4.3. Methanol permeability by densimetry

This technique takes advantage of the density difference between the solvent and the solute (solid or liquid) crossing the membrane. It is suitable for our measurements since methanol ($\rho \approx 0.8$ g cm^{-3}) has a large difference in density with regards to water ($\rho \approx 1.0$ g cm^{-3}), which favours a high resolution in the results.

Seven samples containing different methanol concentrations in water were prepared and their densities measured at 25 °C. It is worth remarking

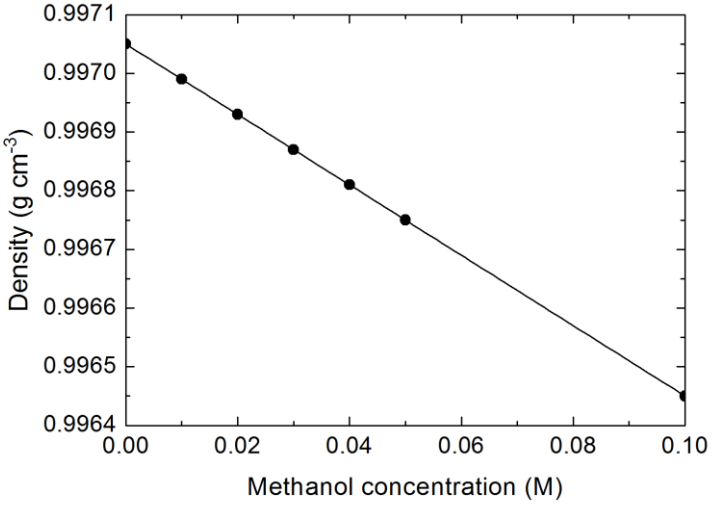

Fig. 9. Calibration curve correlating density of the solution versus methanol concentration at 25 ºC measured by densimetry.

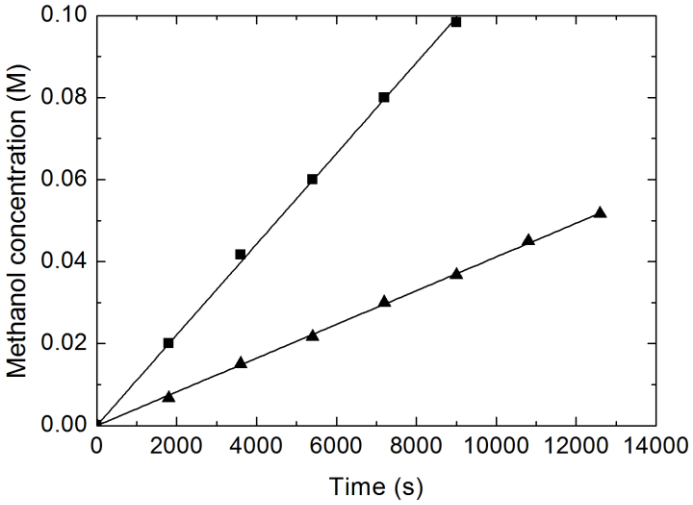

Fig. 10. Methanol concentration (c_R) versus time obtained from measurements of density for (■) pristine Nafion® and (▲) Nafion/PVA composite membranes at 25 ºC and $c_{L,0}$ = 2 M.

the excellent fitting found between densities and methanol concentrations (Figure 9). From this calibration curve and under the same conditions and experimental setup as mentioned for the GC technique, the behaviour of the methanol concentration as a function of time was obtained and it is showed in Figure 10 for the pristine Nafion® and the composite membrane of Nafion/PVA. The apparent permeability coefficients (P) were determined by means of Eq. (7) and the pertinent results are given in Table 1.

A close inspection of Figure 10 shows that the methanol concentrations in the cell R are higher for the pristine Nafion® ($P \approx 2.19 \cdot 10^{-6}$ cm^2 s^{-1}) than for the Nafion/PVA membrane ($P \approx 5.98 \cdot 10^{-7}$ cm^2 s^{-1}). It is similarly found a permeability coefficient for Nafion® identical to those reported values and the composite membrane involves a 3.7 times lower permeability.

4.4. Comparison of results and techniques

We can conclude that the three different experimental techniques have provided very comparable results. In all the cases, the methanol permeability across a Nafion® membrane coincides with the values reported in other studies, and it was also observed that the composite membrane of Nafion/PVA shows a lower permeability coefficient in average 1/3 of the value for pristine Nafion®.

A normalized methanol crossover rate can be defined by means of the following expression [36,37],

$$X_r = \frac{C_R \cdot L}{A \cdot t} \quad \left(\frac{[MeOH]}{cm \cdot s} \right) \tag{11}$$

where X_r is the normalized rate of methanol crossover, c_R/t represents the slope of methanol concentration in reservoir R versus time, and L and A are the thickness and area of the membrane, respectively, which are exposed to the permeation cell.

Assuming that the amount of methanol crossing from side L to side R is much smaller than the total amount of water in R and that the density of water is 1 g cm^{-3} at 25 °C, the molar rate, $q = X_r/L$ ([MeOH]/cm^2 s), is the methanol crossover per unit area of the membrane and second. Thus, the flux density of methanol crossing the membrane can be expressed as,

$$j = q \cdot V_R = \frac{C_R \cdot V_R}{A \cdot t} \quad \left(\frac{mol\ MeOH}{cm^2 \cdot s} \right) \tag{12}$$

in which V_R is the volume of water in the receptor reservoir. The values of flux density calculated for the methanol crossing the membranes in each experiment are reported in Table 1. As expected, the Nafion® film presents a higher flux density of methanol in comparison with the Nafion/PVA membrane.

Regarding the techniques used in this study, we can classify them from an economical point of view as a function of their acquisition cost: Gas chromatography >> densimetry > potentiometry. On the other hand, in terms of accuracy in the measurements of real concentration versus time, the order is as follows: Densimetry ≈ GC >> potentiometry. Another classification involves the time needed to complete a permeation experiment with good results: Densimetry < GC << potentiometry. Although GC requires a similar measurement time as densimetry in order to obtain the permeation curve (c_R versus time), the determination of the methanol concentration by means of the GC setup is more laborious and complex, and thus, globally a higher working time is needed.

Therefore, densimetry can be assigned as the most efficient technique by taking into account the above commented factors. However, if the economical aspect is a limiting factor, the permeation measurements can be carried out by potentiometry. This is a very simple technique and suitable for measuring relative values, such as the slope of the c_R versus time profile, since absolute values of methanol concentration are not required for the corresponding calculations. GC is a precise but expensive technique, and it should be taken into account just in case of being readily available.

5. Conclusions

Ex situ measurements of methanol permeability represent the most unfavourable case in terms of crossover and equivalent to OCV conditions during *in situ* DMFC experiments, as methanol crossover becomes reduced with increasing current density. Therefore, *ex situ* methods are appropriate for a simple and rapid characterization of membranes for DMFC application.

Potentiometry, gas chromatography and densimetry have resulted to be suitable techniques for the *ex situ* determination of methanol crossover through a membrane. In this study, a commercial Nafion® NR-212 film and a novel composite membrane of Nafion/PVA have been used. All those methods showed results in good agreement between each other and with the literature. The novel Nafion/PVA membrane achieved a value of apparent methanol permeability about three times lower than the results reported with pristine Nafion®.

The technique of densimetry performed as the most efficient in terms of accuracy, simplicity, experimental time, and cost. Potentiometry is the most simple and lowest cost option but it seems to be only adequate for relative parameters, such as a slope of concentration versus time. Absolute values of concentration at a given time could not be measured and the time needed to reach a steady-state doubles the experimental time necessary to finish the measurements with the other techniques. In this regard, a previous step of electrochemical activation of the working electrode might be required. On the other hand, GC was also found to be very precise, comparable to densimetry, but the most expensive one, and thus, it should just be taken into account if it is readily available for its use.

Acknowledgements

This work has been supported by the Valencian Institute of Small and Medium-Sized Enterprises (IMPIVA) and the European Regional Development Funds, through the project IMIDIC/2010/13.

References

[1] J. Müller, G. Frank, K. Colbow, D. Wilkinson in Handbook of Fuel Cells-Fundamentals, Technology and Applications, Vol. 3 (Eds. W. Vielstich, A. Lamm, H. Gasteiger), John Wiley & Sons, Chichester, 2003, Chapter 62.
[2] M. Neergat, K. A. Friedrich, U. Stimming, Fuel Cells 2002, 2, 25.
[3] K. A. Mauritz, D. A. Mountz, D. A. Reuschle, R. I. Blackwell, Electrochim. Acta 2004, 50, 565.

[4] Q. Deng, Y. Hu, R. B. Moore, C. L. McCormick, K. A. Mauritz, Chem. Mater. 1997, 9, 36.
[5] Y. M. Kim, K. W. Park, J. H. Choi, I. S. Park, Y. E. Sung, Electrochem. Commun. 2003, 5, 571.
[6] M. A. Smit, A. L. Ocampo, M. A. Espinosa-Medina, P. J. Sebastian, J. Power Sources 2003, 124, 59.
[7] T. Shimizu, T. Naruhashi, T. Momma, T. Osaka, Electrochemistry 2002, 70, 991.
[8] C.-Y. Chen, J. I. Garnica-Rodriguez, M. C. Duke, R. F. Dalla Costa, A. L. Dicks, J. C. Diniz da Costa, J. Power Sources 2007, 166, 324.
[9] F. J. Fernández-Carretero, V. Compañ, E. Riande, J. Power Sources 2007, 173, 68.
[10] F. J. Fernández-Carretero, E. Riande, C. del Río, F. Sanchez, J. L. Acosta, V. Compañ, J. New Mater. Electrochem. Syst. 2010, 13, 83.
[11] N. W. DeLuca, Y. A. Elabd, J. Memb. Sci. 2006, 282, 217.
[12] S. Mollá, V. Compañ, J. Power Sources 2011, 196, 2699.
[13] D. Kreuer, Chem. Mater. 1996, 5, 610.
[14] J. F. Synder, M. A. Ratner, D. F. Shriver, Solid State Ionics 2002, 147, 249.
[15] S. J. P. Ann, Rev. Mat. Res. 2003, 33, 289.
[16] X. Ren, T. A. Zawodzinski, Jr. F. Uribe, H. Dui, S. Gottesfeld in Proton Conducting Membrane Fuel Cells (Eds. I. S. Gottesfeld, G. Halpert, A. Langrebe), The Electrochemical Society Proceedings Series, Penington, 1995, pp. 284.
[17] R. Jiang, D. Chu, Electrochem. Solid State Lett. 2002, 5, A156.
[18] Z. Qi, A. Kaufman, J. Power Sources 2002, 110, 177.
[19] S. Eccarius, B. L. Garcia, C. Hebling, J. W. Weidner, J. Power Sources 2008, 179, 723.
[20] T. Tamaki, A. Yamauchi, T. Ito, H. Ohashi, T. Yamaguchi, Fuel Cells 2011, 11, 394.
[21] B. S. Pivovar, Y. Wang, E. L. Cussler, J. Membr. Sci. 1999, 154, 155.
[22] T. Schaffer, V. Hacker, T. Hejze, T. Tschinder, J. O. Besenhard, P. Prenninger, J. Power Sources 2005, 145, 188.
[23] J. Zhang, Y. Wang, Fuel Cells 2004, 4, 90.
[24] A. Casalegno, P. Grassini, R. Marchesi, Appl. Therm. Eng. 2007, 27, 748.
[25] B. L. García, V. A. Sethuraman, J. W. Weidner, R. E. White, R. Dougal, J. Fuel Cell Sci. Technol. 2004, 1, 43.
[26] N. Munichandraiah, K. McGrath, G. K. Surya, R. Aniszfeld, G. A. Olah, J. Power Sources 2003, 117, 98.
[27] M. Bello, S. M. Javaid, S. U. Rahman, J. Membr. Sci. 2008, 322, 218.
[28] J. Liu, H. Wang, S. Cheng, K.-Y. Chan, J. Membr. Sci. 2005, 246, 95.
[29] S. Mollá, V. Compañ, J. Membr. Sci. 2011, 372, 191.
[30] J. Garrido, V. Compañ, J. Phys. Chem. 1992, 96, 2721.
[31] N. Wakabayashi, H. Uchida, M. Watanabe, Electrochem. Solid State Lett. 2002, 5, E62.
[32] P. Mukoma, B. R. Jooste, H. C. M. Vosloo, J. Membr. Sci. 2004, 243, 293.
[33] D. W. Kim, H.-S. Choi, C. Lee, A. Blumstein, Y. Kang, Electrochim. Acta 2004, 50, 659.
[34] J.-C. Tsai, H.-P. Cheng, J.-F. Kuo, Y.-H. Huang, C.-Y. Chen, J. Power Sources 2009, 189, 958.
[35] T. Schaffer, V. Hacker, T. Hejze, T. Tschinder, J. O. Besenhard, P. Prenninger, J. Power Sources 2005, 145, 188.
[36] H. A. Every, M. A. Hickner, J. E. McGrath, T. A. Zawodzinsk, J. Membr. Sci. 2005, 250, 183.
[37] K. Ramya, K. S. Dhathathreyan, J. Membr. Sci. 2008, 311, 121.

Paper 5

International Journal of Hydrogen Energy 39 (2014) 5121-5136
(Adapted to thesis)

Polymer blends of SPEEK for DMFC application at intermediate temperatures

Sergio Mollá, Vicente Compañ

Dpto. Termodinámica Aplicada, ETSII, Universidad Politécnica de Valencia, 46022 Valencia, Spain.

Abstract

Sulfonated poly(ether-ether-ketone) materials (SPEEK) are good proton conductors at high degrees of sulfonation and appropriate for high temperature application due to their glass transition temperatures around 200 ºC. Nevertheless, high degrees of sulfonation result in excessive swelling and dissolution of the membranes in hot water, preventing their potential use for direct methanol fuel cells. One possible remedy is their chemical stabilization. For this reason, blends of SPEEK with PVA (polyvinyl alcohol), a hydrophilic polymer, were prepared and tested. Above 25 wt% PVA, the membranes were found to be mechanically stable in boiling water, with acceptable proton conductivities but excessive methanol permeabilities. On the other hand, blends of SPEEK with a hydrophobic polymer, PVB (polyvinyl butyral), resulted in extremely stable membranes in boiling water above a 30 wt% PVB content. Those membranes presented excellent mechanical and methanol barrier properties while proton conductivities were very low. A discussion of possible ways to make optimal use of these materials is presented.

Keywords: Sulfonated PEEK, polymer blend, fuel cell membrane, methanol permeability, high temperature DMFC.

1. Introduction

Direct methanol fuel cells (DMFCs) are under attention as promising portable power generators for different electronic applications, e.g. telecommunication, military, leisure, etc. [1]. A high energy capacity due to the liquid nature of the methanol and easy refuelling are their main advantages [1,2]. However, methanol shows low electrochemical oxidation kinetics at the anode in comparison with hydrogen [3,4] and typically high permeability across standard membranes, e.g. Nafion® (DuPont Co.) [2,5,6], which are the most important key issues to overcome. Furthermore, thick membranes are usually used to reduce the methanol crossover that instead causes an increase of the Ohmic losses of the membrane [2]. Mass transport losses due to insufficient concentration of methanol at the anode and possible flooding of water at the cathode need to be taken into account, though they may not be significant if the fuel cell is operated at the right conditions.

Increasing the operating temperature benefits both faster kinetics at the electrodes, e.g. electrochemical oxidation of methanol and oxygen reduction reaction, and enhancement of the proton conductivity as long as water is retained in the membrane [2,7]. Although methanol permeability is also promoted with increasing temperature, the performance of a DMFC improves as the reduction of the electrochemical activation losses counteracts the crossover effect [8]. Unfortunately, not all the polymers are suitable for operation at higher temperatures, and among them, Nafion® starts to loose water [7] and mechanical properties [9] above 80 ºC. The reason is that the glass transition temperature (T_g) of Nafion® ranges between 80 ºC and 100 ºC under hydrated conditions [10-12], and thus, long time stability at higher temperatures cannot be guaranteed [2,12-14].

Sulfonated poly(ether-ether-ketone) materials (SPEEK) are potential candidates to replace Nafion® membranes at a low cost while exhibiting good chemical and thermal stabilities [15,16], that may enable operation at elevated temperatures in which electrochemical reaction rates speed up. The T_g values of SPEEK depend on the degree of sulfonation, i.e. ion-exchange capacity (IEC), and glass transition temperatures above 170 ºC are usually found [15,17]. Therefore, SPEEK membranes have sufficient stability to operate at intermediate temperatures (120-130 ºC) in fuel cells.

Conductivity and water uptake increase with increasing sulfonation degree [17-21] and the dependence of conductivity with water content is stronger for SPEEK materials than in the case of Nafion® [18,19]. Under certain conditions of temperature and degree of sulfonation, the proton conductivity of SPEEK at high levels of hydration surpasses that of Nafion® (≈ 0.1 S cm^{-1}) [17-21]. Thereby, the use of SPEEK for DMFC application, in

which an aqueous methanol solution feeds the anode, seems very appropriate as the membrane could be maintained in a fully hydrated state during a wide range of conditions.

On the other hand, increasing the degree of sulfonation results in higher methanol crossover rates [22-24], which is associated to water uptake, and ion-exchange capacity (IEC) values above 1.8 meq g^{-1} can even make pristine SPEEK membranes to dissolve in hot water [18,25,26].

As mentioned before, water uptake is a key parameter relevant to proton conductivity, methanol crossover and dimensional stability. Furthermore, it even influences long-term operation lifetime as during wet-up and dry-out cycles the mechanical stability strongly depends on the swelling and contraction levels [14].

Methods to control water uptake involve polymer blending [6,27-31] and crosslinking, which can be carried out chemically [32-39] or ionically [40-43]. Other authors have also reported the possibility for additional self-crosslinking reaction in SPEEK via inter-chain polymerization of the sulfonic acid groups at high temperature under vacuum [44]. However, we were not able to observe such a behaviour with our samples at high temperature conditions (140 ºC in vacuum and 200 ºC in air).

A peculiar characteristic of the hydrocarbon-type membranes is the fact that their properties become dependent on the pre-treatment and thermal history [18,45] as well as on the solvent used for the membrane casting [15,17,18,46,47]. In this regard, dimethylformamide (DMF) [17,46,47] and dimethylsulphoxide (DMSO) [15] are reported to affect very negatively to the performance of the membranes, while dimethylacetamide (DMAc) and N-methyl-2-pyrrolidone (NMP) solvents seem more appropriate to achieve better properties [17,46,47].

The purpose of this work is the preparation and fundamental study of the properties of blended SPEEK membranes with two defined goals: (a) Evaluation of the addition effect of hydrophilic or hydrophobic polymers in SPEEK membranes, and (b) application of the membranes for Direct Methanol Fuel Cells operating over 100 ºC in order to profit the advantages that higher temperatures provide.

Solution-cast membranes were prepared by blending SPEEK materials with hydrophilic PVA (polyvinyl alcohol) and hydrophobic PVB (polyvinyl butyral) using DMAc as a solvent. PVA and PVB were selected due to their low cost and wide availability. Although they belong to a same family of polymers (PVB is prepared by reaction of PVA with butyraldehyde), PVA presents a strong hydrophilic character (OH-rich) whereas PVB is hydrophobic due to the butyral side chains and low OH content. The presence of OH groups in a higher or lower degree grants both polymers

with the ability to perform chemical crosslinking with the sulfonic acid moieties of SPEEK. In this matter, it was found that PVB in SPEEK strongly reduced swelling, so an SPEEK grade with a high IEC value, 2.05 meq g^{-1}, was used. For the blended membranes containing PVA, an SPEEK polymer with an IEC value of 1.75 meq g^{-1} was employed since pronounced swelling was observed.

Swelling is one of the most critical features of SPEEK and other kind of hydrocarbon fuel cell membranes. Typically, pristine SPEEK membranes irreversibly swells and start to dissolve above 80 ºC or even at lower temperatures, which makes them impractical for real fuel cell application, especially in DMFCs. Water-methanol solutions are usually pumped into the anodes of DMFCs for the electrochemical reactions and this condition enables the simultaneous hydration of the membranes. Thereby, a pre-treatment step consisting of introducing our membranes in boiling water for 1 h was applied before proceeding with their further characterization in order to ensure their applicability in DMFCs operating above 100 ºC.

The effect of incorporating hydrophilic or hydrophobic polymers into blended membranes has not been generally studied in detail. In our results, different membrane properties were emphasized as a function of the characteristics of the blended polymers. Finally, potential configurations to take full advantage of those properties are proposed.

2. Experimental part

2.1. Materials

Granulated SPEEK (FUMION E ionomers) with IEC of 1.75 mmol g^{-1} and 2.05 mmol g^{-1} were acquired from Fumatech GmbH (St. Ingbert, Germany). SPEEK was dried at 100 ºC for 24 h in vacuum atmosphere and stored in a sealed container to avoid absorption of water before the preparation of membranes.

Polyvinyl alcohol, Mowiol 28-99 grade PVA, and polyvinyl butyral, Mowital B75H grade PVB, were donated by the company Kuraray Europe GmbH (Frankfurt, Germany).

N,N-Dimethylacetamide solvent was purchased from Acros Organics and anhydrous lithium chloride from Sigma-Aldrich.

Polyvinyl alcohol, polyvinyl butyral, dimethylacetamide and lithium chloride were used as received.

2.2. Preparation of membranes

2.2.1. SPEEK-PVA and SPEEK-PVB blends

Initially, solubility of PVA in DMAc solvent was examined and it was found that PVA was not soluble even at temperatures up to 140 ºC. Addition of anhydrous lithium chloride (LiCl) to enhance the solubility was then studied [48]. Incorporation of LiCl in a 0.4 wt% proportion with respect to the weight of DMAc solvent was found optimal for the complete solubilization of PVA until a 5 wt% concentration without affecting later the final aspect of the membranes, while further addition of LiCl caused the appearance of LiCl precipitates on the as-prepared membranes.

Membranes were prepared by casting of solutions with a 10 wt% concentration of polymer blend (SPEEK + PVA) in DMAc incorporating LiCl. Previously, LiCl was dissolved in DMAc at a 0.4 wt% concentration at room temperature. Then, the required amount of PVA was dissolved by stirring at 140 ºC for 1 h and afterwards the solution was let to cool down until room temperature. Finally, SPEEK (IEC = 1.75 meq g^{-1}) was added and the solution was vigorously stirred. SPEEK started to dissolve at room temperature but the solution was heated again at 140 ºC for 1 h in order to ensure a complete homogenisation. Blended compositions ranging from 85%SPEEK-15%PVA to 55%SPEEK-45%PVA were obtained.

PVB is readily soluble in DMAc at room temperature, and therefore, an addition of lithium chloride was not necessary. The required amount of PVB was dissolved in DMAc and stirred at 80 ºC for 1 h to achieve faster dissolution. The solution was let to cool down to room temperature and then SPEEK (IEC = 2.05 meq g^{-1}) was incorporated and the mixture was stirred for 1 h at 80 ºC until complete homogenisation (10 wt% total polymer concentration). Blended membranes with compositions between 75%SPEEK-25%PVB and 45%SPEEK-55%PVB were prepared.

Membranes with a thickness about 100 μm were obtained by casting the solutions on a Teflon® Petri dish and evaporating the solvent at 80 ºC overnight, followed by a treatment at 140 ºC for 2 h and then 1 h at the same temperature under vacuum atmosphere with the purpose of removing trapped DMAc molecules within the polymers. The last thermal step was crosslinking between the SPEEK and the PVA or PVB chains at 200 ºC for 1 h (without vacuum).

The crosslinked membranes were immersed in boiling water for 1 h to examine their mechanical stability as their application is intended for DMFCs operating above 100 ºC with the aim to enhance electrochemical reactions. The swollen membranes were stored in sealed plastic bags containing water.

2.3. Characterization of membranes

2.3.1. Water uptake, swelling and ion-exchange capacity

Water uptake was calculated from the difference between the weight of the membranes wet and dry, according to the following expression,

$$Water\ uptake\,(\%) = \frac{m_{wet} - m_{dry}}{m_{dry}} 100 \qquad (1)$$

Since solubilization of some amounts of polymer from the as-cast membranes was possible to occur during treatment in boiling water, the blended membranes were weighed after 1 h in boiling water (m_{wet}) and after 3 h in an oven at 100 ºC followed by another 3 h in vacuum at that temperature (m_{dry}). This operation was repeated with three samples for each composition in order to obtain an average value.

The swelling degree was measured by the change of area of square membranes with initial 5 x 5 cm^2 dimensions ($A_0 = L_0 \, x \, L_0$). After 1 h in boiling water, the swollen membranes practically maintained the square shape but with enlarged dimensions ($A_f = L_f \, x \, L_f$),

$$Swelling\ (\%) = \frac{A_f - A_0}{A_0} 100 \qquad (2)$$

The ion-exchange capacity (IEC) was obtained by immersing the swollen membranes in the acid form into a 2 M NaCl solution. The protons liberated during the exchange reaction $R\text{-}SO_3H + Na^+ \rightarrow R\text{-}Na + H^+$ were titrated with a 0.01 M NaOH solution and phenolphthalein. The IEC was calculated as,

$$IEC\ (meq\ g^{-1}) = \frac{0.01 \cdot V_{NaOH}}{m_{dry}} \qquad (3)$$

where V_{NaOH} and m_{dry} are the volume in millilitres of NaOH solution used in the titration of the protons released by m grams of dry membrane, respectively. The values of m_{dry} were measured after drying at 100 ºC for 6 h the samples immersed within the NaCl solution.

2.3.2. Scanning electron microscopy (SEM) study

The surface morphology of the blended membranes was investigated using a scanning electron microscope (SEM-model JSM-5410, Jeol Co., Japan). The samples were gold coated before SEM observations.

2.3.3. Infrared (IR) spectroscopy

IR spectroscopy was used to investigate the chemical interactions between the polymer chains of the blended membranes. The spectra were obtained using a Jasco FT/IR-6200 spectrometer.

2.3.4. Differential scanning calorimetry (DSC) analysis

Thermal analysis was carried out by means of a Mettler Toledo DSC 821 differential scanning calorimeter. The heating rate was fixed at 10 ºC min^{-1} and two runs from -50 ºC to 250 ºC were monitored for each sample. The experiments were performed under nitrogen atmosphere using a flux of 50 ml min^{-1}.

2.3.5. Methanol permeability

A typical 2-cell experimental setup was used to measure the methanol permeability coefficient across the blended membranes. The donor chamber (D) was filled with a 2 M or 4 M aqueous solution of methanol, while the receptor chamber (R) was filled with distilled water. Both chambers were kept under stirring and thermostated at 60 ºC. The variation of methanol concentration with time in the receptor reservoir was determined by means of a densimeter (DMA 4500 M, Anton-Paar, Austria). The sample (~1 ml) is introduced into a U-shaped borosilicate glass tube that is being excited to vibrate at its characteristic frequency, which changes depending on the density of the sample. Through a precise determination of the characteristic frequency and a mathematical conversion, the mass density (g cm^{-3}) of the sample can be estimated.

A calibration curve of density versus methanol concentration was obtained before the permeation measurements. During those experiments, a small sample of solution from the receptor compartment was taken at certain time intervals and the density recorded. In order to avoid the volume of liquid in the receptor reservoir (V_R = 150 cm^3) to diminish, the samples were recovered from the densimeter after each measurement. Representing the methanol concentration in the receptor chamber (C_R) versus time (t), the apparent permeability (P) of methanol across a membrane with thickness

L (cm) and surface area A (A = 2.27 cm^2) can be determined from Eq. (4), which is valid during the range in which the gradient $C_{D,0}$ - C_R does not significantly change, that is, for the condition $C_{D,0} >> C_R$ (being $C_{D,0}$ the initial methanol concentration in the donor chamber),

$$P = \frac{V_R \cdot L \cdot C_R}{C_{D,0} \cdot A \cdot (t - t_0)} \qquad (4)$$

2.3.6. Proton conductivity

The proton conductivity of the membranes in the transversal direction was measured by impedance spectroscopy at 25 ºC, 50 ºC, 75 ºC and 90 ºC in the frequency range of $10^{-1} < f < 10^7$ Hz applying a 0.1 V signal amplitude. A Novocontrol broadband dielectric Spectrometer (Hundsangen, Germany) integrated by an SR 830 lock-in amplifier with an Alpha dielectric interface was used. The membranes were previously equilibrated with water and afterwards placed between two gold electrodes in a liquid parallel plate cell coupled to the spectrometer and incorporating deionized water (Milli-Q) to ensure fully hydrated state of the samples. The temperature was controlled by nitrogen jet (QUATRO from Novocontrol) with a temperature error of ~0.1 K during every single sweep in frequency.

The protonic resistance R was taken from the Bode plot as the value of the modulus of the complex impedance at which the phase angle reaches a maximum close to zero in the high frequency region, $|Z| \rightarrow R$. The conductivity of the membranes (σ') was then calculated from the real part of the protonic resistance R by means of Eq. (5),

$$\sigma' = \frac{L}{R \cdot S} \qquad (5)$$

where L is the thickness of the membrane and S the electrode area in contact with the membrane.

3. Results and discussion

3.1. Water uptake and ion-exchange capacity

Immersion in boiling water of pristine membranes of SPEEK with IEC values of 1.75 meq g^{-1} (SPEEK1) and 2.05 meq g^{-1} (SPEEK2) caused first a drastic swelling of the membranes which finally ended in complete

Table 1. Mechanical and dimensional characteristics of the SPEEK1-PVA and SPEEK2-PVB membranes after 1 h in boiling water. Swelling measured by $(A_f - A_0)/A_0$. Initial area (A_0) was 5 x 5 cm^2. Dry thickness of all the cast membranes ~96 ± 4 μm.

Membrane	Hydrated thickness (μm)	Swelling (% area)	Mechanical stability
SPEEK1 (1.75 meq g^{-1})[a]	105 ± 2	∞	Dissolved
SPEEK1-15%PVA	-	-	Very poor
SPEEK1-25%PVA	210 ± 5	58.8 ± 0.01	Poor
SPEEK1-35%PVA	185 ± 3	58.8 ± 0.01	Acceptable
SPEEK1-45%PVA	159 ± 3	58.8 ± 0.01	Good
SPEEK2 (2.05 meq g^{-1})[b]	133 ± 3	∞	Dissolved
SPEEK2-25%PVB	-	-	Partially dissolved
SPEEK2-30%PVB	167 ± 3	0.00	Excellent
SPEEK2-35%PVB	116 ± 2	0.00	Excellent
SPEEK2-45%PVB	103 ± 2	0.00	Excellent
SPEEK2-55%PVB	96 ± 3	0.00	Excellent

[a] Membrane swollen in water at 80 ºC for 1 h.
[b] Membrane swollen in water at 60 ºC for 1 h.

dissolution (Table 1). A limit temperature of 80 ºC and 60 ºC was found for each SPEEK grade, respectively. The membranes were stable in water below those temperatures as swelling did not still reach an irreversible degree.

SPEEK1 (IEC = 1.75 meq g^{-1}) was initially blended with both PVA (hydrophilic) and PVB (hydrophobic) polymers, and the first observations

Table 2. Ion-exchange capacity values of SPEEK1-PVA and SPEEK2-PVB membranes swollen in boiling water for 1 h, and IEC values of those membranes after drying at 100 ºC during 6 h. Water uptake values after swelling in boiling water are also included.

Membrane	IEC after boiling (meq g^{-1})	IEC after drying (meq g^{-1})	Water uptake (%)
SPEEK1 (1.75 meq g^{-1})[a]	1.69 ± 0.05 (dissolved)	0.95 ± 0.02	260 ± 5
SPEEK1-15%PVA	-	-	-
SPEEK1-25%PVA	1.07 ± 0.03	0.040 ± 0.005	695 ± 14
SPEEK1-35%PVA	0.71 ± 0.02	0.12 ± 0.01	490 ± 9
SPEEK1-45%PVA	0.76 ± 0.03	0.17 ± 0.01	296 ± 6
SPEEK2 (2.05 meq g^{-1})[b]	2.02 ± 0.05 (dissolved)	1.08 ± 0.02	343 ± 7
SPEEK2-25%PVB	-	-	-
SPEEK2-30%PVB	0.41 ± 0.02	0.055 ± 0.005	96 ± 2
SPEEK2-35%PVB	Not measured	0.043 ± 0.002	59 ± 1
SPEEK2-45%PVB	Not measured	0.024 ± 0.002	35 ± 1
SPEEK2-55%PVB	Not measured	0.015 ± 0.001	27 ± 1

[a] Membrane swollen in water at 80 ºC for 1 h.
[b] Membrane swollen in water at 60 ºC for 1 h.

pointed out different behaviours in the blended membranes as a function of the polymer characteristics. In the case of PVA, a rubber-like phase was formed in which swelling and water uptake was large but limited enough to allow the formation of stable membranes (Tables 1 and 2). Increasing the amount of PVA improved the stability and reduced the water uptake and swelling degree. Interestingly, in-plane swelling (enlargement of area) was independent of the PVA content but through-plane swelling (the increase of hydrated thickness) diminished with increasing PVA composition (Table 1).

On the other hand, blending of SPEEK1 with PVB resulted in membranes with negligible swelling in boiling water, which in principle are impractical for real DMFC operation as a certain degree of swelling and water uptake are necessary to achieve acceptable conductivities [17-21]. Thereby, SPEEK2 (IEC = 2.05 meq g^{-1}) was selected for blending with PVB due to its higher degree of sulfonation in comparison with SPEEK1 and in consequence less constrained membranes were expected. In Tables 1 and 2 we can observe that above a 30%PVB content the blended SPEEK2 membranes were extremely stable, showing negligible in-plane swelling and relatively small values of water uptake. Through-plane swelling was only significant for the membranes containing 30% and 35% PVB in the composition. Increasing PVB content caused drastically the hydrated thickness and water uptake values of the blended membranes to decrease, while mechanical stability enhanced.

Differences observed between the PVA and PVB blended SPEEK membranes are assigned to the hydrophilic and hydrophobic nature of those polymers, respectively.

With regard to the IEC values in Table 2, a general trend can be distinguished in which the incorporation of PVA or PVB in the membrane composition involves a decrease of the IEC values in relation to the corresponding pristine SPEEK membranes. Two reasons can explain this observation as (1) PVA and PVB lack of sulfonic acid groups ($-SO_3H$) thus diluting the ones provided by the SPEEK, and (2) sulfonic acids of SPEEK will be consumed by crosslinking reactions with OH groups present in PVA and PVB polymers.

The pristine SPEEK membranes (SPEEK1 and SPEEK2) only gave realistic results of IEC, in agreement with those provided by the supplier, when fully dissolved in water. Thus, it is suggested that the measurement of IEC by the NaCl ion-exchange method does not seem to be totally accurate for SPEEK materials. The reason is still not clear and further investigations should be carried out.

It is worth mentioning the large differences observed between the IEC values of membranes in the swollen state and membranes which have been dried at 100 ºC after swelling. The IEC values of the dried membranes were

much lower than those of the same membranes swollen in water. This observation suggests that the properties of this type of membranes are strongly dependent on the thermal history, as it has been reported for explaining differences between swollen and non-swollen SPEEK membranes [18,45]. For this reason, the authors consider that this paper is the first to report that irreversibility of membrane properties between swollen and dried states can take place.

The properties of commercial Nafion® seem to be considerably more reversible than in the case of hydrocarbon based membranes as SPEEK. A possible explanation comes from the fact that in Nafion®, a perfluorinated polymer, phase separation of the hydrophobic and hydrophilic blocks readily occurs whereas in randomly sulfonated hydrocarbon materials such a phase separation is not very pronounced. This results in narrower and less interconnected ionic channels, which in principle are advantageous for reduced permeability and electro-osmotic drag. However, this characteristic leads on the other hand to poor morphological stability, excessive swelling in water while brittleness in the dry state, and to a stronger decrease of proton conductivity with decreasing water content [49,50].

Many recent works deal with the synthesis of hydrocarbon membranes based on ordered block co-polymers in which a block is sulfonated and hydrophilic while the other block remains hydrophobic. This trend seems to be justified by the advantages that an optimal phase separation brings on the final properties [51-55].

3.2. SEM results

Fig. 1 shows the SEM images of a pristine SPEEK2 membrane which was dried after swelling at 60 ºC and it is compared with a SPEEK1-35%PVA and a SPEEK2-30%PVB membrane which were dried after swelling in boiling water (100 ºC). The membranes were dried to avoid problems during the vacuum treatments associated with the SEM procedures.

In Fig. 1 it is observed that both the SPEEK2 and the SPEEK1-35%PVA membranes have a relatively flat surface in a low magnification. However, the SPEEK2-30%PVB membrane revealed a wrinkled morphology indicating the presence of mechanically constrained areas. A close inspection at higher magnifications (zoomed window) showed a very rough surface on the SPEEK2-30%PVB membrane presenting globular structures which are similar to the morphologies observed on sophisticated block co-polymers at the nanoscale. In our method, simple mixing of SPEEK with PVB dissolved in DMAc has produced cast membranes in which well dispersed polymer separation can be found as a consequence of the hydrophobic characteristic of PVB versus the hydrophilic property of

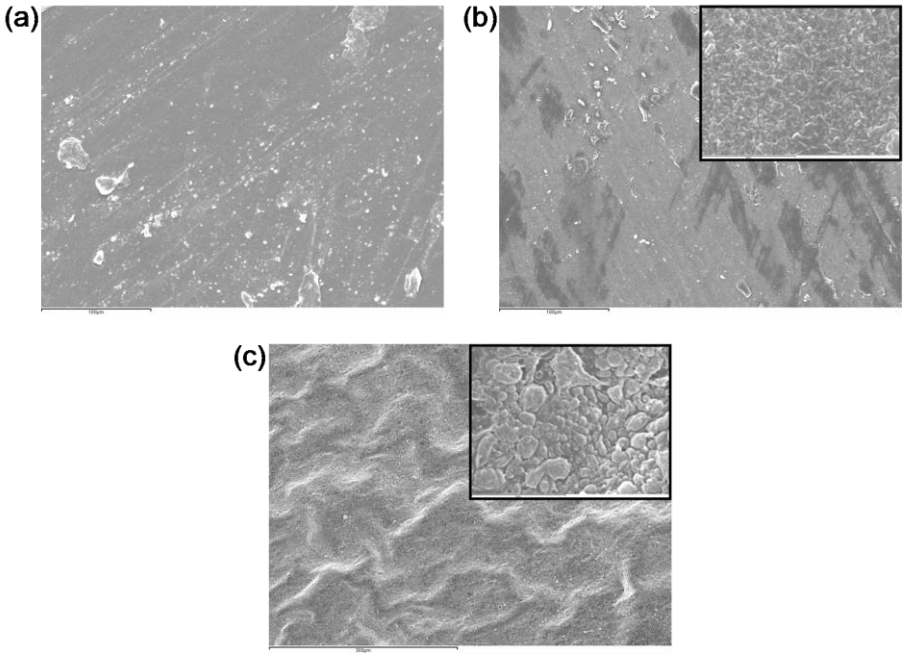

Fig. 1. SEM images of swollen and afterwards dried membranes of (a) pristine SPEEK2 (x350), (b) SPEEK1-35%PVA (x350, zoomed window at x10,000), and (c) SPEEK2-30%PVB (x200, zoomed window at x10,000).

SPEEK. Thus, a morphology presenting phase separation takes place but in this case at a microscale domain.

On the other hand, a flaky surface was observed on the SPEEK1-35%PVA membrane as a result of the shrinking process during drying of the swollen membrane. No evidence of phase separation was found as expected from the hydrophilic nature of the PVA composition containing OH moieties which can establish hydrogen bonding with the sulfonic acid groups of SPEEK.

3.3. FTIR analysis

In Fig. 2 are shown the structures of the SPEEK, PVA and PVB polymers in order to facilitate the interpretation of the FTIR spectra.

The FTIR analysis of the cast PVA sample (Fig. 3) shows a broad peak from 3700 cm^{-1} to 3000 cm^{-1}, centred around 3300 cm^{-1}, indicating stretching of the hydroxyl (OH) groups, whereas the observed peak at 1083 cm^{-1} indicates the C-O stretch of the secondary alcoholic groups. The double peak between 2937 cm^{-1} and 2909 cm^{-1} is due to symmetric C-H stretching in

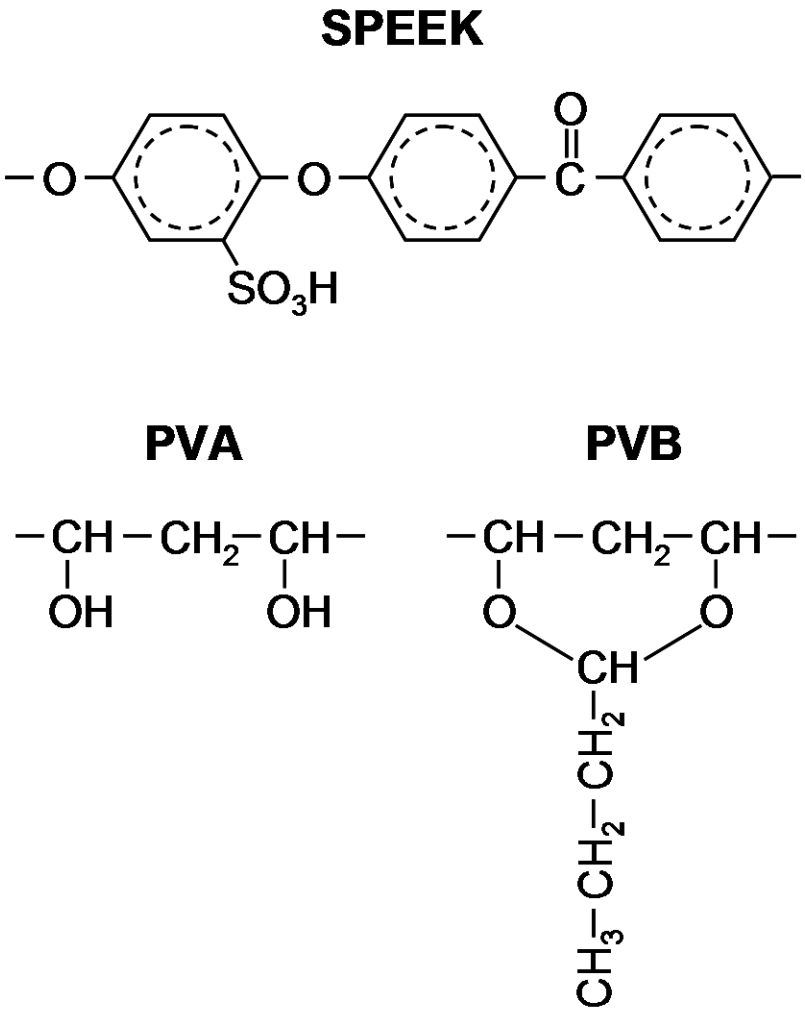

Fig. 2. Schematic representation of the structure of the monomeric units of SPEEK, PVA and PVB.

-CH_2- species and the band between 1718 cm^{-1} and 1709 cm^{-1} is attributed to stretching of C=O [36,56].

After thermal treatment at 200 ºC, the broad peak corresponding to the OH groups decreased indicating partial decomposition of those groups. However, the -CH_2- band remained unaltered thus suggesting that dehydration of the backbone forming C=C units did not occur [56]. On the other hand, the band placed around 1715 cm^{-1} and assigned to C=O groups largely increases after the thermal treatment, which indicates the transformation of C-OH bonds to C=O probably by oxidation in air.

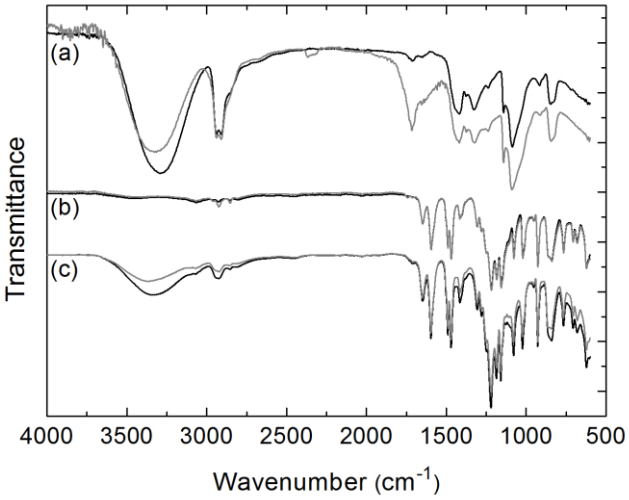

Fig. 3. FTIR spectra of (a) PVA, (b) SPEEK1 and (c) SPEEK1-35%PVA for (black line) as-prepared samples after casting at 80 ºC, and (grey line) samples treated at 200 ºC.

The FTIR profile of the cast SPEEK membrane (SPEEK1) in Fig. 3 shows characteristic peaks around 3450 cm^{-1} (O-H vibration from sulfonic acid groups), at 1247 cm^{-1}, 1079 cm^{-1} and 1025 cm^{-1} (assigned to the sulfonic acid groups), and at 1652 cm^{-1} (carbonyl band) [36], while those peaks at 1491 cm^{-1} and 1221 cm^{-1} are reported to the presence of C-C aromatic ring and aromatic C-O-C, respectively [57]. The profiles are coincident with the cast and the 200 ºC-treated membrane which points out the good thermal and chemical stability of this kind of materials.

The SPEEK-PVA blended membrane (SPEEK1-35%PVA) also observed in Fig. 3 has a profile resembling the one of SPEEK as expected from the fact that it constitutes the main component within the matrix. However, it shows a strong and broad peak at 3330 cm^{-1} in comparison with pristine SPEEK and this is due to overlapping of -OH from PVA and -OH from sulfonic acid groups of SPEEK. After the crosslinking process at 200 ºC, that band largely decreased as a consequence of (a) the direct condensation reaction between sulfonic acid and OH groups thus establishing crosslinking bonds, and (b) the intra- and inter-molecular dehydration of C-OH moieties to C=C units catalysed by the acidity of SPEEK, involving in the latter case direct crosslinking between PVA chains. This is corroborated by the reduction of the -CH_2- absorption band which appears in the blended membrane within the 2923-2937 cm^{-1} range [56]. Therefore, it is plausible the crosslinking to proceed via the formation of bonds between SPEEK-PVA, see Eq. (6), and PVA-PVA chains.

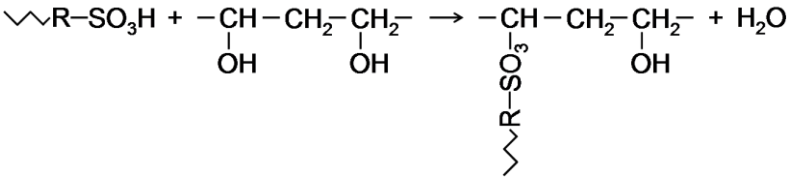

(6)

In Fig. 4, the FTIR spectra of PVB is shown together with those of SPEEK2 and SPEEK-PVB (SPEEK2-30%PVB) membranes. In the case of PVB, a broad peak between 3700 cm^{-1} and 3020 cm^{-1} and centred around at 3430 cm^{-1} is again observed due to OH groups present in the polymer, corresponding to PVA segments which did not react with butyraldehyde (side chains) through an acetal formation-type reaction during the industrial synthesis process. Our commercial sample of PVB (Mowital B75H) is reported by Kuraray Co. to have about an 18-21 wt% of PVA content. Peaks at 2955 cm^{-1} and 2870 cm^{-1} are due to C-H stretching, those at 1341 cm^{-1}, 971 cm^{-1}, 810 cm^{-1} are assigned to C-H symmetry stretching, whereas the one at 1435 cm^{-1} to C-H asymmetry stretching. The band at 1741 cm^{-1} is assigned to C=O stretching, those at 1240 cm^{-1} and 688 cm^{-1} due to C-O-C stretching, and finally the peak at 1131 cm^{-1} is assigned to C-O-C-O-C stretching in accordance with other authors [58].

Heating the PVB in air at 200 ºC causes all the peaks to decrease indicating thermal degradation of the polymer, which was confirmed by the appearance of a yellowish tone in the transparent film assigned to the

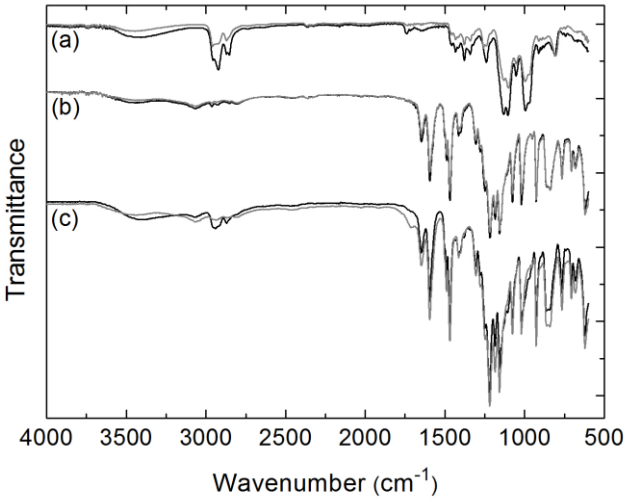

Fig. 4. FTIR spectra of (a) PVB, (b) SPEEK2 and (c) SPEEK2-30%PVB for (black line) as-prepared samples after casting at 80 ºC, and (grey line) samples treated at 200 ºC.

development of conjugated diene units. The OH groups are expected to decrease via a similar dehydration mechanism as mentioned for PVA, while the main decomposition product of degradation at 200 ºC in humid air is reported to be butyraldehyde released from the side chains of the PVB molecule [59]. On the other hand, the FTIR profile of the SPEEK2 membrane shows again an outstanding thermal stability with characteristic peaks placed in same positions as previously cited for the SPEEK1 sample.

The FTIR spectra of the SPEEK-PVB membrane (SPEEK2-30%PVB) is also dominated by the spectra of SPEEK, although the peaks associated to the OH groups (centred at 3400 cm^{-1}) and C-H stretching (2955-2870 cm^{-1}) of the PVB molecule are clearly visible in the cast blend membrane. In the case of the OH groups, the spectra is indeed due to the overlapping of those coming from the PVB (remaining PVA segments) and SPEEK (sulfonic acids) as in the SPEEK-PVA case. Crosslinking at 200 ºC causes those peaks to decrease which should again indicate the fulfilment of condensation reactions between the sulfonic acids and OH groups, and concurrently the degradation of the PVB phase via dehydration mechanisms and removal of butyral side chains. However, those degradation processes might favour further crosslinking reactions between PVB-PVB and SPEEK-PVB chains via reactivity of the very active C=C double bonds which are formed after thermal decomposition. A plausible reaction between a sulfonic acid and a C=C unit is suggested in Eq. (7), although clear understanding and evidence of the principal reaction pathway for the crosslinking of SPEEK with PVB is still needed,

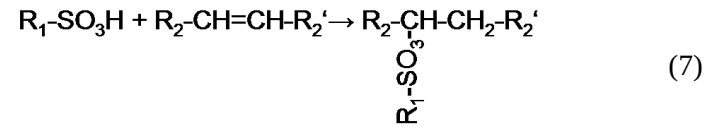

(7)

3.4. DSC results

The DSC curve of PVA in Fig. 5 shows the typical melting of PVA crystallites between 200 ºC and 230 ºC [60]. SPEEK is an amorphous polymer and the glass transition temperature (T_g) of the sample with ion-exchange capacity of 1.75 meq g^{-1} (SPEEK1) is found around 188 ºC (Fig. 7), while the T_g of the SPEEK sample with IEC of 2.05 meq g^{-1} (SPEEK2) increases up to 210 ºC (Fig. 8), in agreement with other authors [15,21,61]. The T_g values shift upwards with the increase of the sulfonation degree as a consequence of stronger intermolecular interactions by hydrogen bonding of sulfonic acid groups and due to increased molecular bulkiness which hinder internal rotations and lead to more rigid materials [15,61].

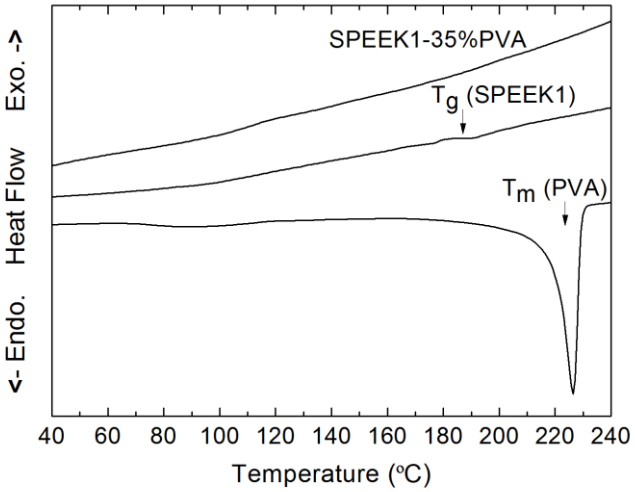

Fig. 5. Second run of DSC profiles for PVA, SPEEK1 (IEC = 1.75 meq g^{-1}) and SPEEK1-35%PVA membranes after thermal treatment at 200 ºC.

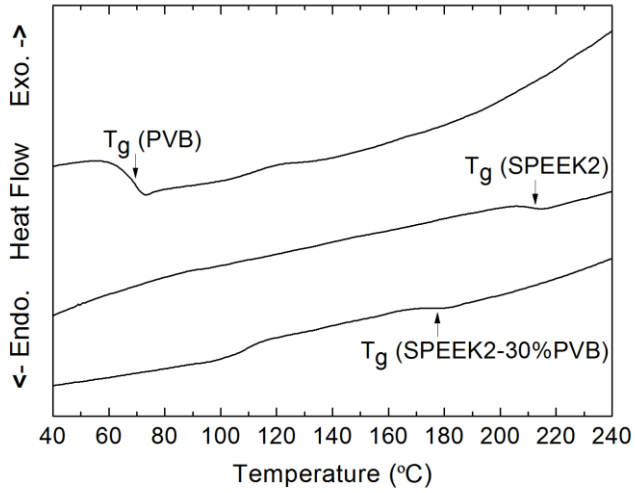

Fig. 6. Second run of DSC profiles for PVB, SPEEK2 (IEC = 2.05 meq g^{-1}) and SPEEK2-30%PVB membranes after thermal treatment at 200 ºC.

The DSC curve of PVB in Fig. 6 shows a large glass transition within the 55-73 ºC range of temperature, which falls into the limits reported for the T_g values of PVB with an 11-19 wt% of PVA content [62]. Increasing the content of butyral side chains in PVB results in lower glass transition

temperatures explained by the plasticizing effect of butyral groups and the decreased hydrogen bonding between OH moieties [62].

The DSC profile of the SPEEK-PVB blended membrane (SPEEK2-30%PVB) in Fig. 6 also shows that the glass transition phase of PVB disappears thus indicating that the PVB chains were crosslinked. Interestingly, a glass transition corresponding to the SPEEK2 phase was found although at reduced temperatures (shifted from 210 ºC to 176 ºC) which corroborates the plasticizing effect of the butyral groups. The reason to explain the presence of a T_g transition in the crosslinked SPEEK-PVB membrane should come from the polymer separation morphology observed in Fig. 1. It seems that all the PVB chains are able to react with an SPEEK chain (SPEEK-PVB) or another PVB chain (PVB-PVB) becoming crosslinked and aggregated in PVB rich clusters. On the other hand, crosslinking reactions are not able to take place in all the SPEEK chains and those free chains become encapsulated within SPEEK-rich clusters and get plasticized by the butyral groups of PVB chains which reacted with neighbouring SPEEK chains.

The result of the SPEEK-PVA blended membrane found in Fig. 5 is different from the one of the SPEEK-PVB composition. In the case of the SPEEK1-35%PVA membrane, the DSC profile does not exhibit any glass transition or melting phases from the SPEEK and PVA content, respectively, thus suggesting that all the SPEEK and PVA chains were mixed and crosslinked forming an interpenetrating polymer network, which is in accordance with the SEM images showing a homogeneous morphology in the SPEEK-PVA composition (Fig. 1).

3.5. Apparent methanol permeability across the membranes

The methanol permeability values for SPEEK1-PVA and SPEEK2-PVB membranes have been characterised as a function of blends composition. The values are reported to be apparent as they incorporate both the effect of boundary layers and the true permeability through the bulk membrane.

The results of methanol permeability and water uptake as a function of the PVA and PVB content are given in Figs. 7 and 8, respectively. The direct relationship between water uptake and methanol permeability is very clear from the profiles observed in those figures, which is indicative that methanol permeates through the water filled channels.

In Fig. 7, it is observed that the methanol permeability decreases with increasing the PVA content as a consequence of the reduced swelling and water uptake via chemical crosslinking. The pristine SPEEK1 membrane shows smaller values of water uptake and methanol permeability as it was immersed 1 h in water just at 80 ºC with the aim to avoid its dissolution.

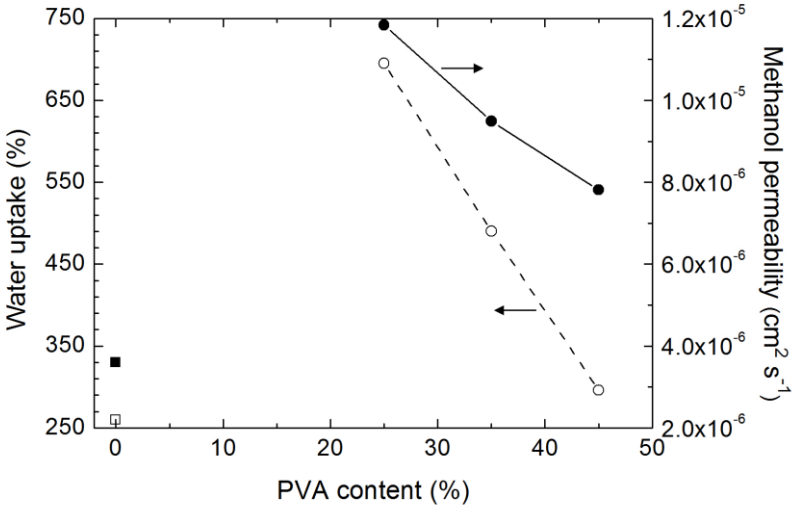

Fig. 7. Values of (closed symbol, solid line) methanol permeability measured at 60 ºC from 2 M methanol solutions and (open symbol, dashed line) water uptake for membranes of SPEEK1-PVA composition. (Square) The pristine SPEEK1 membrane was previously swollen in water at 80 ºC for 1 h, while (circle) the PVA-blended membranes were swollen in boiling water at 100 ºC for 1 h.

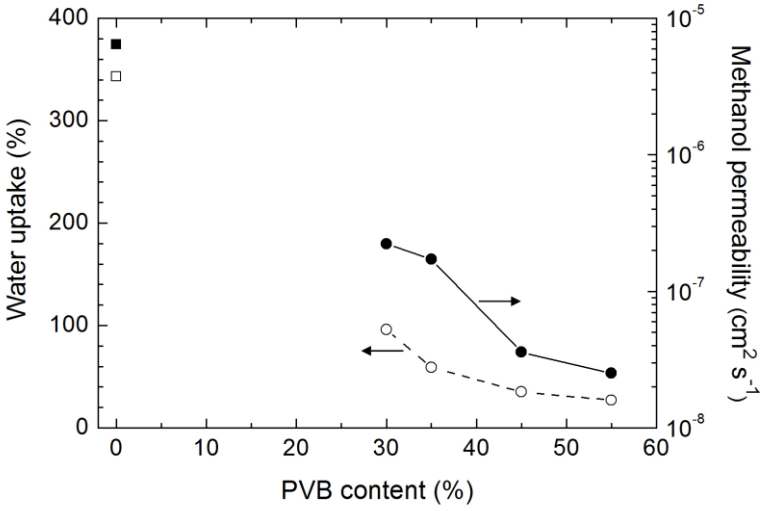

Fig. 8. Values of (closed symbol, solid line) methanol permeability measured at 60 ºC from 4 M methanol solutions and (open symbol, dashed line) water uptake for membranes of SPEEK2-PVB composition. (Square) The pristine SPEEK2 membrane was previously swollen in water at 60 ºC for 1 h, while (circle) the PVB-blended membranes were swollen in boiling water at 100 ºC for 1 h.

The SPEEK-PVA membranes were immersed in boiling water (100 ºC) for 1 h and therefore they were exposed to severer swelling conditions. Values around 10^{-5} cm^2 s^{-1} have been measured in these compositions which are found to be in the same range as other reported SPEEK-PVA membranes [36], although our values lie above those reported ones when similar compositions are compared. Nevertheless, this can be expected from the fact that in the work of T. Yang [36] the blended SPEEK-PVA membranes were just swollen at room temperature despite the methanol permeability measurements were conducted at 80 ºC. Although this temperature surpasses that one of our experimental permeability procedure (60 ºC), it is still below the boiling conditions (100 ºC) at which the membranes in the present study were subjected in order to reach severe swelling levels exceeding the limits of stability usually found in pristine SPEEK membranes. For this reason, the direct comparison of results is not meaningful when the membranes notably differ in their swelling degrees and treatment processes, and this should include comparison with the Nafion® membrane.

Generally, the properties of the SPEEK membranes, mainly reported by the characteristic factor between proton conductivity and methanol permeability (σ/P), are emphasized to surpass the properties of Nafion® in measurements performed at room temperature or at temperatures below the critical irreversible swelling of the corresponding SPEEK materials. However, in our opinion, it should be remarked that those results will only be valid at certain conditions and thus it is not possible to conclude that one material is better than other. Thereby, we have preferred to subject the material compositions in our study to the worst conditions that a hydrated membrane can suffer in a PEM (polymer electrolyte membrane) fuel cell, that is, the boiling point of water. Indeed, our target is the use of these SPEEK-based membranes for DMFC operation above 100 ºC in order to facilitate the electrochemical reactions at the electrodes.

The characteristic factor should be interpreted as a particular parameter for the reasonable comparison of membranes but not as a specific indicator of the DMFC performance properties. This factor gives the same importance to both conductivity and methanol permeability which is not observed in real conditions. A variety of studies have proved that the main membrane property governing the DMFC performance is the proton conductivity since the permeability (crossover) gets reduced with increasing the current density. This is explained by the consumption of methanol in the anode which gradually diminishes the concentration gradient between electrodes, and then the ohmic losses in the membrane become dominant [63-67]. Therefore, although the reduction of methanol permeability diminishes fuel losses thus improving fuel utilization and Faraday efficiency, the proton conductivity should still be emphasized for achieving low resistance membranes and high

power densities. For this reason, the authors suggest the replacement of the commonly accepted characteristic factor (σ/P) by a modified version as σ^2/P, in which the contribution of the conductivity is increased as compared with the permeability.

In Fig. 8, similarly to the SPEEK-PVA case, the same trend is observed for the crosslinked SPEEK-PVB membranes, i.e. decreasing the methanol permeability with increasing the PVB content. However, in this case the decrease in methanol permeability sweeps down within a two orders of magnitude range from the pristine SPEEK2 membrane to the SPEEK2-55%PVB composition. Therefore, the effect of addition of PVB in the SPEEK membrane strongly overtakes PVA in terms of methanol permeability. This conclusion is not surprising from the results in Table 2. It was shown that the water uptake values of the SPEEK-PVB membranes were considerably smaller than those ones of the SPEEK-PVA compositions due to the hydrophobic nature of PVB in opposition to the hydrophilic properties of PVA.

The values of water uptake are given in Table 2 while the values of methanol permeability for each SPEEK-PVA and SPEEK-PVB composition are summarized in Table 3. The methanol permeability of the pristine SPEEK2 membrane, after 1 h in water at 60 ºC, was measured at 50 ºC since in 4 M methanol solution at 60 ºC the membrane was prone to break.

Table 3. Methanol permeability values at 60 ºC for crosslinked membranes of SPEEK1-PVA ($C_{D,0}$ = 2 M) and SPEEK2-PVB ($C_{D,0}$ = 4 M) after 1 h swelling in boiling water. A PVA membrane (after thermal treatment at 200 ºC) and a PVB membrane (after 200 ºC treatment and 1 h in boiling water) are included for comparison ($C_{D,0}$ = 4 M).

Membrane	Swollen thickness (µm)	Apparent methanol permeability ($cm^2\ s^{-1}$)
SPEEK1 (1.75 meq g^{-1})[a]	105 ± 2	$(3.59 \pm 0.07)\cdot10^{-6}$
PVA	175 ± 5	$(4.28 \pm 0.12)\cdot10^{-6}$
SPEEK1-25%PVA	210 ± 5	$(1.18 \pm 0.03)\cdot10^{-5}$
SPEEK1-35%PVA	185 ± 3	$(9.49 \pm 0.15)\cdot10^{-6}$
SPEEK1-45%PVA	159 ± 3	$(7.81 \pm 0.15)\cdot10^{-6}$
SPEEK2 (2.05 meq g^{-1})[b]	133 ±3	$(6.42 \pm 0.14)\cdot10^{-6}$
PVB	80 ± 1	$(3.62 \pm 0.05)\cdot10^{-8}$
SPEEK2-30%PVB	167 ± 3	$(2.23 \pm 0.04)\cdot10^{-7}$
SPEEK2-35%PVB	117 ± 3	$(1.72 \pm 0.04)\cdot10^{-7}$
SPEEK2-45%PVB	103 ± 2	$(3.58 \pm 0.07)\cdot10^{-8}$
SPEEK2-55%PVB	96 ± 3	$(2.51 \pm 0.08)\cdot10^{-8}$

Swollen thickness was measured on the permeating area after methanol permeability experiments.

[a] Membrane swollen in water at 80 ºC for 1 h.

[b] Membrane swollen in water at 60 ºC for 1 h. Methanol permeability was measured at 50 ºC.

The comparison between the pristine SPEEK membranes in Table 3 reflects the increase of methanol permeability with increasing the ion-exchange capacity (permeability of SPEEK2 > SPEEK1) since water uptake is similarly dependent on the IEC level of the ionomer. On the other hand, the SPEEK1-PVA membranes show much higher permeability than the SPEEK2-PVB compositions. A close inspection to the permeability values of pristine PVA and PVB states that PVB is two orders of magnitude less permeable than PVA as a consequence of the hydrophobic characteristic of PVB and the hydrophilic nature of PVA. The latter can swell in water at increasing temperatures and even dissolves in hot water.

Additionally, the methanol permeability at 60 ºC of a pristine PVB membrane was measured without carrying out the thermal treatment at 200 ºC and a value of $(6.73 \pm 0.06)\cdot10^{-8}$ cm^2 s^{-1} was found, about two times higher than the value shown by the thermally treated one (Table 3). This result confirms that thermal degradation of PVB can provide crosslinking reactions via the formed C=C double bonds which leads to a reduction of the permeability. The blended SPEEK2-45%PVB and SPEEK2-55%PVB membranes show even less permeability than the pristine PVB material, inferring that the sulfonic acid groups of SPEEK can also participate in the crosslinking reactions which assist the formation of more compact membranes.

The permeability at 60 ºC of a crosslinked PVA membrane, chemically crosslinked with a 5 wt% solution of glutaraldehyde in 0.1 M HCl, was similarly tested. In this case, its value was found to decrease to $(3.27 \pm 0.21)\cdot10^{-8}$ cm^2 s^{-1} thus remarking the effectiveness of the crosslinking methods in terms of reducing methanol permeability.

The apparent permeability at 60 ºC of a SPEEK1 membrane without pre-treatment in hot water at 80 ºC was also measured, in opposition to the membrane in Table 3, and a value of $(7.68 \pm 0.15)\cdot10^{-7}$ cm^2 s^{-1} was obtained. This result is about 4.7 times below the permeability value of the swollen membrane and highlights the influence of the previous history of treatments on the properties of this type of membranes. This should be taken into account when comparison between different materials and compositions is intended.

The extremely low permeability of pristine PVB has been assigned to the hydrophobic nature of this polymer. However, two reasons make a priori this result unexpected as (i) PVB is an amorphous polymer with a relatively low glass transition temperature (~65 ºC) and (ii) methanol is a less polar molecule than water. Thus, a certain solubility of methanol in the PVB matrix and diffusion through the free volume left by the butyral side groups would be expected. In the case of Nafion®, it is reported that methanol can permeate across both the water filled ionic channels and the perfluorinated

side chains [68-70]. It is assumed that methanol has certain solubility within the Nafion® side chains causing them to expand thus increasing swelling and permeability. Interestingly, it seems that the butyral side chains of PVB do not exhibit such a phenomenon, perhaps due to a strong entanglement between them thus providing a good resistance to methanol solution and swelling. Thereby, we suggest the possible synthesis of ordered block copolymers in which the hydrophobic block might contain butyral side chains (or even longer hydrocarbon chains) for the promotion of phase separation and barrier properties towards methanol, while the hydrophilic blocks might contain the sulfonic acid groups directly attached to the backbone or in short length side chains with the aim to produce narrow ionic channels.

3.6. Proton conduction properties

The behaviour of the proton conductivity as a function of the PVA and PVB compositions are shown in Figs. 9 and 10, respectively. In both cases, conductivity drops with increasing the PVA or PVB content due to the consumption and dilution effects caused on the sulfonic acid groups of SPEEK by those polymers. Constraint of water uptake by the crosslinking of SPEEK with PVA and PVB can also explain the observed reduction of conductivity. In fact, the drop of conductivity by the hydrophobic PVB is

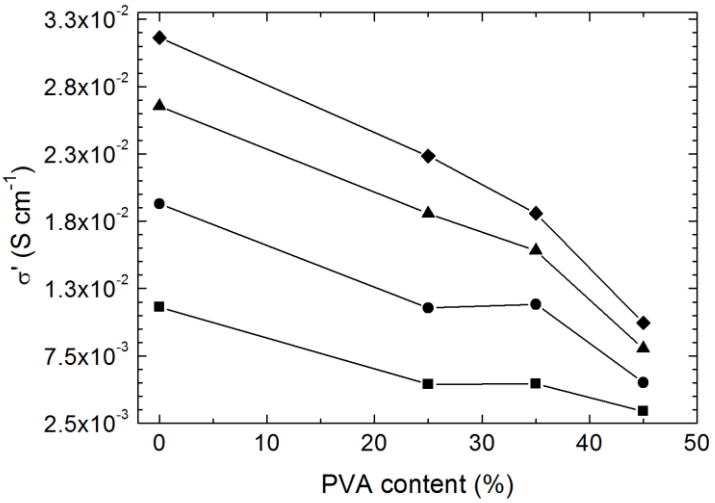

Fig. 9. Proton conductivity values of the swollen SPEEK1-PVA membranes as a function of composition and temperature: (■) 25 ºC, (●) 50 ºC, (▲) 75 ºC, and (♦) 90 ºC. The pristine SPEEK1 (PVA = 0%) was previously swollen in water at 80 ºC for 1 h, whereas the PVA-blended membranes were swollen in boiling water (100 ºC) for 1 h.

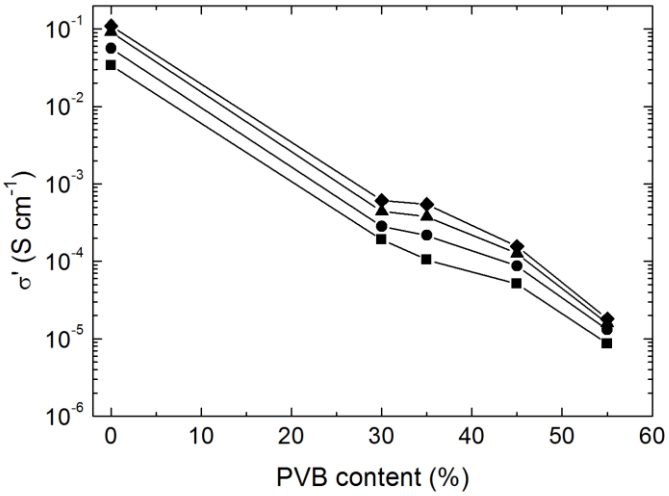

Fig. 10. Proton conductivity values of the swollen SPEEK2-PVB membranes as a function of composition and temperature: (■) 25 ºC, (●) 50 ºC, (▲) 75 ºC, and (♦) 90 ºC. The pristine SPEEK2 (PVB = 0%) was previously swollen in water at 60 ºC for 1 h, whereas the PVB-blended membranes were swollen in boiling water (100 ºC) for 1 h.

very substantial and ranges about 4 orders of magnitude (~10^{-1}-10^{-5} S cm^{-1}). On the other hand, the effect of the hydrophilic PVA is less pronounced and the conductivity just diminishes one order of magnitude (~10^{-2}-10^{-3} S cm^{-1}).

The conductivity of the SPEEK-PVA membranes presented in this study are below the values reported by T. Yang [36], but again we have to consider the different conditions at which the membranes have been subjected. In the work of T. Yang the SPEEK-PVA membranes were crosslinked at 130 ºC while a thermal treatment at 200 ºC has been used in our study. A lower degree of crosslinking is expected for those reported membranes which was not apparently found to be insufficient as the membranes were just swollen in water at room temperature. In our case, achievement of stability at higher temperatures (above 100 ºC) necessarily requires the formation of a highly crosslinked network which on the other hand impacts negatively on the proton conductivity by strong reduction of available sulfonic acid groups. Furthermore, membrane swelling at elevated temperatures as in our work involves the uptake of a large amount of water which until a certain limit can be beneficial since it provides water for the proton conduction. However, beyond such a limit, additional water uptake results in a volume increase which decreases the effective bulk concentration of sulfonic acid groups and causes the proton conductivity to drop.

The values of conductivity at 75 ºC and the calculated values of activation energy for the proton conduction of the SPEEK1-PVA and

Table 4. Proton conductivity (real part, σ') measured at 75 ºC and activation energy values for different compositions of the SPEEK1-PVA and SPEEK2-PVB membranes after 1 h swelling in boiling water. A characteristic factor (σ'/P) for each membrane is included and was obtained from the conductivity values at 75 ºC and the permeability constants at 60 ºC shown in Table 3. A modified version of the characteristic factor as proposed by the authors (σ'^2/P) is also given.

Membrane	σ' (10^{-2} S cm^{-1})	E_a (kJ mol^{-1})	σ'/P (S s cm^{-3})	σ'^{2}/P (S^2 s cm^{-4})
SPEEK1 (1.75 meq g^{-1})[a]	2.61 ± 0.10	12.3 ± 0.1	7270 ± 420	190 ± 20
SPEEK1-25%PVA	1.81 ± 0.08	17.3 ± 0.9	1534 ± 107	27.8 ± 3.2
SPEEK1-35%PVA	1.53 ± 0.05	11.4 ± 0.1	1612 ± 78	24.7 ± 2.0
SPEEK1-45%PVA	0.81 ± 0.03	14.8 ± 0.2	1037 ± 58	8.4 ± 0.8
SPEEK2 (2.05 meq g^{-1})[b]	11.0 ± 0.3	16.6 ± 0.6	17134 ± 841	1885 ± 144
SPEEK2-30%PVB	0.061 ± 0.001	15.9 ± 1.3	2735 ± 94	1.67 ± 0.08
SPEEK2-35%PVB	0.055 ± 0.001	22.6 ± 0.5	3198 ± 133	1.76 ± 0.10
SPEEK2-45%PVB	0.016 ± 0.001	15.3 ± 0.5	4469 ± 367	0.72 ± 0.10
SPEEK2-55%PVB	0.0018 ± 0.0002	10.0 ± 0.9	717 ± 103	0.013 ± 0.003

[a] Membrane swollen in water at 80 ºC for 1 h.
[b] Membrane swollen in water at 60 ºC for 1 h. Methanol permeability was measured at 50 ºC.

SPEEK2-PVB membranes are listed in Table 4. The values of activation energy for the SPEEK1-PVA compositions are in general smaller than those ones of the SPEEK2-PVB membranes as proton conduction is facilitated in a water-rich medium. However, increasing the PVA content tends to increase the activation energy which is explained by the consequent reduction of the effective concentration of sulfonic acid groups. On the other hand, the higher values of activation energy for the SPEEK2-PVB membranes indicate that conductivity becomes more restricted as the water uptake of these compositions is lower. Increasing the PVB content leads to a decrease of the activation energy probably as a consequence of an improved phase separation which facilitates the concentration of sulfonic acid groups in SPEEK-rich clusters.

The deviation in the linear behaviour of the Arrhenius plots for the SPEEK1, SPEEK1-25%PVA and SPEEK1-35%PVA membranes in the range of 25-50 ºC as observed in Fig. 11 is attributed to swelling/water uptake issues which happened during the conductivity measurements in the water filled cell. The Arrhenius plots of the SPEEK2-PVB membranes in Fig. 12 show a complete linear trend along the whole temperature range since swelling gets more constrained with the use of PVB.

A characteristic factor obtained from the commonly accepted relation σ/P has been estimated for each membrane from the conductivity values at 75 ºC given in Table 4 and the apparent methanol permeability constants at

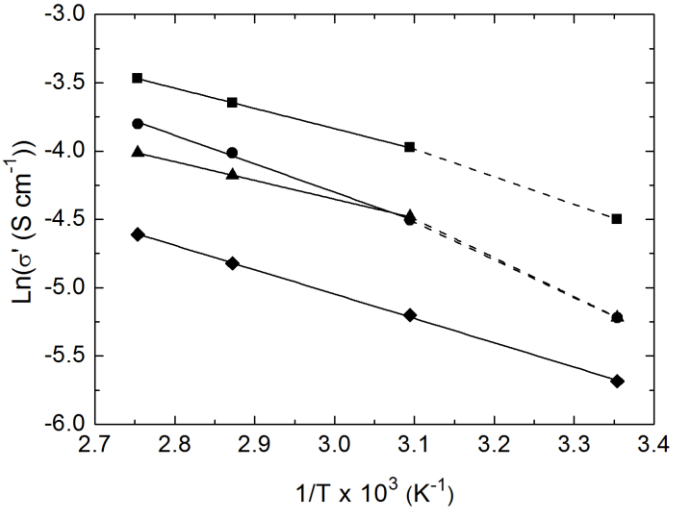

Fig. 11. Arrhenius plots of proton conductivity of the swollen SPEEK1-PVA membranes as a function of composition: (■) SPEEK1, (●) SPEEK1-25%PVA, (▲) SPEEK1-35%PVA, and (♦) SPEEK1-45%PVA. The intervals between 25 ºC and 50 ºC defined by the dashed lines were not used for the calculation of activation energy values.

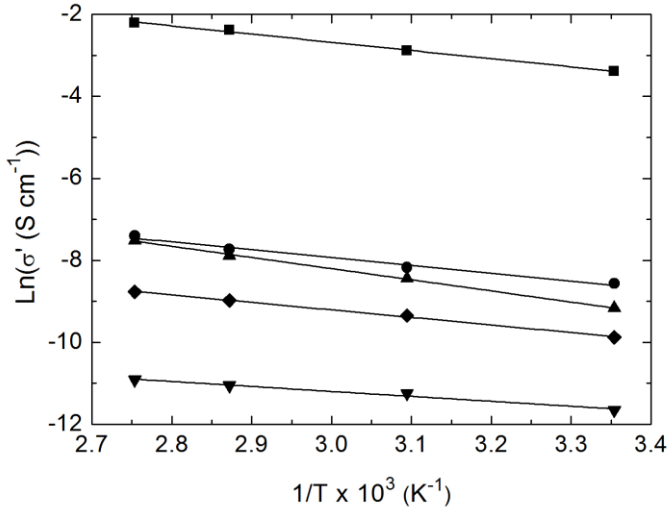

Fig. 12. Arrhenius plots of proton conductivity of the swollen SPEEK2-PVB membranes as a function of composition: (■) SPEEK2, (●) SPEEK2-30%PVB, (▲) SPEEK2-35%PVB, (♦) SPEEK2-45%PVB, and (▼) SPEEK2-55%PVB.

60 ºC in Table 3. It has been compared with a modified version of such a characteristic factor by means of the expression σ^2/P which gives more weight to the proton conductivity. The results are reported in Table 4.

According to the σ/P characteristic factor in which conductivity and methanol permeability have similar importance, the SPEEK2-PVB compositions would be preferably for DMFC operation as they present very reduced methanol permeability despite their low conductivity values. Among the studied compositions, those of SPEEK1-35%PVA and SPEEK2-45%PVB show the most optimal results.

Application of the modified characteristic factor, expressed as σ^2/P, causes the optimal membranes to shift towards the SPEEK1-PVA ones, and among them, the SPEEK1-25%PVA and SPEEK2-35%PVA would be the preferred compositions. It was reported in Table 1 the better mechanical stability of SPEEK1-35%PVA in comparison with SPEEK1-25%PVA. Therefore, we can conclude that the SPEEK1-35%PVA composition is the most optimal membrane for DMFC application at intermediate temperatures in terms of emphasizing proton conductivity.

With regard to the SPEEK2-PVB membranes, the σ^2/P factor suggests two membranes presenting equivalent characteristics, i.e. SPEEK2-30%PVB and SPEEK2-35%PVB. Since their values of methanol permeability are very similar, around $2 \cdot 10^{-7}$ cm^2 s^{-1}, the SPEEK2-30%PVB composition is selected due to its slightly higher proton conductivity. Thereby, SPEEK2-30%PVB represents the best composition in terms of methanol barrier properties while proton conductivity is still taken into account.

It can be observed in Table 4 that the pristine SPEEK membranes display the higher values when both the common and modified characteristic factors are applied. This means that blending other polymers with SPEEK indeed affects the good performance for fuel cell application which would be exhibited by this material alone. Unfortunately, as it has been pointed out previously, pristine SPEEK membranes are prone to excessive swelling and dissolution in hot water thus preventing their practical use. The associated decrease of optimal properties due to blending and crosslinking of the pristine SPEEK materials with other polymers is however compensated by the enhancement of stability at higher temperatures in which other advantages appear. Among those advantages, the thermal activation of the membrane proton conductivity and the accelerated electrochemical reactions at the electrodes, i.e. methanol oxidation and oxygen reduction.

3.7. Strategies for novel composite membranes

Incorporation of PVA and PVB into SPEEK has provided stability towards swelling in boiling water and has revealed two optimal compositions in which a specific characteristic is emphasized as a function of the hydrophilic or hydrophobic characteristics of the blending polymer: SPEEK1-35%PVA

highlights the proton conductivity and SPEEK2-30%PVB the methanol barrier properties.

Despite their good stability at elevated temperatures, the utilization of membranes based on those compositions individually is not desirable for real DMFC application. SPEEK1-35%PVA is expected to show a good performance in terms of power density but presents a relatively large methanol permeability which would decrease considerably the Faraday efficiency, whereas the proton conductivity of SPEEK2-30%PVB is too low for a practical use.

For this reason, we propose the preparation of composite membranes combining adequately both compositions in a single membrane with the purpose of achieving synergy effects between them. The preparation and characterization of these novel membranes is currently under study.

Two potential configurations are schematically represented in Fig. 13: (a) Alternate layers of SPEEK2-30%PVB and SPEEK1-35%PVA (number of layers $n = 3$, 5, etc.), and (b) a matrix of SPEEK1-35%PVA reinforced with nanofibres of SPEEK2-30%PVB.

In the first case, the preparation of thin membranes of SPEEK2-30%PVB and thicker layers of SPEEK1-35%PVA would be preferred. The as-prepared films should be conveniently arranged by alternating the polymer compositions and finally the sandwich should be crosslinked at 200 ºC under pressure in order to chemically attach all the layers.

In reference to the second proposal, the authors have already experienced the preparation of nanofibre reinforced membranes in which the

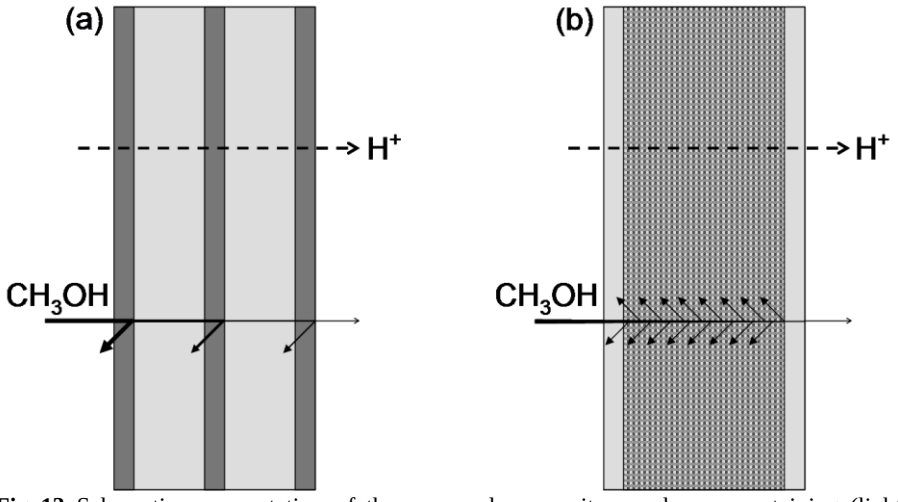

Fig. 13. Schematic representation of the proposed composite membranes containing (light grey) SPEEK1-35%PVA and (dark grey) SPEEK2-30%PVB compositions in (a) an alternate multilayer structure ($n = 5$), and (b) a nanofibre reinforced membrane.

presence of PVA nanofibres blocked methanol permeation within a Nafion® matrix [60]. In the pursuit of this concept, it is desirable to incorporate methanol-blocking nanofibres of SPEEK2-30%PVB into a proton conducting matrix of SPEEK1-35%PVA. In this case, the SPEEK2-30%PVB nanofibres would moreover contribute in some extent to the proton conductivity of the composite membranes and benefit the mechanical properties. Preparation of the SPEEK2-30%PVB nanofibres by electrospinning should be followed by their thermal crosslinking at 200 ºC and consequent infiltration of the SPEEK1-35%PVA matrix from a suitable solution via repeated impregnation and evaporation steps on the nanofibre mat. Finally, the nanocomposite membrane should be crosslinked at 200 ºC under pressure with the aim to favour interfacial adhesion between the nanofibres and the matrix.

4. Conclusions

Pristine SPEEK membranes are impractical for DMFC application at intermediate temperatures (above 100 ºC) due to excessive swelling and dissolution in hot water.

It has been remarked that the swelling conditions and the history of the processes performed on the membranes, e.g. thermal treatments, are important parameters to define the final properties of the SPEEK-based membranes. Comparison of properties should only be accomplished between membranes with similar swelling degrees and history of treatments.

Severe swelling conditions (boiling water) have been applied on the membranes with the aim to filter which compositions are suitable for application in DMFCs operating over 100 ºC, necessary conditions for achieving enhanced electrochemical performances.

Blending and crosslinking SPEEK with other polymers is a suitable method for enhancing stability towards swelling at elevated temperatures in water. Polyvinyl alcohol (PVA) and polyvinyl butyral (PVB) contain functional groups or are able to generate them by thermal degradation. This provides a pathway for crosslinking reactions with SPEEK chains.

PVA is a hydrophilic polymer which forms homogeneous blends with SPEEK suitable for obtaining high proton conductivities. On the other hand, PVB is a hydrophobic polymer and blends with SPEEK result in a phase separation morphology in which very low methanol permeabilities are found. Membrane compositions of SPEEK-35%PVA (for an SPEEK ionomer with IEC = 1.75 meq g^{-1}) and SPEEK-30%PVB (for an SPEEK with IEC = 2.05 meq g^{-1}) exhibited the best properties in terms of mechanical stability, proton conductivity and methanol permeability.

A modified characteristic factor expressed by σ^2/P has been introduced in which more importance is given to the proton conductivity in comparison with the methanol permeability as reported in real DMFC operation.

Two potential configurations for achieving synergy effects between both SPEEK blend compositions have been proposed with the aim to materialize their practical application in DMFCs operating at intermediate temperatures.

This study is intended to assist other researchers involved in the preparation of PEM fuel cell membranes for application at intermediate or high temperatures, especially in DMFCs, providing a useful base for the evaluation of membranes and further development of new approaches.

Acknowledgements

This research has been funded in the frame of Support Programme for Research and Development of the Polytechnic University of Valencia and the Ministry of Science and Innovation through the projects: 24761 and SP-ENE-20120718, respectively.

We thank the group of Prof. Santiago Luis (Universidad Jaume I, Spain) for their support in FTIR measurements and Prof. Koji Nishio (Kyoto University, Japan) for his valuable revision and comments.

References

[1] Kamarudin SK, Achmad F, Daud WRW. Overview on the application of direct methanol fuel cell (DMFC) for portable electronic devices. Int J Hydrogen Energy 2009;34:6902-16.

[2] Neburchilov V, Martin J, Wang H, Zhang J. A review of polymer electrolyte membranes for direct methanol fuel cells. J Power Sources 2007;169:221-38.

[3] Gasteiger HA, Garche J. In: Ertl G, Knözinger H, Schüth F, Weitkamp J, editors. Handbook of heterogeneous catalysis. 2nd ed. Weinheim, Germany: Wiley-VCH; 2008 [Section 13.20.2.7].

[4] Salvatore A, Baglio V, Antonucci V. In: Liu H, Zhang J, editors. Electrocatalysis of direct methanol fuel cells. From fundamentals to applications. Weinheim, Germany: Wiley-VCH; 2009 [Chapter 11].

[5] DeLuca NW, Elabd YA. Nafion®/poly(vinyl alcohol) blends: effect of composition and annealing temperature on transport properties. J Membr Sci 2006;282:217-24.

[6] Tsai J-C, Cheng H-P, Kuo J-F, Huang Y-H, Chen C-Y. Blended Nafion®/SPEEK direct methanol fuel cell membranes for reduced methanol permeability. J Power Sources 2009;189:958-65.

[7] Li Q, He R, Jensen JO, Bjerrum NJ. Approaches and recent development of polymer electrolyte membranes for fuel cells operating above 100 ºC. Chem Mater 2003;15:4896-915.

[8] Song SQ, Zhou WJ, Li WZ, Sun G, Xin Q, Kontou S, Tsiakaras P. Direct methanol fuel cells: methanol crossover and its influence on single DMFC performance. Ionics 2004;10:458-62.

[9] Molla S, Compañ V, Gimenez E, Blazquez A, Urdanpilleta I. Novel ultrathin composite membranes of Nafion/PVA for PEMFCs. Int J Hydrogen Energy 2011;36:9886-95.
[10] Shao Y, Yin G, Wang Z, Gao Y. Proton exchange membrane fuel cell from low temperature to high temperature: material challenges. J Power Sources 2007;167:235-42.
[11] Wasmus S, Küver A. Methanol oxidation and direct methanol fuel cells: a selective review. J Electroanal Chem 1999;461:14-31.
[12] Zhang J, Xie Z, Zhang J, Tang Y, Song C, Navessin T, Shi Z, Song D, Wang H, Wilkinson DP, Liu Z-S, Holdcroft S. High temperature PEM fuel cells. J Power Sources 2006;160:872-91.
[13] Alberti G, Narducci R, Sganappa M. Effects of hydrothermal/thermal treatments on the water-uptake of Nafion membranes and relations with changes of conformation, counter-elastic force and tensile modulus of the matrix. J Power Sources 2008;178:575-83.
[14] Sethuraman VA, Weidner JW, Haug AT, Protsailo LV. Durability of Perfluorosulfonic acid and hydrocarbon membranes: effect of humidity and temperature. J Electrochem Soc 2008;155:B119-24.
[15] Carbone A, Pedicini R, Portale G, Longo A, D'Ilario L, Passalacqua E. Sulphonated poly(ether ether ketone) membranes for fuel cell application: thermal and structural characterization. J Power Sources 2006;163:18-26.
[16] Knauth P, Hou H, Bloch E, Sgreccia E, Di Vona ML. Thermogravimetric analysis of SPEEK membranes: thermal stability, degree of sulfonation and cross-linking reaction. J Anal Appl Pyrolysis 2011;92:361-5.
[17] Kaliaguine S, Mikhailenko SD, Wang KP, Xing P, Robertson G, Guiver M. Properties of SPEEK based PEMs for fuel cell application. Catal Today 2003;82:213-22.
[18] Roziere J, Jones DJ. Non-fluorinated polymer materials for proton exchange membrane fuel cells. Annu Rev Mater Res 2003;33:503-55.
[19] Jiang R, Kunz HR, Fenton JM. Investigation of membrane property and fuel cell behaviour with sulfonated poly(ether ether ketone) electrolyte: temperature and relative humidity effects. J Power Sources 2005;150:120-8.
[20] Paik Y, Chae SA, Han OH, Hwang SY, Ha HY. Influence of water and degree of sulfonation on the structure and dynamics of SPEEK studied by solid-state ^{13}C and ^{1}H NMR. Polymer 2009;50:2664-73.
[21] Do KNT, Kim D. Comparison of homogeneously and heterogeneously sulfonated polyetheretherketone membranes in preparation, properties and cell performance. J Power Sources 2008;185:63-9.
[22] Li L, Zhang J, Wang Y. Sulfonated poly(ether ether ketone) membranes for direct methanol fuel cell. J Membr Sci 2003;226:159-67.
[23] Li X, Zhao C, Lu H, Wang Z, Na H. Direct synthesis of sulfonated poly(ether ether ketone ketone)s (SPEEKKs) proton exchange membranes for fuel cell application. Polymer 2005;46:5820-7.
[24] Xue S, Yin G. Methanol permeability in sulfonated poly(etheretherketone) membranes: a comparison with Nafion membranes. Eur Polym J 2006;42:776-85.
[25] Huang RYM, Shao P, Burns CM, Feng X. Sulfonation of poly(ether ether ketone)(PEEK): kinetic study and characterization. J Appl Polym Sci 2001;82:2651-60.
[26] Kreuer KD. On the development of proton conducting materials for technological applications. Solid State Ionics 1997;97:1-15.
[27] Wu H-L, Ma C-CM, Liu F-Y, Chen C-Y, Lee S-J, Chiang C-L. Preparation and characterization of poly(ether sulfone)/sulfonated poly(ether ether ketone) blend membranes. Eur Polym J 2006;42:1688-95.
[28] Jung H-Y, Park J-K. Long-term performance of DMFC based on the blend membrane of sulfonated poly(ether ether ketone) and poly(vinylidene fluoride). Int J Hydrogen Energy 2009;34:3915-21.

[29] Manea C, Mulder M. Characterization of polymer blends of polyethersulfone/sulfonated polysulfone and polyethersulfone/sulfonated polyetheretherketone for direct methanol fuel cell applications. J Membr Sci 2002;206:443-53.
[30] Wilhelm FG, Pünt IGM, van der Vegt NFA, Strathmann H, Wessling M. Cation permeable membranes from blends of sulfonated poly(ether ether ketone) and poly(ether sulfone). J Membr Sci 2002;199:167-76.
[31] Wei G, Xua L, Huang C, Wang Y. SPE water electrolysis with SPEEK/PES blend membrane. Int J Hydrogen Energy 2010;35:7778-83.
[32] Mikhailenko SD, Wang K, Kaliaguine S, Xing P, Robertson GP, Guiver MD. Proton conducting membranes based on crosslinked sulfonated poly(ether ether ketone) (SPEEK). J Membr Sci 2004;233:93-9.
[33] Zhong S, Fu T, Dou Z, Zhao C, Na H. Preparation and evaluation of a proton exchange membrane based on crosslinkable sulfonated poly(ether ether ketone)s. J Power Sources 2006;162:51-7.
[34] Mikhailenko SD, Robertson GP, Guiver MD, Kaliaguine S. Properties of PEMs based on cross-linked sulfonated poly(ether ether ketone). J Membr Sci 2006;285:306-16.
[35] Zhang W, Gogel V, Friedrich KA, Kerres J. Novel covalently cross-linked poly(etheretherketone) ionomer membranes. J Power Sources 2006;155:3-12.
[36] Yang T. Preliminary study of SPEEK/PVA blend membranes for DMFC applications. Int J Hydrogen Energy 2008;33:6772-9.
[37] Li H, Zhang G, Wu J, Zhao C, Zhang Y, Shao K, Han M, Lin H, Zhu J, Na H. A novel sulfonated poly(ether ether ketone) and cross-linked membranes for fuel cells. J Power Sources 2010;195:6443-9.
[38] Zhang N, Zhang G, Xu D, Zhao C, Ma W, Li H, Zhang Y, Xu S, Jiang H, Sun H, Na H. Crosslinked membranes based on sulfonated poly (ether ether ketone) (SPEEK)/Nafion for direct methanol fuel cells (DMFCs). Int J Hydrogen Energy 2011;36:11025-33.
[39] Zhu Y, Zieren S, Manthiram A. Novel crosslinked membranes based on sulfonated poly(ether ether ketone) for direct methanol fuel cells. Chem Commun 2011;47:7410-2.
[40] Kerres JA. Development of ionomer membranes for fuel cells. J Membr Sci 2001;185:3-27.
[41] Chi NTQ, Luu DX, Kim D. Sulfonated poly(ether ether ketone) electrolyte membranes cross-linked with 4,4'-diaminodiphenyl ether. Solid State Ionics 2011;187:78-84.
[42] Zhao C, Wang Z, Bi D, Lin H, Shao K, Fu T, Zhong S, Na H. Blend membranes based on disulfonated poly(aryl ether ether ketone)s (SPEEK) and poly(amide imide) (PAI) for direct methanol fuel cell usages. Polymer 2007;48:3090-7.
[43] Wu H-L, Ma C-CM, Li C-H, Lee T-M, Chen C-Y, Chiang C-L, Wu C. Sulfonated poly(ether ether ketone)/poly(amide imide) polymer blends for proton conducting membrane. J Membr Sci 2006;280:501-8.
[44] Chen J, Maekawa Y, Asano M, Yoshida M. Double crosslinked polyetheretherketone-based polymer electrolyte membranes prepared by radiation and thermal crosslinking techniques. Polymer 2007;48:6002-9.
[45] Silva V, Silva V, Mendes A, Madeira L, Nunes S. Pre-treatment effect on the transport properties of sulfonated poly(ether ether ketone) membranes for DMFC applications. Desalination 2006;200:645-7.
[46] Robertson GP, Mikhailenko SD, Wang K, Xing P, Guiver MD, Kaliaguine S. Casting solvent interactions with sulfonated poly(ether ether ketone) during proton exchange membrane fabrication. J Membr Sci 2003;219:113-21.
[47] Guan R, Dai H, Li C, Liu J, Xu J. Effect of casting solvent on the morphology and performance of sulfonated polyethersulfone membranes. J Membr Sci 2006;277:148-56.
[48] Tosh B, Saikia CN, Dass NN. Development of a nonaqueous solvent system for poly(vinyl alcohol) and its characterization. J Appl Polym Sci 1999;74:663-9.

[49] Kreuer KD. On the development of proton conducting polymer membranes for hydrogen and methanol fuel cells. J Membr Sci 2001;185:29-39.
[50] Komarov PV, Veselov IN, Chu PP, Khalatur PG. Mesoscale simulation of polymer electrolyte membranes based on sulfonated poly(ether ether ketone) and Nafion. Soft Matter 2010;6:3939-56.
[51] Miyahara T, Hayano T, Matsuno S, Watanabe M, Miyatake K. Sulfonated polybenzophenone/poly(arylene ether) block copolymer membranes for fuel cell applications. ACS Appl Mater Interfaces 2012;4:2881-4.
[52] Na T, Shao K, Zhu J, Sun H, Liu Z, Zhao C, Zhang Z, Lew CM, Zhang G. Block sulfonated poly(arylene ether ketone) containing flexible side-chain groups for direct methanol fuel cells usage. J Membr Sci 2012;417-418:61-8.
[53] Wu L, Zhang Z, Ran J, Zhou D, Li C, Xu T. Advances in proton-exchange membranes for fuel cells: an overview on proton conductive channels (PCCs). Phys Chem Chem Phys 2013;15:4870-87.
[54] Elabd YA, Hickner MA. Block copolymers for fuel cells. Macromolecules 2011;44:1-11.
[55] Krajinovic K, Kaz T, Haering T, Gogel V, Kerres J. Highly sulphonated multiblock-copolymers for direct methanol fuel cells. Fuel Cells 2011;11:787-800.
[56] Gu S, He G, Wu X, Guo Y, Liu H, Peng L, Xiao G. Preparation and characteristics of crosslinked sulfonated poly(phthalazinone ether sulfone ketone) with poly(vinyl alcohol) for proton exchange membrane. J Membr Sci 2008;312:48-58.
[57] Jaafar J, Ismail AF, Mustafa A. Physicochemical study of poly(ether ether ketone) electrolyte membranes sulfonated with mixtures of fuming sulfuric acid and sulfuric acid for direct methanol fuel cell application. Mater Sci Eng A 2007;460-461:475-84.
[58] Hsiang H-I, Chen C-C, Tsai J-Y. Dispersion of nonaqueous Co_2Z ferrite powders with titanate coupling agent and poly(vinyl butyral). Appl Surf Sci 2005;245:252-9.
[59] Seo JJ, Kuk ST, Kim K. Thermal decomposition of PVB (polyvinyl butyral) binder in the matrix and electrolyte of molten carbonate fuel cells. J Power Sources 1997;69:61-8.
[60] Molla S, Compañ V. Polyvinyl alcohol nanofiber reinforced Nafion membranes for fuel cell applications. J Membr Sci 2011;372:191-200.
[61] Zaidi SMJ, Mikhailenko SD, Robertson GP, Guiver MD, Kaliaguine S. Proton conducting composite membranes from polyether ether ketone and heteropolyacids for fuel cell applications. J Membr Sci 2000;173:17-34.
[62] Zhou ZM, David DJ, Macknight WJ, Karasz FE. Synthesis characterization and miscibility of polyvinyl butyrals of varying vinyl alcohol contents. Turkish J Chem 1997;21:229-38.
[63] Silva VSF, Silva VB, Reissner R, Vetter S, Mendes A, Madeira LM, Nunes SP. Non-fluorinated membranes thickness effect on the DMFC performance. Sep Sci Technol 2008;43:1917-32.
[64] Zhang J, Wang Y. Modeling the effects of methanol crossover on the DMFC. Fuel Cells 2004;4:90-5.
[65] Jung G-B, Su A, Tu C-H, Weng F-B. Effect of operating parameters on the DMFC performance. J Fuel Cell Sci Technol 2005;2:81-5.
[66] Jung DH, Lee CH, Kim CS, Shin DR. Performance of a direct methanol polymer electrolyte fuel cell. J Power Sources 1998;71:169-73.
[67] Liu JG, Zhao TS, Liang ZX, Chen R. Effect of membrane thickness on the performance and efficiency of passive direct methanol fuel cells. J Power Sources 2006;153:61-7.
[68] Barragan VM, Villaluenga JPG, Godino MP, Izquierdo-Gil MA, Ruiz-Bauza C, Seoane B. Swelling and electro-osmotic properties of cation-exchange membranes with different structures in methanol-water media. J Power Sources 2008;185:822-7.
[69] Haubold H-G, Vad T, Jungbluth H, Hiller P. Nano structure of Nafion: a SAXS study. Electrochim Acta 2001;46:1559-63.

[70] Chaabane L, Dammak L, Grande D, Larchet C, Huguet P, Nikonenko SV, Nikonenko VV. Swelling and permeability of Nafion®117 in water-methanol solutions: an experimental and modelling investigation. J Membr Sci 2011;377:54-64.

Paper 6

Journal of Membrane Science 492 (2015) 123-136
(Adapted to thesis)

Nanocomposite SPEEK-based membranes for Direct Methanol Fuel Cells at intermediate temperatures

Sergio Mollá, Vicente Compañ

Dpto. Termodinámica Aplicada, ETSII, Universidad Politécnica de Valencia, 46022 Valencia, Spain.

Abstract

Novel nanocomposite membranes were prepared by infiltration of a blend of sulfonated PEEK (SPEEK) with polyvinyl alcohol (PVA), using water as solvent, into electrospun nanofibres of SPEEK blended with polyvinyl butyral (PVB). The membranes were characterized for their application on Direct Methanol Fuel Cells (DMFCs) operating at moderate temperatures (above 80 ºC). An important role of the solvent on the crosslinking temperature for the SPEEK-PVA system was observed. A mat of hydrated SPEEK-30%PVB nanofibres revealed a higher proton conductivity in comparison with a dense membrane of similar composition. Incorporation of the nanofibre mats to the SPEEK-35%PVA matrix provided mechanical stability, methanol barrier properties and certain proton conductivity up to a crosslinking temperature of 120 ºC. Not remarkable effect of the nanofibres was found above that crosslinking temperature. The combined effect of the nanofibres and crosslinking temperature on the properties of the membranes is discussed. DMFC performance experiments concluded promising results for this new low-cost type of membranes, although further optimization steps are still required.

Keywords: Nanofibres, sulfonated PEEK, PVA, PVB, DMFC membranes.

1. Introduction

Direct methanol fuel cells (DMFCs) are electrochemical devices which can offer about 10 times more energy density than hydrogen-fueled proton exchange membrane fuel cells (PEMFCs) and 15 times higher than Li-ion batteries. This is explained by the liquid nature of the methanol fuel which additionally enables an easy refueling [1-3]. Nevertheless, it is well known that methanol crossover through the membrane, commonly a sulfonated perfluorinated polymer so-called Nafion®, causes the DMFC performance to decrease. Methanol adsorbates on the catalyst active sites for oxygen reduction at the cathode is the main reason for performance deterioration [4,5].

Typically, inorganic (nano-)fillers are incorporated into Nafion® via physical or chemical procedures with the aim to block methanol crossover. Preferential sorption of water versus methanol and an increased path tortuosity for mass transport result in lower methanol permeabilities for the hybrid membranes [6-9].

The membranes require to be strong while tough and flexible in order to achieve long mechanical stability. However, introduction of inorganic particles after certain loadings can cause agglomeration and poor dispersion [10,11] and finally a critical embrittlement of the membrane is expected. A different strategy then involves physically, chemically or ionically blending/crosslinking Nafion® with a methanol barrier polymer such us polyvinyl alcohol (PVA), polyvinylidene difluoride (PVDF) and polybenzimidazole (PBI), although in this case proton conductivity is the most affected parameter [12-15].

A pore-filling electrolyte membrane was conceived to overcome the limitations of the polymer blended fuel cell membranes. Such membranes are composed of a polymeric porous substrate with pores on the submicrometer scale which are filled with a proton conductive polymer. The porous substrate must be completely inert to the fuel and mechanically strong to prevent excess swelling of the filling polymer, which can otherwise lead to high methanol crossover [16]. A limited number of materials can be processed to obtain porous frameworks, and among them stand out polyimide (PI) [16,17], polytetrafluoroethylene (PTFE/Teflon®) [18] and ultra-high molecular weight polyethylene (UHMWPE) [19]. Unfortunately, lack of functional groups and difficulty to functionalize the surface of those substrates can result in weak interfaces between both polymer phases thus affecting the long-term stability as it has been reported for a PTFE/Nafion® system [20].

Recently, a similar but more versatile approach enables the utilization of a wide range of materials for the preparation of porous substrates. This

approach involves electrospinning a polymer solution to obtain a nanofibre mat which is afterwards filled with a proton conductive polymer matrix [21-28], although insulating polymers infiltrated into proton conductive nanofibres have also been proposed [29,30]. Interestingly, it has been found that proton conducting nanofibres exponentially increase conductivity with decrease in fibre diameter [25,31]. Higher increment of the proton conductivity is observed along the fibre axis direction than perpendicularly, which is attributed to the preferential orientation of the sulfonated polymeric chains and the consequent alignment of the ionic channels [21,22]. On the other hand, it has been suggested that proton transport takes place preferentially on the surface of the nanofibres, enriched with ionic clusters, rather than inside the nanofibre structure [32]. Probably, a plausible explanation for the enhancement of the proton conductivity of polymer electrolyte nanofibres involves both mechanisms.

Comparison between nanofibre- and blended-type membranes has been carried out with Nafion® and PVA. It was concluded that both types of membranes were effective to reduce methanol crossover, although the nanofibre morphology provided less tortuous proton conduction pathways and better DMFC performance than the blended membranes, in which agglomeration and non-homogeneous distribution of PVA occurred [26]. This is in agreement with the empirical evidence that DMFC performance is mainly governed by proton conductivity of the membrane. This is a consequence of methanol crossover to decrease with increasing current density, thus becoming ohmic losses the dominant parameter [33-35].

Chemical functionalization of the nanofibre surface offers a valuable strategy to improve interface compatibilization with the matrix, thus helping to further reduce methanol permeability and increase mechanical reinforcement and proton conductivity of the nanocomposite membranes [25,36]. Our group has pioneered the development of nanocomposite membranes incorporating surface functionalized nanofibres. We produced PVA nanofibres which were chemically modified on the surface with 4-formyl-1,3-benzenedisulfonic acid groups, with the purpose to promote nanofibre-matrix interaction via hydrogen bonding between sulfonic acid moieties and to assist the proton conduction, and subsequently Nafion® was infiltrated within the nanofibre mats. The resulting nanocomposite membranes were compact and contained a large fraction of PVA phase (~40-50 wt%), which caused about one order of magnitude reduction of methanol permeability while proton conductivity in comparison with pristine Nafion® was just slightly reduced due to the non-conducting behaviour of PVA. Interestingly, the strong reinforcement effect induced by the nanofibres enabled the preparation of very low thickness membranes with

good mechanical properties and low ohmic resistances, which resulted in advantageous fuel cell performances [37-39].

Nafion® is an expensive material and intrinsically limited to temperatures below 80 ºC for an adequate performance [40,41]. Motivated by the replacement of Nafion® with a low-cost alternative polymer electrolyte able to operate at intermediate temperatures (80-140 ºC), suitable for efficient electro-oxidation of methanol and efficient catalyst utilization, our group investigated blended membranes of sulfonated poly-ether-ether-ketone (SPEEK) with a hydrophilic polymer, PVA, and a derived hydrophobic polymer, polyvinyl butyral (PVB) [42]. The purpose was to find optimal compositions for DMFC operation attending to their chemical stability in hot aqueous solutions (evaluated in boiling water). It was found that PVB constrained to a larger extent the water uptake and swelling when blended with SPEEK than PVA, and correspondingly, PVB was preferred for providing methanol barrier properties at the expense of a considerably lower proton conductivity. On the other hand, PVA was suitable for avoiding excessive swelling and dissolution of the blended membrane while permitting acceptable proton conductivities for fuel cell application. The best properties were exhibited by blends of SPEEK and PVA in a ratio of 65:35 w/w, SPEEK-35%PVA, and by SPEEK-30%PVB compositions. SPEEK grades with values of ion-exchange capacity (IEC) of 1.75 meq g^{-1} and 2.05 meq g^{-1} were used, respectively.

Furthermore, an additional goal was the replacement of the PVA nanofibre mats by proton conducting nanofibres simultaneously providing hindrance to methanol crossover. In this sense, the present work represents the research conducted on the preparation and characterization of novel nanocomposite membranes made from nanofibre mats of SPEEK-30%PVB embedded in a SPEEK-35%PVA matrix. A special focus has been laid on the DMFC performance of the nanocomposite membranes at intermediate temperatures.

2. Experimental section

2.1. Materials

Granulated SPEEK (FUMION E ionomers) with ion-exchange capacities of 1.75 mmol g^{-1} and 2.05 mmol g^{-1} were acquired from Fumatech GmbH (St. Ingbert, Germany). These IEC values were confirmed by the authors via titration of samples dissolved in water [42]. The SPEEK materials were dried at 100 ºC for 24 h in vacuum atmosphere and stored in a sealed container to avoid absorption of water before the preparation of membranes.

Polyvinyl alcohol, Mowiol 28-99 grade PVA, and polyvinyl butyral, Mowital B75H grade PVB, were kindly donated by the company Kuraray Europe GmbH (Frankfurt, Germany).

N,N-Dimethylacetamide (DMAc) solvent was purchased from Acros Organics. PVA, PVB and DMAc were used as received. The chemical structures of SPEEK, PVA and PVB are represented in our previous paper [42].

2.2. Preparation of membranes

2.2.1. SPEEK-35%PVA membranes

SPEEK with ion-exchange capacity of 1.75 meq g^{-1} was dissolved in boiling water. An appropriate amount of PVA was separately dissolved in water at 80 ºC (10 wt% PVA concentration) and then both solutions were mixed to prepare a SPEEK-35%PVA composition (SPEEK/PVA 65:35 w/w). Water was added until reaching a 7.5 wt% polymer (SPEEK+PVA) concentration. The solution was vigorously stirred at room temperature until complete homogenization and the membranes cast overnight on a Teflon® Petri dish placed in an oven at 40 ºC. Finally, the membranes were crosslinked at different temperatures, i.e. 110 ºC, 120 ºC, 130 ºC and 140 ºC, for 1 h and immersed in boiling water for another 1 h. The membranes were stored in water at room temperature.

2.2.2. SPEEK-30%PVB nanofibres

A blended solution of SPEEK and PVB in a ratio of 70:30 w/w was prepared in DMAc solvent as follows: A certain amount of PVB was dissolved under stirring in DMAc at 80 ºC for 1 h. When the solution cooled down to room temperature, a specific amount of SPEEK with ion-exchange capacity of 2.05 meq g^{-1} was incorporated. The mixture was heated again at 80 ºC and vigorously stirred for 1 h until complete homogenization. Several polymer (SPEEK+PVB) concentrations were formulated, i.e. 12.5 wt%, 15 wt%, 17.5 wt% and 20 wt%.

Nanofibre mats of SPEEK-30%PVB were electrospun (YFLOW SL, Málaga, Spain) from those prepared solutions. A potential difference of 35 kV was applied between the needle and the planar collector, which were 25 cm apart, and a flow rate of 0.2 ml h^{-1} was fixed during the electrospinning process at a relative humidity (RH) below 40%. An optimal solution for the electrospinning process was selected and used afterwards. Such a solution was electrospun for 15 h and the corresponding mats were heated at 160 ºC for 30 min, in order to remove trapped DMAc molecules,

and then crosslinked at 200 ºC during 1 h in an oven. Round steel frames were placed on the surface of the PVB nanofibres before the crosslinking reaction. The purpose is to pull tight the mats confined within the inner area of the frames as a consequence of their dimensional shrinking. The last step was to fix firmly the crosslinked nanofibre mats in the frames. This was achieved by the attachment of supplementary frames which were mounted on the reverse side of the laying frames.

2.2.3. Nanocomposite SPEEK-based membranes

A 7.5 wt% concentrated solution of SPEEK-35%PVA in water was infiltrated into the SPEEK-30%PVB nanofibre mats with the aim to form the matrix of the nanocomposite membranes. Our method involved the immersion for 5 min of the framed nanofibres inside the cited aqueous solution followed by evaporation of the water for other 5 min. This was carried out by introducing the soaked nanofibre mats in a climate chamber (INELTEC CCSR-0/50, Spain) at 90 ºC with a very low humidity level. This process was repeated 4 times while the nanofibre mat was rotated 90º in each step. In the final step, the formed nanocomposite membrane was dried during 10 min inside the climate chamber. Thereupon, the membrane was cut along the frame boundary and further dried overnight at room temperature.

Finally, square membranes (5 x 5 cm^2) were cut and crosslinked for 1 h under a pressure of 1 kN cm^{-2} between the hot plates of a commercial hand press (Rondol, France). Four crosslinking temperatures were examined, i.e. 110 ºC, 120 ºC, 130 ºC and 140 ºC. The crosslinked nanocomposite membranes were introduced in boiling water for 1 h and stored in water at room temperature.

2.3. Characterization of the nanocomposite membranes

2.3.1 Scanning electron microscopy (SEM) analysis

The morphology of the SPEEK-30%PVB nanofibres and the structure of the nanocomposite membranes were investigated using a scanning electron microscope (SEM-model JSM-5410, Jeol Co., Japan). The samples were gold coated before SEM observations.

For cross-sectional observations, the membranes were cut in a fragile rupture mechanism by previously freezing the samples within liquid nitrogen.

2.3.2. Water uptake, swelling degree and ion-exchange capacity

Water uptake was calculated from the difference between the weight of the nanocomposite membranes in a wet (hydrated after treatment in boiling water) and a dry (dried at 100 ºC in oven) state, according to the expression in Eq. (1),

$$Water\ uptake\ (\%) = \frac{m_{wet} - m_{dry}}{m_{dry}} \times 100 \qquad (1)$$

A value of water uptake was averaged from three similar membranes crosslinked at each temperature.

The swelling degree (in-plane) was measured by the change of area of square membranes with initial 5 x 5 cm^2 dimensions ($A_0 = X_0 \cdot X_0$). After 1 h in boiling water, the swollen membranes practically maintained the square shape but with enlarged dimensions ($A_f = X_f \cdot X_f$), see Eq. (2). Similarly, swelling through the thickness was obtained from the difference between the membrane thickness in dry (L_0) and wet (L_f) states as in Eq. (3),

$$In-plane\ swelling\ (\%) = \frac{A_f - A_0}{A_0} \times 100 \qquad (2)$$

$$Thickness\ swelling\ (\%) = \frac{L_f - L_0}{L_0} \times 100 \qquad (3)$$

The ion-exchange capacity (IEC) was estimated from the swollen membranes, in acid form, by overnight immersion in a 2 M NaCl solution. The protons liberated during the reaction $R\text{-}SO_3H + Na^+ \rightarrow R\text{-}Na + H^+$ were titrated with a 0.01 M NaOH solution and phenolphthalein. The IEC was calculated from,

$$IEC\ (meq\ g^{-1}) = \frac{V_{NaOH} \times 0.01}{m_{dry}} \qquad (4)$$

where V_{NaOH} and m_{dry} are the volume in millilitres of NaOH solution used during the titration of the protons released by m grams of dry membrane, respectively. The values of m_{dry} were measured after drying at 100 ºC the samples utilized for ion-exchange with the NaCl solution.

2.3.3. Infrared (IR) spectroscopy

IR spectroscopy (Jasco FT/IR-6200 spectrometer, United States) was used to investigate the chemical reactions taking place within the nanocomposite membranes at each crosslinking temperature.

2.3.4. Mechanical properties

Static tensile strength testing (DMTA Q800 TA Instruments, United States) was carried out at 25 ºC using samples of SPEEK-35%PVA and nanocomposite membranes both crosslinked at 120 ºC. Samples of 2 mm width were clamped under a torque of 0.113 N m^{-1}, and the clamps were separated 10 mm. The samples were subjected to a preload of 0.001 N and the speed rate was fixed at 1 N min^{-1}. The thickness of the samples was calculated averaging five measurements at different parts. Previously, the membranes, stored in water, were superficially dried with a paper and pressed between two plastic sheets under a weight, which were afterwards placed inside an oven at 35 ºC during 4 days. Five samples of each type of membrane were tested and an average result reported.

2.3.5. Methanol permeability

A typical 2-cell experimental setup [43] was used to measure the coefficient of methanol permeability across the SPEEK-35%PVA and nanocomposite membranes as a function of crosslinking temperature. The donor chamber (D) was filled with a 2 M aqueous solution of methanol, while the receptor chamber (R) was filled with distilled water. Both chambers were stirred and heated at a fixed temperature of 60 ºC. The variation of methanol concentration with time in the receptor reservoir was determined by means of a densimeter (DMA 4500 M, Anton-Paar, Austria). A small sample of solution (approx. 1 ml) is introduced into a thermostated U-shaped borosilicate glass tube with a precise volume being excited to vibrate at its characteristic frequency, which depends on the total mass of the tube and sample. Through a precise determination of the characteristic frequency and a mathematical conversion, the mass density (g cm^{-3}) of the sample can be estimated. Consequently, the methanol concentration of that sample can be mathematically given from a calibration curve of density versus methanol concentration which is previously obtained at the same measurement temperature (50 ºC in our experiments).

During permeability experiments, samples from the receptor compartment were taken at certain time intervals and the density recorded. With the purpose to avoid the volume of solution in the receptor reservoir

(V_R = 150 cm^3) diminishes after each measurement, the samples were recovered from the densimeter and introduced again into the compartment. Representing the methanol concentration in the receptor chamber (C_R) versus time (t), the apparent permeability (P) of methanol across a membrane with thickness L (cm) and surface area A (A = 2.27 cm^2) can be determined from Eq. (5). This is valid while the gradient $C_{D,0}$ - C_R does not significantly change, that is, for the condition $C_{D,0} >> C_R$ (being $C_{D,0}$ the initial methanol concentration in the donor chamber). The parameter t_0 is assigned to the time lag before the pseudo-steady state is reached,

$$P = \frac{V_R \cdot L \cdot C_R}{C_{D,0} \cdot A \cdot (t - t_0)} \qquad (5)$$

2.3.6. Electrochemical impedance spectroscopy (EIS)

The proton conductivities through thickness of the SPEEK-30%PVB nanofibres and the prepared membranes were measured at 60 ºC and 90 ºC by impedance spectroscopy in the frequency range of $10 < f < 10^7$ Hz applying a 0.1 V signal amplitude. A Novocontrol broadband dielectric Spectrometer (Hundsangen, Germany) integrated by an SR 830 lock-in amplifier with an Alpha dielectric interface was used. The membranes were previously equilibrated with deionized water (Milli-Q) and afterwards placed between two gold electrodes in a parallel plate liquid sample cell (BDS 1308, Novocontrol) coupled to the spectrometer. The hydration level of membranes differ between liquid- and vapour-equilibrated, e.g. 100 %RH, environments [44-46]. For this reason and an approximation to the real DMFC conditions (aqueous solution in anode), the samples were soaked in Milli-Q water which was added to the measuring cell in each experiment. The temperature was controlled by nitrogen jet (QUATRO from Novocontrol) with a temperature error less than 0.1 K during every single sweep in frequency.

The protonic resistance R (Ω) was taken from the Bode plot as the value of the real part of the impedance Z' at which the phase angle reaches a maximum close to zero in the high frequency region, $|Z'| \rightarrow R$. The real conductivity (σ') of the membranes (S cm^{-1}) was then calculated from the protonic resistance by means of Eq. (6),

$$\sigma' = \frac{L}{R \cdot S} \qquad (6)$$

where L is the thickness of the membrane (cm) and S the electrode area (0.785 cm^2) in contact with the sample.

2.3.7. Direct methanol fuel cell (DMFC) performance

Membrane electrode assemblies (MEAs) comprising the nanocomposite membranes crosslinked at 110 ºC and 120 ºC were prepared for the evaluation of their DMFC performance with increasing temperatures. MEAs of a commercial Nafion® 115 film (DuPont Co.) were also prepared for comparison.

Anode and cathode gas diffusion electrode layers were acquired from BalticFuelCells GmbH (Schwerin, Germany). The anode was composed of a carbon paper with microlayer (model H2315 T10A) from Freudenberg Group (Weinheim, Germany), which was coated to a 5.0 mg cm^{-2} catalyst loading with particles of an alloy of Pt-Ru black 50:50 (Alfa Aesar) incorporating a 20 wt% content of dry Nafion® ionomer. The cathode consisted of a carbon paper with microlayer from Freudenberg (model H2315 I3C4), which was coated to a 5.0 mg cm^{-2} loading with a catalyst made of platinum nanoparticles supported on advanced carbon (HiSPEC 13100, Alfa Aesar), ratio of 70 wt% Pt on C, containing 20 wt% of Nafion® ionomer.

The electrodes were cut in squares of 2.3 cm side length (about 5 cm^2 area) and sandwiched between fully hydrated membranes. Finally, the MEAs were hot pressed at 110 ºC under a pressure of 300 N cm^{-2} for 3 min. On the other hand, the MEAs of Nafion® membranes were obtained pressing at 135 ºC instead. In all cases, the prepared MEAs were stored in water until fuel cell experiments were performed.

For measuring DMFC performance, the MEAs were placed into a single fuel cell hardware (quick CONNECT, Baltic Fuel Cells GmbH, Germany) containing graphite plates with serpentine flow fields of 5 cm^2 active area, and equipped with a pressure-controlled clamping force system.

An aqueous methanol solution of 2 M concentration was pumped at a flow rate of 6 ml min^{-1} to feed the anode. The cathode was fed with non-humidified oxygen gas at a flow rate of 250 ml min^{-1} and atmospheric pressure.

Polarization curves (i-V) were obtained at several temperatures, i.e. 80 ºC, 100 ºC and 120 ºC, by stepwise increment of the current from open-circuit voltage conditions ($i \approx 0$). Current and power density values were accordingly calculated and represented. Before i-V measurements, the MEAs were electrochemically activated for 5 h running current sweep cycles.

3. Results and discussion

3.1. Electrospinning of SPEEK-30%PVB nanofibres

Electrospinning is a very suitable technique for the scalable fabrication of nanofibres via electrostatic phenomena induced by large electric fields between a needle and a collector [47]. Recently, a novel approach has been proposed in which nanofibres are produced by strong centrifugal forces (centrifugal spinning) enabling higher production rates [48].

Although electrospinning can be defined as a simple technique, the process is influenced by many parameters, i.e. surface tension of polymer solution, polymer concentration, viscosity, solvent volatility, conductivity, flow rate, needle-collector distance, applied potential, surrounding humidity, etc., which makes setting optimal electrospinning parameters rather complicated [47].

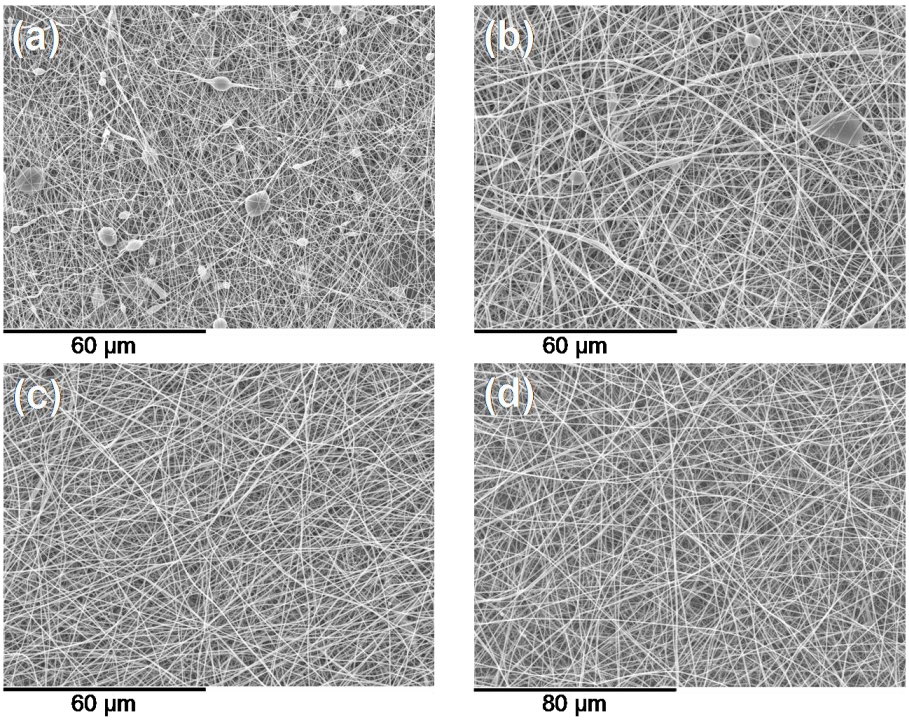

Fig. 1. SEM images of electrospun nanofibres prepared from SPEEK-30%PVB solutions under the same electrospinning conditions but different polymer concentrations: (a) 12.5 wt% (magnified x1,000); (b) 15 wt% (x1,000); (c) 17.5 wt% (x1,000); and (d) 20 wt% (x750).

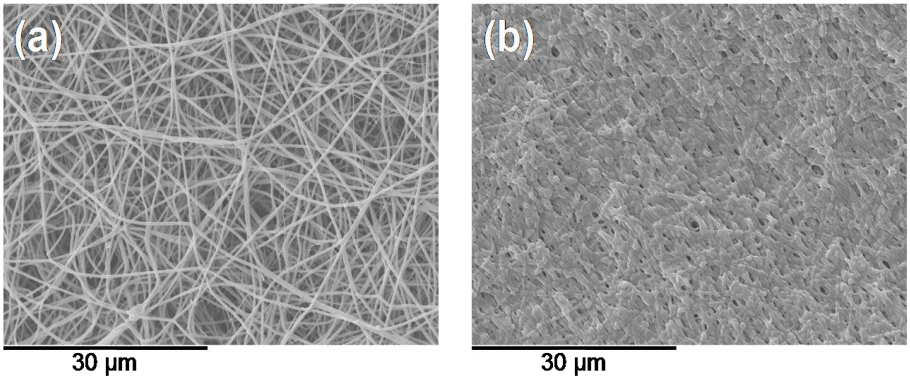

Fig. 2. SEM images of SPEEK-30%PVB nanofibres crosslinked at 200 ºC: (a) As-produced (magnified x2,000); and (b) after 1 h immersion in boiling water (x2,000).

Effect of polymer concentration was analyzed for SPEEK-30%PVB solutions in DMAc solvent under the following electrospinning conditions: The needle and the planar collector were separated 25 cm and energized to a potential of +10 kV and -25 kV, respectively, pumping the polymer solution at a flow rate of 0.2 ml h^{-1} while electrospinning was carried below 40 RH%. Fig. 1 shows the different electrospun nanofibre morphologies prepared from solutions between 12.5 wt% and 20 wt% polymer concentration.

At the lower polymer concentration range, i.e. 12.5 wt% and 15 wt%, defects known as "beads" are visible thus indicating that solution viscosity was insufficient. On the other hand, at the higher concentration range, i.e. 17.5 wt% and 20 wt%, perfect developed nanofibres are observed. The 20 wt% solution was found to be very viscous and it is empirically accepted that nanofibre diameter increases with increasing viscosity. Thereby, the solution with a total polymer concentration of 17.5 wt% was selected for the optimal preparation of SPEEK-30%PVB nanofibres.

The electrospun nanofibre mats, from a SPEEK-30%PVB solution of 17.5 wt% concentration, were first heated at 160 ºC for the removal of remaining DMAc solvent molecules and finally crosslinked at 200 ºC. Fig. 2 shows that the nanofibre morphology is preserved after the crosslinking process and the subsequent immersion in boiling water for 1 h despite densification and welding of the nanofibres are manifested. This confirms that the crosslinked nanofibres have a high chemical stability as required for withstanding hot aqueous environments of methanol solutions (DMFC operation above 80 ºC).

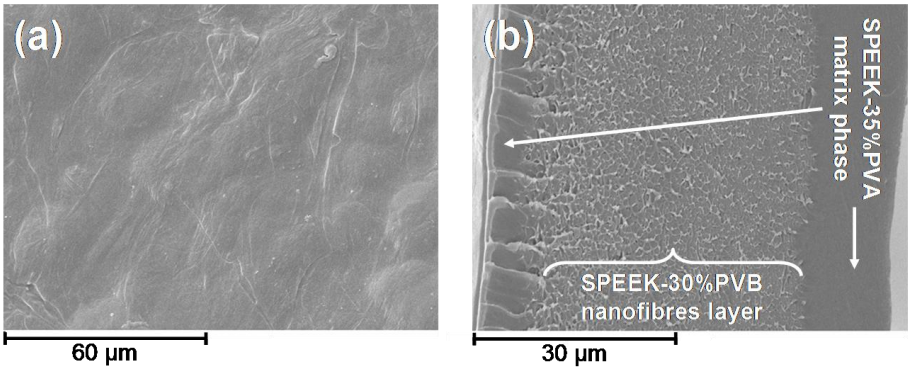

Fig. 3. SEM images of a sample of nanocomposite membrane containing SPEEK-30%PVB nanofibres within a SPEEK-35%PVA matrix: (a) View of the surface (magnified x1,000); and (b) cross-section revealing outer layers of SPEEK-35%PVA and an inner layer of nanofibres embedded in the matrix phase (x2,000).

3.2. Preparation of nanocomposite membranes. SEM analysis

The method applied for the incorporation of the SPEEK-35%PVA matrix between the nanofibres of SPEEK-30%PVB has been analyzed studying superficial and transversal views of the prepared nanocomposite membranes.

The surface and cross-section of a sample of nanocomposite membrane are shown in Fig. 3. The surface is compact with no visible pores, and the cross-section reveals two regions: The outer layers of pure SPEEK-35%PVA phase show a perfect fragile rupture and the inner layer contains evidence of a more plastic rupture, which is assigned to the presence of the nanofibre mat within the SPEEK-35%PVA matrix and the formation of a strong fibre-matrix interface.

These observations confirm that a good penetration of the aqueous SPEEK-35%PVA solution into the nanofibre mats occurs, which leads to the successful impregnation and loading of the matrix phase along the whole nanofibre layer thus forming a perfect sandwich structure.

3.3. Water uptake, swelling degree and ion-exchange capacity

The ion-exchange capacity represents the density of sulfonic acid groups present in the material. The high acid strength of the sulfonic moiety causes water to be incorporated into the ionic channels via hydrated protons (H_3O^+) strongly hydrogen-bonded to water molecules [49], which is represented by the water uptake, and the volume occupied by such an amount of water is measured through the swelling degree. Proton conductivity and methanol

Table 1. Swelling (in-plane and through-thickness), water uptake and ion-exchange capacity (IEC) values of the SPEEK-35%PVA and nanocomposite membranes are reported as a function of crosslinking temperature after 1 h in boiling water. Membrane thickness is given in dry state as a reference.

Membrane	Dry thickness (µm)	In-plane swelling (%)	Thickness swelling (%)	Water uptake (%)	IEC (meq g^{-1})
SPEEK-35%PVA (Cross. 110 ºC)	92 ± 3	203 ± 7	50 ± 5	283 ± 12	0.22 ± 0.01
Nanocomposite (Cross. 110 ºC)	70 ± 5	59 ± 5	109 ± 12	192 ± 12	0.22 ± 0.01
SPEEK-35%PVA (Cross. 120 ºC)	89 ± 3	107 ± 6	37 ± 4	152 ± 7	0.47 ± 0.01
Nanocomposite (Cross. 120 ºC)	72 ± 5	44 ± 5	42 ± 6	86 ± 9	0.31 ± 0.01
SPEEK-35%PVA (Cross. 130 ºC)	86 ± 3	44 ± 5	26 ± 3	67 ± 4	0.50 ± 0.01
Nanocomposite (Cross. 130 ºC)	69 ± 6	21 ± 4	25 ± 4	42 ± 5	0.27 ± 0.01
SPEEK-35%PVA (Cross. 140 ºC)	83 ± 3	21 ± 4	19 ± 2	36 ± 3	0.25 ± 0.01
Nanocomposite (Cross. 140 ºC)	66 ± 5	17 ± 4	21 ± 3	34 ± 5	0.56 ± 0.01

permeability are associated with IEC, water uptake and swelling degree; both generally increasing with those parameters [50-53]. However, if water uptake and swelling degree surpass some critical value, it has been noticed that proton conductivity can be prone to diminish as a consequence of a dilution effect which decreases the local concentration of protons within the ionic channels [54].

Table 1 lists the swelling degree, water uptake and IEC parameters of the nanocomposite membranes as a function of crosslinking temperature. Membranes prepared without nanofibres, i.e. SPEEK-35%PVA, have also been characterized for comparison.

It can be deduced from Table 1 that in-plane swelling, through-thickness swelling and water uptake in both type of membranes diminish with increasing temperature of crosslinking. The nanocomposite membranes remarkably show larger dimensional changes through-thickness than in-plane, which is inferred to the 2-D (plane) mechanical reinforcing effect provided by the nanofibres. This is especially observed with the nanocomposite membranes crosslinked at 110 ºC and 120 ºC; conditions in which the SPEEK-35%PVA matrix is just partially crosslinked as deduced from the high water uptake values. Constraint of the swelling as a

consequence of the reinforcement with nanofibres is clearly demonstrated by comparison of the water uptake values between SPEEK-35%PVA and nanocomposite membranes crosslinked at those temperatures. This suggests the nanocomposite membranes to be mechanically more stable under typical cyclic hydration conditions occurring due to fuel cell operation. Such a cyclic swelling/water uptake of the membrane is prone to generate mechanical stresses and fatigue, thus influencing the long-term operational lifetime [55].

On the other hand, the differences of the swelling and water uptake parameters between both type of membranes diminish with increasing crosslinking temperature and converge at 140 ºC. This result points out that the crosslinking degree approaches a maximum level towards a temperature of about 140 ºC. Consequently, a higher crosslinking degree of the matrix must come accompanied by an important improvement of its mechanical properties, thus decreasing the reinforcement benefit associated with the nanofibres.

Interestingly, the SPEEK-35%PVA membranes prepared in this study by casting from an aqueous solution can be crosslinked at much lower temperatures than those cast with DMAc solvent such us in our previous work [42]. Likely, the strong polar nature and hydrogen-bonding capacity of water favor the orientation of the sulfonic acid groups ($-SO_3H$) of SPEEK against the hydroxide groups (-OH) of PVA, then facilitating the corresponding acid-base reaction.

The ion-exchange capacities measured for the membranes in Table 1 do not represent a meaningful result. The authors suggest that salt rejection, NaCl in this case, might be occurring and, therefore, ion-exchange of protons by sodium ions (Na^+) not taking place. Indeed, some literature reports the salt rejection properties of SPEEK-containing membranes due to the fixed negative charges of the dissociated sulfonic groups which repel anions such us sulfate and chloride [56-58]. An important application for this kind of membranes involves nanofiltration for water purification. Furthermore, salt rejection might be encouraged in our composition by the presence of PVA [59]. It can be then concluded that other salt compositions should be investigated to minimize salt rejection and allow the correct measurement of IEC on this type of membranes. Similarly, this particular phenomenon might take place in other sulfonated hydrocarbon materials different to SPEEK.

3.4. FTIR results

Analysis of the crosslinking reactions between the chains of SPEEK-PVA and SPEEK-PVB mixed in DMAc solvent was conducted by means of the

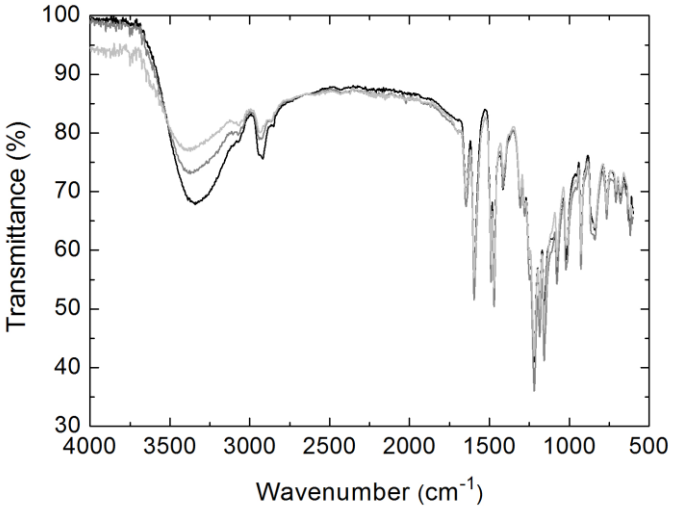

Fig. 4. FTIR spectra as a function of crosslinking temperature for SPEEK-35%PVA membranes prepared from aqueous solutions: (Black) as-prepared, (grey) crosslinked at 120 ºC, and (light grey) crosslinked at 140 ºC.

FTIR and DSC techniques and reported by the authors [42]. Those reactions were mainly assigned to the condensation between sulfonic acids of SPEEK and OH groups of PVA and PVB, and in some extent to reactions between the sulfonic acid groups and intermediate species derived from the thermal degradation of PVA and PVB. In this work, the crosslinking reaction between the SPEEK and PVA polymers blended in water solvent was evaluated preparing samples of SPEEK-35%PVA membranes by casting their aqueous solutions. Samples with similar thickness were obtained and the FTIR spectra associated with such membranes are represented in Fig. 4.

The profiles of the blended SPEEK-PVA membranes predominantly exhibit the characteristic peaks of SPEEK, which can be understood as SPEEK is the principal constituent material of the membranes. Accordingly, the following peaks can be distinguished: O-H species from sulfonic acid groups vibrate at about 3450 cm^{-1}, while other bands assigned to sulfonic acid are found at 1247 cm^{-1}, 1079 cm^{-1} and 1025 cm^{-1}. A peak at 1652 cm^{-1} corresponds to the carbonyl group of the SPEEK structure, and the peaks at 1491 cm^{-1} and 1221 cm^{-1} evidence the presence of C-C aromatic ring and aromatic C-O-C bonds, respectively [60,61].

It is reported that PVA typically shows a broad peak ranging from 3700 cm^{-1} to 3000 cm^{-1} and centered around 3300 cm^{-1}, which is attributed to stretching of the hydroxyl (O-H) groups [60,62]. Consequently, the bands of the vibrating O-H bonds belonging to the sulfonic acid groups of SPEEK and the hydroxide groups of PVA overlap. This should explain the large

peaks observed in Fig. 4 at those wavenumbers. The largest peak appears on the as-prepared sample which has not been crosslinked, and it progressively decreases after crosslinking at 120 ºC and 140 ºC. The condensation reaction between sulfonic acids and hydroxyl groups explains the consumption of OH moieties with the corresponding decrease of the associated peak [42]. This corroborates that crosslinking reactions take place between 110 ºC and 140 ºC in SPEEK-35%PVA compositions prepared from aqueous solutions, in contrast to the SPEEK-PVA formulations mixed in DMAc solvent in which crosslinking was only achieved at about 200 ºC [42].

3.5. Mechanical properties

Static mechanical testing has been carried out on samples of SPEEK-35%PVA and nanocomposite membranes crosslinked at 120 ºC. The purpose is to compare their mechanical properties and evaluate the effect of the nanofibres. It is of special interest to corroborate that the preparation method leads to compact nanocomposite membranes with negligible defects.

Mechanical parameters such us Young's modulus, ultimate tensile strength and tensile rupture strain were obtained and are reported in Table 2. Statistically, no significant differences are found between both membranes and no apparent influence of the nanofibres demonstrated. A plausible explanation can be given taking into account that the previously hydrated membranes were partially dried before the tests by placing them between two plastic sheets under pressure and at 35 ºC for 4 days. At those conditions, the mechanical properties of the matrix and nanofibres seem to coincide. On the other hand, for fully hydrated conditions, the mechanical strength of the swollen matrix will weaken as a function of water uptake and the reinforcing effect of the non-swollen nanofibres would be expected to become evident. Unfortunately, our setup did not allow the samples to be maintained at a fully hydrated state. When hydrated samples were tested, they were losing water during the measurements in air and no reliable data was obtained. Consequently, it was decided to measure samples with lower water content. According to their similar results observed in Table 2, it can be confirmed the successful introduction of the matrix phase between the nanofibres of the mats without evidence of weakening defects such us pores.

Table 2. Average values of Young's modulus (E), ultimate tensile strength (σ_{ult}) and tensile rupture strain (ε_r) for samples crosslinked at 120 ºC of SPEEK-35%PVA and nanocomposite membranes.

Sample	E (GPa)	σ_{ult} (MPa)	ε_r (%)
SPEEK-35%PVA	1.3 ± 0.3	48 ± 8	21 ± 7
Nanocomposite	1.2 ± 0.4	47 ± 7	16 ± 5

An observed advantage of introducing nanofibres arises from the induced mechanical stability of the membranes. It was noted that the SPEEK-based membranes tend to be brittle when their water content decreases up to a dry state as they shrink. However, the nanocomposite membranes were less affected by such a shrinking process and their physical integrity was preserved to a greater extent.

3.6. Methanol permeability

The reduction and limitation of methanol permeability through a membrane is an essential matter for the practical application of direct methanol fuel cells. Fuel loss and decrease of electrochemical efficiency at the cathode are the main issues to avoid.

Methanol permeability has been measured at 60 ºC by analyzing the change of methanol concentration in the receptor chamber (C_R) as a function of time (t) during the pseudo-steady state conditions. Linear trends with R-squared fitted lines are obtained and slopes, expressed by C_R/t, estimated. The values of the slopes are introduced in Eq. (5) and then the apparent methanol permeabilities are calculated from the membrane thickness and other experimental parameters. The methanol permeability is described as 'apparent' due to the fact that includes the effect of the boundary layers in addition to the permeation across the membrane itself.

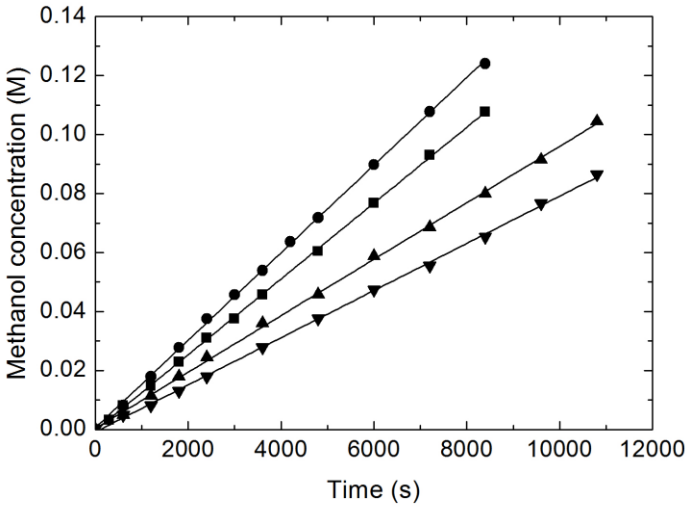

Fig. 5. Profiles of methanol concentration in receptor chamber versus time measured at 60 ºC from a 2 M aqueous methanol solution in donor chamber, which have been obtained for the nanocomposite membranes depending on crosslinking temperature and membrane thickness: (■) 110 ºC, 145 μm; (●) 120 ºC, 107 μm; (▲) 130 ºC, 88 μm; and (▼) 140 ºC, 71 μm.

Table 3. Values at 60 ºC of apparent methanol permeability (P) and proton conductivity (σ') for the SPEEK-35%PVA and nanocomposite membranes as a function of crosslinking temperature. A modified characteristic factor is calculated as $\Phi = \sigma'^2/P$ for theoretical evaluation of materials performance in DMFC operating conditions. A Nafion® 115 membrane is included for reference.

Membrane	Methanol permeability ($cm^2\ s^{-1}$)	Proton conductivity ($S\ cm^{-1}$)	Modified characteristic factor ($S^2\ s\ cm^{-4}$)
SPEEK-35%PVA (Cross. 110 ºC)	$(5.81 \pm 0.20)\cdot10^{-6}$	$(1.11 \pm 0.08)\cdot10^{-2}$	21.2 ± 3.2
Nanocomposite (Cross. 110 ºC)	$(4.43 \pm 0.21)\cdot10^{-6}$	$(1.35 \pm 0.11)\cdot10^{-2}$	41.1 ± 5.8
SPEEK-35%PVA (Cross. 120 ºC)	$(4.70 \pm 0.13)\cdot10^{-6}$	$(1.10 \pm 0.05)\cdot10^{-2}$	25.7 ± 1.9
Nanocomposite (Cross. 120 ºC)	$(3.82 \pm 0.18)\cdot10^{-6}$	$(1.03 \pm 0.08)\cdot10^{-2}$	27.8 ± 3.6
SPEEK-35%PVA (Cross. 130 ºC)	$(2.18 \pm 0.07)\cdot10^{-6}$	$(5.84 \pm 0.32)\cdot10^{-3}$	15.6 ± 1.5
Nanocomposite (Cross. 130 ºC)	$(2.02 \pm 0.11)\cdot10^{-6}$	$(2.50 \pm 0.18)\cdot10^{-3}$	3.1 ± 0.3
SPEEK-35%PVA (Cross. 140 ºC)	$(1.19 \pm 0.06)\cdot10^{-6}$	$(3.53 \pm 0.13)\cdot10^{-3}$	10.5 ± 0.3
Nanocomposite (Cross. 140 ºC)	$(1.34 \pm 0.09)\cdot10^{-6}$	$(1.63 \pm 0.10)\cdot10^{-3}$	2.0 ± 0.1
Nafion® 115	$(3.71 \pm 0.05)\cdot10^{-6}$	$(3.64 \pm 0.11)\cdot10^{-2}$	357 ± 24

Fig. 5 plots the profiles of methanol concentration versus elapsed time for the nanocomposite membranes crosslinked at 110 ºC, 120 ºC, 130 ºC and 140 ºC, which presented a thickness after experiments of 145 μm, 107 μm, 88 μm and 71 μm, respectively. Table 3 shows the values of apparent methanol permeability for all the SPEEK-35%PVA and nanocomposite membranes prepared in this study, which are represented in Fig. 6 as a function of crosslinking temperature.

Methanol permeability is clearly related with the water uptake values of the membranes given in Table 1. Water uptake was particularly constrained by the presence of SPEEK-30%PVB nanofibres when the SPEEK-35%PVA matrix was crosslinked at 110 ºC and 120 ºC, following this order. Fig. 6 corroborates this fact in terms of methanol permeability, and it shows that the nanocomposite membranes crosslinked at 110 ºC and 120 ºC decreased the methanol crossover in comparison with the SPEEK-35%PVA membranes crosslinked at the similar temperatures. Specifically, the latter exhibited relatively high methanol permeabilities when Nafion® is considered as a reference material.

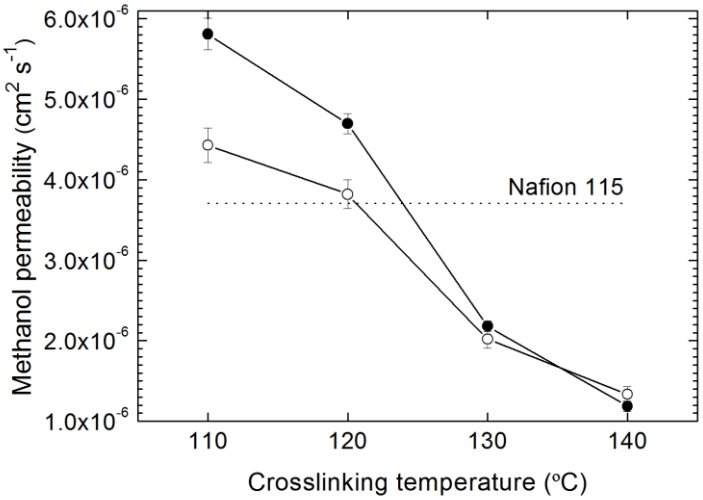

Fig. 6. Representation of the apparent methanol permeabilities at 60 ºC for (closed symbol) SPEEK-35%PVA and (open symbol) nanocomposite membranes in relation to their crosslinking temperatures. The value measured for a commercial Nafion® 115 membrane is included for reference.

Interestingly, the nanocomposite membrane which was crosslinked at 120 ºC had a methanol permeability equivalent to Nafion®, while those membranes crosslinked at 130 ºC and 140 ºC much lower values. Methanol permeability reduced with increasing temperature of crosslinking but no significant differences are observed between SPEEK-35%PVA and nanocomposite membranes crosslinked at 130 ºC and 140 ºC. This is inferred to the higher crosslinking degrees reached at those temperatures which causes no valuable effect of the nanofibres on the crosslinked matrix.

3.7. Proton conductivity

The proton conducting properties of the SPEEK-30%PVB nanofibres and the prepared membranes were examined from impedance measurements at 60 ºC and 90 ºC. Bode diagrams were analyzed by plotting the real part of the conductivity versus frequency. The proton conductivity was obtained at the region of high frequencies in which the real conductivity tends to a plateau when the phase angle value approaches zero.

The Bode diagram of a SPEEK-30%PVB nanofibre mat in Fig. 7 shows the profile of real conductivity versus frequency obtained at 90 ºC. The mat, which previously was placed 1 h in boiling water, was washed with deionized Milli-Q water and the thickness measured (283 μm). Milli-Q water was introduced in the conductivity cell in order to ensure a fully hydrated

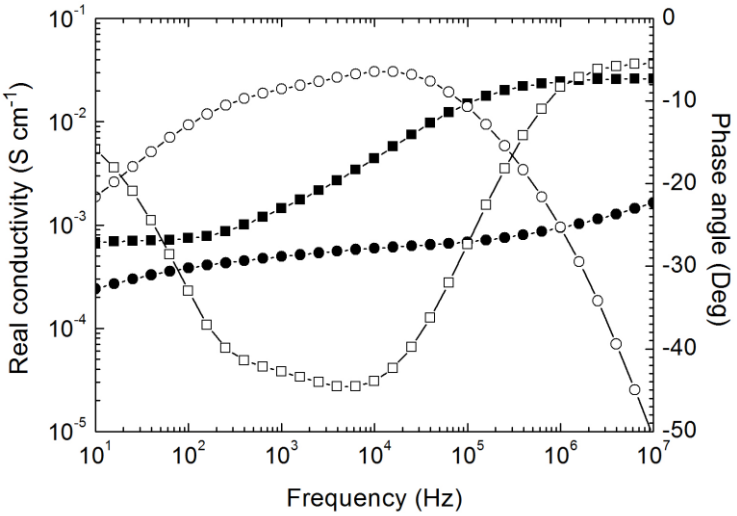

Fig. 7. Bode diagram showing the proton conductivity profiles at 90 ºC of a (square) SPEEK-30%PVB nanofibre mat (283 μm thick) with embedded Milli-Q water, and a (circle) SPEEK-30%PVB membrane (260 μm thick) prepared by casting. Real conductivity and phase angle are represented by solid and open symbols, respectively.

state of the mat during measurements. For comparison, a SPEEK-30%PVB membrane was prepared by casting from a DMAc solution and similar conductivity measurements performed. The membrane was previously swollen in boiling water for 1 h (260 μm thick) and Milli-Q water was also added to the conductivity cell. The result of this membrane at 90 ºC is included in Fig. 7 and displays a conductivity ($6.11 \cdot 10^{-4}$ S cm^{-1}) about 1/43 the conductivity value of the nanofibre mat ($2.61 \cdot 10^{-2}$ S cm^{-1}). This confirms that the SPEEK-30%PVB nanofibres are good proton-conducting materials. Furthermore, the different phase angle profiles shown in Fig. 7 between the nanofibre mat and the SPEEK-30%PVB membrane corroborate that proton conduction takes place along distinct pathways. Two proton conduction mechanisms associated to the nanofibre morphology could explain this large increment of proton conductivity. On one side, conductivity may be improved through the bulk due to an induced preferential orientation of the ionic channels along the nanofibre axis, and on the other side, conductivity may be encouraged on the nanofibre surface through the strong interface formed between water molecules and external sulfonic acid groups [32].

The values of proton conductivity of the SPEEK-35%PVA and nanocomposite membranes obtained at 60 ºC are given in Table 3. Comparison between both types of membranes at each crosslinking temperature reveals the influence of the SPEEK-30%PVB nanofibres on the conductivity. Clearly, when the nanocomposite membrane has been

crosslinked at 110 ºC and water uptake reaches a very high level (see Table 1), the proton conductivity of the nanocomposite membrane exceeds the conductivity of the SPEEK-35%PVA matrix. This confirms a positive contribution of the nanofibres on the conductivity. Crosslinking at 120 ºC has almost no effect on the SPEEK-35%PVA membrane despite the lower water uptake (Table 1), but decreases the conductivity of the nanocomposite membrane until a value close to the pristine SPEEK-35%PVA phase. Further increase of the crosslinking temperature to 130 ºC and 140 ºC results on proton conductivities of the nanocomposite membranes significantly below the conductivities found in the SPEEK-35%PVA membranes. Although the water uptake values at those crosslinking conditions are rather similar between both types of membranes (Table 1), the presence of nanofibres has a negative repercussion. Likely, SPEEK from the nanofibres reacts with PVA from the matrix and the formed interface restricts the presence of water on the nanofibre surface for proton conduction, and in addition, sulfonic acid groups for the donation of protons are consumed. These phenomena could even make the nanofibres to block proton transport through the matrix. Then, apparently, reduction of surface concentration of water molecules and sulfonic acid groups on the SPEEK-30%PVB nanofibres strongly affects their conductivity properties as a consequence of a more limited proton conduction via the water-sulfonic acid association. This conclusion about conductivity preferentially taking place on the nanofibres surface would be in agreement with those reported in other studies [32,63]. Moreover, this explanation can be supported by the fact that nanofibre axis orientation is perpendicular to the proton conduction direction, which might difficult conductivity through the nanofibre bulk but on the nanofibre surface.

Table 3 also compiles the values of a modified characteristic factor which is a theoretical consideration for the suitable estimation of DMFC performance of polymer electrolytes under practical operating conditions. Typically, the characteristic factor is conceived as $\Phi = \sigma'/P$, thus suggesting that both proton conductivity and methanol permeability equally influence DMFC performance. Consequently, a simultaneous and equivalent increment of proton conductivity and methanol permeability would not cause any change on the DMFC performance. However, many authors have empirically demonstrated that proton conductivity is the main parameter governing the DMFC performance during standard operating conditions [33-35]. This is explained by the fact that methanol is electrochemically oxidized at the anode and, thereby, the driving force for methanol permeation, that is the concentration gradient, diminishes with increasing current density. Thus, reaching certain levels of current density makes their associated ohmic losses prevail upon the methanol crossover effect to explain the electrochemical performance. This reason makes us to propose a

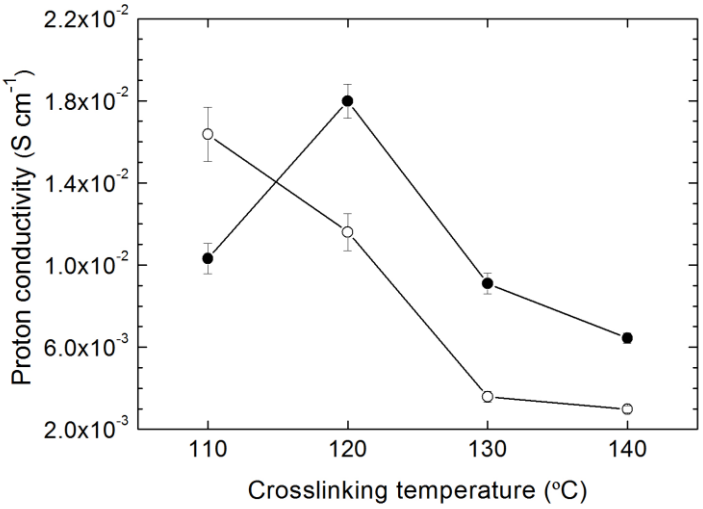

Fig. 8. Proton conductivities at 90 ºC for (closed symbol) SPEEK-35%PVA and (open symbol) nanocomposite membranes as a function of crosslinking temperature. The result of a commercial Nafion® 115 membrane was $5.90 \cdot 10^{-2}$ S cm^{-1} (not shown in graphic).

modified characteristic factor in which proton conductivity is emphasized against methanol permeability without completely neglecting its negative effect. The modified characteristic factor is correspondingly defined as $\Phi = \sigma^{t2}/P$ [42].

Nafion® is an outstanding polymer electrolyte membrane although its main drawback comes from the extremely high cost of this perfluorinated material. We can observe in Table 3 that it is the best performing material according to its modified characteristic factor. Nevertheless, the purpose of this study is replacing Nafion® with more cost effective SPEEK-based materials.

Attending to the modified characteristic factors calculated for the prepared SPEEK-containing membranes in Table 3, the nanocomposite membranes crosslinked at 110 ºC and 120 ºC show a priori the best properties for the achievement of optimal DMFC performances. In this case, it is worth mentioning that the nanocomposite membrane crosslinked at 120 ºC is superior to the former from a mechanical stability point of view.

Fig. 8 encompasses the proton conductivities of the SPEEK-35%PVA and nanocomposite membranes measured at 90 ºC. The conductivity of the nanocomposite membrane crosslinked at 110 ºC ($1.64 \cdot 10^{-2}$ S cm^{-1}) surpasses the conductivity exhibited by the SPEEK-35%PVA membrane crosslinked at the same temperature ($1.03 \cdot 10^{-2}$ S cm^{-1}). The conductivity of the nanocomposite membrane crosslinked at 120 ºC ($1.16 \cdot 10^{-2}$ S cm^{-1}) decreases

in comparison with that one crosslinked at 110 ºC and it is also below the conductivity of the SPEEK-35%PVA membrane crosslinked at 120 ºC ($1.80 \cdot 10^{-2}$ S cm^{-1}). A similar trend is distinguished from the results at 60 ºC in Table 3. On the other hand, the SPEEK-35%PVA membranes crosslinked at 110 ºC and 120 ºC reveal a particular behaviour. The proton conductivities of such membranes are practically similar at 60 ºC (Table 3), but the SPEEK-35%PVA membrane crosslinked at 120 ºC shows a higher conductivity at 90 ºC than the membrane crosslinked at 110 ºC (Fig. 8). Since swelling and water uptake increase with increasing temperature, especially above a critical temperature which depends on the IEC, it is inferred that the lower crosslinking degree reached at 110 ºC will promote a larger water uptake during the measurement at 90 ºC than at 60 ºC. Correspondingly, the larger fraction of water confined within the membrane will cause a diluting effect of the sulfonic acid groups thus decreasing the conductivity [54]. Crosslinking at 120 ºC seems to be optimal for the control of excessive water uptake while still not considerably reducing this parameter for the final achievement of a good proton conduction.

It is then plausible to affirm that proton conductivity of the nanocomposite membranes depends on the nanofibre mats via the conductivity contribution of those nanofibres and their capacity to control swelling and water uptake of the matrix. Membranes with low crosslinking levels are then the most favoured by the nanofibres.

3.8. DMFC performance

The response of the nanocomposite membranes crosslinked at 110 ºC and 120 ºC under DMFC operation is shown in Fig. 9. A standard Nafion® membrane (N115) is included as a reference. Electrochemical performance was evaluated from 80 ºC to 120 ºC at atmospheric pressure with the anode and cathode fed by a 2 M aqueous methanol solution and pure oxygen (without humidification), respectively.

The results at 120 ºC operation have been modeled using Eq. (7), in which mass transport limitation phenomena are not considered for simplification.

$$V = V_{OC} - A_1 \cdot \ln \frac{i}{i_0} - R_{MEA} \cdot i \cdot S \qquad (7)$$

The parameter V represents the cell voltage, V_{OC} the reversible open-circuit voltage, A_1 the sum of the Tafel slopes for anode and cathode, i the cell current density (defined as I/S), i_0 the exchange current density (catalytic function), R_{MEA} the ohmic resistance of the MEA (mainly caused by the ionic

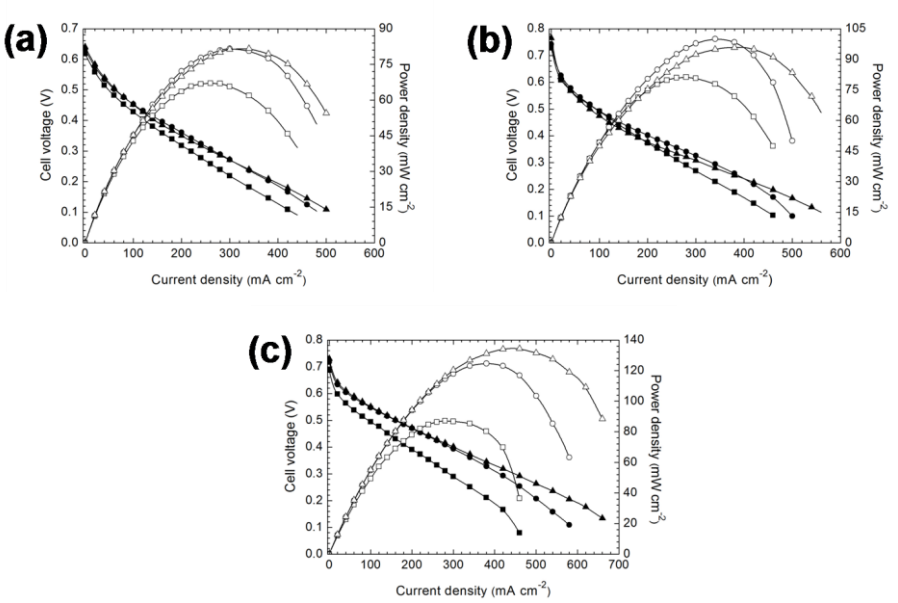

Fig. 9. DMFC performance of the (a) nanocomposite membrane crosslinked at 110 ºC (145 µm thick), (b) nanocomposite membrane crosslinked at 120 ºC (107 µm thick), and (c) Nafion® 115 membrane (157 µm thick) measured at different temperatures: (Square) 80 ºC, (circle) 100 ºC, and (triangle) 120 ºC. Cell voltage profiles are represented by solid symbols and power density curves by open symbols.

resistance of the membrane), *S* the geometrical area of the membrane and *I* the total cell current.

Attempts to estimate the electro-osmotic methanol crossover during DMFC experiments involve the mathematical model given in Eq. (8) [38,64], valid for an equivalent geometrical area of membrane (*S*) of 1 cm^2,

$$V(i, C_{an}) = V_{OC} - A_1 \cdot \ln\left(\frac{i}{i_0}\right) - A_2 \cdot C_{an} - A_3 \cdot i \qquad (8)$$

with,

$$A_3 = \frac{L}{\sigma} + A_{eos} \qquad (9)$$

where A_2 represents the overvoltage caused by diffusion of methanol under a concentration gradient (no current dependent), C_{an} is the methanol concentration at the anode and A_3 represents the overvoltage due to the sum of the protonic resistance and the methanol electro-osmotic effect as both

depend on current density. From Eq. (9), it is detailed that A_3 depends on L and σ, which are the thickness and conductivity of the membrane, respectively, and a term A_{eos} associated with the electro-osmosis of methanol.

The derivative *dV/di* when a constant concentration of methanol in the anode is assumed, is equal to,

$$\frac{dV}{di} = -\frac{A_1}{i} - A_3 \qquad (10)$$

Plotting *dV/di*, preferably between 100-350 mA cm^{-2}, the slope gives the value of A_3 as seen in Eq. (10). Then, A_{eos} can be calculated introducing in Eq. (9) those values of L and σ previously measured experimentally. Although this is a good approach to evaluate the electro-osmotic effect taking place in a membrane, there is a point which weakens this model. In our new consideration, the drawback comes from the fact that proton conductivity can be influenced by methanol crossover. It has been established that an alcohol environment, e.g. methanol, can affect the dissociation of the sulfonic acid groups thus reducing the proton conductivity [65]. This is explained by the lower relative dielectric constant of methanol (33.1 at 20 ºC) in comparison with water (80.4 at 20 ºC). Therefore, the proton conductivity cannot be considered to be a constant independent of methanol crossover and, consequently, this model description becomes strictly not true. Indeed, a new parameter A_3^* should be defined to express the change of membrane resistivity due to the modified proton conductivity of the membrane as a consequence of the mixture of water and methanol within the ionic channels. In this case, A_2 will include the effect of methanol permeation by diffusion on both the membrane conductivity and catalyst performance, while the new A_3^* parameter in Eq. (11) will consider the effect of electro-osmosis of methanol on the conductivity.

$$\frac{dV}{di} = -\frac{A_1}{i} - A_3 - \frac{dA_3}{di}\cdot i = -\frac{A_1}{i} - A_3 - A_3^*\cdot i \qquad (11)$$

It is speculated that the methanol barrier layer should concentrate near the anode side in an asymmetric membrane configuration. Consequently, it would be minimized the accumulation of methanol within the membrane which in turn would decrease the proton conductivity. Following this line, it is predicted the worst situation to occur if the methanol barrier layer would face the cathode site. The nanocomposite membranes of this study contain the nanofibre-based methanol barrier layer in a symmetric centered position (sandwich structure). Next steps should then address the preparation of

asymmetric nanofibre-reinforced membranes and their DMFC performance evaluation as a function of methanol barrier layer position.

Fitting of Eq. (7) to the experimental *i*-*V* values was carried out through the minimum mean square error method, $\Sigma(V_{exp} - V_{mod})^2$, in order to estimate the model parameters. Consequently, every given current density (i) value was associated with an experimentally measured cell voltage (V_{exp}) and a calculated value from the model (V_{mod}). Power density (P) curves were obtained via Eq. (12),

$$P = V \cdot i \tag{12}$$

and thus, two curves were figured, i.e. $P_{exp} = V_{exp} \cdot i$ and $P_{mod} = V_{mod} \cdot i$. Since power density is very sensitive to the cell voltage (V^2) and a function of the ohmic resistance (R_{MEA}), see Eq. (13), this property has been used for a refined determination of the model parameters and especially the ohmic resistance term [66]. In our case, we conceived a global mean square error factor composed of $\Sigma(V_{exp} - V_{mod})^2 \cdot \Sigma(P_{exp} - P_{mod})^2$ which was minimized by iterative calculations using a commercial computer software package. The respective calculated model parameters are reported in Table 4.

$$P = \frac{V^2}{R_{MEA} \cdot S} \tag{13}$$

Turning back to Fig. 9, we can observe that the nanocomposite membrane crosslinked at 120 ºC performed better than the nanocomposite membrane crosslinked at 110 ºC. The former reaches a maximum DMFC performance of 81.2 mW cm^{-2} (at 280 mA cm^{-2}) and the latter 67.1 mW cm^{-2} (at 260 mA cm^{-2}) under an operating cell temperature of 80 ºC. The performance increases to 96.0 mW cm^{-2} (at 400 mA cm^{-2}) and 81.6 mW cm^{-2} (at 340 mA cm^{-2}), respectively, when the cell temperature is 120 ºC. Under similar operating conditions, i.e. at cell temperatures of 80 ºC and 120 ºC, the Nafion® membrane achieved 87.1 mW cm^{-2} (at 280 mA cm^{-2}) and 134.6 mW cm^{-2} (at 440 mA cm^{-2}).

It can be visually distinguished in Fig. 9 that activation polarization losses, observed by the potential drop at the beginning of the *i*-*V* profile, are relatively larger on the nanocomposite membrane crosslinked at 120 ºC. The electrochemical performance of the electrodes decreases with increasing A_1 and decreasing i_0. Clearly, this is corroborated with the values of those parameters given in Table 4 for such a nanocomposite membrane. The reason of this poorer electrochemical performance associated with the

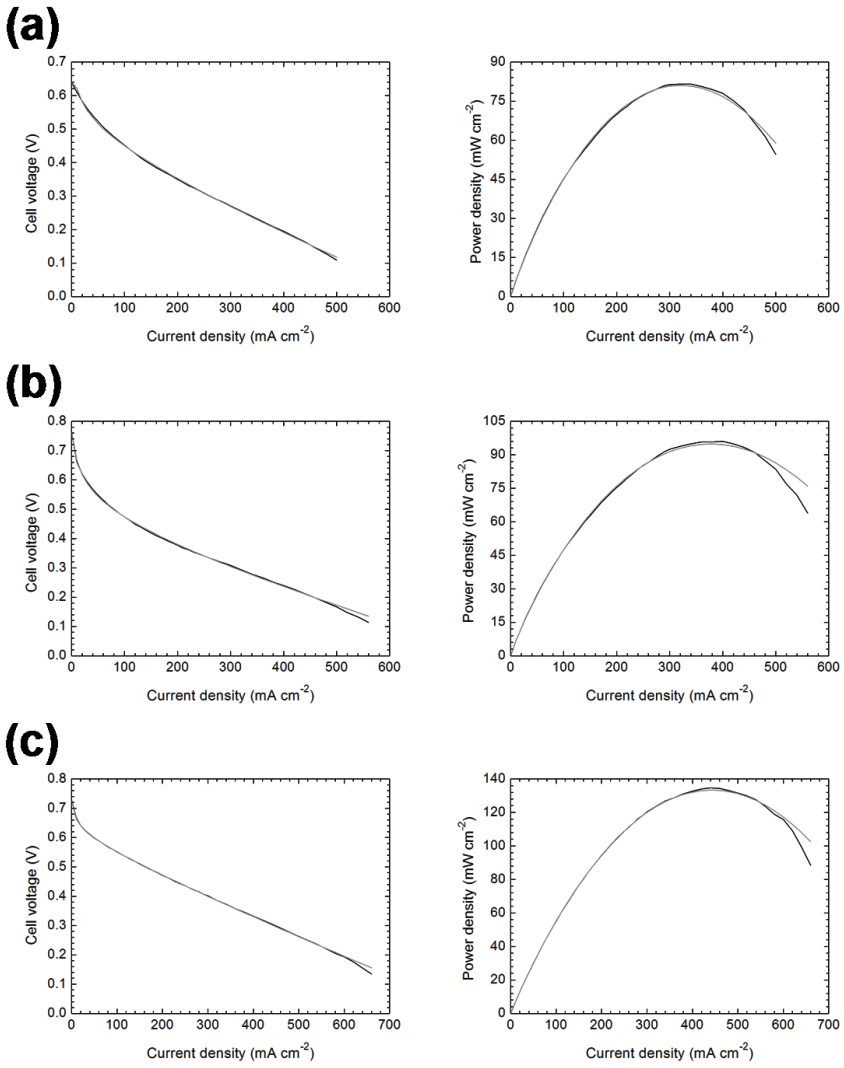

Fig. 10. Fitting between (black line) experimental and (grey line) modeled profiles corresponding to the DMFC performance at 120 ºC of the (a) nanocomposite membrane crosslinked at 110 ºC, (b) nanocomposite membrane crosslinked at 120 ºC, and (c) Nafion® 115 membrane. Left charts describe the cell voltage profiles (*i*-*V*) and right charts represent corresponding power density curves versus current density (*i*-*P*).

catalyst activation remains unclear, although it is assumed that optimization of the MEA preparation still needs to be achieved.

Fig. 10 compares the experimental and modeled profiles for the DMFC performance at 120 ºC of the nanocomposite and Nafion® membranes. A

Table 4. Calculated parameters which fit the model of Eq. (7) for the experimental *i*-*V* curves measured at 120 ºC with the nanocomposite membranes crosslinked at 110 ºC and 120 ºC. The results of the Nafion® 115 membrane are also included.

Membrane	Thickness (μm)	V_{OC} (V)	A_1 (V)	i_0 (A cm^{-2})	R_{MEA} (Ω)	σ_{MEM} (S cm^{-1})
Nanocomposite (Cross. 110ºC)	145 ± 7	0.640	0.050	7.898	0.126	$(2.30 \pm 0.11)\cdot10^{-2}$
Nanocomposite (Cross. 120ºC)	107 ± 5	0.765	0.065	2.430	0.099	$(2.16 \pm 0.10)\cdot10^{-2}$
Nafion® 115	157 ± 2	0.730	0.024	0.865	0.125	$(2.51 \pm 0.03)\cdot10^{-2}$

very good fitting is confirmed which validates the values given in Table 4 for the Eq. (7) model parameters. Nevertheless, the last part of the curves at the highest current densities shows that the experimental profiles tend to be located below those modeled. This is attributed to the appearance of mass transport limitation effects at those conditions, and therefore, it especially occurs in the case of the nanocomposite membrane crosslinked at 120 ºC and Nafion® as both can reach higher currents.

Table 4 also includes the values of open circuit potential (V_{OC}), which are associated with the fuel crossover due to the voltage reduction caused by methanol on the oxygen reduction reaction at the cathode, for the membranes at 120 ºC and a 2 M aqueous methanol solution. In agreement with Fig. 6 and Table 3, the lower V_{OC} value of the nanocomposite membrane crosslinked at 110 ºC confirms its higher methanol permeability characteristics. However, the nanocomposite membrane crosslinked at 120 ºC reveals the largest V_{OC} voltage despite its lower thickness in comparison with the Nafion® membrane. This suggests that although the permeability coefficient at 60 ºC of this nanocomposite membrane was slightly superior to that of Nafion®, the latter seems to increase further its methanol permeability at 120 ºC in relation to the nanocomposite membrane. This might be due to the reaching of the glass transition temperature of Nafion®, ranged between 80-100 ºC under a fully hydrated state [41,67], which would explain an encouragement of its methanol transport properties.

Assuming that the ohmic resistance of a MEA is mainly the ionic resistance of the membrane, the calculated values of R_{MEA} at 120 ºC for the membranes have been converted into proton conductivities (σ_{MEM}) by means of Eq. (6) and are reported in Table 4. The membranes can be ordered in terms of proton conductivity as it was observed at 60 ºC, that is: Nafion® > > Nanocomposite crosslinked at 110 ºC > Nanocomposite crosslinked at 120 ºC. Interestingly, the relative differences in conductivity between Nafion® and the nanocomposite membranes become much smaller at 120 ºC than at 60 ºC. As expected, it can be concluded that SPEEK is a more

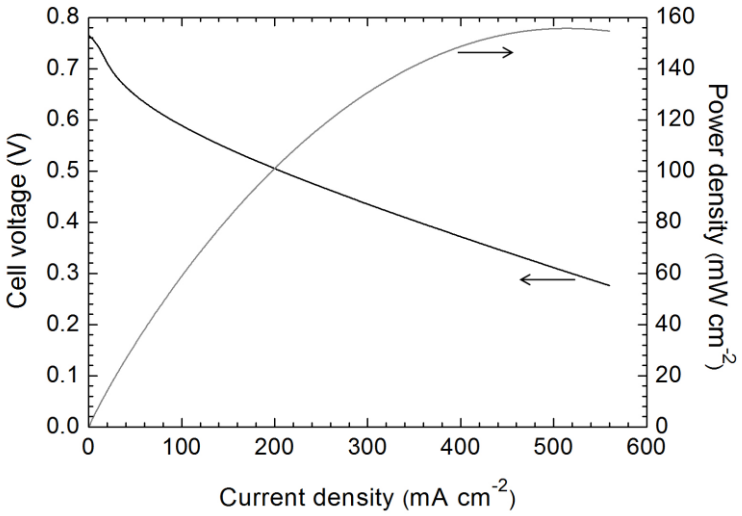

Fig. 11. Simulation of the (black line) *i-V* and (grey line) power density results for the DMFC performance at 120 ºC of the nanocomposite membrane crosslinked at 120 ºC if polarization losses are assumed to be similar to the exhibited by the nanocomposite crosslinked at 110 ºC.

suitable ionomer for fuel cell operation at intermediate temperatures, i.e. above 80 ºC, which is the upper limit temperature of the Nafion® material.

Finally, it is shown in Fig. 11 the simulation of the DMFC performance at 120 ºC for a nanocomposite membrane crosslinked at 120 ºC if the activation polarization losses would be similar to the found for the MEA of the nanocomposite membrane crosslinked at 110 ºC. Therefore, Eq. (7) has been used with V_{OC} and R_{MEA} of the former but A_1 and i_0 parameters of the latter. A maximum power density of 155.8 mW cm^{-2} (at 520 mA cm^{-2}) is obtained. This result surpasses the achieved with the Nafion® membrane and expresses the great potential of these novel nanocomposite membranes for DMFC operation at intermediate temperatures. In this regard, future studies should also focus on the optimization of the MEA preparation, e.g. with SPEEK-bound electrodes, and the favorable electrochemical activation of the electrode catalysts under intermediate temperature conditions.

4. Conclusions

Mats of proton-conducting nanofibres composed of SPEEK blended with PVB (SPEEK-30%PVB) have been successfully obtained by electrospinning. A solution of 17.5 wt% polymer concentration in DMAc was found to be optimal. The conductivity of the nanofibre mats was found

to exceed the conductivity of cast SPEEK-30%PVB membranes at similar conditions. It was suggested that proton conduction in the nanofibre mats mainly takes place on the nanofibre surface, probably induced by the perpendicular orientation of the nanofibre axis towards the proton pathway.

A blend of SPEEK with PVA (SPEEK-35%PVA), which was prepared in water as solvent, was infiltrated as a matrix phase within the nanofibre mats for the formation of novel nanocomposite membranes. The role of the solvent, i.e. water or DMAc, was observed to influence the crosslinking reaction between SPEEK and PVA. Lower crosslinking temperatures (110-140 ºC) were required using water than DMAc (about 200 ºC), which was explained by the polar nature and hydrogen bonding capacity of water. This observation should encourage the consideration of water as a possible solvent for the preparation of other membrane compositions.

Methanol permeability and proton conductivity of the SPEEK-35%PVA and nanocomposite membranes generally decrease with increasing crosslinking temperatures. Comparison between both type of membranes exhibited that the SPEEK-30%PVB nanofibres only benefit the nanocomposite membranes crosslinked at 110 ºC and 120 ºC. The methanol permeability of those membranes was reduced by the nanofibres as a consequence of a more constrained swelling and water uptake of the matrix, while proton conductivity was especially promoted by the nanofibres when crosslinking proceeded at 110 ºC. No effect of the nanofibres on the conductivity was found for the membranes crosslinked at 120 ºC. On the other hand, the nanofibres resulted to be detrimental for proton conductivity when the membranes were crosslinked at 130 ºC and 140 ºC, which was inferred to the low proton conductivity of the nanofibres when water uptake diminishes. This was explained by the fact that higher crosslinking degrees are expected to modify the nanofibre-matrix interface resulting in a hindrance to proton conduction, while low crosslinking levels would enable the simultaneous occurrence of large concentrations of water molecules and sulfonic acid groups on the nanofibre surface thus promoting proton conductivity. In general, the advantages provided by the nanofibres were ascribed to their mechanical reinforcing effect which limits swelling and water uptake of the matrices with lower crosslinking degrees, in turn enhancing physical integrity of the membranes, and to their own contribution to proton conductivity. In this matter, new nanofibre compositions which can achieve high proton conductivities at low water contents are under consideration.

Experimental and simulated polarization curves obtained from DMFC tests revealed that optimized SPEEK-based nanocomposite membranes are prospective candidates to replace costly Nafion® films for DMFC application at intermediate temperatures.

Acknowledgements

This research has been funded by the R&D Support Programmes of the Polytechnic University of Valencia (project 24761) and the Spanish Ministry of Science and Innovation (project SP-ENE-20120718).

We warmly thank the groups of both Prof. Santiago Luis (Universidad Jaume I, Castellon, Spain) and Prof. Javier Pozuelo (Universidad Carlos III, Madrid, Spain) for their valuable contributions to the measurements of IR spectroscopy and mechanical properties, respectively.

References

[1] A. Carbone, R. Pedicini, G. Portale, A. Longo, L. D'Ilario, E. Passalacqua, Sulphonated poly(ether ether ketone) membranes for fuel cell application: Thermal and structural characterization, J. Power Sources 163 (2006) 18-26.
[2] S.K. Kamarudin, F. Achmad, W.R.W. Daud, Overview on the application of direct methanol fuel cell (DMFC) for portable electronic devices, Int. J. Hydrogen Energy 34 (2009) 6902-6916.
[3] V. Neburchilov, J. Martin, H. Wang, J. Zhang, A review of polymer electrolyte membranes for direct methanol fuel cells, J. Power Sources 169 (2007) 221-238.
[4] S. Matar, H. Liu, Effect of cathode catalyst layer thickness on methanol cross-over in a DMFC, Electrochim. Acta 56 (2010) 600-606.
[5] J. Prabhuram, T.S. Zhao, H. Yang, Methanol adsorbates on the DMFC cathode and their effect on the cell performance, J. Electroanal. Chem. 578 (2005) 105-112.
[6] P. Staiti, A.S. Aricò, V. Baglio, F. Lufrano, E. Passalacqua, V. Antonucci, Hybrid Nafion-silica membranes doped with heteropolyacids for application in direct methanol fuel cells, Solid State Ion. 145 (2001) 101-107.
[7] P. Dimitrova, K.A. Friedrich, B. Vogt, U. Stimming, Transport properties of ionomer composite membranes for direct methanol fuel cells, J. Electroanal. Chem. 532 (2002) 75-83.
[8] N. Miyake, J.S. Wainright, R.F. Savinell, Evaluation of a sol-gel derived Nafion/silica hybrid membrane for polymer electrolyte membrane fuel cell applications: II. Methanol uptake and methanol permeability, J. Electrochem. Soc. 148 (2001) A905-A909.
[9] D.H. Jung, S.Y. Cho, D.H. Peck, D.R. Shin, J.S. Kim, Preparation and performance of a Nafion®/montmorillonite nanocomposite membrane for direct methanol fuel cell, J. Power Sources 118 (2003) 205-211.
[10] P.-P. Lu, Z.-L. Xu, H. Yang, Y.-M. Wei, Processing-structure-property correlations of polyethersulfone/perfluorosulfonic acid nanofibers fabricated via electrospinning from polymer-nanoparticle suspensions, ACS Appl. Mater. Interfaces 4 (2012) 1716-1723.
[11] Y. Li, G. He, S. Wang, S. Yu, F. Pan, H. Wu, Z. Jiang, Recent advances in the fabrication of advanced composite membranes, J. Mater. Chem. A 1 (2013) 10058-10077.
[12] Z.G. Shao, X. Wang, I.-M. Hsing, Composite Nafion/polyvinyl alcohol membranes for the direct methanol fuel cell, J. Membr. Sci. 210 (2002) 147-153.
[13] N.W. DeLuca, Y.A. Elabd, Nafion®/poly(vinyl alcohol) blends: Effect of composition and annealing temperature on transport properties, J. Membr. Sci. 282 (2006) 217-224.
[14] K.-Y. Cho, J.-Y. Eom, H.-Y. Jung, N.-S. Choi, Y.M. Lee, J.-K. Park, J.-H. Choi, K.-W. Park, Y.-E. Sung, Characteristics of PVdF copolymer/Nafion blend membrane for direct methanol fuel cell (DMFC), Electrochim. Acta 50 (2004) 583-588.

[15] R. Wycisk, J. Chisholm, J. Lee, J. Lin, P.N. Pintauro, Direct methanol fuel cell membranes from Nafion-polybenzimidazole blends, J. Power Sources 163 (2006) 9-17.
[16] T. Yamaguchi, H. Zhou, S. Nakazawa, N. Hara, An extremely low methanol crossover and highly durable aromatic pore-filling electrolyte membrane for direct methanol fuel cells, Adv. Mater. 19 (2007) 592-596.
[17] T.H. Nguyen, X. Wang, Fabrication of the porous polyimide film as a matrix of the composite membrane of the direct methanol fuel cell, Sep. Purif. Technol. 67 (2009) 208-212.
[18] L.-C. Chen, T.L. Yu, H.-L. Lin, S.-H. Yeh, Nafion/PTFE and zirconium phosphate modified Nafion/PTFE composite membranes for direct methanol fuel cells, J. Membr. Sci. 307 (2008) 10-20.
[19] J. Saleem, P. Gao, J. Barford, G. McKay, Development and characterization of novel composite membranes for fuel cell applications, J. Mater. Chem. A 1 (2013) 14335-14343.
[20] T.-C. Jao, G.-B. Jung, S.-C. Kuo, W.-J. Tzeng, A. Su, Polymer electrolyte membrane water electrolyser with Aquivion® short side chain perfluorosulfonic acid ionomer binder in catalyst layers, Int. J. Hydrogen Energy 37 (2012) 13623-13630.
[21] T. Tamura, R. Takemori, H. Kawakami, Proton conductive properties of composite membranes containing uniaxially aligned ultrafine electrospun polyimide nanofiber, J. Power Sources 217 (2012) 135-141.
[22] T. Tamura, H. Kawakami, Aligned electrospun nanofiber composite membranes for fuel cell electrolytes, Nano Lett. 10 (2010) 1324-1328.
[23] D.M. Yu, S. Yoon, T.-H. Kim, J.Y. Lee, J. Lee, Y.T. Hong, Properties of sulfonated poly(arylene ether sulfone)/electrospun nonwoven polyacrylonitrile composite membrane for proton exchange membrane fuel cells, J. Membr. Sci. 446 (2013) 212-219.
[24] C. Lee, S.M. Jo, J. Choi, K.-Y. Baek, Y.B. Truong, I.L. Kyratzis, Y.-G. Shul, SiO_2/sulfonated poly ether ether ketone (SPEEK) composite nanofiber mat supported proton exchange membranes for fuel cells, J. Mater. Sci. 48 (2013) 3665-3671.
[25] S.-H. Wang, H.-L. Lin, Poly (vinylidene fluoride-co-hexafluoropropylene)/ polybenzimidazole blend nanofiber supported Nafion membranes for direct methanol fuel cells, J. Power Sources 257 (2014) 254-263.
[26] H.-L. Lin, S.-H. Wang, Nafion/poly(vinylalcohol) nano-fiber composite and Nafion/poly(vinylalcohol) blend membranes for direct methanol fuel cells, J. Membr. Sci. 452 (2014) 253-262.
[27] M.M. Hasani-Sadrabadi, I. Shabani, M. Soleimani, H. Moaddel, Novel nanofiber-based triple-layer proton exchange membranes for fuel cell applications, J. Power Sources 196 (2011) 4599-4603.
[28] I. Shabani, M.M. Hasani-Sadrabadi, V. Haddadi-Asl, M. Soleimani, Nanofiber-based polyelectrolytes as novel membranes for fuel cell applications, J. Membr. Sci. 368 (2011) 233-240.
[29] J. Choi, K.M. Lee, R. Wycisk, P.N. Pintauro, P.T. Mather, Nanofiber network ion-exchange membranes, Macromolecules 41 (2008) 4569-4572.
[30] J. Choi, K.M. Lee, R. Wycisk, P.N. Pintauro, P.T. Mather, Sulfonated polysulfone/POSS nanofiber composite membranes for PEM fuel cells, J. Electrochem. Soc. 157 (2010) B914-B919.
[31] B. Dong, L. Gwee, D. Salas-de la Cruz, K.I. Winey, Y.A. Elabd, Super proton conductive high-purity Nafion nanofibers, Nano Lett. 10 (2010) 3785-3790.
[32] Z. Hongwei, Y. Fei, Z. Danying, Fabrication and characterization of electrospun sulfonated poly(phthalazinone ether ketone) mats as potential matrix of reinforced proton exchange membranes, J. Appl. Polym. Sci. 130 (2013) 4581-4586.
[33] J. Zhang, Y. Wang, Modeling the effects of methanol crossover on the DMFC, Fuel Cells 4 (2004) 90-95.
[34] G.-B. Jung, A. Su, C.-H. Tu, F.-B. Weng, Effect of operating parameters on the DMFC performance, J. Fuel Cell Sci. Tech. 2 (2005) 81-85.

[35] J.G. Liu, T.S. Zhao, Z.X. Liang, R. Chen, Effect of membrane thickness on the performance and efficiency of passive direct methanol fuel cells, J. Power Sources 153 (2006) 61-67.
[36] H.-Y. Li, Y.-L. Liu, Nafion-functionalized electrospun poly(vinylidene fluoride) (PVDF) nanofibers for high performance proton exchange membranes in fuel cells, J. Mater. Chem. A 2 (2014) 3783-3793.
[37] S. Mollá, V. Compañ, Polyvinyl alcohol nanofiber reinforced Nafion membranes for fuel cell applications, J. Membr. Sci. 372 (2011) 191-200.
[38] S. Mollá, V. Compañ, Performance of composite Nafion/PVA membranes for direct methanol fuel cells, J. Power Sources 196 (2011) 2699-2708.
[39] S. Mollá, V. Compañ, E. Gimenez, A. Blazquez, I. Urdanpilleta, Novel ultrathin composite membranes of Nafion/PVA for PEMFCs, Int. J. Hydrogen Energy 36 (2011) 9886-9895.
[40] Q. Li, R. He, J.O. Jensen, N.J. Bjerrum, Approaches and recent development of polymer electrolyte membranes for fuel cells operating above 100 ºC, Chem. Mater. 15 (2003) 4896-4915.
[41] Y. Shao, G. Yin, Z. Wang, Y. Gao, Proton exchange membrane fuel cell from low temperature to high temperature: Material challenges, J. Power Sources 167 (2007) 235-242.
[42] S. Mollá, V. Compañ, Polymer blends of SPEEK for DMFC application at intermediate temperatures, Int. J. Hydrogen Energy 39 (2014) 5121-5136.
[43] S. Mollá, V. Compañ, S.L. Lafuente, J. Prats, On the methanol permeability through pristine Nafion® and Nafion/PVA membranes measured by different techniques. A comparison of methodologies, Fuel Cells 11 (2011) 897-906.
[44] P.W. Majsztrik, M.B. Satterfield, A.B. Bocarsly, J.B. Benziger, Water sorption, desorption and transport in Nafion membranes, J. Membr. Sci. 301 (2007) 93-106.
[45] M. Bass, V. Freger, Hydration of Nafion and Dowex in liquid and vapor environment: Schroeder's paradox and microstructure, Polymer 49 (2008) 497-506.
[46] T. Romero, W. Mérida, Water transport in liquid and vapour equilibrated Nafion™ membranes, J. Membr. Sci. 338 (2009) 135-144.
[47] S. Ramakrishna, K. Fujihara, W.-E. Teo, T.-C. Lim, Z. Ma, in: An introduction to electrospinning and nanofibers, World Scientific Publishing Co., 2005 (Chapter 3).
[48] X. Zhang, Y. Lu, Centrifugal spinning: An alternative approach to fabricate nanofibers at high speed and low cost, Polym. Rev. 54 (2014) 677-701.
[49] D. Marx, M.E. Tuckerman, J. Hutter, M. Parrinello, The nature of the hydrated excess proton in water, Nature 397 (1999) 601-604.
[50] J. Roziere, D.J. Jones, Non-fluorinated polymer materials for proton exchange membrane fuel cells, Annu. Rev. Mater. Res. 33 (2003) 503-555.
[51] R. Jiang, H.R. Kunz, J.M. Fenton, Investigation of membrane property and fuel cell behavior with sulfonated poly(ether ether ketone) electrolyte: Temperature and relative humidity effects, J. Power Sources 150 (2005) 120-128.
[52] L. Li, J. Zhang, Y. Wang, Proton conductivity of phosphoric acid doped polybenzimidazole and its composites with inorganic proton conductors, J. Membr. Sci. 226 (2003) 159-167.
[53] X. Li, C. Zhao, H. Lu, Z. Wang, H. Na, Direct synthesis of sulfonated poly(ether ether ketone ketone)s (SPEEKKs) proton exchange membranes for fuel cell application, Polymer 46 (2005) 5820-5827.
[54] T.J. Peckham, S. Holdcroft, Structure-morphology-property relationships of non-perfluorinated proton-conducting membranes, Adv. Mater. 22 (2010) 4667-4690.
[55] H.L. Tang, M. Pan, F. Wang, A mechanical durability comparison of various perfluocarbon proton exchange membranes, J. Appl. Polym. Sci. 109 (2008) 2671-2678.

[56] W.R. Bowen, T.A. Doneva, H.B. Yin, Polysulfone-sulfonated poly(ether ether) ketone blend membranes: systematic synthesis and characterization, J. Membr. Sci. 181 (2001) 253-263.
[57] T. He, M. Frank, M.H.V. Mulder, M. Wessling, Preparation and characterization of nanofiltration membranes by coating polyethersulfone hollow fibers with sulfonated poly(ether ether ketone) (SPEEK), J. Membr. Sci. 307 (2008) 62-72.
[58] W.J. Lau, A.F. Ismail, Theoretical studies on the morphological and electrical properties of blended PES/SPEEK nanofiltration membranes using different sulfonation degree of SPEEK, J. Membr. Sci. 334 (2009) 30-42.
[59] J.M. Gohil, P. Ray, Polyvinyl alcohol as the barrier layer in thin film composite nanofiltration membranes: Preparation, characterization, and performance evaluation, J. Colloid Interface Sci. 338 (2009) 121-127.
[60] T. Yang, Preliminary study of SPEEK/PVA blend membranes for DMFC applications, Int. J. Hydrogen Energy 33 (2008) 6772-6779.
[61] J. Jaafar, A.F. Ismail, A. Mustafa, Preparation of high performance SPEEK/Cloisite 15A nanocomposite membrane via advanced membrane formulation method, Mater. Sci. Eng. A 460-461 (2007) 475-484.
[62] S. Gu, G. He, X. Wu, Y. Guo, H. Liu, L. Peng, G. Xiao, Preparation and characteristics of crosslinked sulfonated poly(phthalazinone ether sulfone ketone) with poly(vinyl alcohol) for proton exchange membrane, J. Membr. Sci. 312 (2008) 48-58.
[63] X. Li, X. Hao, D. Xu, G. Zhang, S. Zhong, H. Na, D. Wang, Fabrication of sulfonated poly(ether ether ketone ketone) membranes with high proton conductivity, J. Membr. Sci. 281 (2006) 1-6.
[64] H.-L. Lin, T.L. Yu, L.-N. Huang, L.-C. Chen, K.-S. Shen, G.-B. Jung, Nafion/PTFE composite membranes for direct methanol fuel cell applications, J. Power Sources 150 (2005) 11-19.
[65] A.M. Affoune, A. Yamada, M. Umeda, Conductivity and surface morphology of Nafion membrane in water and alcohol environments, J. Power Sources 148 (2005) 9-17.
[66] X. Dominguez-Benetton, S. Sevda, K. Vanbroekhoven, D. Pant, The accurate use of impedance analysis for the study of microbial electrochemical systems, Chem. Soc. Rev. 41 (2012) 7228-7246.
[67] J. Zhang, Z. Xie, J. Zhang, Y. Tang, C. Song, T. Navessin, Z. Shi, D. Song, H. Wang, D.P. Wilkinson, Z.-S. Liu, S. Holdcroft, High temperature PEM fuel cells, J. Power Sources 160 (2006) 872-891.

Summary of results

3.1. Nafion/PVA membranes

The general effect of incorporating PVA nanofibres within a Nafion® polymer electrolyte is summarized in the following points attending to important membrane parameters for DMFC characterization. In this regard, a pristine Nafion® film with a thickness of 46 ± 1 μm and a nanocomposite Nafion/PVA membrane of 47 ± 3 μm thickness are concisely compared.

3.1.1. Water uptake and ion-exchange capacity

In Fig. 26 are represented the values of water uptake and ion-exchange capacity (IEC) for the pristine Nafion® film and the Nafion/PVA membrane. Both exhibit very similar water uptake levels despite the IEC of Nafion/PVA is about the half of the Nafion® value. This is inferred to the strong hydrophilic character of PVA, due to the polar OH groups, which contributes to hold water even though sulfonic acid moieties are absent in its bulk structure (surface functionalization is not expected to have any significant influence in this matter). Perhaps, this property might be further exploited in fuel cells operating with hydrogen at temperatures higher than 100 ºC and relatively lower humidities. In this case, PVA would be expected to add a higher water retention capacity.

Therefore, the decrease of IEC observed in the Nafion/PVA membrane is justified by the lack of sulfonic acid groups in the PVA phase. Taking into consideration that the measured IEC comes from the Nafion® matrix, with a dry density of 2 g cm^{-3}, and that the density of PVA is 1.3 g cm^{-3}, the composition of the Nafion/PVA membrane can be estimated. The obtained result is: 62.4 wt% Nafion® and 37.6 wt% PVA, i.e. 37.4 vol% Nafion® and 62.6 vol% PVA.

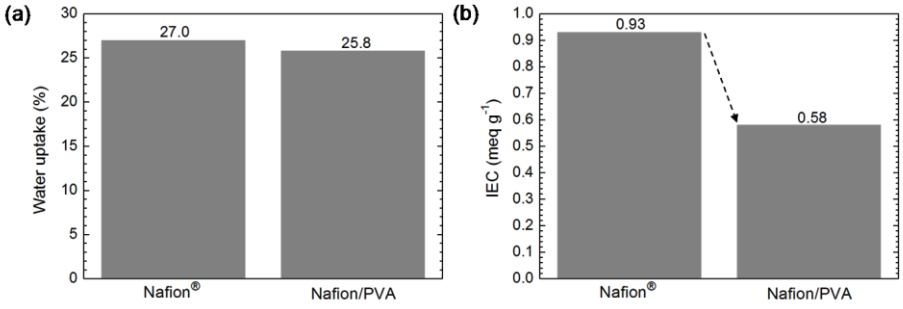

Fig. 26. Values of (a) water uptake and (b) ion-exchange capacity for the reported membranes of Nafion® (no nanofibres) and Nafion/PVA (with nanofibres).

3.1.2. Mechanical properties

The Young's modulus, yield strength (σ_y) and ultimate tensile strength (σ_{ult}) of the Nafion® film and Nafion/PVA membrane are shown in Fig. 27. Clearly, the introduction of PVA nanofibres inside a Nafion® matrix provides a greater stiffness as revealed by the Nafion/PVA membrane. While the yield strength and ultimate tensile strength were practically doubled, the Young's modulus was remarkably increased by a factor of 5.

The improved mechanical properties of the nanocomposite membranes are suggested to increase their physical durability during fuel cell operation, which would also make them good candidates for high pressure PEM electrolysers.

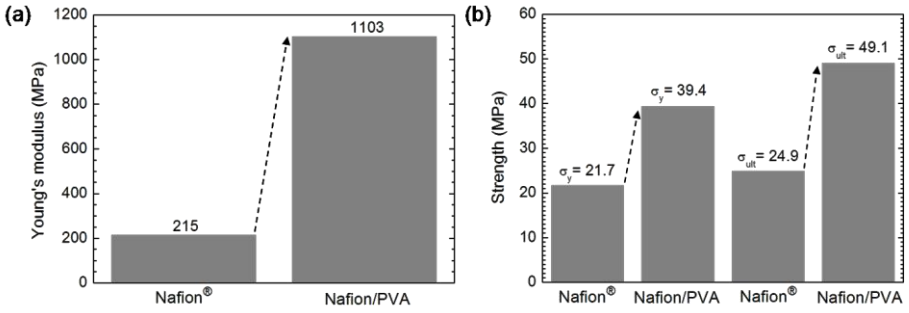

Fig. 27. Mechanical properties of the Nafion film and Nafion/PVA membrane expressed in terms of (a) Young's modulus, (b) yield strength (σ_y) and ultimate tensile strength (σ_{ult}).

3.1.3. Methanol permeability

The PVA nanofibres are found to cause a large reduction of methanol permeability as observed in Fig. 28 by comparison of Nafion® and Nafion/PVA.

The reason for such a decrease is mainly given attending to the intrinsic methanol barrier property of PVA, which is attributed to its semi-crystalline structure, thus inducing a significant increase of tortuosity for diffusion of the methanol molecules. In addition, some contribution of a more constrained swelling of the Nafion® matrix due to the reinforcing effect of the nanofibres cannot be neglected.

Consequently, introduction of organic nanofibres instead of inorganic nanoparticles is a good strategy to limit methanol crossover without compromising the toughness of the membranes.

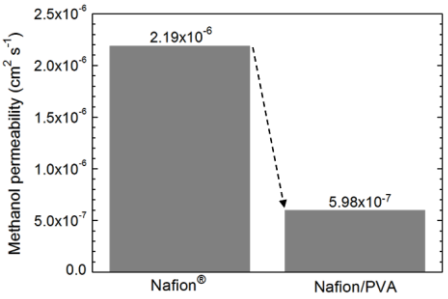

Fig. 28. Methanol permeability coefficients at 25 ºC of the membranes of Nafion® and Nafion/PVA measured by densimetry from a 2 M methanol solution.

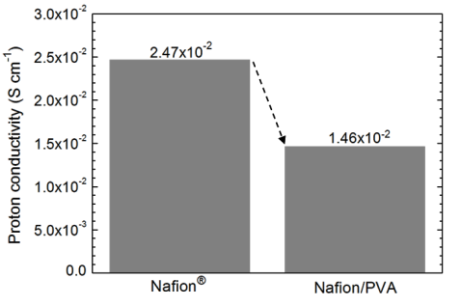

Fig. 29. Proton conductivies at 25 ºC of the membranes of Nafion® and Nafion/PVA, which were measured soaked in deionized water by impedance spectroscopy.

3.1.4. Proton conductivity

The measured decrease of proton conductivity between the Nafion® and Nafion/PVA membrane in Fig. 29 is associated with the reduction of IEC as a result of the insertion of nanofibres.

Interestingly, the relative drop in conductivity of the Nafion/PVA membrane is lower than the relative drop in its methanol permeability (Figs. 28 and 29), which reveals that methanol permeation becomes more affected by the nanofibres than proton conduction.

3.1.5. DMFC performance

The Nafion/PVA membrane performs slightly below the Nafion® film in spite of its lower methanol permeability and higher OCV (Fig. 30). This

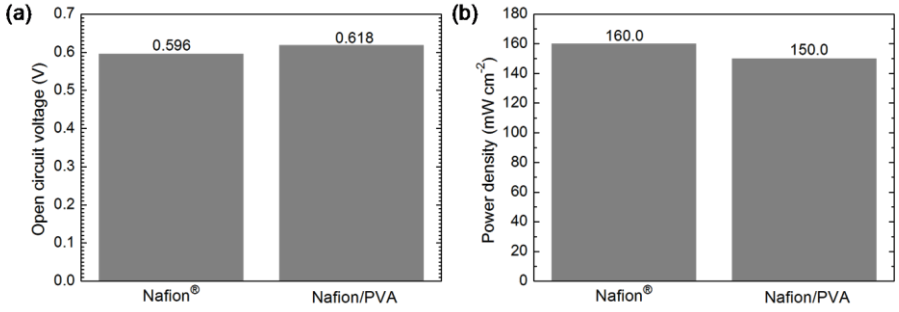

Fig. 30. DMFC results of (a) open circuit voltage and (b) maximum power density measured at 70 ºC feeding a 2 M methanol solution.

corroborates the empirical observation that proton conductivity is the main parameter governing DMFC performance. Remarkably, such a performance is reached in the case of the Nafion/PVA membrane with a Nafion® content about 60 vol% less than the Nafion® polymer present in the film of similar thickness with which is compared.

It can then be concluded that replacement of expensive Nafion® with PVA nanofibres is a suitable approach for the preparation of cost-effective DMFC membranes showing good performances.

3.2. SPEEK-PVA/SPEEK-PVB membranes

The properties for DMFC application given by the SPEEK-30%PVB nanofibres (IEC of SPEEK 2.05 meq g^{-1}) to the SPEEK-35%PVA matrix (IEC of SPEEK 1.75 meq g^{-1}) are schematically analyzed. For this purpose, a cast SPEEK-35%PVA membrane (with a thickness of 122 ± 6 μm) and a nanocomposite membrane of SPEEK-PVA/SPEEK-PVB (with a thickness of 107 ± 5 μm) are contrasted after crosslinking at 120 ºC and swelling in boiling water. The SPEEK-35%PVA matrix composition was blended in water as a solvent. DMFC performance of the nanocomposite membrane is represented against a commercial 157 ± 2 μm thick Nafion® 115 film.

3.2.1. Water uptake and swelling degree

The values of water uptake and in-plane swelling (relative change of area) of the nanocomposite membrane fall well below those ones reached by the membrane without nanofibres. This observation reveals that swelling of the SPEEK-35%PVA phase is constrained by the nanofibres, which is inferred to their mechanical reinforcement contribution.

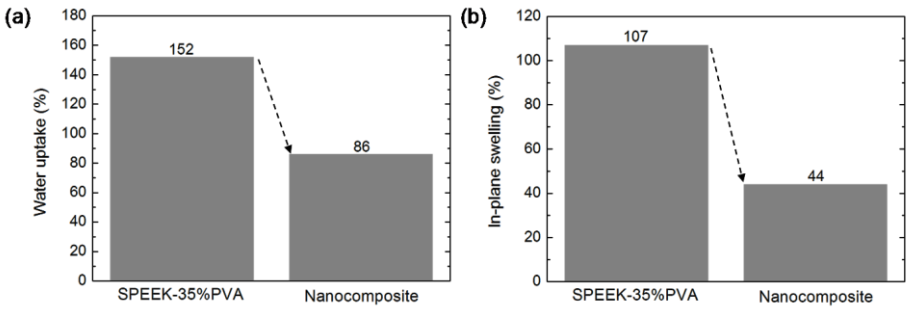

Fig. 31. Values of (a) water uptake and (b) in-plane swelling for the developed SPEEK-based membranes of SPEEK-35%PVA (no nanofibres) and nanocomposite (with nanofibres).

3.2.2. Mechanical properties

The mechanical properties of the SPEEK-35%PVA and nanocomposite membranes shown in Fig. 32 do not exhibit statistically significant differences. Although this disagrees with the conclusion derived from the observed swelling constraint, it can be explained by the dry state of the membranes. The swollen membranes had to be dried before carrying out the mechanical tests and, in this condition, the results do not allow to distinguish between the presence or absence of nanofibres.

The Young's modulus of both membranes are in the 1.2-1.3 GPa range, slightly above the nanofibre-reinforced Nafion/PVA membrane (1.1 GPa) as shown in Fig. 27. This confirms that a dry phase of SPEEK-35%PVA itself possesses good mechanical properties and conceals the reinforcing effect of the nanofibres. On the other hand, the nanofibres are considered to mechanically influence the membrane under a swollen state as previously discussed for the water uptake and swelling degree behaviours.

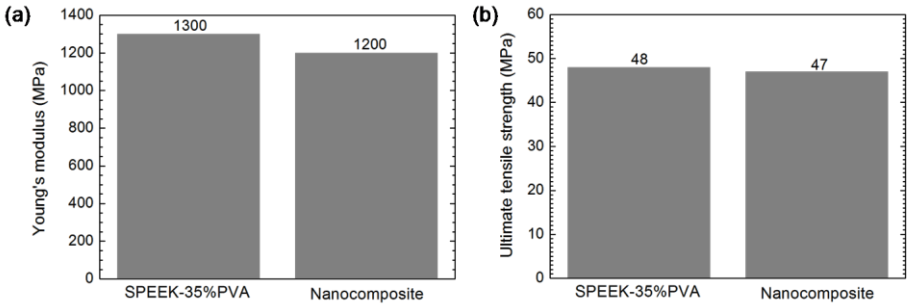

Fig. 32. Mechanical properties of the dry SPEEK-35%PVA and nanocomposite membranes expressed in terms of (a) Young's modulus and (b) ultimate tensile strength.

3.2.3. Methanol permeability

The methanol permeability is found to decrease in the nanocomposite membrane as a consequence of the SPEEK-30%PVB nanofibres (Fig. 33). This is attributed to their constraining effect on the SPEEK-35%PVA swelling behaviour.

However, analysis of Figs. 28 and 33 suggests that the SPEEK-30%PVB nanofibres are less effective for the reduction of methanol crossover than the crosslinked PVA nanofibres, despite the intrinsically good methanol barrier characteristics of the SPEEK-30%PVB composition. A plausible reason for this result comes then from the large water uptake value of the SPEEK-based

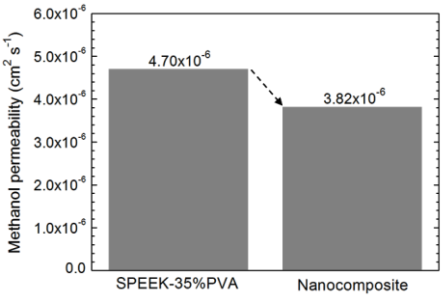

Fig. 33. Methanol permeability coefficients at 60 ºC of the SPEEK-35%PVA and nanocomposite membranes measured by densimetry from a 2 M methanol solution.

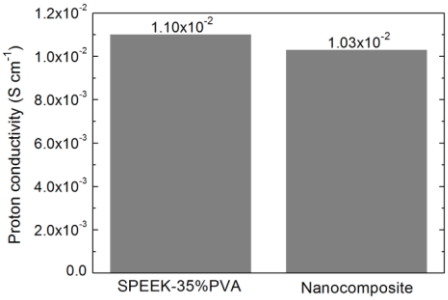

Fig. 34. Proton conductivity values at 60 ºC of the SPEEK-35%PVA and nanocomposite membranes, which were measured soaked in deionized water by impedance spectroscopy.

nanocomposite membrane (~86 wt%) in comparison with the nanocomposite Nafion/PVA membrane (~26 wt%). Under such a high level of water uptake, it seems difficult to achieve a profound drop in methanol permeability independently of the material properties of the incorporated nanofibres.

3.2.4. Proton conductivity

According to Fig. 34, there are no important differences in proton conductivity between the SPEEK-35%PVA and nanocomposite membranes. This is especially relevant taking into consideration the much lower water uptake of the latter. Therefore, the SPEEK-30%PVB nanofibres do not significantly affect the conductivity of the nanocomposite membrane, in contrast to the result obtained with the incorporation of PVA nanofibres within the Nafion® matrix as observed in Fig. 29.

The influence of the SPEEK-30%PVB nanofibres on the conductivity can be described in terms of swelling constraint, thus compensating the lower water content with a higher relative concentration of sulfonic acids, and due to intrinsic proton conductivity of the nanofibres at these conditions.

3.2.5. DMFC performance

DMFC results at an operating temperature of 120 ºC are represented in Fig. 35. At this temperature, methanol permeability of the nanocomposite membrane will be below the permeability of the Nafion® 115 film in line with the obtained values of OCV.

On the other hand, the maximum power density exhibited by the Nafion® film clearly surpasses the nanocomposite membrane. The principal

cause is ascribed to the higher proton conductivity of Nafion®, although it was detected a way for improvement via optimization of the MEA preparation and activation. Moreover, a better long-term stability is predicted for the nanocomposite membranes operating above 100 ºC as a consequence of their inherent high glass transition temperatures.

In summary, the developed SPEEK-based nanocomposite membrane is a suitable candidate for operating DMFCs at higher temperatures than those appropriate for Nafion®. The incorporation of SPEEK-30%PVB nanofibres benefits the control of matrix swelling, thus reducing methanol permeability and improving mechanical properties and physical stability, while proton conductivity is maintained.

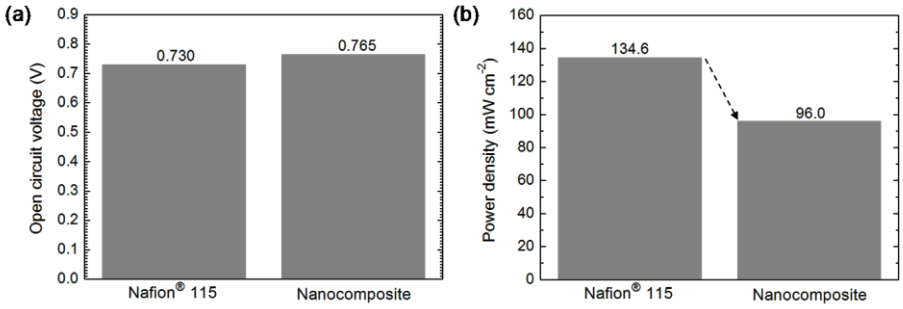

Fig. 35. DMFC results of (a) open circuit voltage and (b) maximum power density measured at 120 ºC feeding a 2 M methanol solution.

Future proposals

4.1. Catalytic fuel oxidation within membranes

The role of the nanofibres for the reduction of methanol crossover in the prepared nanocomposite membranes has been assigned to their increased tortuosity for methanol permeation and the constraint of membrane swelling by their induced mechanical reinforcement.

Further evolution of the nanofibre role would involve direct methanol decomposition/oxidation of the crossing molecules along the membrane thickness before they can reach the cathode and affect its electrochemical performance. This might be achieved by loading catalytic nanoparticles or compounds on the nanofibre surface with high activity towards methanol oxidation assisted by the permeating oxygen molecules which move from the air electrode (cathode) to the anode. Suitable catalysts are reported to be platinum [50-52], platinum-ruthenium alloys [52], manganese-palladium oxides [53], gold [54], and polyoxometalate (POM) systems [55]. Indeed, a study shows that Pt-incorporated Nafion® membranes (via ion-exchange between Pt cations and sulfonic groups) can increase its DMFC performance by catalitically oxidizing the crossover methanol to carbon dioxide (CO_2) and water, although a Pt loading over a 3 wt% caused the water uptake and proton conductivity to decrease [51]. Therefore, it is expected that incorporation of Pt nanoparticles on the nanofibre surface would represent a more optimised method. Besides, more complex catalytic compositions with tailored nanostructures could be prepared in a simpler way by different chemical steps on the nanofibre surface without the presence of the ionomer.

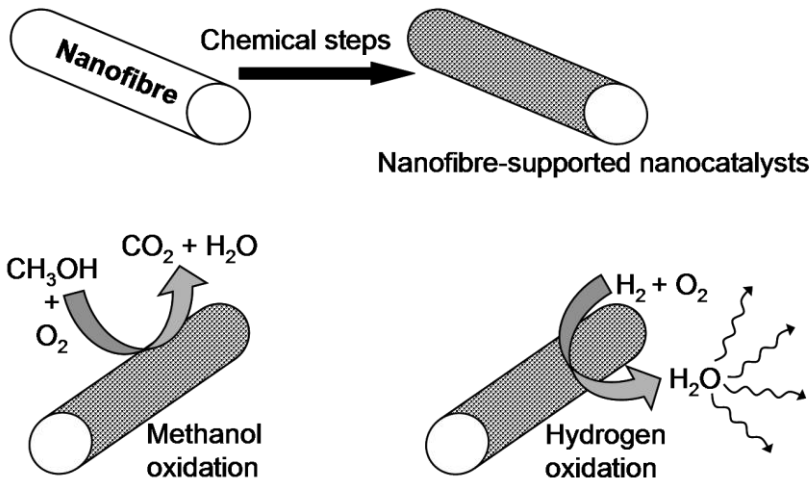

Fig. 36. Scheme of catalyst nanoparticles supported on the surface of a nanofibre for the oxidation/combustion of methanol (elimination of fuel crossover) or hydrogen (self-humidifying membrane).

Fig. 36 depicts the principle of methanol oxidation to carbon dioxide by a nanofibre-supported catalyst. This approach is very promising for the total elimination of the methanol crossover problem. An additional advantage is inferred to come from the associated heat generation by the methanol combustion, which should thermally activate the proton conductivity of the membrane.

On the other hand, a pursued goal in fuel cell technology is the development of membranes able to operate at low humidity levels and preferably at dry conditions. Attempts to resolve this issue deal with the introduction of platinum or palladium nanoparticles into the membrane [56,57]. This causes the combustion of the crossover hydrogen and oxygen molecules and the produced water is used for the self-humidification of the membrane. Other studies report the utilization of supported platinum nanoparticles on different substrates, such us Pt/SiO_2 [58,59], Pt/zeolite [60], Pt/clay [61], Pt/sulfated zirconia [62], Pt/heteropolyacid [63], etc., which can be easier prepared and then homogeneously dispersed inside the membrane. However, excess of inorganic filler has been found to rather block proton conduction [64]. Consequently, it seems reasonable to propose the loading of nanocatalysts for the H_2-O_2 reaction, e.g. platinum, on nanofibres which might be externally functionalised with appropriate grafted moieties to help the stabilization of the nanoparticles (see Fig. 36). Additionally, a more prospective concept would even consider the utilization of high proton-conducting nanofibres to mitigate the reduction of conductivity derived from non-conducting materials.

4.2. High proton-conducting nanofibres

Solid polymer electrolytes composed of a crosslinked PVA matrix incorporating heteropolyacids (HPAs), such us $H_3PW_{12}O_{40}$ (PWA) and $H_4SiW_{12}O_{40}$ (SiWA), have been reported to exhibit high proton conductivities (~0.01 S cm^{-1}) at room temperature [65,66]. This is ascribed to the large number of crystallized water molecules and the large density of free protons in this kind of compounds.

These blended PVA-HPAs compositions are very promising for the preparation of proton conducting nanofibres presenting high values of conductivity as represented in Fig. 37. Additionally, these PVA-HPAs nanofibres are also expected to constrain methanol permeability as discussed for the Nafion-PVA nanocomposite membranes. Similarly, HPAs could be introduced into SPEEK-PVB nanofibres for enhancing their proton conductivity at the lower water contents associated with higher crosslinking degrees of the SPEEK-PVA matrix phase.

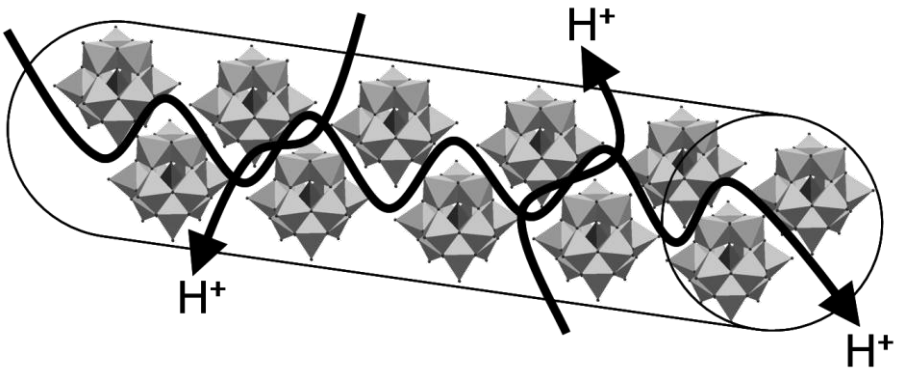

Fig. 37. Proton conduction in a crosslinked PVA nanofibre as a consequence of the incorporation of suitable heteropolyacids (polyoxometalates).

Furthermore, the heteropolyacids (polyoxometalates) could be used as supports for nanocatalysts such us platinum, i.e. Pt/HPA systems, thus combining proton conductivity with synergistic effects for the catalytic fuel oxidation within the membrane [55,63].

4.3. Increased mechanical properties of membranes

A long lifetime is required for the succesful commercialization of fuel cells. In the case of membranes, chemical and mechanical stability is necessary to achieve a good durability. The chemical stability depends on the polymer composition but the mechanical properties can be influenced by other materials such us inorganic fillers, reinforcing fibres, etc. In this regard, we have presented the mechanical reinforcement effect provided by PVA and SPEEK-based nanofibres and its influence on the membrane properties.

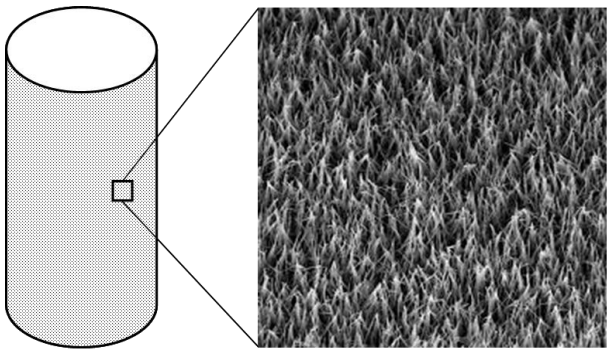

Fig. 38. Growth of a nanowire interphase on a nanofibre surface for increasing interface strength and the global mechanical properties of the corresponding composite membranes.

It is well known that one of the most critical components of a fibre-matrix system in a composite material is the interface. The global mechanical behaviour is correspondingly governed by the mechanical characteristics of the interface.

A novel strategy for enhancing interface strength entails the growth of ZnO nanowires on the surface of the reinforcing fibre. This results in large increments of the interface and laminar shear strengths and the energy absorption capacity of the composite materials [67,68].

A fuel cell membrane is typically subjected to stresses, creep and fatigue induced by larger swelling and temperature levels and by repetitive cycles of swelling/drying. Therefore, it is proposed the fabrication and study of nanofibres with the surface modified by the growth of inorganic nanowires, as shown in Fig. 38, with the aim to improve further the mechanical properties and thus durability of the nanocomposite membranes under fuel cell operating conditions.

Conclusions

Polymeric nanofibres are prospective fillers to improve the characteristics of fuel cell membranes without affecting their flexibility. Electrospinning is a suitable and standard technique for the production of nanofibres made from a broad selection of materials, although new more productive methods are being developed.

The nanofibre morphology exhibits large surface areas which can be functionalised and modified to tailor the interface properties. As a result, mechanical reinforcement of the composite membranes leads to lower water uptake and swelling values which cause the methanol permeability to decrease in DMFC conditions. Additionally, low thickness membranes with reduced ohmic losses can be fabricated.

In this thesis work, nanocomposite membranes have been prepared based on (*i*) a Nafion® matrix with PVA nanofibres (Nafion/PVA) and (*ii*) a blended SPEEK-PVA matrix phase with SPEEK-PVB nanofibres (SPEEK-PVA/SPEEK-PVB). The former are focused on DMFC application below 80 ºC and the latter for operation within the 80-140 ºC range.

The surface of the PVA nanofibres were functionalised with sulfonic acid moieties through the reactivity of the OH groups of PVA via an acetal formation reaction. The interface compatibility was attributed to hydrogen bonding between the sulfonic acid species ($-SO_3H$). An associated advantage was blocking the condensation of sulfonic acids of Nafion® with OH groups of PVA on the nanofibre surface, thus avoiding a larger decrease in proton conductivity as expected from the presence of a non-conducting PVA phase.

The intrinsic methanol barrier properties of the crosslinked PVA nanofibres caused the nanocomposite membranes to show a significant reduction in methanol permeability in comparison with pristine Nafion®.

Proton conductivity measurements of Nafion® and Nafion/PVA membranes within a range of thicknesses revealed a correlation between conductivity and thickness, which was linear in the case of Nafion®.

The PVA nanofibre mats also provided a strong mechanical reinforcing effect to the Nafion® matrix which resulted in the succesful preparation of low thickness membranes (< 20 μm). This could counteract their lower proton conductivity and achieve reduced ohmic losses. Generally, thin membranes are preferred for operation of hydrogen fuel cells at lower relative humidity levels since water transport between cathode and anode is facilitated. Furthermore, important savings of materials and costs are expected with the utilization of thin Nafion/PVA membranes based on nanofibres of the inexpensive PVA polymer.

A disadvantage of Nafion® added up to its high methanol permeability and cost is a glass transition temperature (T_g) in the vicinity of 100 ºC, at hydrated conditions, which limits its maximum operating temperature to 80 ºC. Increasing this temperature is fundamental for enhancing the

electrochemical processes occurring in the DMFC electrodes. With a goal targetted at intermediate temperatures, i.e. 80-140 ºC range, the research was focused on SPEEK polymers due to their high thermal (T_g > 170 ºC) and chemical stabilities, availability of materials and low cost.

The main drawback of SPEEK was found to be excessive swelling and dissolution in hot water, which prevented its practical use in DMFCs at intermediate temperatures. Crosslinking SPEEK with other polymers was considered for enhancing its mechanical stability at those conditions. Immersion of the membranes in boiling water for 1 h was the selected examination procedure.

Hydrophilic PVA and hydrophobic PVB were blended with SPEEK at different compositions and the corresponding membranes crosslinked and characterised. A crosslinking temperature of 200 ºC was required when DMAc solvent was used to blend the polymers. However, this temperature was observed to decrease up to 110 ºC for the SPEEK-PVA compositions mixed in water.

Both PVA and PVB formed crosslinked networks with SPEEK and stabilized it against dissolution in boiling water. This was assigned to the condensation reaction between sulfonic acids of SPEEK and OH groups of PVA and PVB, although intermediate species derived from their thermal degradation were also suggested to play a certain role. Swelling of the membranes was larger with PVA than PVB. Consequently, the proton conductivities of the SPEEK-PVA compositions reached acceptable values for fuel cell systems, while SPEEK-PVB compositions were superior in terms of methanol permeability reduction. Optimal compositions attending their mechanical properties, proton conductivities and methanol permeabilities were found to be SPEEK-35%PVA and SPEEK-30%PVB using SPEEK polymers with IEC values of 1.75 and 2.05 meq g^{-1}, respectively.

Nanofibre mats of SPEEK-30%PVB exhibited proton conductivites well above the shown by cast membranes of similar composition. This increment was inferred to promoted proton conduction on the nanofibre surface. Nanocomposite membranes composed of SPEEK-30%PVB nanofibres embedded in a SPEEK-35%PVA matrix phase (mixed in water) were fabricated and characterised. Benefits provided by the nanofibres were mainly achieved at lower crosslinking degrees and attributed to their mechanical reinforcing effect thus constraining water uptake and swelling. As a result, the mechanical stability of the membranes was enhanced, a good proton conductivity maintained and methanol permeability reduced. A nanocomposite membrane crosslinked at 120 ºC revealed prospective characteristics for application in DMFCs at intermediate temperatures, although further optimization should be explored.

References

[1] H. Zhang, P.K. Shen, Chem. Soc. Rev. 41 (2012) 2382-2394.
[2] L. Carrette, K.A. Friedrich, U. Stimming, Fuel Cells 1 (2001) 5-39.
[3] P. Divya, S. Ramaprabhu, J. Mater. Chem. A 1 (2013) 13605-13611.
[4] A. Su, Y.M. Ferng, J. Hou, T.L. Yu, Int. J. Hydrogen Energ. 37 (2012) 7710-7718.
[5] A. Hamnett, Catal. Today 38 (1997) 445-457.
[6] T.J. Schmidt, H.A. Gasteiger, R.J. Behm, Electrochem. Commun. 1 (1999) 1-4.
[7] A.N. Kuznetsov, P.A. Simonov, V.I. Zaikovskii, V.N. Parmon, E.R. Savinova, J. Solid State Electr. 17 (2013) 1903-1912.
[8] X. Wang, J. Zhang, H. Zhu, Chinese J. Catal. 32 (2011) 74-79.
[9] X. Guo, D.-J. Guo, X.-P. Qiu, L.-Q. Chen, W.-T. Zhu, J. Power Sources 194 (2009) 281-285.
[10] S.-Y. Huang, P. Ganesan, S. Park, B.N. Popov, J. Am. Chem. Soc. 131 (2009) 13898-13899.
[11] K. Senevirathne, R. Hui, S. Campbell, S. Ye, J. Zhang, Electrochim. Acta 59 (2012) 538-547.
[12] S. Sharma, B.G. Pollet, J. Power Sources 208 (2012) 96-119.
[13] F. Lufrano, V. Baglio, P. Staiti, V. Antonucci, A.S. Aricò, J. Power Sources 243 (2013) 519-534.
[14] S. Subianto, M. Pica, M. Casciola, P. Cojocaru, L. Merlo, G. Hards, D.J. Jones, J. Power Sources 233 (2013) 216-230.
[15] F.J. Fernández-Carretero, E. Riande, C. Del Rio, F. Sanchez, J.L. Acosta, V. Compañ, J. New Mat. Electr. Sys. 13 (2010) 83.
[16] L. Unnikrishnan, S. Mohanty, S.K. Nayak, High Perform. Polym. 25 (2013) 854-867.
[17] Y. Zhao, Z. Jiang, D. Lin, A. Dong, Z. Li, H. Wu, J. Power Sources 224 (2013) 28-36.
[18] S.J. Peighambardoust, S. Rowshanzamir, M. Amjadi, Int. J. Hydrogen Energ. 35 (2010) 9349-9384.
[19] Y. Li, G. He, S. Wang, S. Yu, F. Pan, H. Wu, Z. Jiang, J. Mater. Chem. A 1 (2013) 10058-10077.
[20] T. Yamaguchi, F. Miyata, S.-I. Nakao, J. Membrane Sci. 214 (2003) 283-292.
[21] T. Yamaguchi, H. Zhou, S. Nakazawa, N. Hara, Adv. Mater. 19 (2007) 592-596.
[22] L. Gubler, S.A. Gürsel, G.G. Scherer, Fuel Cells 5 (2005) 317-335.
[23] K. Jetsrisuparb, S. Balog, C. Bas, L. Perrin, A. Wokaun, L. Gubler, Eur. Polym. J. 53 (2014) 75-89
[24] S. Cavaliere, S. Subianto, I. Savych, D.J. Jones, J. Rozière, Energ. Environ. Sci. 4 (2011) 4761-4785.
[25] Z. Dong, S.J. Kennedy, Y. Wu, J. Power Sources 196 (2011) 4886-4904.
[26] M.M. Hasani-Sadrabadi, I. Shabani, M. Soleimani, H. Moaddel, J. Power Sources 196 (2011) 4599-4603.
[27] C. Lee, S.M. Jo, J. Choi, K.-Y. Baek, Y.B. Truong, I.L. Kyratzis, Y.-G. Shul, J. Mater. Sci. 48 (2013) 3665-3671.
[28] H.-L. Lin, S.-H. Wang, C.-K. Chiu, T.L. Yu, L.-C. Chen, C.-C. Huang, T.-H. Cheng, J.-M. Lin, J. Membrane Sci. 365 (2010) 114-122.
[29] H.-Y. Li, Y.-L. Liu, J. Mater. Chem. A 2 (2014) 3783-3793.
[30] J.-R. Lee, N.-Y. Kim, M.-S. Lee, S.-Y. Lee, J. Membrane Sci. 367 (2011) 265-272.
[31] D.M. Yu, S. Yoon, T.-H. Kim, J.Y. Lee, J. Lee, Y.T. Hong, J. Membrane Sci. 446 (2013) 212-219.
[32] J. Choi, K.M. Lee, R. Wycisk, P.N. Pintauro, P.T. Mather, Macromolecules 41 (2008) 4569-4572.
[33] J. Choi, K.M. Lee, R. Wycisk, P.N. Pintauro, P.T. Mather, J. Mater. Chem. 20 (2010) 6282-6290.
[34] B. Dong, L. Gwee, D. Salas-de la Cruz, K.I. Winey, Y.A. Elabd, Nano Lett. 10 (2010) 3785-3790.

[35] T. Tamura, H. Kawakami, Nano Lett. 10 (2010) 1324-1328.
[36] Z. Hongwei, Y. Fei, Z. Danying, J. Appl. Polym. Sci. 130 (2013) 4581-4586.
[37] T. Tamura, R. Takemori, H. Kawakami, J. Power Sources 217 (2012) 135-141.
[38] O.E. Kongstein, T. Berning, B. Børresen, F. Seland, R. Tunold, Energy 32 (2007) 418-422.
[39] M. Mamlouk, K. Scott, N. Hidayati, J. Fuel Cell Sci. Tech. 8 (2011) 061009-061009-8.
[40] L. Gubler, D. Kramer, J. Belack, Ö. Ünsal, T.J. Schmidt, G.G. Scherer, J. Electrochem. Soc. 154 (2007) B981-B987.
[41] A.A. Argun, J.N. Ashcraft, P.T. Hammond., Adv. Mater. 20 (2008) 1539-1543.
[42] S. Ramakrishna, K. Fujihara, W.-E. Teo, T.-C. Lim, Z. Ma, In: An Introduction to Electrospinning and Nanofibers, World Scientific Publishing Co. Pte. Ltd., June 2005, ISBN: 978-981-256-454-2.
[43] H. Qu, S. Wei, Z. Guo, J. Mater. Chem. A 1 (2013) 11513-11528.
[44] J. Lyons, C. Li, F. Ko, Polymer 45 (2004) 7597-7603.
[45] P.D. Dalton, D. Grafahrend, K. Klinkhammer, D. Klee, M. Möller, Polymer 48 (2007) 6823-6833.
[46] H. Fong, I. Chun, D.H. Reneker, Polymer 40 (1999) 4585-4592.
[47] Y.H. Jung, H.Y. Kim, D.R. Lee, S.Y. Park, Macromol. Res. 13 (2005) 385-390.
[48] C.Y. Du, T.S. Zhao, W.W. Yang, Electrochim. Acta 52 (2007) 5266-5271.
[49] V.A. Paganin, E. Sitta, T. Iwasita, W. Vielstich, J. Appl. Electrochem. 35 (2005) 1239-1243.
[50] J.R. Applegate, D. McNally, H. Pearlman, S.D. Bakrania, Energy Fuels 27 (2013) 4014-4020.
[51] P.-C. Lee, T.-H. Han, D.O. Kim, J.-H. Lee, S.-J. Kang, C.-H. Chung, Y. Lee, S.M. Cho, H.-G. Choi, T. Kim, E. Lee, J.-D. Nam, J. Membrane Sci. 322 (2008) 441-445.
[52] L.C. Battirola, J.F. Schneider, I.C.L. Torriani, G. Tremiliosi-Filho, U.P. Rodrigues-Filho, Int. J. Hydrogen Energ. 38 (2013) 12060-12068.
[53] M.C. Álvarez-Galván, B. Pawelec, V.A. de la Peña O'Shea, J.L.G. Fierro, P.L. Arias, Appl. Catal. B-Environ. 51 (2004) 83-91.
[54] M. Haruta, A. Ueda, S. Tsubota, R.M.T. Sanchez, Catal. Today 29 (1996) 443-447.
[55] P. Li, W.Mi, Q. Su, C. Luo, Fuel Cells 14 (2014) 56-63.
[56] Y. Liu, T. Nguyen, N. Kristian, Y. Yu, X. Wang, J. Membrane Sci. 330 (2009) 357-362.
[57] J.Y. Lee, W.K. Lee, S.W. Hong, H.K. Lee, J. Nanosci. Nanotechno. 13 (2013) 7886-7890.
[58] C.-H. Tsai, F.-L. Yang, C.-H. Chang, Y.W. Chen-Yang, Int. J. Hydrogen Energ. 37 (2012) 7669-7676.
[59] H.N. Yang, D.C. Lee, S.H. Park, W.J. Kim, J. Membrane Sci. 443 (2013) 210-218.
[60] D.-H. Son, R.K. Sharma, Y.-G. Shul, H. Kim, J. Power Sources 165 (2007) 733-738.
[61] W. Zhang , M.K.S. Li , P.-L. Yue, P. Gao, Langmuir 24 (2008) 2663-2670.
[62] Y. Zhang, H. Zhang, Y. Zhai, X. Zhu, C. Bi, J. Power Sources 168 (2007) 323-329.
[63] S.J. Peighambardoust, S. Rowshanzamir, M.G. Hosseini, M. Yazdanpour, Int. J. Hydrogen Energ. 36 (2011) 10940-10957.
[64] D.C. Lee, H.N. Yang, S.H. Park, K.W. Park, W.J. Kim, J. Membrane Sci. 474 (2015) 254-262.
[65] H. Gao, Q. Tian, K. Lian, Solid State Ionics 181 (2010) 874-876.
[66] H. Gao, K. Lian, J. Mater. Chem. 22 (2012) 21272-21278.
[67] Y. Lin, G. Ehlert, H.A. Sodano, Adv. Funct. Mater. 19 (2009) 2654-2660.
[68] H.-S. Hwang, M.H. Malakooti, B.A. Patterson, H.A. Sodano, Compos. Sci. Technol. 107 (2015) 75-81.